Exploring the Role of Tertiary Lymphoid Structures Using a Mouse Model of Bacteria-Infected Lungs

Jean-Luc Teillaud, Lucile Regard, Clémence Martin, Sophie Sibéril, Pierre-Régis Burgel

Methods in Molecular Biology 1845

Springer Protocols

Marie-Caroline Dieu-Nosjean *Editor*

Tertiary Lymphoid Structures

Methods and Protocols

Humana Press

METHODS IN MOLECULAR BIOLOGY

Series Editor
John M. Walker
School of Life and Medical Sciences
University of Hertfordshire
Hatfield, Hertfordshire, AL10 9AB, UK

For further volumes:
http://www.springer.com/series/7651

Tertiary Lymphoid Structures

Methods and Protocols

Edited by

Marie-Caroline Dieu-Nosjean

Laboratory "Cancer, Immune Control and Escape", UMRS 1138 INSERM, Cordeliers Research Center, Sorbonne University, UMR 1138, Paris Descartes University, Sorbonne Paris City, UMR 1138, Paris, France

Humana Press

Editor
Marie-Caroline Dieu-Nosjean
Laboratory "Cancer, Immune Control and Escape"
UMRS 1138 INSERM
Cordeliers Research Center
Sorbonne University, UMR 1138
Paris Descartes University
Sorbonne Paris City, UMR 1138
Paris, France

ISSN 1064-3745 ISSN 1940-6029 (electronic)
Methods in Molecular Biology
ISBN 978-1-4939-8708-5 ISBN 978-1-4939-8709-2 (eBook)
https://doi.org/10.1007/978-1-4939-8709-2

Library of Congress Control Number: 2018950391

This Humana Press imprint is published by the registered company Springer Science+Business Media, LLC part of Springer Nature.
The registered company address is: 233 Spring Street, New York, NY 10013, U.S.A.

Preface

The immune system has developed many mechanisms to build up a protective response against pathogens or abnormal cells. Some of them take place in organs (i.e. secondary lymphoid organs, SLO) or structures (such as gut-associated lymphoid tissue (GALT) and mucosa-associated lymphoid tissue (MALT)) that are lifelong and fully dedicated to the elaboration of adaptive immune responses. However, there are also inducible lymphoid structures that develop transiently in response to chronic inflammation. These structures, also known as tertiary lymphoid structures (TLS), exhibit features similar to those of SLO, with the segregation of B, T, and dendritic cells in two distinct B-cell and T-cell rich areas.

TLS are found in upper and even lower vertebrates that emerged more than 500 million years ago, suggesting that the ability to form TLS is anterior to the development of SLO during the evolution of the species. It is intriguing to note that TLS that are transient structures persisted in mammals despite the emergence of SLO and other constitutive lymphoid organizations. The advantage gained in conserving TLS during evolution raises many questions about their role in the setting and maintenance of local immune responses in inflammatory environments. It is through the various chapters that make up this book that different aspects of TLS can be discovered. How they can be studied in preclinical models or in the clinics is also presented.

After an introductory chapter that discusses where TLS stand among all the existing lymphoid organizations (Chapter 1), two chapters (Chapters 2 and 3) detail TLS composition, organization, and location. They also present particular situations such as the presence of TLS in the central nervous system. The next chapters describe original and innovative methods allowing the study of TLS in humans and mice. One of the first questions arising when TLS are studied is how to define a TLS in a pathological context. Are we detecting only lymphocyte aggregates or true TLS? Which marker(s) should be used for TLS identification? What are the criteria that should be taken into account to characterize and quantify TLS for prognostic and predictive studies? Thus, Chapters 4, 5, 6, and 7 describe various methods and tools to detect, image, quantify, and analyze TLS. From single or double immunohistochemical staining performed on serial tissue sections to multiplex staining on a single tissue section, an array of methods that make it possible to investigate TLS structure and function is proposed. Similarly, different strategies are offered to quantify TLS in an automated way using stained tissue sections. In particular, a methodology is proposed to visualize TLS from a number of immunostainings made on serial sections by reconstructing images with an open-source software (Chapter 4).

The investigation of TLS immune functions may require switching from cellular to molecular approaches due to the low number of immune cells that can be isolated from these structures or to study a given area of interest. One method of choice is the use of laser capture microdissection to study functional signatures of TLS from frozen tissues (Chapter 8). The search for TLS presence can be also performed by identifying a gene signature from fixed and paraffin-embedded tissues (Chapter 9).

The study of B and T lymphocyte subsets present in TLS has been made also possible, thanks to the optimization of well-known technologies and the development of protocols

adapted to the tissue contexture of these structures. Thus, the analysis of B-cell repertoires and the functionality of the corresponding antibodies produced has been performed by generating a large number of recombinant monoclonal antibodies from isolated single B cells (Chapter 10). The development of protocols for the sorting of lymphocyte subpopulations by negative selection or of very rare populations such as follicular-helper T lymphocytes by positive selection will allow the performance of ex vivo functional tests (Chapters 11 and 12).

Finally, Chapters 13, 14, 15, and 16 are entirely dedicated to the development of murine inflammatory models allowing the functional study of TLS in the context of infection or malignancy.

Overall, this book entitled *Tertiary Lymphoid Structures: Methods and Protocols* is intended to guide our colleagues in the many techniques and methods that can be used to study TLS in pathological situations in patients. Some preclinical models are also depicted in detail in order to show that TLS structure, development, and maintenance can be studied in vivo and targeted. This will undoubtedly increase our knowledge on the immune function and the targeting of these structures paving the way to possible therapeutic applications.

Paris, France ***Marie-Caroline Dieu-Nosjean***

Contents

Contributors

Ann Ager • *Division of Infection and Immunity, School of Medicine and Systems Immunity Research Institute, Cardiff University, Heath Park, Cardiff, UK*

Francesca Barone • *Rheumatology Research Group, Institute of Inflammation and Ageing (IIA), University of Birmingham, Queen Elizabeth Hospital, Birmingham, UK*

Michele Bombardieri • *Centre for Experimental Medicine & Rheumatology, John Vane Science Centre, William Harvey Research Institute, Barts and The London School of Medicine and Dentistry, Queen Mary University of London, London, UK*

Charles Brown • *MedImmune LLC, Gaithersburg, MD, USA*

Pierre-Régis Burgel • *Paris Descartes University, Sorbonne Paris Cité, Faculté de Médecine, UPRES EA 2511, Paris, France; Service de Pneumologie et Service de Physiologie, Hôpital Cochin, AP-HP, Paris, France*

Chiara Burkhardt • *Institute of Experimental Immunology, University of Zurich, Zurich, Switzerland*

Ruben Casanova • *Institute of Pathology and Molecular Pathology, University Hospital Zurich, Zurich, Switzerland*

Kelli A. Connolly • *Department of Immunobiology, Yale University School of Medicine, New Haven, CT, USA*

Elisa Corsiero • *Centre for Experimental Medicine and Rheumatology, John Vane Science Centre, William Harvey Research Institute, Barts and The London School of Medicine and Dentistry, Queen Mary University of London, London, UK*

Coline Couillault • *Laboratory "Targeting of the Tumor and Its Immune Microenvironment", Institut National de la Santé et de la Recherche Médicale (INSERM) U1052, CNRS 5286, Centre Léon Bérard, Centre de Recherche en Cancérologie de Lyon, University Claude Bernard Lyon 1, Lyon, France*

Priyanka Devi-Marulkar • *Cordeliers Research Center, Sorbonne University, UMRS 1138, Paris, France; Cordeliers Research Center, Paris Descartes University, Sorbonne Paris Cité, UMRS 1138, Paris, France; Cordeliers Research Center, Laboratory "Cancer, Immune Control and Escape", INSERM, UMRS 1138, Paris, France; "Cytokine Signaling" Unit, INSERM U1221, Department of Immunology, Institut Pasteur, Paris, France*

Marie-Caroline Dieu-Nosjean • *Laboratory "Cancer, Immune Control and Escape", UMRS 1138 INSERM, Cordeliers Research Center, Sorbonne University, UMR 1138, Paris Descartes University, Sorbonne Paris City, UMR 1138, Paris, France*

Bertrand Dubois • *Laboratory "Targeting of the Tumor and Its Immune Microenvironment", Institut National de la Santé et de la Recherche Médicale (INSERM) U1052, CNRS 5286, Centre Léon Bérard, Centre de Recherche en Cancérologie de Lyon, University Claude Bernard Lyon 1, Lyon, France*

Victor H. Engelhard • *Beirne B. Carter Center for Immunology Research and Department of Microbiology, Immunology and Cancer Biology, University of Virginia, Charlottesville, VA, USA*

Yang-Xin Fu • *Department of Pathology, University of Texas Southwestern Medical Center, Dallas, TX, USA*

Awen Gallimore • *Division of Infection and Immunity, School of Medicine and Systems Immunity Research Institute, Heath Park, Cardiff University, Cardiff, UK*

Soizic Garaud • *Molecular Immunology Unit, Institut Jules Bordet, Université Libre de Bruxelles, Brussels, Belgium*

David Gardner • *Rheumatology Research Group, Institute of Inflammation and Ageing (IIA), University of Birmingham, Queen Elizabeth Hospital, Birmingham, UK*

Claire Germain • *Cordeliers Research Center, Sorbonne University, UMRS 1138, Paris, France; Cordeliers Research Center, Paris Descartes University, Sorbonne Paris Cité, UMRS 1138, Paris, France; Cordeliers Research Center, Laboratory "Cancer, Immune Control and Escape", INSERM, UMRS 1138, Paris, France; Laboratory "Immune Intervention and Biotherapies", Centre d'Immunologie et des Maladies Infectieuses (CIMI), UPMC UMRS CR7—INSERM U1135—CNRS ERL 8255, Paris, France*

Jérémy Goc • *Cordeliers Research Center, Laboratory "Cancer, Immune Control and Escape", Institut National de la Santé et de la Recherche Médicale (INSERM), UMRS 1138, Paris, France; Cordeliers Research Center, Paris Descartes University, Sorbonne Paris Cité, UMRS 1138, Paris, France; Cordeliers Research Center, Sorbonne University, UMRS 1138, Paris, France; Division of Gastroenterology and Hepatology, Joan and Sanford I. Weill Department of Medicine, Weill Cornell Medicine, Cornell University, New York, NY, USA; Department of Microbiology and Immunology, Weill Cornell Medicine, Cornell University, New York, NY, USA; The Jill Robert's Institute for Research in Inflammatory Bowel Disease, Weill Cornell Medicine, Cornell University, New York, NY, USA*

Claudia Gutierrez-Chavez • *Cordeliers Research Center, Laboratory "Cancer, Immune Control and Escape", Institut National de la Santé et de la Recherche Médicale (INSERM), UMRS 1138, Paris, France; Cordeliers Research Center, Paris Descartes University, Sorbonne Paris Cité, UMRS 1138, Paris, France; Cordeliers Research Center, Sorbonne University, UMRS 1138, Paris, France; Department of Radiation Oncology, Albert Einstein College of Medicine, Bronx, NY, USA*

Chunyan Gu-Trantien • *Molecular Immunology Unit, Institut Jules Bordet, Université Libre de Bruxelles, Brussels, Belgium; Institute for Medical Immunology, Université Libre de Bruxelles, Charleroi, Belgium*

Lucas Jagemann • *Centre for Experimental Medicine and Rheumatology, John Vane Science Centre, William Harvey Research Institute, Barts and The London School of Medicine and Dentistry, Queen Mary University of London, London, UK*

Emma Jones • *Division of Infection and Immunity, School of Medicine and Systems Immunity Research Institute, Heath Park, Cardiff University, Cardiff, UK*

Nikhil Joshi • *Department of Immunobiology, Yale University School of Medicine, New Haven, CT, USA*

Hélène Kaplon • *Cordeliers Research Center, Laboratory "Cancer, Immune Control and Escape", Institut National de la Santé et de la Recherche Médicale (INSERM), UMRS 1138, Paris, France; Cordeliers Research Center, Paris Descartes University, Sorbonne Paris Cité, UMRS 1138, Paris, France; Cordeliers Research Center, Sorbonne University, UMRS 1138, Paris, France*

Christophe Klein • *Cordeliers Research Center, Center of Cellular Imaging and Cytometry, Institut National de la Santé et de la Recherche Médicale (INSERM), UMRS 1138, Paris, France; Cordeliers Research Center, Sorbonne University, UMRS 1138, Paris, France; Cordeliers Research Center, Paris Descartes University, Paris Cité, UMRS 1138, Paris, France*

Samantha Knockaert • *Cordeliers Research Center, Laboratory "Cancer, Immune Control and Escape", Institut National de la Santé et de la Recherche Médicale (INSERM), UMRS 1138, Paris, France; Cordeliers Research Center, Paris Descartes University, Sorbonne Paris Cité, UMRS 1138, Paris, France; Cordeliers Research Center, Sorbonne University, UMRS 1138, Paris, France; Center for Therapeutic Innovation in Oncology, Institut de Recherches Servier, Croissy sur Seine, France*

Myriam Lawand • *Cordeliers Research Center, Laboratory "Cancer, Immune Control and Escape", Institut National de la Santé et de la Recherche Médicale (INSERM), UMRS 1138, Paris, France; Cordeliers Research Center, Paris Descartes University, Sorbonne Paris Cité, UMRS 1138, Paris, France; Cordeliers Research Center, Sorbonne University, UMRS 1138, Paris, France; Centre d'immunothérapie, Unité 932, Institut Curie, Paris, France*

Jean-Nicolas Lodewyckx • *Molecular Immunology Unit, Institut Jules Bordet, Université Libre de Bruxelles, Brussels, Belgium*

Antoine Louveau • *Center for Brain Immunology and Glia (BIG), Department of Neuroscience, University of Virginia, Charlottesville, VA, USA*

Clémence Martin • *Paris Descartes University, Sorbonne Paris Cité, Faculté de Médecine, UPRES EA 2511, Paris, France; Service de Pneumologie et Service de Physiologie, Hôpital Cochin, AP-HP, Paris, France*

Selene Meza-Perez • *Division of Clinical Immunology and Rheumatology, Department of Medicine, University of Alabama at Birmingham, Birmingham, AL, USA*

Edoardo Migliori • *Molecular Immunology Unit, Institut Jules Bordet, Université Libre de Bruxelles, Brussels, Belgium*

Christopher George Mueller • *Laboratoire d'Immunologie, Immunopathologie et Chimie Thérapeutique, Institut de Biologie Moléculaire et Cellulaire (IBMC), CNRS UPR3572, University of Strasbourg, Strasbourg, France*

Mursal Nader • *Department of Immunobiology, Yale University School of Medicine, New Haven, CT, USA*

Saba Nayar • *Rheumatology Research Group, Institute of Inflammation and Ageing (IIA), University of Birmingham, Queen Elizabeth Hospital, Birmingham, UK*

J. David Peske • *Beirne B. Carter Center for Immunology Research and Department of Microbiology, Immunology and Cancer Biology, University of Virginia, Charlottesville, VA, USA*

Costantino Pitzalis • *Centre for Experimental Medicine and Rheumatology, John Vane Science Centre, William Harvey Research Institute, Barts and The London School of Medicine and Dentistry, Queen Mary University of London, London, UK*

Xiangyan Qiu • *Department of Pathology, University of Texas Southwestern Medical Center, Dallas, TX, USA*

Troy D. Randall • *Division of Clinical Immunology and Rheumatology, Department of Medicine, University of Alabama, Birmingham, AL, USA*

Lucile Regard • *Paris Descartes University, Sorbonne Paris Cité, Faculté de Médecine, UPRES EA 2511, Paris, France; Service de Pneumologie et Service de Physiologie, Hôpital Cochin, AP-HP, Paris, France*

Anthony B. Rodriguez • *Beirne B. Carter Center for Immunology Research and Department of Microbiology, Immunology and Cancer Biology, University of Virginia, Charlottesville, VA, USA*

Sophie Sibéril • *Cordeliers Research Center, Laboratory "Cancer, Immune Control and Escape", Institut National de la Santé et de la Recherche Médicale (INSERM), UMRS 1138, Paris, France; Cordeliers Research Center, Paris Descartes University, Sorbonne Paris Cité, UMRS 1138, Paris, France; Cordeliers Research Center, Sorbonne University, UMRS 1138, Paris, France*

Karīna Siliņa • *Institute of Experimental Immunology, University of Zurich, Zurich, Switzerland*

Aaron Silva-Sanchez • *Division of Clinical Immunology and Rheumatology, Department of Medicine, University of Alabama, Birmingham, AL, USA*

Cinzia Solinas • *Molecular Immunology Unit, Institut Jules Bordet, Université Libre de Bruxelles, Brussels, Belgium*

Alex Solterman • *Institute of Pathology and Molecular Pathology, University Hospital Zurich, Zurich, Switzerland*

Keith E. Steele • *MedImmune LLC, Gaithersburg, MD, USA*

Haidong Tang • *Department of Pathology, University of Texas Southwestern Medical Center, Dallas, TX, USA*

Jean-Luc Teillaud • *Cordeliers Research Center, Laboratory "Cancer, Immune Control and Escape", Institut National de la Santé et de la Recherche Médicale (INSERM), UMRS 1138, Paris, France; Cordeliers Research Center, Paris Descartes University, Sorbonne Paris Cité, UMRS 1138, Paris, France; Cordeliers Research Center, Sorbonne University, UMRS 1138, Paris, France*

Casey Timmerman • *Department of Pathology, University of Texas Southwestern Medical Center, Dallas, TX, USA*

Maries van den Broek • *Institute of Experimental Immunology, University of Zurich, Zurich, Switzerland*

Karen Willard-Gallo • *Molecular Immunology Unit, Institut Jules Bordet, Université Libre de Bruxelles, Brussels, Belgium*

Chapter 1

Tertiary Lymphoid Structures Among the World of Noncanonical Ectopic Lymphoid Organizations

Aaron Silva-Sanchez, Troy D. Randall, and Selene Meza-Perez

Abstract

Tertiary lymphoid structures (TLOs), also known as ectopic lymphoid structures, are associated with chronic infections and inflammatory diseases. Despite their association with pathology, these structures are actually a normal, albeit transient, component of the immune system and facilitate local immune responses that are meant to mitigate inflammation and resolve infection. Many of the mechanisms controlling the formation and function of tertiary lymphoid structures have been identified, in part by experimentally triggering their formation using defined stimuli under controlled conditions. Here, we introduce the experimental and pathological conditions in which tertiary lymphoid tissues are formed, describe the mechanisms linked to their formation, and discuss their functions in the context of both infection and inflammation.

Key words Tertiary lymphoid organ (TLO), Ectopic lymphoid tissue, Secondary lymphoid organ (SLO), Follicular dendritic cell (FDC), Fibroblastic reticular cell (FRC), B-cell follicle, Germinal center, Autoimmunity

1 Introduction

Immune responses are initiated in secondary lymphoid organs (SLOs), which collect antigens and cells from surrounding tissues, recruit naïve B and T cells from the blood, and provide an environment that maximizes encounters between antigen-presenting cells and lymphocytes and supports the proliferation and differentiation of effector cells. All SLOs share a similar cellular architecture that includes primary and secondary B-cell follicles organized around a network of follicular dendritic cells (FDCs); a T-cell zone organized around a network of fibroblastic reticular cells (FRCs); macrophages and dendritic cells (DCs) strategically placed to capture antigen and prime T cells; high endothelial venules (HEVs) for lymphocyte extravasation; and lymphatic vessels (except in spleen) for collection of antigens and cells from tissues as well as for the release of cells into the blood [1, 2].

Marie-Caroline Dieu-Nosjean (ed.), *Tertiary Lymphoid Structures: Methods and Protocols*, Methods in Molecular Biology, vol. 1845, https://doi.org/10.1007/978-1-4939-8709-2_1,

SLOs form during embryogenesis at predetermined locations, independently of antigen or inflammation, using a well-defined program of cellular and molecular interactions [3, 4]. In contrast, architecturally and functionally similar tissues, known as tertiary lymphoid organs (TLOs) or tertiary lymphoid structures (TLS), form after birth at unpredictable sites, due to persistent local inflammation triggered by infection, autoimmune diseases, malignancy, allograft recognition, and other conditions [5–7]. In each of these situations, lymphocytes and other cells that make up TLOs are likely responding to locally produced antigens or autoantigens. In turn, antigen-stimulated lymphocytes provide the signals needed for TLO organogenesis and maintenance. Once antigen is cleared and inflammation resolves, TLOs often disappear [4, 8].

The accumulation of lymphocytes and the degree to which they become organized in peripheral, nonlymphoid tissues vary depending on the strength, type, and duration of the inflammatory and antigenic stimuli. As a result, lymphoid aggregates range from loose collections of a few B cells to highly organized tissues with all the hallmarks of TLOs. As a result, investigators have made efforts to classify the spectrum of lymphoid aggregates, under the hypothesis that not all aggregates are functionally equivalent [9–11]. Although the minimal attributes needed to form a functional TLO are not known, we will define a TLO as a lymphoid aggregate with differentiated stromal components (FDCs, FRCs, or HEVs) that would not normally reside in that tissue. This type of definition would exclude inflammatory aggregates of B or T cells that lack differentiated stromal compartments.

2 Development of TLOs

Many of the mechanisms controlling TLO formation are similar to those governing SLO development. Both involve reciprocal interactions between fibroblastic stromal cell types, such as FDCs and FRCs, and lymphocytes such as B cells, T cells, and innate lymphoid cells (ILCs). On one side of this interaction, stromal cells in SLOs and mature TLOs express homeostatic chemokines, such as CCL19, CCL21, CXCL13, and CXCL12 [12], that attract lymphoid and myeloid cells and also express cytokines like RANKL and IL-7 that promote survival and expansion of lymphocytes. On the other side of this interaction, lymphocytes express TNF family members, including lymphotoxin (LT), TNF-α, and LIGHT [4, 13, 14] that maintain stromal cell differentiation.

Although this model generally applies to both SLOs and TLOs, the details differ considerably. For example, although SLOs typically require specialized ILCs known as lymphoid tissue inducer (LTi) cells to express LT and TNF-α, these same cytokines are

provided by B and T cells in the context of TLO formation [15–17]. More importantly, SLOs form in the absence of inflammation, whereas the formation of TLOs is triggered by inflammatory cytokines, including IL-1α [18], IL-6 [19], IL-17 [15], and IL-22 [20]. Interestingly, these cytokines are often associated with either the development or the function of Th17 cells, which are often associated with the formation of TLOs in autoimmune, infectious, and inflammatory diseases. Intriguingly, many of these same cytokines are involved in the function of the SLO-inducing LTi cells, suggesting that they may have overlapping functions. Although Th17 cells and IL-17 are often associated with the formation of TLOs, there are additional inflammatory pathways that trigger TLO formation. Regardless of the inflammatory stimuli that trigger TLO formation, the end result still requires LT-triggered stromal cell differentiation and homeostatic chemokine production.

Despite some commonalities in their development, TLOs form under a wide variety of conditions and cytokine milieus that depend on the initiating stimulus (infection, autoimmunity, transplantation, malignancy) and the tissue in which the TLO is forming. Consequently, it is likely that TLOs forming in response to diverse stimuli in different tissues will have unique characteristics that may impart distinctive attributes to immune responses occurring in those TLOs. Thus, it will be important for future studies to identify both the shared and unique features of individual TLO-associated diseases, in order to understand disease progression and to develop therapies that specifically target TLO formation or function.

3 Role of TLOs in Pathogenic Immune Responses

TLOs are often observed in tissues damaged by autoimmune responses. For example, TLOs are observed in the inflamed synovium of patients with rheumatoid arthritis [21–25], the salivary and lacrimal glands of patients with Sjögren's syndrome [26–28], the brains and spinal cords of patients with multiple sclerosis [29–35], the kidneys of patients with lupus nephritis [36], the pancreata of patients with diabetes [37–39], and the thymus of patients with myasthenia gravis [40, 41]. In many cases, increased severity of disease is associated with more or larger TLOs in the affected tissue [42, 43]. As a result, many investigators conclude that TLOs exacerbate local immune reactivity and contribute to pathogenesis.

Consistent with the idea that TLOs exacerbate local autoimmune-mediated inflammation and tissue damage, TLOs in target tissues often contain B and T cells responding to local autoantigens [44]. For example, B cells in TLOs from the synovium or lungs of rheumatoid arthritis patients often produce antibodies that bind citrullinated histones [45, 46], which are target antigens

in this disease. Similarly, B cells in TLOs from patients with rheumatoid arthritis [47, 48], Sjögren's syndrome [49], and lupus nephritis [44] have evidence of clonal expansion and somatic hypermutation, suggesting that they are actively responding to local antigens.

In many cases, the formation of TLOs in the context of autoimmunity is associated with the presence of Th17 cells. For example, patients with lupus nephritis, rheumatoid arthritis, diabetes, and multiple sclerosis commonly have Th17 cells in TLOs that form in target tissues [15, 31, 32, 50–54]. Unfortunately, it is difficult to dissociate cause from consequence in snapshots of human disease. As a result, it is not entirely clear whether these Th17 cells are produced by TLOs under these conditions, or alternatively whether TLOs are forming in response to the activities of Th17 cells that were produced elsewhere [32, 55, 56]. Nevertheless, the role of IL-17 in the formation of TLOs is well documented in mouse studies [15, 32, 57, 58], suggesting that IL-17 or its downstream mediators may be important therapeutic targets for pathogenic immune responses that involve TLOs.

The role of IL-17 in the formation of TLOs is complex. Although Th17 cells are the primary producers of IL-17 in many autoimmune diseases, IL-17 is also made by γδT cells, ILC3 cells, LTi cells, and some Tfh cells, all of which may contribute to TLO formation under various conditions. These same cells make other cytokines, such as IL-22, TNF-α, and LT, which also contribute to TLO formation in both autoimmunity and infection [20, 59, 60]. Importantly, IL-17 can directly trigger fibroblastic cells to express CXCL13 and CCL19, which attract B cells, T cells, and DCs and are required for the formation of B-cell follicles and T-cell zones, respectively [15, 58]. IL-17 also promotes the expression of CXCL8, CXCL9, and CXCL10, inflammatory chemokines that potently recruit neutrophils [61]. In fact, neutrophils are instrumental in the formation of some TLOs [62], possibly by providing B-cell-activating cytokines, such as APRIL [63], or because they release serine proteases that damage local tissues and trigger repair processes [64].

Although IL-17 is important for initiating TLO formation, the reciprocal interactions between stroma-derived homeostatic cytokines/chemokines and LT-producing lymphocytes and DCs are required to maintain the structure of TLOs. In fact, the blockade of IL-17 has little effect on established TLOs, whereas the blockade of LT causes their dissolution [15]. In the context of autoimmunity or other chronic inflammatory conditions, IL-17-driven inflammation and LT-driven homeostasis most likely occur simultaneously, making therapeutic intervention more difficult.

4 TLOs and Protective Immunity

Despite the fact that TLOs are often associated with pathogenic immune responses, the mere presence of a TLO in a particular organ does not promote autoimmune or inflammatory responses. For example, the Ruddle lab generated mice that expressed TNF-α or LT under the control of the rat insulin promoter, with the idea that these cytokines would promote inflammation in the pancreas and lead to the development of diabetes. In fact, the transgenic mice did develop inflammatory infiltrates in the pancreas consisting of B cells, $CD4^+$ and $CD8^+$ T cells, as well as $ICAM^+VCAM^+$ stromal cells, but surprisingly did not develop diabetes [65–67]. Subsequent studies defined these lymphoid infiltrates as TLOs, complete with B-cell follicles with FDCs and T-cell areas with HEVs [38, 39, 60, 68].

In fact, the tissue-specific transgenic expression of a variety of cytokines or chemokines leads to the spontaneous development of TLOs—each revealing a new level of complexity to the mechanisms that promote TLO formation. For example, using the same rat insulin promoter to drive transgene expression, multiple investigators show that LT [69], TNF-α [70, 59], LIGHT [60], CXCL13 [71], and CCL21, CCL19, and CXCL12 [72, 73] independently promote the formation of local TLOs in the pancreas. Moreover, the transgenic expression of these same cytokines or chemokines in other tissues also triggers TLO formation in those tissues [74–77]. Each cytokine or chemokine generated TLOs with slightly different features as a consequence of what cell types that particular molecule activated or attracted. Although tissue-specific expression of cytokines and chemokines is associated with TLO development at that site, the systemic expression of some cytokines, such as IL-7, can trigger the formation of TLOs (and even additional SLOs) in multiple tissues due to the expansion and persistence of LTi cells [78]. Thus, a variety of cytokines impact TLO formation either directly or indirectly without triggering autoimmunity.

Although the examples above demonstrate that TLOs are not always associated with pathogenesis, there are also cases in which TLOs are distinctly protective, particularly in the context of infection. For example, TLOs form in the lungs following infection with a variety of viruses or microbes [57, 58, 79–85]. Interestingly, mice lacking all SLOs, but retaining TLOs in the lung, are actually more resistant to influenza infection than conventional mice [13]. These mice make normal primary B- and T-cell responses, generate long-lived antibody-secreting cells, maintain memory T cells, and are resistant to secondary challenge infections [13]. Similarly, memory $CD8^+$ T cells accumulate in the lung after infection in TLO-like structures termed repair-associated memory depots (RAMDs) [86]. These sites are similar to nodular inflammatory

foci (NIFs), which develop in mice infected with murine cytomegalovirus (MCMV) [11]. Myeloid cells accumulate in these sites, differentiate into antigen-presenting DCs, and promote $CD8^+$ T-cell responses against infection. Thus, TLOs can provide effective primary immunity and maintain memory cells, independently of conventional SLOs.

The role of TLOs in controlling pulmonary infection with *Mycobacterium tuberculosis* (Mtb) is particularly instructive [45, 81, 83, 87]. For example, numerous well-organized TLOs are found in the lungs of primates with well-controlled, latent tuberculosis, whereas fewer and less organized TLOs are observed in the lungs of primates with active disease [88]. In fact, TLOs are an important component of the granuloma structure that helps contain Mtb, in part because stromal cells in TLOs recruit CCR7- and CXCR5-expressing T cells [83, 89], which are necessary to activate pulmonary macrophages that engulf and kill Mtb.

Similar to the formation of TLOs in autoimmune diseases, the formation of TLOs in response to infection with Mtb requires the IL-23/IL-17 axis as well as the LT signaling pathway [90–94]. Mtb-infected mice lacking IL-17A, IL-22, or IL-23 develop smaller and fewer TLOs and are less able to restrain bacterial growth [81]. Although IL-17 works by triggering chemokine expression and thereby calling in inflammatory cells, IL-22 seems to be more important for the formation of B-cell follicles [15, 20], perhaps due to expansion of CXCL13-expressing FDC networks in TLOs. These data demonstrate that the formation of TLOs, even when triggered by IL-17, can be protective in the context of infection.

5 Regulatory Functions of TLOs

One might conclude that TLOs simply amplify local immune responses. In the case of autoimmunity or other inflammatory responses, augmented immunity would exacerbate inflammation, whereas in the case of infection augmented immunity would facilitate pathogen clearance and accelerate the healing process. In addition to these two scenarios, some data suggest that TLOs can mediate protective functions *via* regulatory functions. For example, in the $ApoE^{-/-}$ model of atherosclerosis, TLOs form beneath atherosclerotic plaques [95]. Although atherosclerosis is considered an inflammatory disease, these TLOs appear to temper inflammation by promoting the differentiation of regulatory T cells (Tregs). In the absence of TLOs (eliminated by conditional knockout of the LTβR), $ApoE^{-/-}$ mice developed more and larger plaques [95]. Thus, some aspect of TLO function, perhaps Treg generation, is immunoprotective, even in the context of inflammatory diseases.

What might confer regulatory properties on TLOs? One possibility is the activities of fibroblastic stromal cells that make up the scaffolding of TLOs. In addition to their organizational properties, FRCs in conventional SLOs can present self-antigens and promote tolerance rather than immune activation [96, 97]. This activity is achieved in part by promoting Treg differentiation [98, 99], and by expressing inducible nitric oxide synthase [100–102], which suppresses T-cell proliferation *via* the production of nitric oxide [100, 103]. Although, TLOs appear to have FDCs and FRCs like conventional SLOs, it is not clear where these cells come from or whether they have additional or different functions that may influence local immune reactions.

The example of Mtb infection highlights another potential role of TLOs—containment. Granulomas not only support the activation of Mtb-killing macrophages, but they also physically contain the infection and prevent dissemination. In a similar way, TLOs may be collecting and sequestering antigens, as well as activated effector T cells, and thereby preventing them from disseminating to target tissues and causing further damage. For example, TLOs in the lungs of asthmatics may collect and sequester Th2 cells and limit their ability to promote airway hyper-responsiveness. The idea seems plausible, as treatment with the S1P agonist, FTY720 (a drug that downregulates the S1PR1 and prevents lymphocyte egress from SLOs [104]), blocks airway hypersensitivity in mice [105, 106]. Moreover, FTY720 treatment promotes TLO development [107], in part by preventing the recirculation of lymphocytes. In fact, FTY720 (fingolimod) is now used clinically to treat autoimmune diseases like multiple sclerosis [108], which is characterized by the development of TLOs in the CNS. Thus, the ability of TLOs to sequester antigens and potentially damaging effector cells may by one way in which they attenuate disease progression.

Importantly, the ability of TLOs to sequester antigens or cells is dependent on their ability to collect those cells. Conventional SLOs have well-described methods for antigen collection. For example, lymph nodes collect antigens and cells from regional tissues via lymphatic vessels [109–112], mucosal tissues like Peyer's patches collect antigens across a specialized epithelium [3, 5], and fat-associated lymphoid clusters (FALCs) in the mesentery and pericardium and the milky spots of the omentum collect antigens from body cavities [5, 113–115]. However, it is less clear how TLOs, which are often embedded in solid tissues, might collect antigens.

In many cases, TLOs form in response to autoantigens or alloantigens that are expressed in the tissues in which TLOs are formed, so there is no need to collect antigen from distal sites. In some cases however, the formation of TLOs is linked with the local development of lymphatic vessels. For example, pulmonary infection promotes the VEGF-dependent growth of lymphatic vessels

surrounding TLOs in the lung [45, 79]. However, it is unclear whether these vessels are afferent lymphatics that bring antigens and cells to the TLOs or are efferent lymphatics that drain to downstream lymph nodes. Understanding how TLOs are connected to the lymphatic vasculature will be important for understanding how TLOs function in many settings.

6 What Controls Whether TLOs Promote or Prevent Immune Activation?

Much like chronic infections, tumors and transplanted organs persistently stimulate the immune system, leading to sustained inflammation. Not surprisingly, TLOs are often observed in these situations [116] and the mechanisms underlying their formation and function are clinically important [117]. For example, in some cases, the formation of TLOs in lung transplants is associated with sustained alloreactivity and chronic graft rejection [118, 119]. In fact, the presence of TLOs in allografts is primarily associated with local lymphocyte activation and increased rejection [120], probably via many of the mechanisms discussed above. However, in other cases, the formation of TLOs is associated with acceptance of allografts [121], possibly by priming Tregs that help mediate tolerance [121]. Similarly, the transfer of lymphocytes from accepted transplants into new transplant recipients leads to allograft acceptance [122], due to the expansion of alloantigen-specific Tregs in local TLOs [123]. Thus, it is important to understand the features of TLOs that distinguish whether they promote T-cell activation and rejection or Treg expansion and tolerance.

Although tolerance is a desired outcome in transplantation, the opposite is true in the case of cancer. TLOs are often observed in or near areas of non-small cell lung cancer (NSCLC) [124–126]. Not surprisingly, these areas are associated with the expression of homeostatic chemokines linked to TLO formation and T-cell recruitment. Consistent with this idea, tumor-associated TLO areas have PNAd$^+$ HEVs that co-localize with CD62L$^+$ T cells, suggesting that they can recruit T cells from the blood [127]. Although the formation of TLOs in tumors is sometimes prognostic of favorable outcomes to treatment [128], tumor-associated TLOs sometimes exhibit an immunosuppressive phenotype, characterized by a high density of Tregs and absence of NK cells [129, 130]. This functional discrepancy may be partly due to their location, as TLOs within pancreatic tumors are correlated with favorable outcomes, whereas TLOs at the periphery of tumors are not [129]. Unfortunately, our understanding of these observations is incomplete and we do not know why tumor-associated TLOs might form in one location or another, whether their location changes the phenotype of responding T cells, or whether they are

differentially supplying T cells to the tumor or sequestering them. Nevertheless, these results dramatically illustrate the importance of TLOs in both protective immunity and pathogenesis and highlight our gaps in knowledge that need to be filled in order to therapeutically target the activities of TLOs in the context of inflammation, infection, and malignancy.

7 Conclusion

In summary, we now know that TLOs are formed by a wide variety of stimuli under diverse conditions and, depending on factors that we do not entirely understand, can either exacerbate or restrain inflammation and local immunity. Enhanced immunity is clearly beneficial for clearing infections or tumors, but is also detrimental in the context of autoimmunity and transplantation. As a result, the details of how TLOs form and function under different conditions are critically important, as they will undoubtedly make the difference between transplant rejection or tolerance, tumor killing or progression, and pathogen clearance or chronic infection. In our view, some of the important unanswered questions are these: What are the origins of the fibroblastic stromal cells in TLOs? Are they developmentally or functionally different in TLOs that form in different tissues or in different locations in the same tissue? What controls whether TLOs promote T-cell activation or Treg expansion, thereby leading to opposite clinical outcomes? An understanding of the answers to these questions will almost certainly lead to methods allowing us to control the activity of TLOs and promote desired clinical outcomes, regardless of the type of immune response.

References

1. Cyster JG (2010) B cell follicles and antigen encounters of the third kind. Nat Immunol 11(11):989–996. https://doi.org/10.1038/ni.1946
2. Drayton DL, Liao S, Mounzer RH, Ruddle NH (2006) Lymphoid organ development: from ontogeny to neogenesis. Nat Immunol 7(4):344–353. https://doi.org/10.1038/ni1330
3. Dieu-Nosjean MC, Goc J, Giraldo NA et al (2014) Tertiary lymphoid structures in cancer and beyond. Trends Immunol 35(11):571–580. https://doi.org/10.1016/j.it.2014.09.006
4. Jones GW, Jones SA (2016) Ectopic lymphoid follicles: inducible centres for generating antigen-specific immune responses within tissues. Immunology 147(2):141–151. https://doi.org/10.1111/imm.12554
5. Randall TD, Mebius RE (2014) The development and function of mucosal lymphoid tissues: a balancing act with micro-organisms. Mucosal Immunol 7(3):455–466. https://doi.org/10.1038/mi.2014.11
6. van de Pavert SA, Mebius RE (2010) New insights into the development of lymphoid tissues. Nat Rev Immunol 10(9):664–674. https://doi.org/10.1038/nri2832
7. Yin C, Mohanta S, Maffia P, Habenicht AJ (2017) Editorial: tertiary lymphoid organs (TLOs): powerhouses of disease immunity. Front Immunol 8:228. https://doi.org/10.3389/fimmu.2017.00228
8. Carragher DM, Rangel-Moreno J, Randall TD (2008) Ectopic lymphoid tissues and local immunity. Semin Immunol 20(1):26–42. https://doi.org/10.1016/j.smim.2007.12.004

9. Cruz-Migoni S, Caamano J (2016) Fat-associated lymphoid clusters in inflammation and immunity. Front Immunol 7:612. https://doi.org/10.3389/fimmu.2016.00612
10. Jones GW, Bombardieri M, Greenhill CJ et al (2015) Interleukin-27 inhibits ectopic lymphoid-like structure development in early inflammatory arthritis. J Exp Med 212(11):1793–1802. https://doi.org/10.1084/jem.20132307
11. Stahl FR, Heller K, Halle S et al (2013) Nodular inflammatory foci are sites of T cell priming and control of murine cytomegalovirus infection in the neonatal lung. PLoS Pathog 9(12):e1003828. https://doi.org/10.1371/journal.ppat.1003828
12. Pitzalis C, Jones GW, Bombardieri M, Jones SA (2014) Ectopic lymphoid-like structures in infection, cancer and autoimmunity. Nat Rev Immunol 14(7):447–462. https://doi.org/10.1038/nri3700
13. Moyron-Quiroz JE, Rangel-Moreno J, Kusser K et al (2004) Role of inducible bronchus associated lymphoid tissue (iBALT) in respiratory immunity. Nat Med 10(9):927–934. https://doi.org/10.1038/nm1091
14. van de Pavert SA, Olivier BJ, Goverse G et al (2009) Chemokine CXCL13 is essential for lymph node initiation and is induced by retinoic acid and neuronal stimulation. Nat Immunol 10(11):1193–1199. https://doi.org/10.1038/ni.1789
15. Rangel-Moreno J, Carragher DM, de la Luz Garcia-Hernandez M et al (2011) The development of inducible bronchus-associated lymphoid tissue depends on IL-17. Nat Immunol 12(7):639–646. https://doi.org/10.1038/ni.2053
16. Lochner M, Ohnmacht C, Presley L et al (2011) Microbiota-induced tertiary lymphoid tissues aggravate inflammatory disease in the absence of RORgamma t and LTi cells. J Exp Med 208(1):125–134. https://doi.org/10.1084/jem.20100052
17. Cherrier M, Sawa S, Eberl G (2012) Notch, Id2, and RORgammat sequentially orchestrate the fetal development of lymphoid tissue inducer cells. J Exp Med 209(4):729–740. https://doi.org/10.1084/jem.20111594
18. Kuroda E, Ozasa K, Temizoz B et al (2016) Inhaled fine particles induce alveolar macrophage death and interleukin-1alpha release to promote inducible bronchus-associated lymphoid tissue formation. Immunity 45(6):1299–1310. https://doi.org/10.1016/j.immuni.2016.11.010
19. Goya S, Matsuoka H, Mori M et al (2003) Sustained interleukin-6 signalling leads to the development of lymphoid organ-like structures in the lung. J Pathol 200(1):82–87. https://doi.org/10.1002/path.1321
20. Barone F, Nayar S, Campos J et al (2015) IL-22 regulates lymphoid chemokine production and assembly of tertiary lymphoid organs. Proc Natl Acad Sci U S A 112(35):11,024–11,029. https://doi.org/10.1073/pnas.1503315112
21. Wengner AM, Hopken UE, Petrow PK et al (2007) CXCR5- and CCR7-dependent lymphoid neogenesis in a murine model of chronic antigen-induced arthritis. Arthritis Rheum 56(10):3271–3283. https://doi.org/10.1002/art.22939
22. Thurlings RM, Wijbrandts CA, Mebius RE et al (2008) Synovial lymphoid neogenesis does not define a specific clinical rheumatoid arthritis phenotype. Arthritis Rheum 58(6):1582–1589. https://doi.org/10.1002/art.23505
23. Takemura S, Braun A, Crowson C et al (2001) Lymphoid neogenesis in rheumatoid synovitis. J Immunol 167(2):1072–1080
24. Shi K, Hayashida K, Kaneko M et al (2001) Lymphoid chemokine B cell-attracting chemokine-1 (CXCL13) is expressed in germinal center of ectopic lymphoid follicles within the synovium of chronic arthritis patients. J Immunol 166(1):650–655
25. Humby F, Bombardieri M, Manzo A et al (2009) Ectopic lymphoid structures support ongoing production of class-switched autoantibodies in rheumatoid synovium. PLoS Med 6(1):e1. https://doi.org/10.1371/journal.pmed.0060001
26. Holdgate N, St Clair EW (2016) Recent advances in primary Sjogren's syndrome. F1000Res 5. https://doi.org/10.12688/f1000research.8352.1
27. Fava RA, Kennedy SM, Wood SG et al (2011) Lymphotoxin-beta receptor blockade reduces CXCL13 in lacrimal glands and improves corneal integrity in the NOD model of Sjogren's syndrome. Arthritis Res Ther 13(6):R182. https://doi.org/10.1186/ar3507
28. Bombardieri M, Barone F, Lucchesi D et al (2012) Inducible tertiary lymphoid structures, autoimmunity, and exocrine dysfunction in a novel model of salivary gland inflammation in C57BL/6 mice. J Immunol 189(7):3767–3776. https://doi.org/10.4049/jimmunol.1201216
29. Serafini B, Rosicarelli B, Magliozzi R et al (2004) Detection of ectopic B-cell follicles with germinal centers in the meninges of patients with secondary progressive multiple sclerosis. Brain Pathol 14(2):164–174
30. Pikor NB, Prat A, Bar-Or A, Gommerman JL (2015) Meningeal tertiary lymphoid tissues and multiple sclerosis: a gathering place for diverse types of immune cells during CNS auto-

immunity. Front Immunol 6:657. https://doi.org/10.3389/fimmu.2015.00657
31. Pikor NB, Astarita JL, Summers-Deluca L et al (2015) Integration of Th17- and lymphotoxin-derived signals initiates meningeal-resident stromal cell remodeling to propagate neuroinflammation. Immunity 43(6):1160–1173. https://doi.org/10.1016/j.immuni.2015.11.010
32. Peters A, Pitcher LA, Sullivan JM et al (2011) Th17 cells induce ectopic lymphoid follicles in central nervous system tissue inflammation. Immunity 35(6):986–996. https://doi.org/10.1016/j.immuni.2011.10.015
33. Mitsdoerffer M, Peters A (2016) Tertiary lymphoid organs in central nervous system autoimmunity. Front Immunol 7:451. https://doi.org/10.3389/fimmu.2016.00451
34. Magliozzi R, Columba-Cabezas S, Serafini B, Aloisi F (2004) Intracerebral expression of CXCL13 and BAFF is accompanied by formation of lymphoid follicle-like structures in the meninges of mice with relapsing experimental autoimmune encephalomyelitis. J Neuroimmunol 148(1-2):11–23. https://doi.org/10.1016/j.jneuroim.2003.10.056
35. Columba-Cabezas S, Griguoli M, Rosicarelli B et al (2006) Suppression of established experimental autoimmune encephalomyelitis and formation of meningeal lymphoid follicles by lymphotoxin beta receptor-Ig fusion protein. J Neuroimmunol 179(1-2):76–86. https://doi.org/10.1016/j.jneuroim.2006.06.015
36. Hsieh C, Chang A, Brandt D et al (2011) Predicting outcomes of lupus nephritis with tubulointerstitial inflammation and scarring. Arthritis Care Res (Hoboken) 63(6):865–874. https://doi.org/10.1002/acr.20441
37. Ludewig B, Odermatt B, Landmann S et al (1998) Dendritic cells induce autoimmune diabetes and maintain disease via de novo formation of local lymphoid tissue. J Exp Med 188(8):1493–1501
38. Henry RA, Kendall PL (2010) CXCL13 blockade disrupts B lymphocyte organization in tertiary lymphoid structures without altering B cell receptor bias or preventing diabetes in nonobese diabetic mice. J Immunol 185(3):1460–1465. https://doi.org/10.4049/jimmunol.0903710
39. Astorri E, Bombardieri M, Gabba S et al (2010) Evolution of ectopic lymphoid neogenesis and in situ autoantibody production in autoimmune nonobese diabetic mice: cellular and molecular characterization of tertiary lymphoid structures in pancreatic islets. J Immunol 185(6):3359–3368. https://doi.org/10.4049/jimmunol.1001836
40. Zhang X, Liu S, Chang T et al (2016) Intrathymic Tfh/B cells interaction leads to ectopic GCs formation and anti-AChR antibody production: central role in triggering MG occurrence. Mol Neurobiol 53(1):120–131. https://doi.org/10.1007/s12035-014-8985-1
41. Hill ME, Shiono H, Newsom-Davis J, Willcox N (2008) The myasthenia gravis thymus: a rare source of human autoantibody-secreting plasma cells for testing potential therapeutics. J Neuroimmunol 201-202:50–56. https://doi.org/10.1016/j.jneuroim.2008.06.027
42. Pei G, Zeng R, Han M et al (2014) Renal interstitial infiltration and tertiary lymphoid organ neogenesis in IgA nephropathy. Clin J Am Soc Nephrol 9(2):255–264. https://doi.org/10.2215/CJN.01150113
43. Magliozzi R, Howell O, Vora A et al (2007) Meningeal B-cell follicles in secondary progressive multiple sclerosis associate with early onset of disease and severe cortical pathology. Brain 130(Pt 4):1089–1104. https://doi.org/10.1093/brain/awm038
44. Chang A, Henderson SG, Brandt D et al (2011) In situ B cell-mediated immune responses and tubulointerstitial inflammation in human lupus nephritis. J Immunol 186(3):1849–1860. https://doi.org/10.4049/jimmunol.1001983
45. Rangel-Moreno J, Hartson L, Navarro C et al (2006) Inducible bronchus-associated lymphoid tissue (iBALT) in patients with pulmonary complications of rheumatoid arthritis. J Clin Invest 116(12):3183–3194. https://doi.org/10.1172/JCI28756
46. Corsiero E, Bombardieri M, Carlotti E et al (2016) Single cell cloning and recombinant monoclonal antibodies generation from RA synovial B cells reveal frequent targeting of citrullinated histones of NETs. Ann Rheum Dis 75(10):1866–1875. https://doi.org/10.1136/annrheumdis-2015-208356
47. Scheel T, Gursche A, Zacher J et al (2011) V-region gene analysis of locally defined synovial B and plasma cells reveals selected B cell expansion and accumulation of plasma cell clones in rheumatoid arthritis. Arthritis Rheum 63(1):63–72. https://doi.org/10.1002/art.27767
48. Kim HJ, Berek C (2000) B cells in rheumatoid arthritis. Arthritis Res 2(2):126–131. https://doi.org/10.1186/ar77
49. Salomonsson S, Jonsson MV, Skarstein K et al (2003) Cellular basis of ectopic germinal center formation and autoantibody production in the target organ of patients with Sjogren's syndrome. Arthritis Rheum 48(11):3187–3201. https://doi.org/10.1002/art.11311
50. Zhang Z, Kyttaris VC, Tsokos GC (2009) The role of IL-23/IL-17 axis in lupus nephritis. J Immunol 183(5):3160–3169. https://doi.org/10.4049/jimmunol.0900385

51. Pisitkun P, Ha HL, Wang H et al (2012) Interleukin-17 cytokines are critical in development of fatal lupus glomerulonephritis. Immunity 37(6):1104–1115. https://doi.org/10.1016/j.immuni.2012.08.014
52. Hirota K, Yoshitomi H, Hashimoto M et al (2007) Preferential recruitment of CCR6-expressing Th17 cells to inflamed joints via CCL20 in rheumatoid arthritis and its animal model. J Exp Med 204(12):2803–2812. https://doi.org/10.1084/jem.20071397
53. Genovese MC, Durez P, Richards HB et al (2014) One-year efficacy and safety results of secukinumab in patients with rheumatoid arthritis: phase II, dose-finding, double-blind, randomized, placebo-controlled study. J Rheumatol 41(3):414–421. https://doi.org/10.3899/jrheum.130637
54. Crispin JC, Oukka M, Bayliss G et al (2008) Expanded double negative T cells in patients with systemic lupus erythematosus produce IL-17 and infiltrate the kidneys. J Immunol 181(12):8761–8766
55. Nistala K, Adams S, Cambrook H et al (2010) Th17 plasticity in human autoimmune arthritis is driven by the inflammatory environment. Proc Natl Acad Sci U S A 107(33):14751–14756. https://doi.org/10.1073/pnas.1003852107
56. Harbour SN, Maynard CL, Zindl CL et al (2015) Th17 cells give rise to Th1 cells that are required for the pathogenesis of colitis. Proc Natl Acad Sci U S A 112(22):7061–7066. https://doi.org/10.1073/pnas.1415675112
57. Fleige H, Ravens S, Moschovakis GL et al (2014) IL-17-induced CXCL12 recruits B cells and induces follicle formation in BALT in the absence of differentiated FDCs. J Exp Med 211(4):643–651. https://doi.org/10.1084/jem.20131737
58. Eddens T, Elsegeiny W, Garcia-Hernadez ML et al (2017) Pneumocystis-driven inducible bronchus-associated lymphoid tissue formation requires Th2 and Th17 immunity. Cell Rep 18(13):3078–3090. https://doi.org/10.1016/j.celrep.2017.03.016
59. Rehal S, von der Weid PY (2017) TNFDeltaARE mice display abnormal lymphatics and develop tertiary lymphoid organs in the mesentery. Am J Pathol 187(4):798–807. https://doi.org/10.1016/j.ajpath.2016.12.007
60. Lee Y, Chin RK, Christiansen P et al (2006) Recruitment and activation of naive T cells in the islets by lymphotoxin beta receptor-dependent tertiary lymphoid structure. Immunity 25(3):499–509. https://doi.org/10.1016/j.immuni.2006.06.016
61. Song HW, Yang C, Liu W et al (2017) Interleukin-17A plays the same role on mice acute lung injury respectively induced by lipopolysaccharide and paraquat. Inflammation 40:1509–1519. https://doi.org/10.1007/s10753-017-0592-7
62. Foo SY, Zhang V, Lalwani A et al (2015) Regulatory T cells prevent inducible BALT formation by dampening neutrophilic inflammation. J Immunol 194(9):4567–4576. https://doi.org/10.4049/jimmunol.1400909
63. Mohr E, Serre K, Manz RA et al (2009) Dendritic cells and monocyte/macrophages that create the IL-6/APRIL-rich lymph node microenvironments where plasmablasts mature. J Immunol 182(4):2113–2123. https://doi.org/10.4049/jimmunol.0802771
64. Solleti SK, Srisuma S, Bhattacharya S et al (2016) Serpine2 deficiency results in lung lymphocyte accumulation and bronchus-associated lymphoid tissue formation. FASEB J 30(7):2615–2626. https://doi.org/10.1096/fj.201500159R
65. Picarella DE, Kratz A, Li CB et al (1993) Transgenic tumor necrosis factor (TNF)-alpha production in pancreatic islets leads to insulitis, not diabetes. Distinct patterns of inflammation in TNF-alpha and TNF-beta transgenic mice. J Immunol 150(9):4136–4150
66. Picarella DE, Kratz A, Li CB et al (1992) Insulitis in transgenic mice expressing tumor necrosis factor beta (lymphotoxin) in the pancreas. Proc Natl Acad Sci U S A 89(21):10036–10040
67. Flavell RA, Kratz A, Ruddle NH (1996) The contribution of insulitis to diabetes development in tumor necrosis factor transgenic mice. Curr Top Microbiol Immunol 206:33–50
68. Penaranda C, Tang Q, Ruddle NH, Bluestone JA (2010) Prevention of diabetes by FTY720-mediated stabilization of peri-islet tertiary lymphoid organs. Diabetes 59(6):1461–1468. https://doi.org/10.2337/db09-1129
69. Mounzer RH, Svendsen OS, Baluk P et al (2010) Lymphotoxin-alpha contributes to lymphangiogenesis. Blood 116(12):2173–2182. https://doi.org/10.1182/blood-2009-12-256065
70. Zhang Q, Lu Y, Proulx ST et al (2007) Increased lymphangiogenesis in joints of mice with inflammatory arthritis. Arthritis Res Ther 9(6):R118. https://doi.org/10.1186/ar2326
71. Ansel KM, Ngo VN, Hyman PL et al (2000) A chemokine-driven positive feedback loop organizes lymphoid follicles. Nature 406(6793):309–314. https://doi.org/10.1038/35018581
72. Luther SA, Bidgol A, Hargreaves DC et al (2002) Differing activities of homeostatic chemokines CCL19, CCL21, and CXCL12 in

lymphocyte and dendritic cell recruitment and lymphoid neogenesis. J Immunol 169(1):424–433
73. Cyster JG (1999) Chemokines and the homing of dendritic cells to the T cell areas of lymphoid organs. J Exp Med 189(3):447–450
74. Marinkovic T, Garin A, Yokota Y et al (2006) Interaction of mature CD3+CD4+ T cells with dendritic cells triggers the development of tertiary lymphoid structures in the thyroid. J Clin Invest 116(10):2622–2632. https://doi.org/10.1172/JCI28993
75. Marchesi F, Martin AP, Thirunarayanan N et al (2009) CXCL13 expression in the gut promotes accumulation of IL-22-producing lymphoid tissue-inducer cells, and formation of isolated lymphoid follicles. Mucosal Immunol 2(6):486–494. https://doi.org/10.1038/mi.2009.113
76. Furtado GC, Pacer ME, Bongers G et al (2014) TNFalpha-dependent development of lymphoid tissue in the absence of RORgammat(+) lymphoid tissue inducer cells. Mucosal Immunol 7(3):602–614. https://doi.org/10.1038/mi.2013.79
77. Chen L, He Z, Slinger E et al (2015) IL-23 activates innate lymphoid cells to promote neonatal intestinal pathology. Mucosal Immunol 8(2):390–402. https://doi.org/10.1038/mi.2014.77
78. Meier D, Bornmann C, Chappaz S et al (2007) Ectopic lymphoid-organ development occurs through interleukin 7-mediated enhanced survival of lymphoid-tissue-inducer cells. Immunity 26(5):643–654. https://doi.org/10.1016/j.immuni.2007.04.009
79. Baluk P, Adams A, Phillips K et al (2014) Preferential lymphatic growth in bronchus-associated lymphoid tissue in sustained lung inflammation. Am J Pathol 184(5):1577–1592. https://doi.org/10.1016/j.ajpath.2014.01.021
80. Gaur S, Trayner E, Aish L, Weinstein R (2004) Bronchus-associated lymphoid tissue lymphoma arising in a patient with bronchiectasis and chronic Mycobacterium avium infection. Am J Hematol 77(1):22–25. https://doi.org/10.1002/ajh.20136
81. Khader SA, Guglani L, Rangel-Moreno J, Gopal R et al (2011) IL-23 is required for long-term control of Mycobacterium tuberculosis and B cell follicle formation in the infected lung. J Immunol 187(10):5402–5407. https://doi.org/10.4049/jimmunol.1101377
82. Kaushal D, Foreman TW, Gautam US et al (2015) Mucosal vaccination with attenuated Mycobacterium tuberculosis induces strong central memory responses and protects against tuberculosis. Nat Commun 6:8533. https://doi.org/10.1038/ncomms9533
83. Kahnert A, Hopken UE, Stein M et al (2007) Mycobacterium tuberculosis triggers formation of lymphoid structure in murine lungs. J Infect Dis 195(1):46–54. https://doi.org/10.1086/508894
84. GeurtsvanKessel CH, Willart MA, Bergen IM et al (2009) Dendritic cells are crucial for maintenance of tertiary lymphoid structures in the lung of influenza virus-infected mice. J Exp Med 206(11):2339–2349. https://doi.org/10.1084/jem.20090410
85. Kocks JR, Adler H, Danzer H et al (2009) Chemokine receptor CCR7 contributes to a rapid and efficient clearance of lytic murine gamma-herpes virus 68 from the lung, whereas bronchus-associated lymphoid tissue harbors virus during latency. J Immunol 182(11):6861–6869. https://doi.org/10.4049/jimmunol.0801826
86. Takamura S, Yagi H, Hakata Y et al (2016) Specific niches for lung-resident memory CD8+ T cells at the site of tissue regeneration enable CD69-independent maintenance. J Exp Med 213(13):3057–3073. https://doi.org/10.1084/jem.20160938
87. Nakayama M, Ozaki H, Itoh Y et al (2016) Vaccination against H9N2 avian influenza virus reduces bronchus-associated lymphoid tissue formation in cynomolgus macaques after intranasal virus challenge infection. Pathol Int 66(12):678–686. https://doi.org/10.1111/pin.12472
88. Slight SR, Rangel-Moreno J, Gopal R et al (2013) CXCR5(+) T helper cells mediate protective immunity against tuberculosis. J Clin Invest 123(2):712–726. https://doi.org/10.1172/JCI65728
89. Khader SA, Gaffen SL, Kolls JK (2009) Th17 cells at the crossroads of innate and adaptive immunity against infectious diseases at the mucosa. Mucosal Immunol 2(5):403–411. https://doi.org/10.1038/mi.2009.100
90. Shen H, Gu J, Xiao H et al (2017) Selective destruction of interleukin 23-induced expansion of a major antigen-specific gammadelta T-cell subset in patients with tuberculosis. J Infect Dis 215(3):420–430. https://doi.org/10.1093/infdis/jiw511
91. Shen H, Chen ZW (2017) The crucial roles of Th17-related cytokines/signal pathways in M. tuberculosis infection. Cell Mol Immunol 15:216–225. https://doi.org/10.1038/cmi.2017.128
92. Quesniaux VF, Jacobs M, Allie N et al (2010) TNF in host resistance to tuberculosis infection. Curr Dir Autoimmun 11:157–179. https://doi.org/10.1159/000289204
93. Day TA, Koch M, Nouailles G et al (2010) Secondary lymphoid organs are dispensable for the development of T-cell-mediated

immunity during tuberculosis. Eur J Immunol 40(6):1663–1673. https://doi.org/10.1002/eji.201040299
94. Allie N, Keeton R, Court N et al (2010) Limited role for lymphotoxin alpha in the host immune response to Mycobacterium tuberculosis. J Immunol 185(7):4292–4301. https://doi.org/10.4049/jimmunol.1000650
95. Hu D, Mohanta SK, Yin C et al (2015) Artery tertiary lymphoid organs control aorta immunity and protect against atherosclerosis via vascular smooth muscle cell lymphotoxin beta receptors. Immunity 42(6):1100–1115. https://doi.org/10.1016/j.immuni.2015.05.015
96. Fletcher AL, Lukacs-Kornek V, Reynoso ED et al (2010) Lymph node fibroblastic reticular cells directly present peripheral tissue antigen under steady-state and inflammatory conditions. J Exp Med 207(4):689–697. https://doi.org/10.1084/jem.20092642
97. Cohen JN, Guidi CJ, Tewalt EF et al (2010) Lymph node-resident lymphatic endothelial cells mediate peripheral tolerance via Aire-independent direct antigen presentation. J Exp Med 207(4):681–688. https://doi.org/10.1084/jem.20092465
98. Warren KJ, Iwami D, Harris DG et al (2014) Laminins affect T cell trafficking and allograft fate. J Clin Invest 124(5):2204–2218. https://doi.org/10.1172/JCI73683
99. Baptista AP, Roozendaal R, Reijmers RM et al (2014) Lymph node stromal cells constrain immunity via MHC class II self-antigen presentation. Elife 3. https://doi.org/10.7554/eLife.04433
100. Siegert S, Huang HY, Yang CY et al (2011) Fibroblastic reticular cells from lymph nodes attenuate T cell expansion by producing nitric oxide. PLoS One 6(11):e27618. https://doi.org/10.1371/journal.pone.0027618
101. Lukacs-Kornek V, Malhotra D, Fletcher AL et al (2011) Regulated release of nitric oxide by nonhematopoietic stroma controls expansion of the activated T cell pool in lymph nodes. Nat Immunol 12(11):1096–1104. https://doi.org/10.1038/ni.2112
102. Khan O, Headley M, Gerard A et al (2011) Regulation of T cell priming by lymphoid stroma. PLoS One 6(11):e26138. https://doi.org/10.1371/journal.pone.0026138
103. Zinocker S, Vaage JT (2012) Rat mesenchymal stromal cells inhibit T cell proliferation but not cytokine production through inducible nitric oxide synthase. Front Immunol 3:62. https://doi.org/10.3389/fimmu.2012.00062
104. Matloubian M, Lo CG, Cinamon G et al (2004) Lymphocyte egress from thymus and peripheral lymphoid organs is dependent on S1P receptor 1. Nature 427(6972):355–360. https://doi.org/10.1038/nature02284
105. Sawicka E, Zuany-Amorim C, Manlius C et al (2003) Inhibition of Th1- and Th2-mediated airway inflammation by the sphingosine 1-phosphate receptor agonist FTY720. J Immunol 171(11):6206–6214
106. Idzko M, Hammad H, van Nimwegen M et al (2006) Local application of FTY720 to the lung abrogates experimental asthma by altering dendritic cell function. J Clin Invest 116(11):2935–2944. https://doi.org/10.1172/JCI28295
107. Kocks JR, Davalos-Misslitz AC, Hintzen G et al (2007) Regulatory T cells interfere with the development of bronchus-associated lymphoid tissue. J Exp Med 204(4):723–734. https://doi.org/10.1084/jem.20061424
108. Brinkmann V, Billich A, Baumruker T et al (2010) Fingolimod (FTY720): discovery and development of an oral drug to treat multiple sclerosis. Nat Rev Drug Discov 9(11):883–897. https://doi.org/10.1038/nrd3248
109. Shin K, Kataru RP, Park HJ et al (2015) TH2 cells and their cytokines regulate formation and function of lymphatic vessels. Nat Commun 6:6196. https://doi.org/10.1038/ncomms7196
110. Randolph GJ, Angeli V, Swartz MA (2005) Dendritic-cell trafficking to lymph nodes through lymphatic vessels. Nat Rev Immunol 5(8):617–628. https://doi.org/10.1038/nri1670
111. Loo CP, Nelson NA, Lane RS et al (2017) Lymphatic vessels balance viral dissemination and immune activation following cutaneous viral infection. Cell Rep 20(13):3176–3187. https://doi.org/10.1016/j.celrep.2017.09.006
112. Kataru RP, Lee YG, Koh GY (2014) Interactions of immune cells and lymphatic vessels. Adv Anat Embryol Cell Biol 214:107–118. https://doi.org/10.1007/978-3-7091-1646-3_9
113. Roozendaal R, Mebius RE (2011) Stromal cell-immune cell interactions. Annu Rev Immunol 29:23–43. https://doi.org/10.1146/annurev-immunol-031210-101357
114. Meza-Perez S, Randall TD (2017) Immunological functions of the omentum. Trends Immunol 38(7):526–536. https://doi.org/10.1016/j.it.2017.03.002
115. Benezech C, Luu NT, Walker JA et al (2015) Inflammation-induced formation of fat-associated lymphoid clusters. Nat Immunol 16(8):819–828. https://doi.org/10.1038/ni.3215
116. Wagnetz D, Sato M, Hirayama S et al (2012) Rejection of tracheal allograft by intrapulmonary lymphoid neogenesis in the absence of

secondary lymphoid organs. Transplantation 93(12):1212–1220. https://doi.org/10.1097/TP.0b013e318250fbf5
117. Sautes-Fridman C, Fridman WH (2016) TLS in tumors: what lies within. Trends Immunol 37(1):1–2. https://doi.org/10.1016/j.it.2015.12.001
118. Nasr IW, Reel M, Oberbarnscheidt MH et al (2007) Tertiary lymphoid tissues generate effector and memory T cells that lead to allograft rejection. Am J Transplant 7(5):1071–1079. https://doi.org/10.1111/j.1600-6143.2007.01756.x
119. Gelman AE, Li W, Richardson SB et al (2009) Cutting edge: acute lung allograft rejection is independent of secondary lymphoid organs. J Immunol 182(7):3969–3973. https://doi.org/10.4049/jimmunol.0803514
120. Sicard A, Chen CC, Morelon E, Thaunat O (2016) Alloimmune-induced intragraft lymphoid neogenesis promotes B-cell tolerance breakdown that accelerates chronic rejection. Curr Opin Organ Transplant 21(4):368–374. https://doi.org/10.1097/MOT.0000000000000329
121. Li W, Bribriesco AC, Nava RG, Brescia AA et al (2012) Lung transplant acceptance is facilitated by early events in the graft and is associated with lymphoid neogenesis. Mucosal Immunol 5(5):544–554. https://doi.org/10.1038/mi.2012.30
122. Le Texier L, Thebault P, Lavault A et al (2011) Long-term allograft tolerance is characterized by the accumulation of B cells exhibiting an inhibited profile. Am J Transplant 11(3):429–438. https://doi.org/10.1111/j.1600-6143.2010.03336.x
123. Legoux FP, Lim JB, Cauley AW et al (2015) CD4+ T cell tolerance to tissue-restricted self antigens is mediated by antigen-specific regulatory T cells rather than deletion. Immunity 43(5):896–908. https://doi.org/10.1016/j.immuni.2015.10.011
124. Hiraoka N, Ino Y, Yamazaki-Itoh R (2016) Tertiary lymphoid organs in cancer tissues. Front Immunol 7:244. https://doi.org/10.3389/fimmu.2016.00244
125. Dieu-Nosjean MC, Giraldo NA, Kaplon H et al (2016) Tertiary lymphoid structures, drivers of the anti-tumor responses in human cancers. Immunol Rev 271(1):260–275. https://doi.org/10.1111/imr.12405
126. Dieu-Nosjean MC, Antoine M, Danel C et al (2008) Long-term survival for patients with non-small-cell lung cancer with intratumoral lymphoid structures. J Clin Oncol 26(27):4410–4417. https://doi.org/10.1200/JCO.2007.15.0284
127. de Chaisemartin L, Goc J, Damotte D et al (2011) Characterization of chemokines and adhesion molecules associated with T cell presence in tertiary lymphoid structures in human lung cancer. Cancer Res 71(20):6391–6399. https://doi.org/10.1158/0008-5472.CAN-11-0952
128. Weinstein AM, Chen L, Brzana EA et al (2017) Tbet and IL-36gamma cooperate in therapeutic DC-mediated promotion of ectopic lymphoid organogenesis in the tumor microenvironment. Oncoimmunology 6(6):e1322238. https://doi.org/10.1080/2162402X.2017.1322238
129. Hiraoka N, Ino Y, Yamazaki-Itoh R et al (2015) Intratumoral tertiary lymphoid organ is a favourable prognosticator in patients with pancreatic cancer. Br J Cancer 112(11):1782–1790. https://doi.org/10.1038/bjc.2015.145
130. Joshi NS, Akama-Garren EH, Lu Y et al (2015) Regulatory T cells in tumor-associated tertiary lymphoid structures suppress anti-tumor T cell responses. Immunity 43(3):579–590. https://doi.org/10.1016/j.immuni.2015.08.006

Chapter 2

Cellular and Vascular Components of Tertiary Lymphoid Structures

Christopher George Mueller, Saba Nayar, David Gardner, and Francesca Barone

Abstract

Inflammatory immune cells recruited at the site of chronic inflammation form structures that resemble secondary lymphoid organs (SLO). These are characterized by segregated areas of prevalent T- or B-cell aggregation, differentiation of high endothelial venules, and local activation of resident stromal cells, including lymphatic endothelial cells. B-cell proliferation and affinity maturation toward locally displayed autoantigens have been demonstrated at these sites, known as tertiary lymphoid structures (TLS). TLS formation during chronic inflammation has been associated with local disease persistence and progression, as well as increased systemic manifestations. While bearing a similar histological structure to SLO, the signals that regulate TLS and SLO formation can diverge and a series of pro-inflammatory cytokines have been ascribed as responsible for TLS formation at different anatomical sites. Moreover, for a long time the structural compartment that regulates TLS homeostasis, including survival and recirculation of leucocytes has been neglected. In this chapter, we summarize the novel data available on TLS formation, structural organization, and the functional and anatomical links connecting TLS and SLOs.

Key words Tertiary lymphoid organ, TNF-α, Lymphotoxin, Lymphatic vessel, Stromal cell, CXCL13, CCL21, Lymphocyte, Sjogren's syndrome

1 Introduction

The ectopic process that results in the close interaction between leukocytes and stromal cells in the context of inflammation results in the formation of anatomical structures defined as ectopic or tertiary lymphoid structures (TLS).

TLS form to satisfy the local requirement for lymphocyte maintenance within an inflamed tissue. As such, these structures develop in organs not previously predisposed to support the independent generation of an immune response, making the process of lympho-neogenesis the progressive acquisition of features able to support basic lymphocyte functions, such as antigen presentation, co-stimulation, survival, affinity maturation, and exit [1]. As such

Marie-Caroline Dieu-Nosjean (ed.), *Tertiary Lymphoid Structures: Methods and Protocols*, Methods in Molecular Biology, vol. 1845, https://doi.org/10.1007/978-1-4939-8709-2_2,

TLS are best defined as the organoid assembly of cells of the adaptive immune system (B and T lymphocytes and by dendritic cells) in nonimmune tissue; they comprise one or more B-cell follicles that may cluster around fibroblastic stromal cells that share features of follicular dendritic cells (FDC) [2]. TLS are also characterized by T cells that, along with interdigitating mature dendritic cells (DCs), are placed around fibroblastic reticular cells (FRCs) [3]. High endothelial venules (HEVs), flat vessels, and lymphatic vessels (LVs) can also be found within TLS, but fail to acquire the complex organization of SLOs [4, 5].

2 Molecular Cues Regulating TLS Assembly, the TNFRS

It is now clear that the process of ectopic TLS formation does not fully recapitulate the embryological development of SLOs and while the same molecules might be expressed at some stage during TLS establishment the sequence of events that regulate SLO formation may not be quite the same in TLS [1].

The tumor necrosis factor superfamily (TNFSF) members TNFα, lymphotoxin (LT) α and β, and their signaling receptors TNFRI/II and LTβR were suspected to promote the formation of TLS when their critical role in SLO development emerged. Seminal work by Dr. Ruddle and her group showed that ectopic expression of TNFα or LTα, but not LTβ, under the control of rat insulin promoter led to the formation of TLS [6, 7]. Stronger effects in mesenchyme maturation and leucocyte recruitment were observed when LTα and LTβ were co-expressed, resulting in an invasive leukocyte accumulation of the pancreatic islets and significantly larger TLS than in LTα transgenic mice [7]. Differentiation of specialized vascular structures with high endothelium and expression of peripheral node addressin (PNAd), ligand for L-selectin, were also observed in this model providing the molecular mechanisms for naïve T-cell and B-cell recruitment at these sites [7]. Of the two TNFRs, the TNFRI, the principal mediator of lymphoid tissue organogenesis and germinal center reaction [8], plays the major role in mediating LTα-induced pancreatic TLS [9]. Investigators have more recently demonstrated that LTα expression in tumor cells leads to the formation of intra-tumoral lymphoid tissue able to sustain an efficient immune response [10].

The inclusion of inducible bronchial-associated lymphoid tissue (iBALT), fat-associated lymphoid clusters (FALC), and nasal-associated lymphoid tissue (NALT) in the TLS category is debated [11]. Similarly to classical TLS, iBALT, tear duct-associated lymphoid tissues, and NALTs appear to develop independently of LTαβ and LTβR [12–15]. However, LT signaling is crucial for the maintenance and organization of these structures; accordingly, iNALT are disrupted in LTα$^{-/-}$ mice [12]. Interestingly, the expan-

sion of the lymphatic network in iBALT appears to be directly dependent on LTβR signaling [16].

While an effect of LTα, alone or with LTβ, appears manifest, the role of TNFα is conflicting. In some inflammatory diseases, including those with TLS, TNFα actually exhibits anti-inflammatory activities [17]. For instance, insulitis in NOD mice and lupus in New Zealand lupus-prone mice are improved after injection of TNFα [18, 19]. Nevertheless, the activation of both LTβR and TNFRI has been implicated in the formation of aortic TLS (ATLS) that form in association with atherosclerotic lesions within the adventitia of apolipoprotein-deficient ($apoE^{-/-}$) mice. Here, interruption of the LTβR signaling has been demonstrated to suppress lymphoid chemokine (CXCL13 and CCL21) expression and to reduce HEV formation, thereby disrupting the anatomical structure and maintenance of the TLS [20, 21]. In NOD mice, pancreatic TLS show local upregulation of LTαβ and LIGHT, an alternative LTβR ligand [22, 23]. Similarly, in a model of TLS formation in the meningeal tissue, LTβ is expressed and important for TLS establishment [24].

LIGHT is an alternative ligand for LTβR and its transgenic overexpression drives TLS formation in animal models of melanoma and fibrosarcoma [10, 25]. In the TLS of NOD mice there was a local upregulation of LTαβ and LIGHT [26]. Pancreatic LIGHT overexpression in NOD mice also exacerbates local inflammation and disease development [27].

3 Cellular Requirements for TLS Establishment, ILC3

SLO development depends on the interaction between hematopoietic lymphoid tissue inducer (LTi) cells and lymphoid tissue organizers (LTo) of mesenchymal origin [28]. Recently, in addition, the importance of LTi cell interaction with RANK-activated lymphatic endothelial cells has been highlighted [29]. LTi cells are the major producer of LTαβ in response to IL-7, TNFα, and RANKL [30] and their attraction into the lymph node (LN) anlagen in sufficient numbers for complete organogenesis is regulated by chemoattractive signaling mediated by CXCL13 and CCL21 [31]. Their assembly is secured by the reciprocal interaction of integrins with MAdCAM-1 and VCAM-1 that are upregulated on the vascular endothelium and the mesenchyme of the anlagen [28].

The requirement for innate lymphoid cell type 3 (ILC3) for TLS formation is debated. ILC3 cells have been suggested to support isolated lymphoid follicle (ILF) formation, via IL-22 production. However, the extent to which the structures can be considered TLS is controversial [11]. Indeed, there is evidence from different animal models that ILCs, including LTi/ILC3 cells, are not essential for the formation of ectopic lymphoid aggregates. In a model of thyroid

CCL21 overexpression, TLS formation occurs in the absence of transcription factor Id2 that is required for LTi/ILC3 cell maturation [11]. IL-17-mediated iBALT formation also appears to be independent on LTi cells [12].

4 Proinflammatory Cells and Cytokines

It is now accepted that in inflammatory conditions, the signals required for TLS establishment and maturation can be provided by a variety of proinflammatory immune cells that reprise the role of LTi cells during SLO formation [13]. B cells and T cells can provide an alternative source of LTαβ when appropriately stimulated, and a similar role can be played by dendritic cells, both in terms of TLS formation and maintenance [1, 11]. Myeloid $CD68^+$ cells have also been demonstrated to be able to produce lymphoid chemokines such as CXCL13 or CXCL12 [32].

Intriguingly, the signals delivered by these inflammatory cells exceed the classical lymphotoxin/TNFR activation pathway. For instance, the ubiquitous transgenic co-expression of IL-6 and IL-6R leads to perivascular accumulation of lymphocytes with a substantial proportion of B cells and mature plasma B cells [33]. Additionally, overexpression of IL-5 in the respiratory epithelium also results in the development of organized iBALT. However, unlike the models of homeostatic chemokines or TNF-family ligands mentioned above, which do not necessarily develop associated pathology despite TLS formation, the IL-5-dependent induction of iBALT leads to epithelial hypertrophy, goblet cell hyperplasia, accumulation of eosinophils in the airway lumen and peribronchial areas, and focal collagen deposition, which are all signs of severe lung pathology [34].

IL-17 has emerged as an important mediator or iBALT induced by lipopolysaccharides [12]. IL-17 elicits inflammatory and homeostatic chemokine production in the absence of LTα and LTβ, including the aberrant production of CXCL12 [35]. Using a T-cell transgenic animal model of experimental autoimmune encephalomyelitis (EAE) that mimics multiple sclerosis, Peters and colleagues demonstrated that T cells expressing IL-17 can support the formation of ectopic lymphoid tissues in the central nervous system (CNS) [36]. BALTs induced by *Mycobacterium tuberculosis* are also dependent on IL-17 [37].

Studies of human SS have detected IL-22 mRNA in the affected salivary glands [38] and serum levels of IL-22 have been shown to correlate with clinical manifestations of the disease, including hypergammaglobulinemia and autoantibody production [39]. In a mouse model of viral induced SS, inhibition of IL-22 but not of IL-17 has been shown to strongly reduce TLS size [40].

5 Lymphoid Chemokines and Survival Factors

Ectopic lympho-neogenesis has been typically associated with the aberrant expression of lymphoid chemokines, classically implicated in the compartmentalization of adult SLO. CXCL13 is expressed by fibroblastic stromal cells in SLO. It is required for the embryonic migration of LTi cells in the anlagen and, in postnatal life, for the compartmentalization of the lymphocytes in the follicles. Overexpression of CXCL13 under the rat insulin promoter (RIP) in the pancreas and kidneys [41] leads to TLS characterized by segregated B/T-cell zones, presence of conventional DCs, and a dense network of stromal cells and HEV-type blood vessels (Fig. 1) [42]. Similarly, increased expression of CXCL13 and B-cell infiltration has been observed in the central nervous tissue of mice in experimental autoimmune encephalomyelitis (EAE) [43] and, among other chemokines (notably CXCL10), CXCL13 has been found in the spontaneous mouse model of autoimmune gastritis [44].

The expression of several other chemokines has been described in TLS. For instance, spontaneous TLS formation in the pancreas of diabetic NOD mice is associated with local upregulation of CXCL13, CXCL12, and CCL19 concomitant with FDC formation and B-cell activation [26]. ATLS that form in the aortic adventitia display expression of CXCL13 and CCL21 [20].

CXCL12 (or stromal cell-derived factor 1, SDF1) is critical in bone marrow hematopoiesis and B-cell development, where it is expressed by bone marrow stromal cells [45]. CXCL12 is displayed by HEVs in SLO and acts as an important B-cell recruiting factor [46]. RIP-CXCL12 transgenic mice present small infiltrates comprising few T cells but enriched in DCs, B cells, and plasma cells [47]. Significant upregulation of CXCL12 is observed in TLS associated with lymphoma development in the salivary glands of patients with Sjögren's syndrome [32].

CCL19 and CCL21, expressed by endothelial cells and some stromal cells, are ligands for CCR7 carried by T cells, dendritic cells, and LTi cells. CCL21 is more effective than CCL19 in forming ectopic lymphoid structures [47, 48]; however they lack B-cell follicles [47]. Ectopic expression of CCL21 in the thyroid gland was sufficient to induce TLS formation that resembled the structures seen in Hashimoto's thyroiditis and Graves' disease [49] and both chemokines were detected in RA and SS [5, 50].

In human pathology, CXCL13, CCL21, and CXCL12 were found in Sjögren's syndrome tissue [32, 51, 52], Hashimoto's thyroiditis [53], rheumatoid arthritis [5], and non-small cell lung cancer (NSCLC) [54]. While different patterns of lymphoid arrangements usually coexist, inflamed tissues harboring highly organized TLS tend to express significantly higher levels of LTα, CXCL13, and CCL21 than those with diffuse lymphoid infiltrates

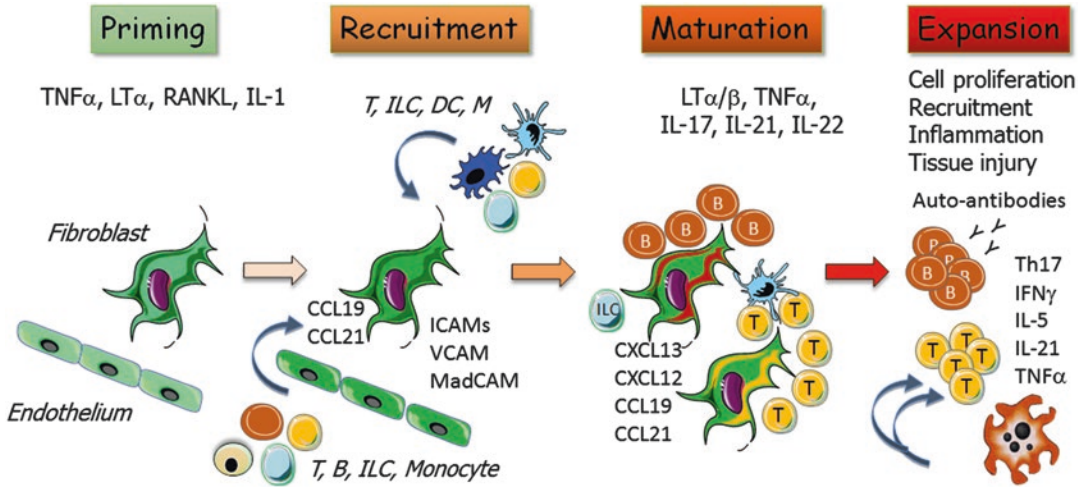

Fig. 1 Four-stage process of TLS formation. Inflammatory cytokines prime endothelium, tissue-resident fibroblasts, or possibly other structural cells (i.e. pericytes, epithelial cells) to express chemokines and adhesion molecules leading to the recruitment of circulatory or tissue-resident hematopoietic cells. Adhesion molecules subsequently anchor the cells to fibroblasts and/or endothelial cells. During the maturation phase, cytokines such as lymphotoxin and TNF-α foster fibroblast differentiation into lymphoid tissue organizers that more specifically and more efficiently cluster B cells and T cells. Innate lymphoid cells (ILCs) are thought to play an important role by the production of lymphotoxin α and β, but possibly also through Th-17. Similar to SLOs, these structures support B- and T-cell activation leading to TLS expansion through cell proliferation and recruitment. These chronic inflammatory lymphoid structures can then cause severe immunopathology

[5, 50, 55–57]. In fact, the expression levels of CXCL13 and LTβ may be highly predictive of the presence of ectopic germinal centers in synovial biopsies of patients with RA and SS [5, 50, 55–58].

One of the primary functions of TLS is to support the survival of incoming lymphocytes. Accordingly, ectopic expression of B- and T-cell survival factors has been found in TLS. B-cell-activating factor (BAFF) regulates B-cell survival and has been found to be overproduced in meninges-associated ectopic GC formation in a mouse model of CNS inflammation [43]. Similarly, LTα-dependent IL-7 overexpression leads to ectopic lymphoid structures in different nonlymphoid tissues [59] and has been attributed to increased local survival of lymphocytes and disease persistence.

6 Non-hematopoietic Compartments of TLS

6.1 Mesenchymal Cells

The organizational program that regulates the maturation of the embryonic LTo into adult lymph nodes is tightly regulated and gives rise, in postembryonic life, to a distinct and well-organized anatomical structure. This organization is maintained by mature fibroblastic reticular cells (FRCs) in the T-cell zone, marginal reticular cells (MRCs) of the marginal zone, and FDCs of the B-cell follicle. Together, these stromal cell populations regulate organ compart-

mentalization, cell mobility, and distribution of cells and small molecules [60]. The modification of local stromal cells into functional lymphoid tissue fibroblasts together with the mostly segregated expression of lymphoid chemokines (CCL19, CCL21, CXCL12, and CXCL13) and survival factors (IL-7, BAFF, and APRIL) define most TLS [11].

Once fully matured, TLS can display a specialized network of FDCs capable of driving a functional GC response and differentiation of HEVs [61]. FDCs predominantly form in aggregates where B-cell follicles and/or a germinal center are observed [62]. FRCs, commonly characterized by the expression of gp38 and the production of CCL21, are generally found within the T-cell area of the TLS in primary biliary cirrhosis, RA, and other conditions [3, 11, 50, 63, 64].

Different expression of chemokines and stromal cell markers has been reported in diverse TLS models [35, 40, 65–67], suggesting that the production of different chemokines can be elicited in response to diverse stimuli dependent on the locations.

Although epithelial cells can transform into mesenchymal cells, there is so far little evidence of this occurring during TLS formation. In a model of skin inflammation (not characterized by full TLS maturation), stromal cells are derived from local fibroblasts but not from keratinocytes [66]. Epithelial cells appear involved in SS, where CXCL12 is expressed by the salivary duct epithelium and CXCL13 in acini and ducts [32, 68].

6.2 Vascular System

Conceptually, TLS develop when the forces that recruit and retain leukocytes exceed those that expel them from the tissue. This results either through an overactive recruitment *via* blood endothelial cells or as a consequence of a diminished lymphatic endothelial cell-regulated cell output. Nonetheless, lymphedema is unlikely to be sufficient to create TLS when the retaining force is underdeveloped [61]. Therefore, a coordinated interplay between entry-retention-exit is probably required for TLS formation. Moreover, lymphocyte retention within the tissue rarely achieves the level of organization sufficient to form a TLS, thus suggesting that an active process of recruitment and organization is required for TLS formation [11].

Nonetheless, the activation of the resident vascular structures, that includes upregulation of homing molecules to enable lymphocyte recruitment, appears to be a prerequisite of TLS assembly. Blood endothelial vessels undergo remodeling during inflammation signaling for the entry of blood-derived hematopoietic cells through expression of integrins, addressins, and chemokines in response to LTαβ signals [47]. Endothelial cells and fibroblasts express cell adhesion factors such as mucosal vascular addressin cell adhesion molecule-1 (MAdCAM-1), vascular addressin cell adhesion molecule-1 (VCAM-1), or intercellular adhesion molecule-1 (ICAM-1). This active expression of adhesion molecules is accom-

panied by the loss of vascular integrity, which results in exposure of the sub-endothelium matrix and efflux of plasma from the intravascular space [69]. This newly formed extravascular matrix supports leukocyte extravasation [70, 71]. The process of angiogenesis in TLS is supported by local release of VEGFα, angiopoietin, PDGF, IL-1, TNFα, and CXCL8, some of which are expressed by fibroblasts under inflammatory conditions [11]. Ectopic expression of proinflammatory chemokines such as CXCL8/IL-8 and CCL2/MCP-1 support the chemotactic gradient necessary for influx of various inflammatory cells into peripheral tissue [72]. Blood endothelial cells are also involved in leukocyte activation by expressing MHC class II molecules [73] and co-stimulatory molecules including OX40L, ICOSL, and CD25 [74].

Within TLS, blood endothelial cells undergo a complex process of conversion of flat venular endothelial cells into tall and plump endothelial cells that closely resemble the HEVs present in the T-cell areas of the lymph nodes. TLS-associated HEVs are characterized by expression of the lymph node trafficking code, peripheral node addressin (PNAd) which recognizes and binds L-selectin (also named CD62L), expressed on naïve/central memory T lymphocytes and mature dendritic cells. This is responsible, together with the ectopic expression of CCL21, ligand for CCR7, for the homing of naïve and central memory T cells within those structures [4, 5, 75]. HEV differentiation and in particular PNAd expression are regulated by lymphotoxin [76–78].

6.3 Lymphatic Vessels

Under homeostatic conditions lymphatic vessels drain and transport extracellular fluid and macromolecules into the systemic circulation. While blood endothelial vessels mainly deliver cells to inflamed tissues, the lymphatic bed is responsible for the transport of tissue-derived cells (i.e. DCs, T cells) and antigens toward the draining lymph node. LVs also regulate interstitial fluid drainage preventing excessive swelling of the inflamed organ. LVs undergo dramatic remodeling during inflammation to support the increased need for tissue exit of cellular material [79]. Lymphangiogenesis in embryonic life is tightly regulated, so that LV development is intimately connected with the process of lympho-neogenesis. LVs sprout out from the cardinal vein, in a process that is orchestrated by the homeobox genes Prox1 and Sox18, the growth factor VEGF-C, and its receptor VEGFR3. However, a non-venous origin of lymphatic vasculature has been also demonstrated [80]. Recent studies have shown that lymphatic vessel formation also requires interaction between lymphatic vessels and platelet-derived Clec-2 for separation of lymphatic vessels from the blood endothelial vessels [81, 82].

Within immunized lymph nodes, a significant expansion of the lymphatic vessels occurs that coincides with an increased influx of immune cells, thereby maximizing the potential for interaction between different cell types and enabling an effective immune response to occur.

This process is very tightly regulated by LTβR signaling and remodels the LN in a manner that allows an effective balance between the input and output of the cells. This in turn helps in the recovery of the LN to homeostatic conditions [83]. The expansion of LV endothelial cells not only supports the need for cellular interaction but may also play an important role in immunological function, as lymphatic endothelial cells express peripheral tissue antigens (PTA) under the control of AIRE for presentation to T cells as well as immunoregulatory factors that are able to modulate the local immune responses [84].

LVs also undergo remodeling in peripheral tissue during inflammatory conditions, whereby the activation of NF-κB pathway can stimulate the expression of Prox1 and increase the transcripts for the VEGFR3 [85, 86]. Neo-lymphoangiogenesis in TLS is also supported by the expression of LT, IL-1, and TNFα [87–91]. Immune cell migration into the developing LVs has been suggested, alongside proliferation of existing endothelial progenitors [92–94].

Interestingly TLS, that lack differentiated marginal reticular cells and a proper capsule, are devoid of a subcapsular sinus, contributing to the anatomical disorganization of the vascular system in TLS. However, LVs are present in TLS and to a certain extent localized mainly in the outer follicular area. While there is no evidence that an organized lymphatic afferent system exists in TLS, the presence of efferent lymphatics draining antigens and activated immune cells to the draining lymph nodes has been demonstrated [95]. Similar to the SLO, LVs in inflamed tissue act in an immune-regulatory role, upregulating the expression of D6/CCBP2, a decoy receptor capable of reducing the inflammatory response by scavenging inflammatory CC chemokines [96] and suppressing dendritic cell maturation [97]. There is no evidence that this function is not maintained in TLS. Lymphangiogenesis in TLS is believed to represent a productive attempt to resolve inflammation; however, it is not clear whether the newly formed LVs are able to establish viable connection with preexisting lymphatic vessels, which would hamper the drainage of activated dendritic cells, macrophages, and locally displayed antigens to the draining LN [98–103] (Bugatti et al., EULAR Communication, 2011). It is also unclear to what extent the newly formed lymphatic vessels contribute to the chemokine gradient established in the TLS and whether or not the ectopic expression of CCL21 on LVs can be considered a positive factor for the functional development of TLS [99, 100]. Of interest is the finding that RANK activation of LVs plays a critical factor in SLO formation [29]. While the underlying mechanisms are still unclear, the finding that lymphatic and blood endothelial cells express cell adhesion molecules upon RANK stimulation [104] suggests that the endothelial cells function as a first retention signal to LTi cells. Indeed, pharmacological blocking lymphocyte exit by acting on lymphatic sphingosine-1-phosphate (S1P) receptors lead to an additional LN in about half of the animals [29].

Nayar et al. demonstrated that expansion of the lymphatic bed within TLS follows a bimodal course, with a first phase of expansion induced by IL-7 and the second phase that coincides with the peak of organization of the TLS, being mediated by LTβR signaling [95]. While we could not identify a direct effect of LTβR in lymphatic cell proliferation, others have recently showed that LT might act as a proliferative factor for LV endothelial cells *via* NF-κB activation [105]. Other proinflammatory cytokines have been implicated in this process, some with positive and some with detrimental effects on lymphangiogenesis. Interestingly, blocking some of these cytokines has been sought after as a therapeutic intervention in inflammation, leaving open the possibility that counteracting the inflammatory cascade might hamper the same innate attempt to its resolution [95].

7 Conclusions

TLS assembly is a complex phenomenon and can be regulated at different sites by diverse cytokines and cellular requirements. While the pathogenic *versus* tolerogenic role of those structures is still debated [106, 107], in chronic autoimmune disease TLS persistence is considered a negative predictive factor for disease progression [2, 32]. Recent advances in the understanding of SLO biology and the development of novel tools to dissect leukocytes/stromal cell interaction provided critical insights into TLS assembly and regulation [12, 108]. This will translate to the development of compounds able to interfere with TLS structure and persistence in the tissue, thus decreasing local autoimmunity and risks associated with ectopic lymphocytic expansion.

Acknowledgments

F.B. is an ARUK Senior Fellow and is part of the NIHR Birmingham Biomedical Research Centre.

References

1. Barone F, Gardner DH, Nayar S et al (2016) Stromal fibroblasts in tertiary lymphoid structures: a novel target in chronic inflammation. Front Immunol 7:477
2. Aloisi F, Pujol-Borrell R (2006) Lymphoid neogenesis in chronic inflammatory diseases. Nat Rev Immunol 6:205–217
3. Link A, Hardie DL, Favre S et al (2011) Association of T-zone reticular networks and conduits with ectopic lymphoid tissues in mice and humans. Am J Pathol 178:1662–1675
4. Barone F, Bombardieri M, Manzo A et al (2005) Association of CXCL13 and CCL21 expression with the progressive organization of lymphoid-like structures in Sjogren's syndrome. Arthritis Rheum 52:1773–1784
5. Manzo A, Paoletti S, Carulli M et al (2005) Systematic microanatomical analysis of CXCL13 and CCL21in situ production and progressive lymphoid organization in rheumatoid synovitis. Eur J Immunol 35:1347–1359
6. Kratz A, Campos-Neto A, Hanson MS, Ruddle NH (1996) Chronic inflammation

caused by lymphotoxin is lymphoid neogenesis. J Exp Med 183:1461–1472
7. Drayton DL, Ying X, Lee J et al (2003) Ectopic LT directs lymphoid organ neogenesis with concomitant expression of peripheral node addressin and a HEV-restricted sulfotransferase. J Exp Med 197:1153–1163
8. Matsumoto M, Mariathasan S, Nahm MH et al (1996) Role of lymphotoxin and the type I TNF receptor in the formation of germinal centers. Science 271:1289–1291
9. Sacca R, Kratz A, Campos-Neto A et al (1995) Lymphotoxin: from chronic inflammation to lymphoid organs. J Inflamm 47:81–84
10. Schrama D, thor Straten P, Fischer WH et al (2001) Targeting of lymphotoxin-alpha to the tumor elicits an efficient immune response associated with induction of peripheral lymphoid-like tissue. Immunity 14:111–121
11. Buckley CD, Barone F, Nayar S et al (2015) Stromal cells in chronic inflammation and tertiary lymphoid organ formation. Annu Rev Immunol 33:715–745
12. Rangel-Moreno J, Carragher DM, de la Luz Garcia-Hernandez M et al (2011) The development of inducible bronchus-associated lymphoid tissue depends on IL-17. Nat Immunol 12:639–646
13. Nagatake T, Fukuyama S, Kim DY et al (2009) Id2-, RORgammat-, and LTbetaR-independent initiation of lymphoid organogenesis in ocular immunity. J Exp Med 206:2351–2364
14. Harmsen A, Kusser K, Hartson L et al (2002) Cutting edge: organogenesis of nasal-associated lymphoid tissue (NALT) occurs independently of lymphotoxin-alpha (LT alpha) and retinoic acid receptor-related orphan receptor-gamma, but the organization of NALT is LT alpha dependent. J Immunol 168:986–990
15. Fukuyama S, Hiroi T, Yokota Y et al (2002) Initiation of NALT organogenesis is independent of the IL-7R, LTbetaR, and NIK signaling pathways but requires the Id2 gene and CD3(−)CD4(+)CD45(+) cells. Immunity 17:31–40
16. Furtado GC, Marinkovic T, Martin AP et al (2007) Lymphotoxin beta receptor signaling is required for inflammatory lymphangiogenesis in the thyroid. Proc Natl Acad Sci U S A 104:5026–5031
17. Kollias G (2005) TNF pathophysiology in murine models of chronic inflammation and autoimmunity. Semin Arthritis Rheum 34:3–6
18. Jacob CO, Aiso S, Michie SA et al (1990) Prevention of diabetes in nonobese diabetic mice by tumor necrosis factor (TNF): similarities between TNF-alpha and interleukin 1. Proc Natl Acad Sci U S A 87:968–972
19. Ernandez T, Mayadas TN (2009) Immunoregulatory role of TNFalpha in inflammatory kidney diseases. Kidney Int 76:262–276
20. Grabner R, Lotzer K, Dopping S et al (2009) Lymphotoxin beta receptor signaling promotes tertiary lymphoid organogenesis in the aorta adventitia of aged ApoE$^{-/-}$ mice. J Exp Med 206:233–248
21. Lotzer K, Dopping S, Connert S et al (2010) Mouse aorta smooth muscle cells differentiate into lymphoid tissue organizer-like cells on combined tumor necrosis factor receptor-1/lymphotoxin beta-receptor NF-kappaB signaling. Arterioscler Thromb Vasc Biol 30:395–402
22. Fletcher D, Triantafyllou A (2007) Mast cells in the salivary glands and tongue of the ferret: demonstration and some histochemical observations. Anat Histol Embryol 36:38–42
23. Gommerman JL, Browning JL (2003) Lymphotoxin/light, lymphoid microenvironments and autoimmune disease. Nat Rev Immunol 3:642–655
24. Pikor NB, Astarita JL, Summers-Deluca L et al (2015) Integration of Th17- and lymphotoxin-derived signals initiates meningeal-resident stromal cell remodeling to propagate neuroinflammation. Immunity 43:1160–1173
25. Yu P, Lee Y, Liu W et al (2004) Priming of naive T cells inside tumors leads to eradication of established tumors. Nat Immunol 5:141–149
26. Astorri E, Bombardieri M, Gabba S et al (2010) Evolution of ectopic lymphoid neogenesis and in situ autoantibody production in autoimmune nonobese diabetic mice: cellular and molecular characterization of tertiary lymphoid structures in pancreatic islets. J Immunol 185:3359–3368
27. Lee Y, Chin RK, Christiansen P et al (2006) Recruitment and activation of naive T cells in the islets by lymphotoxin beta receptor-dependent tertiary lymphoid structure. Immunity 25:499–509
28. Mebius RE (2003) Organogenesis of lymphoid tissues. Nat Rev Immunol 3:292–303
29. Onder L, Morbe U, Pikor N et al (2017) Lymphatic endothelial cells control initiation of lymph node organogenesis. Immunity 47:80–92.e4
30. Yoshida H, Naito A, Inoue J et al (2002) Different cytokines induce surface lymphotoxin-alphabeta on IL-7 receptor-alpha cells that differentially engender lymph

nodes and Peyer's patches. Immunity 17:823–833
31. van de Pavert SA, Mebius RE (2014) Development of secondary lymphoid organs in relation to lymphatic vasculature. Adv Anat Embryol Cell Biol 214:81–91
32. Barone F, Bombardieri M, Rosado MM et al (2008) CXCL13, CCL21, and CXCL12 expression in salivary glands of patients with Sjogren's syndrome and MALT lymphoma: association with reactive and malignant areas of lymphoid organization. J Immunol 180:5130–5140
33. Goya S, Matsuoka H, Mori M et al (2003) Sustained interleukin-6 signalling leads to the development of lymphoid organ-like structures in the lung. J Pathol 200:82–87
34. Lee JJ, McGarry MP, Farmer SC et al (1997) Interleukin-5 expression in the lung epithelium of transgenic mice leads to pulmonary changes pathognomonic of asthma. J Exp Med 185:2143–2156
35. Fleige H, Ravens S, Moschovakis GL et al (2014) IL-17-induced CXCL12 recruits B cells and induces follicle formation in BALT in the absence of differentiated FDCs. J Exp Med 211:643–651
36. Peters A, Pitcher LA, Sullivan JM et al (2011) Th17 cells induce ectopic lymphoid follicles in central nervous system tissue inflammation. Immunity 35:986–996
37. Khader SA, Guglani L, Rangel-Moreno J et al (2011) IL-23 is required for long-term control of Mycobacterium tuberculosis and B cell follicle formation in the infected lung. J Immunol 187:5402–5407
38. Ciccia F, Accardo-Palumbo A, Alessandro R et al (2012) Interleukin-22 and interleukin-22-producing NKp44+ natural killer cells in subclinical gut inflammation in ankylosing spondylitis. Arthritis Rheum 64:1869–1878
39. Lavoie TN, Stewart CM, Berg KM et al (2011) Expression of interleukin-22 in Sjogren's syndrome: significant correlation with disease parameters. Scand J Immunol 74:377–382
40. Barone F, Nayar S, Campos J et al (2015) IL-22 regulates lymphoid chemokine production and assembly of tertiary lymphoid organs. Proc Natl Acad Sci U S A 112:11024–11029
41. Drayton DL, Liao S, Mounzer RH, Ruddle NH (2006) Lymphoid organ development: from ontogeny to neogenesis. Nat Immunol 7:344–353
42. Luther SA, Lopez T, Bai W et al (2000) BLC expression in pancreatic islets causes B cell recruitment and lymphotoxin-dependent lymphoid neogenesis. Immunity 12:471–481
43. Magliozzi R, Columba-Cabezas S, Serafini B, Aloisi F (2004) Intracerebral expression of CXCL13 and BAFF is accompanied by formation of lymphoid follicle-like structures in the meninges of mice with relapsing experimental autoimmune encephalomyelitis. J Neuroimmunol 148:11–23
44. Katakai T, Hara T, Sugai M et al (2003) Th1-biased tertiary lymphoid tissue supported by CXC chemokine ligand 13-producing stromal network in chronic lesions of autoimmune gastritis. J Immunol 171:4359–4368
45. Greenbaum A, Hsu YM, Day RB et al (2013) CXCL12 in early mesenchymal progenitors is required for haematopoietic stem-cell maintenance. Nature 495:227–230
46. Okada T, Ngo VN, Ekland EH et al (2002) Chemokine requirements for B cell entry to lymph nodes and Peyer's patches. J Exp Med 196:65–75
47. Luther SA, Bidgol A, Hargreaves DC et al (2002) Differing activities of homeostatic chemokines CCL19, CCL21, and CXCL12 in lymphocyte and dendritic cell recruitment and lymphoid neogenesis. J Immunol 169:424–433
48. Chen SC, Vassileva G, Kinsley D et al (2002) Ectopic expression of the murine chemokines CCL21a and CCL21b induces the formation of lymph node-like structures in pancreas, but not skin, of transgenic mice. J Immunol 168:1001–1008
49. Marinkovic T (2006) Interaction of mature CD3+CD4+ T cells with dendritic cells triggers the development of tertiary lymphoid structures in the thyroid. J Clin Investig 116:2622–2632
50. Manzo A, Bugatti S, Caporali R et al (2007) CCL21 expression pattern of human secondary lymphoid organ stroma is conserved in inflammatory lesions with lymphoid neogenesis. Am J Pathol 171:1549–1562
51. Salomonsson S, Dorner T, Theander E et al (2002) A serologic marker for fetal risk of congenital heart block. Arthritis Rheum 46:1233–1241
52. Amft N, Bowman SJ (2001) Chemokines and cell trafficking in Sjogren's syndrome. Scand J Immunol 54:62–69
53. Aust G, Sittig D, Becherer L et al (2004) The role of CXCR5 and its ligand CXCL13 in the compartmentalization of lymphocytes in thyroids affected by autoimmune thyroid diseases. Eur J Endocrinol 150:225–234
54. de Chaisemartin L, Goc J, Damotte D et al (2011) Characterization of chemokines and adhesion molecules associated with T cell presence in tertiary lymphoid structures in

human lung cancer. Cancer Res 71:6391–6399
55. Takemura S, Braun A, Crowson C et al (2001) Lymphoid neogenesis in rheumatoid synovitis. J Immunol 167:1072–1080
56. Bugatti S, Manzo A, Bombardieri M et al (2011) Synovial tissue heterogeneity and peripheral blood biomarkers. Curr Rheumatol Rep 13:440–448
57. Humby F, Bombardieri M, Manzo A et al (2009) Ectopic lymphoid structures support ongoing production of class-switched autoantibodies in rheumatoid synovium. PLoS Med 6:e1
58. Weyand CM, Goronzy JJ (2003) Ectopic germinal center formation in rheumatoid synovitis. Ann N Y Acad Sci 987:140–149
59. Meier D, Bornmann C, Chappaz S et al (2007) Ectopic lymphoid-organ development occurs through interleukin 7-mediated enhanced survival of lymphoid-tissue-inducer cells. Immunity 26:643–654
60. Roozendaal R, Mebius RE (2011) Stromal cell-immune cell interactions. Annu Rev Immunol 29:23–43
61. Ruddle NH (2014) Lymphatic vessels and tertiary lymphoid organs. J Clin Invest 124:953–959
62. Bombardieri M, Barone F, Humby F et al (2007) Activation-induced cytidine deaminase expression in follicular dendritic cell networks and interfollicular large B cells supports functionality of ectopic lymphoid neogenesis in autoimmune sialoadenitis and MALT lymphoma in Sjogren's syndrome. J Immunol 179:4929–4938
63. Drumea-Mirancea M, Wessels JT, Muller CA et al (2006) Characterization of a conduit system containing laminin-5 in the human thymus: a potential transport system for small molecules. J Cell Sci 119:1396–1405
64. Pitzalis C, Jones GW, Bombardieri M, Jones SA (2014) Ectopic lymphoid-like structures in infection, cancer and autoimmunity. Nat Rev Immunol 14:447–462
65. Krautler NJ, Kana V, Kranich J et al (2012) Follicular dendritic cells emerge from ubiquitous perivascular precursors. Cell 150:194–206
66. Peduto L, Dulauroy S, Lochner M et al (2009) Inflammation recapitulates the ontogeny of lymphoid stromal cells. J Immunol 182:5789–5799
67. Dutertre CA, Clement M, Morvan M et al (2014) Deciphering the stromal and hematopoietic cell network of the adventitia from non-aneurysmal and aneurysmal human aorta. PLoS One 9:e89983
68. Salomonsson S, Larsson P, Tengner P et al (2002) Expression of the B cell-attracting chemokine CXCL13 in the target organ and autoantibody production in ectopic lymphoid tissue in the chronic inflammatory disease Sjogren's syndrome. Scand J Immunol 55:336–342
69. Pober JS, Sessa WC (2007) Evolving functions of endothelial cells in inflammation. Nat Rev Immunol 7:803–815
70. Clark PR, Manes TD, Pober JS, Kluger MS (2007) Increased ICAM-1 expression causes endothelial cell leakiness, cytoskeletal reorganization and junctional alterations. J Invest Dermatol 127:762–774
71. Adams DH, Shaw S (1994) Leucocyte-endothelial interactions and regulation of leucocyte migration. Lancet 343:831–836
72. Middleton J, Neil S, Wintle J et al (1997) Transcytosis and surface presentation of IL-8 by venular endothelial cells. Cell 91:385–395
73. Pober JS, Orosz CG, Rose ML, Savage CO (1996) Can graft endothelial cells initiate a host anti-graft immune response? Transplantation 61:343–349
74. Shiao SL, McNiff JM, Pober JS (2005) Memory T cells and their costimulators in human allograft injury. J Immunol 175:4886–4896
75. Girard JP, Springer TA (1995) High endothelial venules (HEVs): specialized endothelium for lymphocyte migration. Immunol Today 16:449–457
76. Carragher D, Johal R, Button A et al (2004) A stroma-derived defect in NF-kappaB2$^{-/-}$ mice causes impaired lymph node development and lymphocyte recruitment. J Immunol 173:2271–2279
77. Browning JL, Allaire N, Ngam-Ek A et al (2005) Lymphotoxin-beta receptor signaling is required for the homeostatic control of HEV differentiation and function. Immunity 23:539–550
78. Onder L, Danuser R, Scandella E et al (2013) Endothelial cell-specific lymphotoxin-beta receptor signaling is critical for lymph node and high endothelial venule formation. J Exp Med 210:465–473
79. Huggenberger R, Siddiqui SS, Brander D et al (2011) An important role of lymphatic vessel activation in limiting acute inflammation. Blood 117:4667–4678
80. Martinez-Corral I, Ulvmar MH, Stanczuk L et al (2015) Nonvenous origin of dermal lymphatic vasculature. Circ Res 116:1649–1654
81. Osada M, Inoue O, Ding G et al (2012) Platelet activation receptor CLEC-2 regulates blood/lymphatic vessel separation by inhibiting proliferation, migration, and tube formation of lym-

phatic endothelial cells. J Biol Chem 287:22241–22252
82. Watson SP, Lowe K, Finney BA (2014) Platelets in lymph vessel development and integrity. Adv Anat Embryol Cell Biol 214:93–105
83. Liao S, Ruddle NH (2006) Synchrony of high endothelial venules and lymphatic vessels revealed by immunization. J Immunol 177:3369–3379
84. Fletcher AL, Malhotra D, Turley SJ (2011) Lymph node stroma broaden the peripheral tolerance paradigm. Trends Immunol 32:12–18
85. Alitalo K (2011) The lymphatic vasculature in disease. Nat Med 17:1371–1380
86. Flister MJ, Wilber A, Hall KL et al (2010) Inflammation induces lymphangiogenesis through up-regulation of VEGFR-3 mediated by NF-kappaB and Prox1. Blood 115:418–429
87. Mounzer RH, Svendsen OS, Baluk P et al (2010) Lymphotoxin-alpha contributes to lymphangiogenesis. Blood 116:2173–2182
88. Alitalo K, Tammela T, Petrova TV (2005) Lymphangiogenesis in development and human disease. Nature 438:946–953
89. Kunder CA, St John AL, Abraham SN (2011) Mast cell modulation of the vascular and lymphatic endothelium. Blood 118:5383–5393
90. Cursiefen C, Chen L, Borges LP et al (2004) VEGF-A stimulates lymphangiogenesis and hemangiogenesis in inflammatory neovascularization via macrophage recruitment. J Clin Invest 113:1040–1050
91. Hamrah P, Chen L, Zhang Q, Dana MR (2003) Novel expression of vascular endothelial growth factor receptor (VEGFR)-3 and VEGF-C on corneal dendritic cells. Am J Pathol 163:57–68
92. Lee JY, Park C, Cho YP et al (2010) Podoplanin-expressing cells derived from bone marrow play a crucial role in postnatal lymphatic neovascularization. Circulation 122:1413–1425
93. Kerjaschki D, Huttary N, Raab I et al (2006) Lymphatic endothelial progenitor cells contribute to de novo lymphangiogenesis in human renal transplants. Nat Med 12:230–234
94. Maruyama K, Ii M, Cursiefen C et al (2005) Inflammation-induced lymphangiogenesis in the cornea arises from CD11b-positive macrophages. J Clin Invest 115:2363–2372
95. Nayar S, Campos J, Chung MM et al (2016) Bimodal expansion of the lymphatic vessels is regulated by the sequential expression of IL-7 and lymphotoxin alpha1beta2 in newly formed tertiary lymphoid structures. J Immunol 197:1957–1967
96. Jamieson T, Cook DN, Nibbs RJ et al (2005) The chemokine receptor D6 limits the inflammatory response in vivo. Nat Immunol 6:403–411
97. Podgrabinska S, Kamalu O, Mayer L et al (2009) Inflamed lymphatic endothelium suppresses dendritic cell maturation and function via Mac-1/ICAM-1-dependent mechanism. J Immunol 183:1767–1779
98. Thaunat O, Kerjaschki D, Nicoletti A et al (2006) Is defective lymphatic drainage a trigger for lymphoid neogenesis? Trends Immunol 27:441–445
99. Burman A, Haworth O, Bradfield P et al (2005) The role of leukocyte-stromal interactions in chronic inflammatory joint disease. Joint Bone Spine 72:10–16
100. Kerjaschki D, Regele HM, Moosberger I et al (2004) Lymphatic neoangiogenesis in human kidney transplants is associated with immunologically active lymphocytic infiltrates. J Am Soc Nephrol 15:603–612
101. von der Weid PY, Rehal S, Ferraz JG (2011) Role of the lymphatic system in the pathogenesis of Crohn's disease. Curr Opin Gastroenterol 27:335–341
102. Kajiya K, Detmar M (2006) An important role of lymphatic vessels in the control of UVB-induced edema formation and inflammation. J Invest Dermatol 126:919–921
103. Wilkinson LS, Edwards JC (1991) Demonstration of lymphatics in human synovial tissue. Rheumatol Int 11:151–155
104. Cordeiro OG, Chypre M, Brouard N et al (2016) Integrin-alpha IIb identifies murine lymph node lymphatic endothelial cells responsive to RANKL. PLoS One 11:e0151848
105. Yang CY, Vogt TK, Favre S et al (2014) Trapping of naive lymphocytes triggers rapid growth and remodeling of the fibroblast network in reactive murine lymph nodes. Proc Natl Acad Sci U S A 111:E109–E118
106. Theander E, Vasaitis L, Baecklund E et al (2011) Lymphoid organisation in labial salivary gland biopsies is a possible predictor for the development of malignant lymphoma in primary Sjogren's syndrome. Ann Rheum Dis 70(8):1363
107. Hu D, Mohanta SK, Yin C et al (2015) Artery tertiary lymphoid organs control aorta immunity and protect against atherosclerosis via vascular smooth muscle cell lymphotoxin beta receptors. Immunity 42:1100–1115
108. Barone F, Campos J, Bowman S, Fisher BA (2015) The value of histopathological examination of salivary gland biopsies in diagnosis, prognosis and treatment of Sjogren's syndrome. Swiss Med Wkly 145:w14168

Chapter 3

Meningeal Immunity, Drainage, and Tertiary Lymphoid Structure Formation

Antoine Louveau

Abstract

For decades, the brain has been considered an immune-privileged organ, meaning that the brain was mainly ignored by the immune system and that the presence of immune cells, notably of the adaptive arm, was a hallmark of pathological conditions. Over the past few decades, the definition of the immune privilege continues to be refined. There has been evidence accumulating that shows that the immune system plays a role in proper brain function. This evidence may represent an effective source of therapeutic targets for neurological disorders. In this chapter, we discuss the recent advances in understanding the immunity of the brain and describe how tertiary lymphoid structures can be generated in the central nervous system, which might represent a new avenue to treat neurological disorders.

Key words Tertiary lymphoid structure, Drainage, Meningeal lymphatic vasculature, Glymphatic system, Cervical lymph node

1 Immune Privilege Concept and Immunity of the Central Nervous System

The central nervous system (CNS) is a compartmentalized organ composed of the parenchyma (brain and spinal cord) surrounded by meninges. The meninges are comprised of the pia mater which covers the parenchyma, the arachnoid mater, and the dura mater that is attached to the skull. The subarachnoid space lies between the arachnoid and the pia mater and contains the cerebrospinal fluid (CSF). Both the CSF and the meninges ensure the protection of the parenchyma from endogenous/exogenous threats and provide buoyancy. The CNS is also protected from the entry of pathogens, circulating immune cells, and blood factors by the blood–brain barrier (BBB), which is formed by a unique set of tight junctions expressed by the endothelial cells of the brain along with a lining of astrocyte end-feet.

In the mid-1940s, Sir Peter Medawar proposed the concept of immune privilege to describe tissues in which the introduction of a foreign tissue does not elicit an immune response. Indeed, implan-

Marie-Caroline Dieu-Nosjean (ed.), *Tertiary Lymphoid Structures: Methods and Protocols*, Methods in Molecular Biology, vol. 1845, https://doi.org/10.1007/978-1-4939-8709-2_3,

tation of tumors or fetal tissues into the brain parenchyma leads to their successful growth and maintenance [1–3]. Similarly, transplantation of skin allograft inside of the brain parenchyma only elicited a delayed graft rejection compared to a similar graft in the periphery [4]. These findings suggest that the brain is a tolerogenic organ unable to induce an immune response as efficient as peripheral tissues. Several features of the CNS were proposed to explain this unique feature: (1) the lack of professional antigen-presenting cells in the brain parenchyma, (2) the lack of lymphatic drainage from the brain parenchyma, and (3) the blood–brain barrier. Interestingly, if an immune response against the graft's antigens was induced prior to the transplantation in the parenchyma, the brain's immune response to the allograft is similar to the peripheral organs' response [4]. This suggests that while antigens within the brain fail to prime an efficient immune response, they can maintain and potentiate it. This highlights that immune cells can cross the BBB if activated in the periphery. Furthermore, if the allograft was implanted close to the ventricle or within the subarachnoid spaces, the rejection rate was similar to peripheral graft suggesting that the CSF/meningeal compartments behave differently than the parenchyma and are more in touch with peripheral immunity [5, 6]. Overall these pioneer experiments revealed that the different CNS compartments have a different relationship toward the immune system.

1.1 Brain Parenchyma Versus Meningeal Compartment: Drainage System

One major difference between the brain parenchyma and its surroundings is their drainage capacity. Indeed waste clearance out of the brain relies on the brain interstitial fluid and the CSF [7, 8]. Injection of tracers (blue dextran or horseradish peroxidase) directly into the brain parenchyma resulted in their accumulation in the perivascular spaces of cerebral blood vessels [9, 10]. These observations were confirmed with a large variety of compounds of vastly different molecular weights [11, 12]. Similarly, horseradish peroxidase (HRP), or other compounds injected into the CSF of mammals, appears to use similar perivascular pathways to rapidly enter the brain [12–14]. A system was therefore proposed where the CSF and the interstitial fluid (ISF) would intermix at the level of the perivascular space (the degree of mixture of both fluids remains a matter of debate [15–17]), allowing the removal of molecular waste from the brain parenchyma into the CSF, and consequently might favor the delivery of beneficial CSF constituents and nutrients to deeper structure of the brain parenchyma. The exact mechanism allowing the efflux of CSF into the brain remains a matter of debate between a bulk fluid flow and a simple diffusion mechanism [9, 17–19]. Pioneer work from the laboratory of Maiken Nedergaard has demonstrated that this system is dependent on cerebral arterial pulsation [20], CSF volume, and homeostasis [21]. Sleep states, anesthesia, and postural altera-

tions have been shown to modulate the perivascular draining system [22, 23]. Reports have identified the water-channel AQP4, expressed on the end-feet of astrocyte, as a major regulator of perivascular drainage and driving of the CSF into the brain. This leads to the nomenclature of glial associated lymphatic system or glymphatic system [7, 21, 24]. More recent reports have challenged the role of AQP4 in that system [19]. While immune cells are unlikely to use that system to exit the brain parenchyma [25], perivascular drainage of molecular waste might play a major, and central, role in neurological disorders [15, 17, 26]. In aged mice, and in murine transgenic model of Alzheimer's disease, glymphatic CSF influx is reduced and results in impaired β amyloid (Aβ) clearance [7, 27, 28], suggesting that the glymphatic system might play a major role in the pathology of Alzheimer's disease. Furthermore, glymphatic impairment seems to be a hallmark of multiple neurological disorders, including subarachnoid hemorrhage, multiple microinfarction, and traumatic brain injury [29, 30]. Reduced perivascular clearance of solute also appears to be associated with motor and cognitive deficits [31]. Overall, perivascular drainage represents the system for the brain to remove its waste into the CSF.

Injection of tracer into the CSF leads to its accumulation into the brain parenchyma via perivascular drainage (as described earlier), but also can be seen accumulating in the periphery into the lymph nodes of the neck [32–37]. Similarly, immune cells with migrating properties, mainly T cells and dendritic cells, when injected into the CSF have been shown to migrate into the cervical lymph nodes [38–42]. These observations suggest that, contrary to the brain parenchyma, the meningeal spaces have a direct access to the periphery. The ability of CSF constituents to drain out of the CNS, using both classical and nonclassical paths, which will be described in detail in the next section of this chapter, demonstrates that the CNS is neither excluded nor ignored by the immune system.

1.2 Brain Parenchyma Versus Meningeal Compartment: Immune Cells

Another major discrepancy between the brain and the meningeal compartment is the presence of immune cells. Meningeal endothelial cells present different features than parenchymal and lack astrocytic end-feet, resulting in a more permissive barrier compared to the BBB [43]. While the brain parenchyma is virtually devoid of immune cells (with the exception of the brain-resident macrophages, that is, microglia, but also potentially mast cells [44]), the meningeal compartment is populated by numerous immune cells, even under physiological conditions [45–49]. The meningeal immune compartment appears to be a dynamic compartment [50], participating in brain immune surveillance [45, 47, 51, 52] and ensuring brain function [45, 53]. Indeed, meningeal T cells have notably been implicated in the regulation of cognitive behavior

[45, 53–57], social behavior [54], and adult neurogenesis [56, 57] by way of cytokine secretions. These works illustrate how the immune compartment, residing in the surrounding of the brain, can have a direct impact on its function. All cell types in the brain parenchyma express receptor for cytokines [54, 58–61], including neurons, and can therefore have their function modulated by cytokines released in the CSF [54]. Under pathological conditions, the meningeal immune compartment is also gaining momentum. Longitudinal clinical studies have revealed that in multiple sclerosis patients, inflammatory events can be observed prior to being detected in the brain parenchyma [62, 63]. In experimental autoimmune encephalomyelitis (EAE), the animal model of multiple sclerosis, encephalitogenic T cells have been shown to enter the CNS through the meningeal blood vasculature where they will encounter local macrophages [64]. It appears that the meningeal compartment serves as a key checkpoint for encephalitogenic T cells, where they could supposedly acquire the phenotype that allows them to infiltrate the brain parenchyma. Recently, locally residing NKp46^{+} innate lymphoid cells (ILCs) have been shown to coordinate meningeal inflammation during EAE and facilitate the invasion of the brain parenchyma by encephalitogenic T cells [65]. Moreover, meningeal resident mast cells have also been proposed as a sentinel, controlling the activation and invasion of the brain parenchyma by encephalitogenic T cells [66]. The meningeal immune compartment has started being studied in other pathological conditions. In a stroke model, IL-17-producing T cells have been reported to migrate into the meningeal compartment and influence ischemic neuroinflammation [67]. In animal models of Alzheimer's disease, targeting the meningeal immune system through blockade of PD-1 resulted in an amelioration of disease pathology and clinical symptoms [68], suggesting that the meningeal immune compartment represents a key therapeutic target for neurological disorders.

While the brain parenchyma and the meningeal spaces have different features, they are not isolated from one another and can communicate. Indeed, molecular waste from the brain is removed via perivascular drainage and accumulates in the CSF where it would then drain into the cervical lymph nodes via lymphatic drainage. Molecules, including cytokines produced by the meningeal immune compartment, can directly affect (*via* perivascular drainage) brain function.

2 Meningeal Lymphatic Vasculature and Regulation Of Brain Immunity

2.1 Lymphatic Vasculature in the CNS

As described earlier, injection of tracers or immune cells into the CSF leads to their drainage into the cervical lymph nodes, mostly the deep cervical lymph nodes, but also the superficial cervical

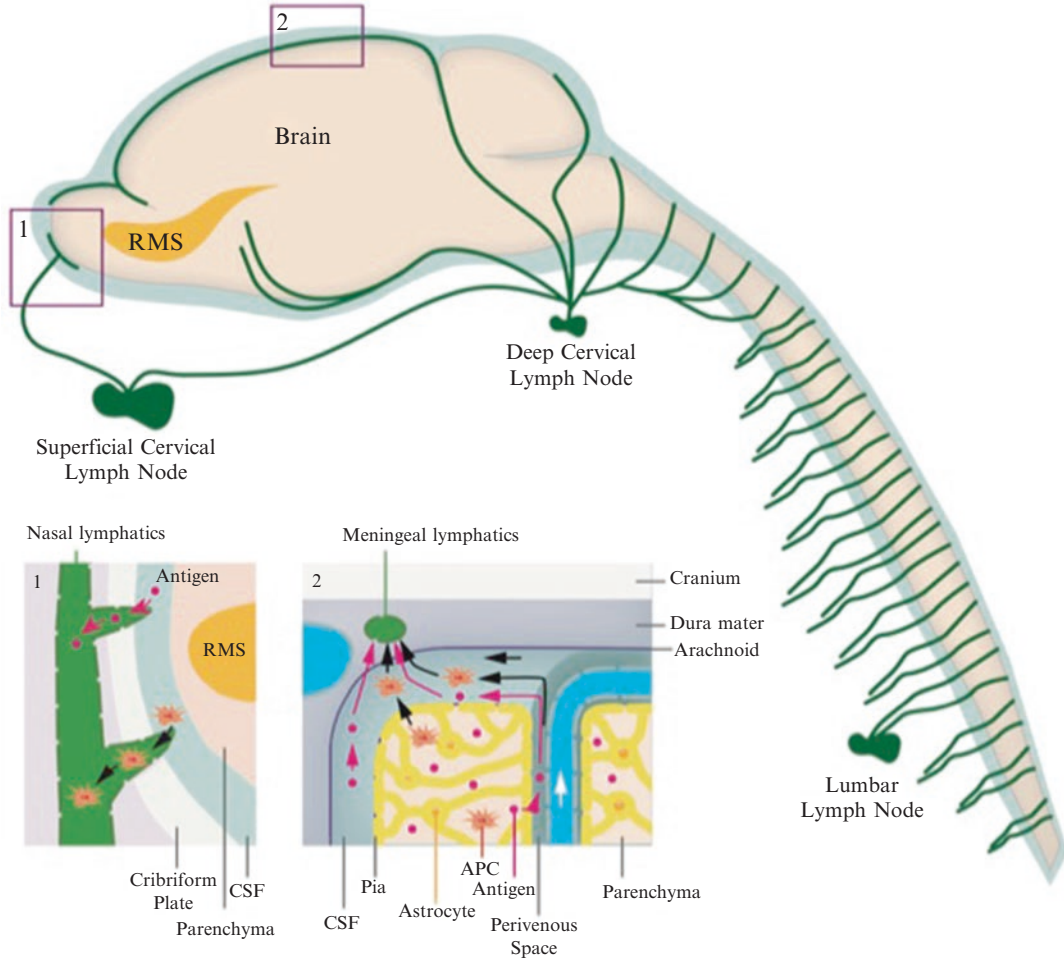

Fig. 1 CNS-lymphatic system drainage. Schematic illustration of the CNS-draining route *via* lymphatic vasculature for antigens and immune cells. Macromolecules and antigen-presenting cells are proposed to exit *via* (1) the lymphatics of the nasal region crossing the cribriform plate or (2) the meningeal lymphatic network. Abbreviations: *APC* Antigen-presenting cell, *CSF* Cerebrospinal fluid, *RMS* Rostral migratory stream

lymph nodes and, in some instances, the lumbar lymph nodes [15, 17] (Fig. 1). In almost all peripheral tissues, drainage of extracellular fluids and immune cells is ensured by the lymphatic system [69]. The lymphatic vasculature is a unique blind-ended, unidirectional absorptive and transport system [70]. Unlike blood vessels, the lymphatic network does not form a closed circulatory network. The presence of lymphatic vessels in the dura mater has been suggested over the years [71–75] and has been recently molecularly and functionally characterized in both rodents [49, 76] and humans [77]. The meningeal lymphatic vasculature, expressing all the hallmark markers of lymphatic endothelial cells [49, 76], runs along the major veins of the meninges, but also along the middle meningeal artery [49, 76]. Furthermore, lymphatic vessels can be

seen in the vicinity of the cribriform plate, and even crossing the cribriform plate [76], a route previously described as a major route for CSF, immune cells, and macromolecules to drain into the peripheral lymph nodes [34, 39, 41, 78, 79]. While most work has focused on the meningeal lymphatic of the brain region, a similar network of lymphatic appears to be present in the meninges covering the spinal cord, enabling drainage into lower back lymph nodes such as the lumbar lymph nodes [36, 80–82].

2.2 Routes of Drainage and Contributions

Over the years, several routes have been proposed for macromolecules and immune cells to drain into the cervical lymph nodes: (1) clearance along perineural sheaths of cranial and spinal nerves, (2) meningeal lymphatic vasculature, and (3) arachnoid granulations. Arachnoid granulations are protrusions of the arachnoid mater into the sinuses of the dura and allow the drainage of water content of the CSF directly into the venous system *via* channels of the arachnoid cap of the granulation. Their roles in the maintenance of CSF homeostasis in human have been extensively described [83–87] but appear to have a more limited role in sheep and rodents [88]. Accordingly, a recent study suggested that CSF drainage out of the CNS is carried predominantly by the lymphatic vasculature in mice [89]. Furthermore, this system appears unlikely to allow the excretion of large macromolecules or immune cells [90]. Tracers, when injected into the CSF, have been observed into the nasal mucous membrane and its associated lymphatics [34, 78, 79] suggesting a direct drainage of the CSF and its constituents through the cribriform plate into the nasal mucosa prior to reaching the cervical lymph nodes. Immune cells have been suggested to use a similar route when injected into the subarachnoid space or into the brain parenchyma [39, 41, 42] (Fig. 1). Similar injections of tracers and immune cells into the CSF, or into the brain parenchyma, lead to their accumulation into the meningeal lymphatic vasculature prior to being observed in the cervical lymph nodes [49, 76]. This suggests that the meningeal vasculature could represent a major route for drainage of CSF constituents (Fig. 1). The exact mechanism is however unknown. Indeed the meningeal lymphatic system is localized in the dura [49, 71, 76, 77], therefore separated from the CSF by the impermeable arachnoid mater. Further works are therefore necessary to understand how the CSF and its constituents can reach the meningeal lymphatic and drain into the cervical lymph nodes.

The contribution of the cribriform plate route *versus* the meningeal lymphatic route in CNS homeostasis and immune surveillance will require more work and the development of a targeted approach. Those routes however seem to play different roles in terms of CSF maintenance. Surgical blockade of the cribriform plate route results in an instantaneous and sustained increase of intracranial pressure in sheep, suggesting that the cribriform plate

route is a major regulator of CSF homeostasis [91]. However, mice born without meningeal lymphatic vessels do not appear to have any defect in intracranial pressure nor brain water content [76]. Because the lack of meningeal lymphatic came from birth, it is possible that compensatory or adaptive mechanisms took place in this model. However, substantiated by the low diameter of the meningeal lymphatic network compared to peripheral tissues, it is plausible that the meningeal lymphatic vasculature is not a major contributor in the regulation of intracranial pressure.

Immune cells, notably T cells and dendritic cells, have been shown to be naturally present in the meningeal lymphatic network [49], suggesting that this system could play a major role in the regulation of the meningeal immune system and participate in the generation and/or maintenance of the immune response in the CNS. We are only starting to explore the contribution of the meningeal lymphatic network under normal and pathological conditions. The meningeal lymphatics are efferent vessels allowing exit of immune cells into the periphery. The potential function of these vessels as afferent vessels participating in the entry of immune cells into the CNS under pathological conditions has however never been addressed.

3 Tertiary Lymphoid Organ Formation in CNS Disorders

Tertiary lymphoid organs (TLOs) also named tertiary lymphoid structures (TLS) are ectopic lymphoid formations developing in inflamed, infected, injured, or tumoral tissues [92]. They are characterized by the accumulations of lymphoid cells in a structured manner reminiscent of lymph nodes with the presence of high endothelial venules and lymphatic vessels [92–95]. Structurally, TLS have T- and B-cell compartmentalization with intercalated dendritic cells, follicular dendritic cells, and stromal cells. TLS can be found in many tissues under conditions of chronic inflammation, and while their contribution in pathologies is still a matter of debate, correlation studies are strongly suggesting that their formation is a good prognosis in cancer, while detrimental in transplantation and autoimmune diseases [92, 94]. The formation of TLS in the CNS has been described, notably in the context of multiple sclerosis (MS) and its animal model [96], but little is known about their formation and the role of the meningeal immune compartment/lymphatic network in the formation and maintenance of such structure. In this section, we discuss the existing literature about TLS formation in the CNS and hypothesize the potential role of TLS in neurological disorders.

3.1 TLS in Multiple Sclerosis

Multiple sclerosis is a chronic inflammatory disease of the CNS, which results in permanent neuronal damage and substantial motor

disability in patients [97, 98]. While autoreactive T cells are a major driver of the disease, B cells have been proven essential for disease pathogenesis [99–101]. Morphological studies have demonstrated, in a fraction of patients with MS [102–104], a large degree of meningeal inflammation associated with aggregates of B cells and T cells with various degrees of organization [105]. Some aggregates even presented a reticular network of follicular dendritic cells [104], suggesting the formation of TLS in the meninges of MS patients. Contrary to TLS described in peripheral tissues, meningeal TLS do not appear to harbor high endothelial venules, suggesting particular features for the meningeal TLS (Fig. 2). Interestingly, these aggregates were observed in patients at different stages of the disease but were not systematically observed, suggesting that these structures might be only transiently formed in MS patients [103, 104], or that only a fraction of patients develop such structures for a reason that remains to be determined. The incidence of meningeal TLS in MS pathology remains unclear. However, the presence of such structures correlates with a more severe disease course. In MS, B-cell repertoire analysis revealed a high degree of overlap between the CSF and the brain lesions in patients, suggesting that local hypermutation and affinity maturation of immunoglobulins might occur locally [106, 107]. Meningeal TLS would represent a perfect structure enabling such an event. This hypothesis was recently demonstrated in a mouse model of MS [108]. Meningeal TLS have been shown to form in some mouse models of MS, especially the ones that present dependency on B cells [108–115]. Similarly to patients, meningeal TLS particularly developed on the brain meninges lining the brainstem and ventricles [96]. Again, most meningeal TLS did not present high endothelial venule structures but are formed within the highly vascularized meninges suggesting that meningeal TLS might function using their niche environment. The mechanism for the induction of meningeal TLS during EAE remains unclear but reports have identified lymphotoxins as a driver of B cells attracting CXCL13 in the CNS, a known chemokine for the formation of TLS [110, 113]. Moreover, infiltrating Th17 cells have been described to be capable of functioning similarly to lymphoid tissue inducer (LTi) cells and induce remodeling of meningeal fibroblast into follicular dendritic cells to promote TLS formation [114, 115].

3.2 Meningeal Lymphatics and CNS TLS

The presence of lymphatic vessels, normally observed in peripheral TLS [95], in meningeal TLS has not been described yet (Fig. 2). Because of their preferential formation in the brain meninges, they could be inducing the invasion of the meningeal lymphatic vessels directly into the TLS. It is also possible that if localized in close vicinity to the meningeal lymphatics, TLS might use the endogenous network without inducing de novo formation of lymphatic vessels, similarly to what is suggested for high endothelial venules.

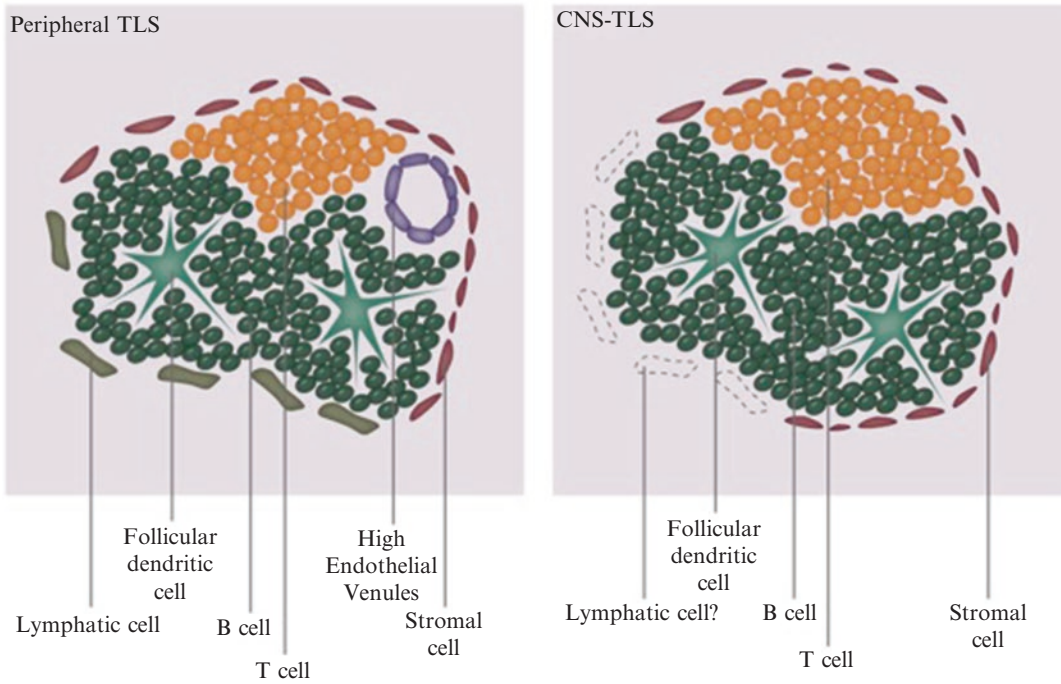

Fig. 2 Peripheral *versus* CNS tertiary lymphoid structure. Schematic illustration of the different organizations of peripheral and CNS tertiary lymphoid structures

CCL21 has been shown as a key chemokine for the formation of TLS [116]. CCL21 is highly expressed by the meningeal lymphatic endothelial cells [49, 76] and could therefore represent a source of chemokines capable of initiating the formation of TLS in the CNS. Furthermore, the communication of the TLS with the periphery in the context of MS/EAE remains understudied, but B-cell repertoire studies do suggest a degree of communication of the TLS/meningeal compartment with the cervical lymph nodes [105, 106].

3.3 TLS in Other Neurological Disorders

As of now, the presence of TLS has only been described in the context of MS/EAE. The meningeal compartment is representing a major, yet understudied, site and further studies are necessary to analyze the immune activity of this compartment, most notably the formation of TLS in many more neurological disorders such as injury and brain tumors. We are only starting to decipher the regulation of meningeal immunity under physiological conditions: How are immune cells maintained in the meningeal compartment? How are they responding to changes in homeostasis? How do those changes affect the brain both structurally and functionally? It is possible that dysregulation of the meningeal immune compartment contributes to the incidence of neurological disorders. Similarly, we do not understand the mechanisms of regulation of

meningeal immunity during CNS inflammation, including the contribution of naturally resident immune cells in the formation of TLS. Therefore, understanding the mechanism of meningeal TLS formation might uncover a new therapeutic approach in context where the immune system fails to mount a sufficient immune response in the brain, notably in the context of primary brain tumors.

4 Conclusion

In conclusion, while initial experiments conducted by Peter Medawar established the idea that the CNS was an immune-privileged organ by way of being ignored by the immune system, studies over the past 50 years or so have clearly demonstrated immune activity in the brain under both physiological and pathological conditions. Indeed, the homeostatic meningeal spaces are dynamically populated by numerous cells and can communicate with the periphery through the meningeal lymphatic network. Moreover, tertiary lymphoid structures can form in those spaces and participate in the local inflammatory response. However, Medawar's initial observations remain valid, suggesting that the CNS is immunologically unique, and understanding the dynamic of the immune response in the CNS will uncover new therapeutic avenue to impact neurological disease.

Acknowledgments

We would like to thank D. Preston for editing the manuscript and L. Louveau for the artwork.
Funding: This work was supported by LE&RN Postdoctoral Fellowship Award to A.L.

References

1. Murphy JB, Sturm E (1923) Conditions determining the transplantability of tissues in the brain. J Exp Med 38:183–197
2. Shirai Y (1921) Transplantation of the rat sarcoma in adult heterogenous animals. Japn Med World 1:14–15
3. Willis RA (1935) Experiments on the intracerebral implantation of embryo tissues in rats. Proc R Soc Lond Ser B 117:400–412
4. Medawar PB (1948) Immunity to homologous grafted skin; the fate of skin homografts transplanted to the brain, to subcutaneous tissue, and to the anterior chamber of the eye. Br J Exp Pathol 29(1):58–69
5. Mason DW, Charlton HM, Jones AJ et al (1986) The fate of allogeneic and xenogeneic neuronal tissue transplanted into the third ventricle of rodents. Neuroscience 19(3):685–694
6. Nicholas MK, Antel JP, Stefansson K, Arnason BG (1987) Rejection of fetal neocortical neural transplants by H-2 incompatible mice. J Immunol 139(7):2275–2283
7. Iliff JJ, Wang M, Liao Y et al (2012) A paravascular pathway facilitates CSF flow through the brain parenchyma and the clearance of interstitial solutes, including amyloid β. Sci Transl Med 4(147):147ra111–147ra111

8. Weller RO, Subash M, Preston SD et al (2008) Perivascular drainage of amyloid-beta peptides from the brain and its failure in cerebral amyloid angiopathy and Alzheimer's disease. Brain Pathol Zurich Switz 18(2):253–266
9. Cserr HF, Ostrach LH (1974) Bulk flow of interstitial fluid after intracranial injection of Blue Dextran 2000. Exp Neurol 45(1):50–60
10. Cserr HF, Cooper DN, Milhorat TH (1977) Flow of cerebral interstitial fluid as indicated by the removal of extracellular markers from rat caudate nucleus. Exp Eye Res 25(Supplement 1):461–473
11. Cserr HF, Cooper DN, Suri PK, Patlak CS (1981) Efflux of radiolabeled polyethylene glycols and albumin from rat brain. Am J Physiol 240(4):F319–F328
12. Morris AWJ, Sharp MM, Albargothy NJ et al (2016) Vascular basement membranes as pathways for the passage of fluid into and out of the brain. Acta Neuropathol (Berl) 131(5):725–736
13. Rennels ML, Gregory TF, Blaumanis OR et al (1985) Evidence for a "paravascular" fluid circulation in the mammalian central nervous system, provided by the rapid distribution of tracer protein throughout the brain from the subarachnoid space. Brain Res 326(1):47–63
14. Rennels ML, Blaumanis OR, Grady PA (1990) Rapid solute transport throughout the brain via paravascular fluid pathways. Adv Neurol 52:431–439
15. Engelhardt B, Carare RO, Bechmann I et al (2016) Vascular, glial, and lymphatic immune gateways of the central nervous system. Acta Neuropathol (Berl) 132(3):317–338
16. Engelhardt B, Vajkoczy P, Weller RO (2017) The movers and shapers in immune privilege of the CNS. Nat Immunol 18(2):123–131
17. Louveau A, Plog BA, Antila S et al (2017) Understanding the functions and relationships of the glymphatic system and meningeal lymphatics. J Clin Invest 127(9):3210–3219
18. Asgari M, Zélicourt D, de Kurtcuoglu V (2016) Glymphatic solute transport does not require bulk flow. Sci Rep 6:srep38635
19. Smith AJ, Yao X, Dix JA et al (2017) Test of the "glymphatic" hypothesis demonstrates diffusive and aquaporin-4-independent solute transport in rodent brain parenchyma. Elife 6:e27679
20. Iliff JJ, Wang M, Zeppenfeld DM et al (2013) Cerebral arterial pulsation drives paravascular CSF–interstitial fluid exchange in the murine brain. J Neurosci 33(46):18,190–18,199
21. Plog BA, Dashnaw ML, Hitomi E et al (2015) Biomarkers of traumatic injury are transported from brain to blood via the glymphatic system. J Neurosci Off J Soc Neurosci 35(2):518–526
22. Lee H, Xie L, Yu M et al (2015) The effect of body posture on brain glymphatic transport. J Neurosci 35(31):11,034–11,044
23. Xie L, Kang H, Xu Q et al (2013) Sleep drives metabolite clearance from the adult brain. Science 342(6156):373–377
24. Garbage NM (2013) Truck of the brain. Science 340(6140):1529–1530
25. Carare RO, Bernardes-Silva M, Newman TA et al (2008) Solutes, but not cells, drain from the brain parenchyma along basement membranes of capillaries and arteries: significance for cerebral amyloid angiopathy and neuroimmunology. Neuropathol Appl Neurobiol 34(2):131–144
26. Jessen NA, Munk ASF, Lundgaard I, Nedergaard M (2015) The glymphatic system: a beginner's guide. Neurochem Res 7:1–17
27. Kress BT, Iliff JJ, Xia M et al (2014) Impairment of paravascular clearance pathways in the aging brain. Ann Neurol 76(6):845–861
28. Peng W, Achariyar TM, Li B et al (2016) Suppression of glymphatic fluid transport in a mouse model of Alzheimer's disease. Neurobiol Dis 93:215–225
29. Gaberel T, Gakuba C, Goulay R et al (2014) Impaired glymphatic perfusion after strokes revealed by contrast-enhanced MRI: a new target for fibrinolysis? Stroke 45(10):3092–3096
30. Wang M, Ding F, Deng S et al (2017) Focal solute trapping and global glymphatic pathway impairment in a murine model of multiple microinfarcts. J Neurosci Off J Soc Neurosci 37(11):2870–2877
31. Iliff JJ, Chen MJ, Plog BA et al (2014) Impairment of glymphatic pathway function promotes tau pathology after traumatic brain injury. J Neurosci 34(49):16,180–16,193
32. Bradbury MW, Cserr HF, Westrop RJ (1981) Drainage of cerebral interstitial fluid into deep cervical lymph of the rabbit. Am J Physiol 240(4):F329–F336
33. Clapham R, O'Sullivan E, Weller RO, Carare RO (2010) Cervical lymph nodes are found in direct relationship with the internal carotid artery: significance for the lymphatic drainage of the brain. Clin Anat N Y N 23(1):43–47
34. Kida S, Pantazis A, Weller RO (1993) CSF drains directly from the subarachnoid space into nasal lymphatics in the rat. Anatomy, histology and immunological significance.

Neuropathol Appl Neurobiol 19(6):480–488
35. Szentistványi I, Patlak CS, Ellis RA, Cserr HF (1984) Drainage of interstitial fluid from different regions of rat brain. Am J Physiol 246(6 Pt 2):F835–F844
36. Weller RO, Djuanda E, Yow H-Y, Carare RO (2009) Lymphatic drainage of the brain and the pathophysiology of neurological disease. Acta Neuropathol (Berl) 117(1):1–14
37. Yamada S, DePasquale M, Patlak CS, Cserr HF (1991) Albumin outflow into deep cervical lymph from different regions of rabbit brain. Am J Physiol Heart Circ Physiol 261(4):H1197–H1204
38. Clarkson BD, Walker A, Harris MG et al (2017) CCR7 deficient inflammatory dendritic cells are retained in the central nervous system. Sci Rep 7:42,856
39. Goldmann J, Kwidzinski E, Brandt C et al (2006) T cells traffic from brain to cervical lymph nodes via the cribroid plate and the nasal mucosa. J Leukoc Biol 80(4):797–801
40. Hatterer E, Davoust N, Didier-Bazes M et al (2006) How to drain without lymphatics? Dendritic cells migrate from the cerebrospinal fluid to the B-cell follicles of cervical lymph nodes. Blood 107(2):806–812
41. Kaminski M, Bechmann I, Pohland M et al (2012) Migration of monocytes after intracerebral injection at entorhinal cortex lesion site. J Leukoc Biol 92(1):31–39
42. Mohammad MG, Tsai VWW, Ruitenberg MJ et al (2014) Immune cell trafficking from the brain maintains CNS immune tolerance. J Clin Invest 124(3):1228–1241
43. Shechter R, London A, Schwartz M (2013) Orchestrated leukocyte recruitment to immune-privileged sites: absolute barriers versus educational gates. Nat Rev Immunol 13(3):206–218
44. Silver R, Silverman A-J, Vitković L, Lederhendler II (1996) Mast cells in the brain: evidence and functional significance. Trends Neurosci 19(1):25–31
45. Derecki NC, Cardani AN, Yang CH et al (2010) Regulation of learning and memory by meningeal immunity: a key role for IL-4. J Exp Med 207(5):1067–1080
46. Goldmann T, Wieghofer P, Jordão M et al (2016) Origin, fate and dynamics of macrophages at CNS interfaces. Nat Immunol 17(7):797–805
47. Kivisäkk P, Mahad DJ, Callahan MK et al (2003) Human cerebrospinal fluid central memory CD4+ T cells: evidence for trafficking through choroid plexus and meninges via P-selectin. Proc Natl Acad Sci U S A 100(14):8389–8394
48. Korin B, Ben-Shaanan TL, Schiller M et al (2017) High-dimensional, single-cell characterization of the brain's immune compartment. Nat Neurosci 20(9):1300–1309
49. Louveau A, Smirnov I, Keyes TJ et al (2015) Structural and functional features of central nervous system lymphatic vessels. Nature 523(7560):337–341
50. Radjavi A, Smirnov I, Derecki N, Kipnis J (2014) Dynamics of the meningeal CD4(+) T-cell repertoire are defined by the cervical lymph nodes and facilitate cognitive task performance in mice. Mol Psychiatry 19(5):531–533
51. Kipnis J (2016) Multifaceted interactions between adaptive immunity and the central nervous system. Science 353(6301):766–771
52. Ransohoff RM, Engelhardt B (2012) The anatomical and cellular basis of immune surveillance in the central nervous system. Nat Rev Immunol 12(9):623–635
53. Brombacher TM, Nono JK, De Gouveia KS et al (2017) IL-13-mediated regulation of learning and memory. J Immunol Baltim MD 1950 198(7):2681–2688
54. Filiano AJ, Xu Y, Tustison NJ et al (2016) Unexpected role of interferon-γ in regulating neuronal connectivity and social behaviour. Nature 535(7612):425–429
55. Kipnis J, Gadani S, Derecki NC (2012) Pro-cognitive properties of T cells. Nat Rev Immunol 12(9):663–669
56. Wolf SA, Steiner B, Akpinarli A et al (2009) CD4-positive T lymphocytes provide a neuroimmunological link in the control of adult hippocampal neurogenesis. J Immunol Baltim Md 1950 182(7):3979–3984
57. Ziv Y, Ron N, Butovsky O et al (2006) Immune cells contribute to the maintenance of neurogenesis and spatial learning abilities in adulthood. Nat Neurosci 9(2):268–275
58. Blank T, Prinz M (2017) Type I interferon pathway in CNS homeostasis and neurological disorders. Glia 65(9):1397–1406
59. Choi GB, Yim YS, Wong H et al (2016) The maternal interleukin-17a pathway in mice promotes autism-like phenotypes in offspring. Science 351(6276):933–939
60. Shin Yim Y, Park A, Berrios J et al (2017) Reversing behavioural abnormalities in mice exposed to maternal inflammation. Nature 549(7673):482–487
61. Srinivasan D, Yen J-H, Joseph DJ, Friedman W (2004) Cell type-specific interleukin-1beta signaling in the CNS. J Neurosci Off J Soc Neurosci 24(29):6482–6488

62. Gh Popescu BF, Lucchinetti CF (2012) Meningeal and cortical grey matter pathology in multiple sclerosis. BMC Neurol 12:11
63. Howell OW, Reeves CA, Nicholas R et al (2011) Meningeal inflammation is widespread and linked to cortical pathology in multiple sclerosis. Brain J Neurol 134(Pt 9):2755–2771
64. Bartholomäus I, Kawakami N, Odoardi F et al (2009) Effector T cell interactions with meningeal vascular structures in nascent autoimmune CNS lesions. Nature 462(7269):94–98
65. Kwong B, Rua R, Gao Y et al (2017) T-bet-dependent NKp46(+) innate lymphoid cells regulate the onset of TH17-induced neuroinflammation. Nat Immunol 18(10):1117–1127
66. Russi AE, Walker-Caulfield ME, Guo Y et al (2016) Meningeal mast cell-T cell crosstalk regulates T cell encephalitogenicity. J Autoimmun 73:100–110
67. Benakis C, Brea D, Caballero S et al (2016) Commensal microbiota affects ischemic stroke outcome by regulating intestinal γδ T cells. Nat Med 22(5):516–523
68. Baruch K, Deczkowska A, Rosenzweig N et al (2016) PD-1 immune checkpoint blockade reduces pathology and improves memory in mouse models of Alzheimer's disease. Nat Med 22(2):135–137
69. Alitalo K (2011) The lymphatic vasculature in disease. Nat Med 17(11):1371–1380
70. Wang Y, Oliver G (2010) Current views on the function of the lymphatic vasculature in health and disease. Genes Dev 24(19):2115–2126
71. Andres KH, von Düring M, Muszynski K, Schmidt RF (1987) Nerve fibres and their terminals of the dura mater encephali of the rat. Anat Embryol 175(3):289–301
72. Foldi M, Csanda E, Obal F et al (1963) Uber Wirkungen der Unterbindung der Lymphgefasse und Lymphknoten des Halses auf das Zentralnervensystem im Tierversuch. Z Gesamte Exp Med 137:483–510
73. Furukawa M, Shimoda H, Kajiwara T et al (2008) Topographic study on nerve-associated lymphatic vessels in the murine craniofacial region by immunohistochemistry and electron microscopy. Biomed Res Tokyo Jpn 29(6):289–296
74. Gausas RE, Daly T, Fogt F (2007) D2-40 expression demonstrates lymphatic vessel characteristics in the dural portion of the optic nerve sheath. Ophthal Plast Reconstr Surg 23(1):32–36
75. Mascagni P, Bellini G (1816) Istoria Completa Dei Vasi Linfatici. Presso Eusebio Pacini e Figlio, Florence, p 195
76. Aspelund A, Antila S, Proulx ST et al (2015) A dural lymphatic vascular system that drains brain interstitial fluid and macromolecules. J Exp Med 212(7):991–999
77. Absinta M, Ha S-K, Nair G et al (2017) Human and nonhuman primate meninges harbor lymphatic vessels that can be visualized noninvasively by MRI. Elife 3:6
78. Johnston M, Zakharov A, Papaiconomou C et al (2004) Evidence of connections between cerebrospinal fluid and nasal lymphatic vessels in humans, non-human primates and other mammalian species. Cerebrospinal Fluid Res 1(1):2
79. Johnston M, Zakharov A, Koh L, Armstrong D (2005) Subarachnoid injection of Microfil reveals connections between cerebrospinal fluid and nasal lymphatics in the non-human primate. Neuropathol Appl Neurobiol 31(6):632–640
80. Brierley JB, Field EJ (1948) The connexions of the spinal sub-arachnoid space with the lymphatic system. J Anat 82(3):153–166
81. Kwon S, Janssen CF, Velasquez FC, Sevick-Muraca EM (2017) Fluorescence imaging of lymphatic outflow of cerebrospinal fluid in mice. J Immunol Methods 449:37–43
82. Antila S, Karaman S, Nurmi H et al (2017) Development and plasticity of meningeal lymphatic vessels. J Exp Med 214(12):3645–3667
83. Go KG, Houthoff HJ, Hartsuiker J et al (1986) Fluid secretion in arachnoid cysts as a clue to cerebrospinal fluid absorption at the arachnoid granulation. J Neurosurg 65(5):642–648
84. Kido DK, Gomez DG, Jr AMP, Potts DG (1976) Human spinal arachnoid villi and granulations. Neuroradiology 11(5):221–228
85. Mawera G, Asala SA (1996) The function of arachnoid villi/granulations revisited. Cent Afr J Med 42(9):281–284
86. Upton ML, Weller RO (1985) The morphology of cerebrospinal fluid drainage pathways in human arachnoid granulations. J Neurosurg 63(6):867–875
87. Whedon JM, Glassey D (2009) Cerebrospinal fluid stasis and its clinical significance. Altern Ther Health Med 15(3):54–60
88. Boulton M, Young A, Hay J et al (1996) Drainage of CSF through lymphatic pathways and arachnoid villi in sheep: measurement of 125I-albumin clearance. Neuropathol Appl Neurobiol 22(4):325–333
89. Ma Q, Ineichen BV, Detmar M, Proulx ST (2017) Outflow of cerebrospinal fluid is predominantly through lymphatic vessels and is

reduced in aged mice. Nat Commun 8(1):1434
90. Tripathi BJ, Tripathi RC (1974) Vacuolar transcellular channels as a drainage pathway for cerebrospinal fluid. J Physiol 239(1):195–206
91. Mollanji R, Bozanovic-Sosic R, Zakharov A et al (2002) Blocking cerebrospinal fluid absorption through the cribriform plate increases resting intracranial pressure. Am J Physiol Regul Integr Comp Physiol 282(6):R1593–R1599
92. Dieu-Nosjean M-C, Goc J, Giraldo NA et al (2014) Tertiary lymphoid structures in cancer and beyond. Trends Immunol 35(11):571–580
93. Drayton DL, Liao S, Mounzer RH, Ruddle NH (2006) Lymphoid organ development: from ontogeny to neogenesis. Nat Immunol 7(4):344–353
94. Pitzalis C, Jones GW, Bombardieri M, Jones SA (2014) Ectopic lymphoid-like structures in infection, cancer and autoimmunity. Nat Rev Immunol 14(7):447–462
95. Ruddle NH (2014) Lymphatic vessels and tertiary lymphoid organs. J Clin Invest 124(3):953–959
96. Mitsdoerffer M, Peters A. (2016) Tertiary lymphoid organs in central nervous system autoimmunity. Front Immunol [Internet]. Oct 25 [cited 2017 Nov 3];7. Available from: https://www.ncbi.nlm.nih.gov/pmc/articles/PMC5078318/
97. Compston A, Coles A (2002) Multiple sclerosis. Lancet Lond Engl 359(9313):1221–1231
98. Compston A, Coles A (2008) Multiple sclerosis. Lancet Lond Engl 372(9648):1502–1517
99. Blauth K, Owens GP, Bennett JL. (2015) The ins and outs of B cells in multiple sclerosis. Front Immunol [Internet]. [cited 2017 Nov 3];6. Available from: https://www.frontiersin.org/articles/10.3389/fimmu.2015.00565/full
100. Liblau RS, Gonzalez-Dunia D, Wiendl H, Zipp F (2013) Neurons as targets for T cells in the nervous system. Trends Neurosci 36(6):315–324
101. Weiner HL (2004) Multiple sclerosis is an inflammatory T-cell-mediated autoimmune disease. Arch Neurol 61(10):1613–1615
102. Kooi E-J, Geurts JJG, van Horssen J et al (2009) Meningeal inflammation is not associated with cortical demyelination in chronic multiple sclerosis. J Neuropathol Exp Neurol 68(9):1021–1028
103. Magliozzi R, Howell O, Vora A et al (2007) Meningeal B-cell follicles in secondary progressive multiple sclerosis associate with early onset of disease and severe cortical pathology. Brain J Neurol 130(Pt 4):1089–1104
104. Serafini B, Rosicarelli B, Magliozzi R et al (2004) Detection of ectopic B-cell follicles with germinal centers in the meninges of patients with secondary progressive multiple sclerosis. Brain Pathol Zurich Switz 14(2):164–174
105. Lucchinetti CF, Popescu BFG, Bunyan RF et al (2011) Inflammatory cortical demyelination in early multiple sclerosis. N Engl J Med 365(23):2188–2197
106. Palanichamy A, Apeltsin L, Kuo TC et al (2014) Immunoglobulin class-switched B cells form an active immune axis between CNS and periphery in multiple sclerosis. Sci Transl Med 6(248):248ra106
107. Stern JNH, Yaari G, Vander Heiden JA et al (2014) B cells populating the multiple sclerosis brain mature in the draining cervical lymph nodes. Sci Transl Med 6(248):248ra107
108. Lehmann-Horn K, Wang S-Z, Sagan SA et al (2016) B cell repertoire expansion occurs in meningeal ectopic lymphoid tissue. JCI Insight 1(20):e87234
109. Bettelli E, Baeten D, Jäger A et al (2006) Myelin oligodendrocyte glycoprotein-specific T and B cells cooperate to induce a Devic-like disease in mice. J Clin Invest 116(9):2393–2402
110. Columba-Cabezas S, Griguoli M, Rosicarelli B et al (2006) Suppression of established experimental autoimmune encephalomyelitis and formation of meningeal lymphoid follicles by lymphotoxin beta receptor-Ig fusion protein. J Neuroimmunol 179(1–2):76–86
111. Dang AK, Tesfagiorgis Y, Jain RW, et al (2015) Meningeal infiltration of the spinal cord by non-classically activated B cells is associated with chronic disease course in a spontaneous B cell-dependent model of cns autoimmune disease. Front Immunol [Internet]. Sep 15 [cited 2017 Nov 3];6. Available from: https://www.ncbi.nlm.nih.gov/pmc/articles/PMC4584934/
112. Kuerten S, Schickel A, Kerkloh C et al (2012) Tertiary lymphoid organ development coincides with determinant spreading of the myelin-specific T cell response. Acta Neuropathol (Berl) 124(6):861–873
113. Magliozzi R, Columba-Cabezas S, Serafini B, Aloisi F (2004) Intracerebral expression of CXCL13 and BAFF is accompanied by formation of lymphoid follicle-like structures in the meninges of mice with relapsing experimental autoimmune encephalomyelitis. J Neuroimmunol 148(1–2):11–23

114. Peters A, Pitcher LA, Sullivan JM et al (2011) Th17 cells induce ectopic lymphoid follicles in central nervous system tissue inflammation. Immunity 35(6):986–996

115. Pikor NB, Astarita JL, Summers-Deluca L et al (2015) Integration of Th17- and lymphotoxin-derived signals initiates meningeal-resident stromal cell remodeling to propagate neuroinflammation. Immunity 43(6):1160–1173

116. Sautès-Fridman C, Lawand M, Giraldo NA, et al (2016) Tertiary lymphoid structures in cancers: prognostic value, regulation, and manipulation for therapeutic intervention. Front Immunol [Internet]. Oct 3 [cited 2018 Jan 27];7. Available from: https://www.ncbi.nlm.nih.gov/pmc/articles/PMC5046074/

Chapter 4

Development of Tools for the Selective Visualization and Quantification of TLS-Immune Cells on Tissue Sections

Christophe Klein, Priyanka Devi-Marulkar, Marie-Caroline Dieu-Nosjean, and Claire Germain

Abstract

Tertiary lymphoid structures (TLS) are considered as genuine markers of inflammation. Their presence within inflamed tissues or within the tumor microenvironment has been associated with the local development of an active immune response. While high densities of TLS are correlated with disease severity in autoimmune diseases or during graft rejection, it has been associated with longer patient survival in many cancer types. Their efficient visualization and quantification within human tissues may represent new tools for helping clinicians in adjusting their therapeutic strategy. Some immunohistochemistry (IHC) protocols are already used in the clinic to appreciate the level of immune infiltration in formalin-fixed, paraffin-embedded (FFPE) tissues. However, the use of two or more markers may sometimes be useful to better characterize this immune infiltrate, especially in the case of TLS. Besides the growing development of multiplex labeling approaches, imaging can also be used to overcome some technical difficulties encountered during the immunolabeling of tissues with several markers.

This chapter describes IHC methods to visualize in a human tissue (tumoral or not) the presence of TLS. These methods are based on the immunostaining of four TLS-associated immune cell populations, namely follicular B cells, follicular dendritic cells (FDCs), mature dendritic cells (mDCs), and follicular helper T cells (T_{FH}), together with non-T_{FH} T cells. Methodologies for subsequent quantification of TLS density are also proposed, as well as a virtual multiplexing method based on image registration using the open-source software ImageJ (IJ), aiming at co-localizing several immune cell populations from different IHC stainings performed on serial tissue sections.

Key words Tertiary lymphoid structure, Double immunohistochemistry, Virtual multiplexing, Image registration, CD20, DC-LAMP, PD-1, B-cell follicle, Mature dendritic cell, Follicular helper T cell, Open-source software, ImageJ

Abbreviations

AID	Activation-induced cytidine deaminase
AP	Alkaline phosphatase
APAAP	Alkaline phosphatase anti-alkaline phosphatase
Bcl6	B-cell lymphoma 6

Marie-Caroline Dieu-Nosjean (ed.), *Tertiary Lymphoid Structures: Methods and Protocols*, Methods in Molecular Biology, vol. 1845, https://doi.org/10.1007/978-1-4939-8709-2_4,

CSR	Class-switch recombination
FDC	Follicular dendritic cell
FFPE	Formalin-fixed, paraffin-embedded
GC	Germinal center
HRP	Horseradish peroxidase
HS	Human serum
IF	Immunofluorescence
IHC	Immunohistochemistry
IJ	ImageJ
mDC	Mature dendritic cell
NSCLC	Non-small cell lung cancer
RA	Rheumatoid arthritis
ROA	Region of analysis
ROI	Region of interest
SHM	Somatic hypermutation
SIFT	Scale invariant feature transform
SLO	Secondary lymphoid organ
T_{FH}	Follicular helper T cell
TLS	Tertiary lymphoid structure
WSI	Whole-slide image

1 Introduction

Under pathological conditions, the infiltration of tissues by immune cells, the density of this immune infiltrate, and its potential organization in tertiary lymphoid structures (TLS) often mirror the development of an active immune response.

TLS are transient ectopic lymphoid aggregates displaying the same organization and functionality as canonical secondary lymphoid organs (SLOs), with a T-cell-rich area characterized by DC-LAMP$^+$ mature dendritic cells (mDCs) forming clusters with T cells, and a B-cell-rich area characterized by CD20$^+$ B cells [1, 2]. Like in conventional SLOs, B-cell follicles are composed of a mantle of IgD$^+$ naive B cells, surrounding a germinal center (GC) identified by highly proliferating Ki67$^+$ B cells, a network of CD21$^+$ follicular dendritic cells (FDCs), presence of CD3$^+$ CD4$^+$ CXCL13$^+$ PD-1^{high} follicular helper T cells (T_{FH}), and expression of activation-induced cytidine deaminase (AID) and Bcl6 (B-cell lymphoma 6), both associated with class-switch recombination (CSR) and somatic hypermutation (SHM) activities [2–5]. An increasing number of studies over the past decades have provided evidence that TLS represent sites for the local initiation and expansion of antigen-specific T- and B-cell responses [2, 6, 7], subverting the dogma that adaptive immune responses only take place in SLOs.

So far, these TLS have been observed in many situations of chronic inflammation, including lung inflammatory diseases (fibrosis, pneumonia, hypersensitivity pneumonitis, diffuse pan-

bronchiolitis, tobacco-induced inflammation, …), infectious diseases, graft rejection, autoimmune disorders (rheumatoid arthritis (RA), multiple sclerosis …), allergy, atherosclerosis, and cancer [8–10]. While in autoimmune diseases and transplantation the presence of TLS was associated with disease exacerbation and poor outcome [11–15], T- and B-cell responses initiated within TLS during infections were shown to be associated with pathogen clearance and reduced morbidity [16]. Similarly, in cancer, many studies demonstrated that the presence of TLS in the tumor microenvironment was associated with anti-tumor immune responses and prolonged patient survival, such as in non-small cell lung cancer (NSCLC), oral squamous cell carcinoma, metastatic colorectal cancer, and breast cancer [1, 2, 4, 6, 10, 17–20].

Most of these studies based their analysis on the quantification by immunohistochemistry (IHC) of $CD20^+$ B-cell aggregates in the tumor tissue or of DC-$LAMP^+$ mDCs, as a hallmark of TLS [21]. However, proper TLS visualization and quantification within tissues may be challenging, and the complete characterization of fully active TLS may require the use of additional markers and thus the development of multiplexed immunolabeling. A way to achieve multiplexing is to perform sequential IHC stainings on the same tissue section, with tyramide-based signal amplification and antibody striping between each staining. However, the analysis of the sequential stainings obtained requires the use of sophisticated methods of image acquisition, as well as image processing by a spectral unmixing algorithm, especially when cell-to-cell interactions have to be studied at high resolution. In the case when the desired information are the absolute quantification and/or the potential co-localization of different immune cell types within a same structure, at a relatively lower resolution, virtual multiplexing of different IHC stainings performed on serial tissue sections can be developed more easily. The first step is the digitalization of the immunostained tissue sections as whole-slide images (WSI), which can be performed using more accessible slide scanners. These WSI can then be analyzed with an image analysis software, and high-throughput quantitative studies can then be achieved by counting a large amount of cells on a large number of tissue sections. Another advantage of WSI is that vast areas of tissue can be imaged at high magnification, giving the opportunity to detect and quantify rare isolated cells within the entire tissue section. Finally, the spatial relationship between different cell types can also be investigated starting from different WSI, provided that a step of image registration, extensively described in this chapter, has been performed before the analysis.

Here we propose three standardized IHC protocols for the visualization and/or subsequent quantification of TLS-associated $CD20^+$ B-cell follicles, TLS-associated DC-$LAMP^+$ mDCs, and TLS-associated PD-1^{high} T_{FH}, on formalin-fixed, paraffin-embedded

(FFPE) human tissue sections, using NSCLC tumor samples as an example. The computer-assisted semiquantitative and quantitative analysis of IHC stainings proposed here represents a solution superior to the manual method in terms of reproducibility and applicability in the clinic, on large cohorts of patients. We also describe a virtual multiplexing method based on image registration, using an open-source software broadly used in scientific imaging and microscopy, ImageJ (IJ), to visualize the co-localization of several immune cell populations within a same structure, starting from different IHC stainings performed on serial tissue sections.

2 Materials

2.1 Samples

FFPE NSCLC tumor tissue sections, 5 μm thick.

2.2 Buffers

1. 100% Xylene or Clearene (Leica).
2. 100% Ethanol.
3. Distilled water.
4. Ethanol solutions at 90%, 70%, and 50%.
5. 10× TBS: 47.4 g Trizma® hydrochloride + 263 g sodium chloride, in 3 L distilled water; pH adjusted at 7.4.
6. 1× TBS: 1 volume of 10× TBS + 9 volumes of distilled water.
7. 1× TBS-T: 1 volume of 10× TBS + 9 volumes of distilled water + 0.04% Tween20.
8. 1× Phosphate-buffered saline (PBS).
9. 0.1M Tris–HCl: 15.76 g of Tris–HCl in 1 L distilled water; pH adjusted at 8.2.

2.3 Reagents

All specific antibodies used in the three following protocols are additionally listed in Table 1.

1. 1× Antigen retrieval solutions:
   (a) For double IHC anti-human CD20/anti-human CD21 and anti-human CD20/anti-human PD-1: Target retrieval solution (TRS) pH6 (Dako, 10×; 1 volume + 9 volumes of distilled water, pH adjusted at 6).
   (b) For double IHC anti-human DC-LAMP/anti-human CD3: Citrate buffer pH6 (4.5 mL of 0.1 M citric acid + 20.5 mL of 0.1 M sodium citrate in 225 mL of distilled water; pH adjusted at 6).
2. 3% H_2O_2.
3. 5% HS: 5% Decomplemented human serum (HS) in PBS.
4. Antibody diluent (Dako REAL™, Dako).

Table 1
Antibodies and reagents used in IHC protocols

Antibody or reagent	Conjugate	Host	Clone or reference	Source	Dilution
Human CD20	UC	Mouse IgG2a	L26	Agilent/Dako	1/250
Human CD21	UC	Mouse IgG1	1F8	Agilent/Dako	1/30
Human DC-LAMP *(cross-reactivity with canine, feline, murine, and sheep DC-LAMP)*	UC	Rat IgG2a	1010 E1.01	Dendritics	1/80
Human CD3	UC	Rabbit IgG	A0452	Agilent/Dako	1/80
Human PD-1	UC	Mouse IgG1	NAT105	Roche	Pre-diluted
Mouse IgG2a	Biotin	Goat IgG	115-065-206	Jackson ImmunoResearch	1/100
Mouse IgG1	UC	Goat IgG	115-005-205	Jackson ImmunoResearch	1/30
Rat IgG	Biotin	Donkey $F(ab')_2$	712-066-153	Jackson ImmunoResearch	1/500
Rabbit IgG	AP	Goat $F(ab')_2$	111-056-045	Jackson ImmunoResearch	1/300
Streptavidin	HRP	NA	P039701	Agilent/Dako	1/300
APAAP	AP	Mouse IgG1	D0651	Agilent/Dako	1/30

Abbreviations: AP Alkaline phosphatase, *APAAP* Alkaline phosphatase anti-alkaline phosphatase, *HRP* Horseradish peroxidase, *NA* Nonapplicable, *UC* Uncoupled

5. Primary antibodies:
   (a) For double IHC anti-human CD20/anti-human CD21: Anti-human CD20 (mouse IgG2a, clone L26, Dako, working dilution 1/250e) and anti-human CD21 (mouse IgG1, clone 1F8, Dako, working dilution 1/30e).
   (b) For double IHC anti-human DC-LAMP/anti-human CD3: Anti-human DC-LAMP (CD208, rat IgG2b, clone 1010E1.01, Dendritics/Clinisciences, working dilution 1/80e, *see* **Note 1**) and anti-human CD3 (rabbit polyclonal IgG antibodies, Dako, working dilution 1/80e).
   (c) For double IHC anti-human CD20/anti-human PD-1: Anti-human CD20 (mouse IgG2a, clone L26, Dako, working dilution 1/250e) and anti-human PD-1 (mouse

IgG1, clone NAT105, VENTANA/ROCHE, pre-diluted).

6. Secondary antibodies:
   (a) For double IHC anti-human CD20/anti-human CD21 and anti-human CD20/anti-human PD-1: Anti-mouse IgG2a-biotin ($F(ab')_2$, goat, JIR, working dilution 1/100e) and anti-mouse IgG1 (goat, JIR, working dilution 1/30e).
   (b) For double IHC anti-human DC-LAMP/anti-human CD3: Anti-rat IgG-biotin ($F(ab')_2$, donkey, JIR, working dilution 1/500e) and anti-rabbit IgG-AP ($F(ab')_2$, goat, JIR, working dilution 1/300e).
7. Tertiary reagents:
   (a) Streptavidin-HRP (Dako) 1/300e.
   (b) APAAP (Dako) 1/30e.
8. Substrates:
   (a) AEC (3-amino-9-ethylcarbazole) horseradish peroxidase (HRP) Substrate Kit (VECTOR).
   (b) SAP Blue Alkaline Phosphatase (AP) Substrate Kit (VECTOR).
9. Levamisole Endogenous Alkaline Phosphatase Inhibitor (Dako).
10. Mounting Medium (Glycergel®, Dako).

2.4 Specialist Equipment

1. Drying oven.
2. Laboratory fume hood.
3. Glass containers for slides.
4. Plastic containers for slides.
5. Water bath.
6. Absorbent papers.
7. Humidified chamber.
8. Microscope (magnification x100).
9. Glass coverslips.
10. Slide scanner (NanoZoomer slide scanner, Hamamatsu).
11. Analysis software (Calopix, Tribvn).
12. ImageJ software.

3 Methods

3.1 Double Immunohistochemistry Anti-human CD20/Anti-human CD21 for TLS-Associated B-Cell Follicle Quantification

1. Dry the tissue sections a minimum of 30 min (or overnight) in a drying oven at 37 °C.
2. Deparaffinize the tissue sections: Under a laboratory fume hood, immerse the slides in three successive baths of 100% xylene (or Clearene) for 5 min each, then in one bath of absolute ethanol for 5 min, one bath of 90% ethanol for 5 min, one bath of 70% ethanol for 5 min, one bath of 50% ethanol for 5 min, and one bath of distilled water for 5 min (use glass containers for slides).
3. Retrieve antigen: Immerse the slides in a bath of pre-warmed antigen retrieval solution (TRS, pH6) for 30 min at 97 °C (in a water bath; use a plastic container for slides).
4. Take out the plastic container from the water bath and let it cool for 30 min at room temperature, on the bench.
5. Wash the slides in TBS for 5 min under agitation (use a glass container for slides) (*see* **Note 2**).
6. Remove the excess of buffer with absorbent papers (*see* **Notes 3** and **4**).
7. Place the slides in a humidified chamber.
8. Cover the tissue with 200 µL of 3% H_2O_2 for 10 min at room temperature (for saturation of the endogenous peroxidases).
9. Wash the slides in 1× TBS for 1 min.
10. Remove the excess of buffer with absorbent papers.
11. Cover the tissue with 200 µL of 5% HS, for 30 min at room temperature (for saturation of the receptors for the Fc portion of immunoglobulins).
12. Simply remove the excess of 5% HS with absorbent papers (do not wash).
13. Cover the tissue with 200 µL of primary antibody solution (anti-human CD20 1/250e + anti-human CD21 1/30e in antibody diluent Dako REAL™), for 1 h at room temperature.
14. Wash the slides in 1× TBS-T for 5 min, under gentle agitation, twice.
15. Remove the excess of buffer with absorbent papers.
16. Cover the tissue with 200 µL of secondary antibody solution (anti-mouse IgG2a-biotin 1/100e + anti-mouse IgG1 1/30e in 1× TBS), for 30 min at room temperature.
17. Wash the slides in 1× TBS-T for 5 min, under gentle agitation, twice.
18. Remove the excess of buffer with absorbent papers.

19. Cover the tissue with 200 µL of tertiary reagents (streptavidin-HRP 1/300e + APAAP 1/30e in 1× TBS), for 30 min at room temperature.
20. Wash the slides in 1× TBS-T for 5 min, under gentle agitation, twice.
21. Wash the slides in 1× TBS for 5 min, under gentle agitation.
22. Remove the excess of buffer with absorbent papers.
23. CD20 immunostaining revelation with AEC: Cover the tissue with 200 µL of AEC solution (prepared according to the manufacturer's instructions, in distilled water), for up to 30 min at room temperature (CD20-immunostained cells appear in red (Fig. 1a), check under the microscope) (*see* **Note 5**).
24. Stop the reaction in a bath of 1× TBS, for 5 min, under gentle agitation.
25. Remove the excess of buffer with absorbent papers.
26. CD21 immunostaining revelation with SAP: Cover the tissue with 200 µL of SAP solution (prepared according to the manufacturer's instructions, in 0.1 M Tris–HCl pH 8.2, and supplemented with Levamisole, to inhibit endogenous alkaline phosphatases, 1 drop per mL of SAP solution), for 10–30 min maximum at room temperature (CD21-immunostained cells appear in blue (Fig. 1a), check under the microscope) (*see* **Note 6**).
27. Stop the reaction in a bath of 1× TBS, for 5 min, under gentle agitation.
28. Wash the slides in distilled water, for 5 min, under gentle agitation.
29. Remove the excess of buffer with absorbent papers.
30. Mount the slides with glass coverslips using glycergel (liquefied by heating at 70 °C).
31. Let the slides dry overnight at room temperature before storing.

3.2 Double Immunohistochemistry Anti-human DC-LAMP/Anti-human CD3 for TLS-Associated mDC Quantification

1. Dry the tissue sections a minimum of 30 min (or overnight) in a drying oven at 37 °C.
2. Deparaffinize the tissue sections: Under a laboratory fume hood, immerse the slides in three successive baths of 100% xylene (or Clearene) for 5 min each, then in one bath of absolute ethanol for 5 min, one bath of 90% ethanol for 5 min, one bath of 70% ethanol for 5 min, one bath of 50% ethanol for 5 min, and one bath of distilled water for 5 min (use glass containers for slides).

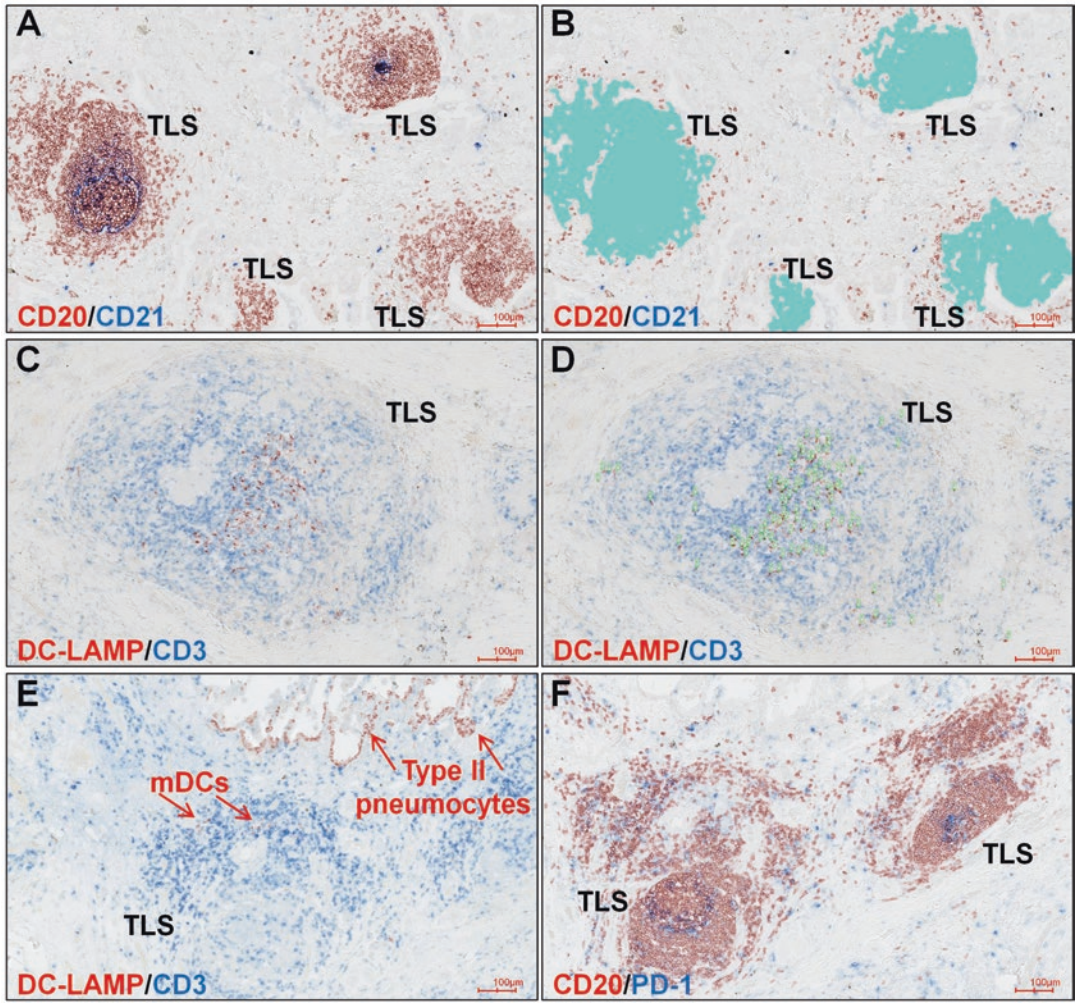

Fig. 1 TLS visualization and quantification through three different double IHC. (**a**, **b**) IHC staining of a FFPE section from NSCLC tumor with anti-human CD20 (in red) and anti-human CD21 (in blue). (**a**) Visualization of four TLS-associated B-cell follicles, subsequently identified by Calopix software (**b**) during automatic quantification. (**c–e**) IHC staining of a FFPE section from NSCLC tumor with anti-human DC-LAMP (in red) and anti-human CD3 (in blue). (**c** and **e**) Visualization of DC-LAMP$^+$ mDCs forming clusters with CD3$^+$ T cells within a TLS. (**d**) DC-LAMP$^+$ mDCs are manually identified (small numbers "1") and counted by two independent observers using Calopix software. (**e**) Illustration of the difficulty of performing an automatic counting of DC-LAMP$^+$ cells with Calopix software in NSCLC tumors, as type II pneumocytes are also visualized with DC-LAMP staining. (**f**) IHC staining of a FFPE section from NSCLC tumor with anti-human CD20 (in red) and anti-human PD-1 (in blue), for T_{FH} cell visualization within two TLS. (**a–f**) Scale bar = 100 μm. Abbreviations: *IHC* Immunohistochemistry, *FFPE* Formalin-fixed paraffin-embedded, *mDC* Mature dendritic cell, *NSCLC* Non-small cell lung cancer, *TLS* Tertiary lymphoid structure

3. Retrieve antigen: Immerse the slides in a bath of pre-warmed antigen retrieval solution (citrate, pH6) for 30 min at 97 °C (in a water bath; use a plastic container for slides).
4. Take out the plastic container from the water bath and let it cool for 30 min at room temperature, on the bench.
5. Wash the slides in TBS for 5 min under agitation (use a glass container for slides) (*see* **Note 2**).
6. Remove the excess of buffer with absorbent papers (*see* **Notes 3** and **4**).
7. Place the slides in a humidified chamber.
8. Cover the tissue with 200 µL of 3% H_2O_2, for 10 min, at room temperature (for saturation of the endogenous peroxidases).
9. Wash the slides in 1× TBS for 1 min.
10. Remove the excess of buffer with absorbent papers.
11. Cover the tissue with 200 µL of 5% HS, for 30 min, at room temperature (for saturation of the receptors for the Fc portion of immunoglobulins).
12. Simply remove the excess of 5% HS with absorbent papers (do not wash).
13. Cover the tissue with 200 µL of primary antibody solution (anti-human DC-LAMP 1/80e + anti-human CD3 1/80e in antibody diluent Dako REAL™), for 1 h, at room temperature.
14. Wash the slides in 1× TBS-T for 5 min, under gentle agitation, twice.
15. Remove the excess of buffer with absorbent papers.
16. Cover the tissue with 200 µL of secondary antibody solution (anti-rat IgG-biotin 1/500e + anti-rabbit IgG-AP 1/300e in 1× TBS), for 30 min, at room temperature.
17. Wash the slides in 1× TBS-T for 5 min, under gentle agitation, twice.
18. Remove the excess of buffer with absorbent papers.
19. Cover the tissue with 200 µL of tertiary reagent (streptavidin-HRP 1/300e in 1× TBS), for 30 min, at room temperature.
20. Wash the slides in 1× TBS-T for 5 min, under gentle agitation, twice.
21. Wash the slides in 1× TBS for 5 min, under gentle agitation.
22. Remove the excess of buffer with absorbent papers.
23. DC-LAMP immunostaining revelation with AEC: Cover the tissue with 200 µL of AEC solution (prepared according to the manufacturer's instructions, in distilled water), for up to 30 min, at room temperature (DC-LAMP-immunostained

cells appear in red (Fig. 1c), check under the microscope) (*see* **Note 5**).

24. Stop the reaction in a bath of 1× TBS, for 5 min, under gentle agitation.
25. Remove the excess of buffer with absorbent papers.
26. CD3 immunostaining revelation with SAP: Cover the tissue with 200 µL of SAP solution (prepared according to the manufacturer's instructions, in 0.1 M Tris–HCl pH 8.2, and supplemented with Levamisole, to inhibit endogenous alkaline phosphatases, 1 drop per mL of SAP solution), for 10–30 min maximum, at room temperature (CD3-immunostained cells appear in blue (Fig. 1c), check under the microscope).
27. Stop the reaction in a bath of 1× TBS, for 5 min, under gentle agitation.
28. Wash the slides in distilled water, for 5 min, under gentle agitation.
29. Remove the excess of buffer with absorbent papers.
30. Mount the slides with glass coverslips using glycergel (liquefied by heating at 70 °C).
31. Let the slides dry overnight at room temperature before storing.

3.3 Double Immunohistochemistry Anti-human CD20/Anti-human CD21 for TLS-Associated T_{FH} Cell Visualization

1. Dry the tissue sections for a minimum of 30 min (or overnight) in a drying oven at 37 °C.
2. Deparaffinize the tissue sections: Under a laboratory fume hood, immerse the slides in three successive baths of 100% xylene (or Clearene) for 5 min each, then in one bath of absolute ethanol for 5 min, one bath of 90% ethanol for 5 min, one bath of 70% ethanol for 5 min, one bath of 50% ethanol for 5 min, and one bath of distilled water for 5 min (use glass containers for slides).
3. Retrieve antigen: Immerse the slides in a bath of pre-warmed antigen retrieval solution (TRS, pH6) for 30 min at 97 °C (in a water bath; use a plastic container for slides).
4. Take out the plastic container from the water bath and let it cool for 30 min at room temperature, on the bench.
5. Wash the slides in TBS for 5 min under agitation (use a glass container for slides) (*see* **Note 2**).
6. Remove the excess of buffer with absorbent papers (*see* **Notes 3** and **4**).
7. Place the slides in a humidified chamber.
8. Cover the tissue with 200 µL of 3% H_2O_2, for 10 min, at room temperature (for saturation of the endogenous peroxidases).

9. Wash the slides in 1× TBS for 1 min.
10. Remove the excess of buffer with absorbent papers.
11. Cover the tissue with 200 µL of 5% HS, for 30 min, at room temperature (for saturation of the receptors for the Fc portion of immunoglobulins).
12. Simply remove the excess of 5% HS with absorbent papers (do not wash).
13. Cover the tissue with 200 µL of primary antibody solution (anti-human PD-1 pre-diluted + anti-human CD20 1/250e, in anti-human PD-1 pre-diluted solution), for 1 h and 30 min, at room temperature.
14. Wash the slides in 1× TBS-T for 5 min, under gentle agitation, twice.
15. Remove the excess of buffer with absorbent papers.
16. Cover the tissue with 200 µL of secondary antibody solution (anti-mouse IgG2a-biotin 1/100e + anti-mouse IgG1 1/30e in 1× TBS), for 30 min, at room temperature.
17. Wash the slides in 1× TBS-T for 5 min, under gentle agitation, twice.
18. Remove the excess of buffer with absorbent papers.
19. Cover the tissue with 200 µL of tertiary reagent (streptavidin-HRP 1/300e + APAAP 1/30e in 1× TBS), for 30 min, at room temperature.
20. Wash the slides in 1× TBS-T for 5 min, under gentle agitation, twice.
21. Wash the slides in 1× TBS for 5 min, under gentle agitation.
22. Remove the excess of buffer with absorbent papers.
23. CD20 immunostaining revelation with AEC: Cover the tissue with 200 µL of AEC solution (prepared according to the manufacturer's instructions, in distilled water), for up to 30 min, at room temperature (CD20-immunostained cells appear in red (Fig. 1f), check under the microscope) (*see* **Note 5**).
24. Stop the reaction in a bath of 1× TBS, for 5 min, under gentle agitation.
25. Remove the excess of buffer with absorbent papers.
26. PD-1 immunostaining revelation with SAP: Cover the tissue with 200 µL of SAP solution (prepared according to the manufacturer's instructions, in 0.1 M Tris–HCl pH 8.2, and supplemented with Levamisole, to inhibit endogenous alkaline phosphatases, 1 drop per mL of SAP solution), for 10–30 min maximum, at room temperature (PD-1-immunostained cells appear in blue (Fig. 1f), check under the microscope).

27. Stop the reaction in a bath of 1× TBS, for 5 min, under gentle agitation.
28. Wash the slides in distilled water, for 5 min, under gentle agitation.
29. Remove the excess of buffer with absorbent papers.
30. Mount the slides with glass coverslips using glycergel (liquefied by heating at 70 °C).
31. Let the slides dry overnight at room temperature before storing.

4 Image Analysis and TLS Quantification

4.1 TLS-Associated B-Cell Follicle Quantification

TLS-associated B-cell follicle quantification can be performed automatically, using an image analysis software (Calopix software), after scanning of the whole slide using a slide scanner (NanoZoomer slide scanner).

1. Import the image generated after scanning of the slide into the Calopix database.
2. Delineate the "region of analysis" (ROA): In the case of NSCLC tumor tissue, the region of analysis corresponds to the tumor area, including the invasive margin; necrotic areas are excluded.
3. Use the "Ilastik" tool to educate the software: Create a protocol with five different classes, for (1) red $CD20^+$ B cells, (2) blue $CD21^+$ FDCs, (3) black anthracosis, (4) white empty spaces, and (5) the rest of the tissue (i.e., the tumor nests, tumor stroma, and remodeled lung tissue at the invasive margin); save the protocol for subsequent application to the complete tissue.
4. Launch a "Tissue recognition for surface quantification" analysis on Calopix: This protocol determines the ratio (expressed as a percentage) between a numerator corresponding to the surface (in mm^2) of the area of interest and a denominator corresponding to the surface (in mm^2) of the total tissue. In this case, the numerator is the total surface of all TLS-associated B-cell follicles, identified by red $CD20^+$ B cells (class 1) and/or blue $CD21^+$ FDCs (class 2) (Fig. 1a), and the denominator is the total surface of the region of analysis, after exclusion of white empty spaces (class 4):

$$\frac{[\text{class 1} + \text{class 2}]}{[\text{class 1} + \text{class 2} + \text{class 3} + \text{class 5}]} \times 100 = \frac{\text{TLS-associated B-cell follicles}\left(\text{in mm}^2\right)}{\text{Total tissue}\left(\text{in mm}^2\right)} \times 100$$
$$= \text{Density of TLS-associated B-cell follicles}(\%)$$

During the analysis, a size criterion for TLS-associated B-cell follicle surface is used: only TLS-associated B-cell follicles with a minimum surface of 7000 μm² are considered and included in the numerator (Fig. 1b) (*see* **Note 7**).

4.2 TLS-Associated mDC Quantification

When immunostained with anti-DC-LAMP antibody, mDCs within TLS are visualized as very small red dots (like nuclear circular structures), scattered among blue CD3⁺ T cells (Fig. 1c, e). Sometimes, very thin, free dendrites are visible. However, in lungs including NSCLC, immunostaining with DC-LAMP marker stains not only mDCs but also type II pneumocytes (Fig. 1e). The presence of two different types of red-colored cells in a same area limits the full-automated counting of mDCs using the aforementioned Calopix software. However, TLS-associated mDC quantification can be performed semiautomatically, using Calopix for determining total tissue surface area, but with the manual counting of the red DC-LAMP⁺ mDCs within blue CD3⁺ T cell areas by two independent observers.

1. Import the image generated after scanning of the slide (on NanoZoomer slide scanner) into the Calopix database.
2. Delineate the "region of analysis" (ROA): In the case of NSCLC tumor tissue, the region of analysis corresponds to the tumor area, including the invasive margin; necrotic areas are excluded.
3. Use the "Ilastik" tool to educate the software: Create a protocol with three different classes, for (1) tissue, (2) black anthracosis, and (3) white empty spaces; save the protocol for subsequent application to the complete tissue.
4. Launch a "Tissue recognition for surface quantification" analysis on Calopix: Exclude class 3 while launching the protocol. This protocol determines the surface (in mm²) of the total tissue within the ROA, that is, tumor nests, tumor stroma, and invasive margin.
5. For counting manually DC-LAMP⁺ mDCs, first screen the entire slide to pre-visualize the mDCs within the T-cell areas of TLS.
6. In the window "Annotations" of Calopix, use the tool "counter" to start the manual counting. On the slide, left click on each DC-LAMP⁺ mDC within the predetermined ROA: each click appears as a small number "1" on the slide (Fig. 1d), and is incremented in the "Annotations" window of Calopix.
7. The final count can be exported from the "Annotations" window into a separate Excel file.
8. Divide this final count by the surface area (in mm²) previously determined to get the density of DC-LAMP⁺ mDCs in the tissue section (expressed as a number of cells per mm²).

4.3 Full TLS Visualization After Image Registration of Three Serial Tissue Sections: CD20/CD21 (B-Cell Follicles and FDCs), DC-LAMP/CD3 (mDCs and T-Cell Areas), and CD20/PD-1 (B-Cell Follicles and T_{FH})

The complete characterization of fully active TLS within a (tumoral) inflamed tissue may require the simultaneous identification, localization, and quantification of several immune cell populations and subpopulations on the same tissue section. By IHC, it is theoretically possible to distinguish up to three different immuno-markers, as images are usually recorded with RGB cameras. However, in practice, it is difficult to distinguish more than two chromogens on the same slide. In this regard, immunofluorescence (IF) presents some advantages, as signals from different fluorochromes can be acquired independently. In conventional fluorescence microscopy, up to four biomarkers (or three biomarkers plus counterstained nuclei) can be easily recorded with standard equipment. For higher degrees of multiplexing, several problems may arise, including potential antibodies' cross-reaction but also difficulties in secondary fluorescence signal detection and separation. Indeed, when more than four biomarkers are used simultaneously, in order to distinguish the different fluorochromes, image acquisition has to be done with a spectral imager, either a spectral confocal laser scanning microscope or a conventional optical microscope equipped with a spectral detector. The multispectral data acquired have then to be processed with a spectral unmixing software. This method allows the simultaneous detection of up to six fluorescent biomarkers associated with nuclear counterstaining, but still suffers from some drawbacks, including a time-consuming process of labeling, pricey reagents, and expensive equipment for image acquisition. In addition, those equipment are usually not able to acquire very large image mosaics (WSI), or only at low speed as compared to conventional slide scanners. Finally, some errors in spectral unmixing, which is an image processing step, can arise.

Virtual multiplexing methods have also been proposed and represent affordable alternatives. One strategy is to perform on the same tissue section sequential standard immuno-peroxidase labelings, with imaging and then erasing of the staining obtained between each labeling ("SIMPLE" method). It has been shown that up to six consecutive staining/erasing steps can be achieved [22]. This method has the advantage to allow the use of standard reagents and imaging equipment but is still time consuming. A more simple approach consists of performing IHC (and/or IF) labelings on serial tissue sections [23]. This technique has to be performed on maximum 3–5 μm thick consecutive sections to obtain good results, and has for main limitation that antigen co-expression at the cell level can only be checked on one unique tissue section. However, this method can be performed with standard procedures and equipment, and enables to determine the co-localization and thus the potential interactions of several different cell types in specific tissue areas.

A crucial point for these two methods is the image registration process, which allows the comparison of different labelings from

consecutive (different) tissue sections in the same tissue area. Image registration consists of computing a geometric transform that maps points from one image, the moving image, to homologous points in a fixed reference image. This transform is called rigid when the spatial transform is limited to translation, rotation, scaling, shearing, or a combination of those operations, and is called deformable or elastic when local displacements are also allowed. Usually, B splines are used to keep the track of those local deformations. An optimizer routine then tests different geometric transforms by evaluating the similarity between the moving image and the reference image until an optimal transform is found. The similarity is quantified at each step of the optimization by some metrics, for example the sum of squared differences between the pixel intensity of the two images.

Image registration methods have been well developed for many years in different domains such as satellite imagery, radiology imagery, and even histology, for example for the reconstruction of monomodal (single stained) 3D serial sections. Indeed, registration of histological images is a well-studied field of research, and issues such as nonlinear deformation, steering, shearing, folding, or shrinking due to tissue processing have been addressed and have received some solutions. Multimodal image series (images of different labelings from different tissue sections) registration presents additional challenges. As pixel values can vary a lot for different labelings in the same area of tissue, the metrics used to quantify the similarity between the modalities has to be chosen carefully. Usually, the metrics successfully used in monomodal image series registration fail when applied to the registration of multimodal image series. Alternatively, landmark points positioned on remarkable features of the images can be used by the registration algorithm so that their distance in both images is minimized at the end of the process. The landmark points can be selected manually by the user or determined automatically by an algorithm. The use of landmark points is generally a good strategy for the registration of multimodal images; however the selection of landmark point positions can be imprecise, hence limiting the accuracy of the registration.

Finally, an additional challenge is the usually huge size of the WSI created by the slide scanners. The most straightforward strategy for WSI registration is to perform at first a registration at low magnification, followed by a registration at high magnification on a small field of view based on the results of the low-magnification registration.

4.3.1 Registration with ImageJ Software

ImageJ (IJ) is a well-known image processing and analysis open-source software [24]. It is used in many domains of scientific imaging and especially in microscopy. The FIJI version of ImageJ [25] is bundled with many plug-ins dedicated to microscopy image processing and analysis, including image registration tools. However,

the main drawback of IJ is its limitation regarding the size of the images it can manage. Indeed, IJ is only able to deal with images smaller than 2^{31} pixels (about 46,000 × 46,000 pixels), even if enough memory is allocated to the software. This restrains the use of this tool to small or low-resolution virtual sections. Another limitation of IJ is the slide scanner's file formats it can open. Nearly each slide scanner vendor uses its own file format. To open those different file formats in FIJI, the "LOCI's Bio-Formats importer" plug-in [26] may be useful. However, it can only deal with some of them. Fortunately, regarding the file format generated by the NanoZoomer slide scanner (Hamamatsu), an IJ plug-in, "NDPItools," has been developed recently [27], making those files convenient for IJ.

Among the different tools for image registration available in FIJI we used two plug-ins based on their performances and ease of use: the "Linear stack alignment with SIFT" written by Dr. Stephan Saalfeld, based on the SIFT algorithm [28], and the "Stackreg" plug-in [29], which is based on the minimization of the sum of squared differences between the pixel intensity of the two images. The "Scale Invariant Feature Transform" (SIFT) algorithm finds automatically distinctive features in both images, and identifies those that are matched. Then, a geometric transform is applied to the moving image so that the distance between matching points is minimized. This tool gave good results in our hands. In contrast, because of the metrics it uses, "Stackreg" is not well adapted to the registration of multimodal images and is more suited to the registration of monomodal images. However, "Stackreg" is very fast and easy to use and we found that it gives satisfactory results when the labelings present in the different images to register are roughly localized in the same tissue areas.

In the case when significant physical deformations of the tissue sections appeared during sample preparation, elastic registration may be required. In this situation "BUnwarpJ" [30] proved its usefulness. This plug-in can run fully automatically, or with user-defined landmarks. It also accepts landmarks automatically defined by the SIFT algorithm which is also present in FIJI, as a stand-alone plug-in (plugin>feature extraction>Extract SIFT correspondences). Unfortunately, "BUnwarpJ" will function only on small images as it requires a large amount of memory, and thus can only be used for the registration of WSI at very low resolution.

4.3.2 Installation of FIJI and Required Plug-ins

1. Download and install the FIJI version corresponding to your computer's operating system from this web page: https://fiji.sc/#download.
2. Check that enough memory is allocated to IJ: Edit>Options>Memory & threads. Usually about 75% of the computer RAM can be used by IJ.

3. Download and install "NDPItools" plug-in from this web page: http://www.imnc.in2p3.fr/pagesperso/deroulers/software/ndpitools/.
4. Download NDPItools.jar and copy this file in the /Fiji.app/plugins folder or alternatively drag and drop the NDPItools.jar file on the FIJI menu bar when FIJI is started.

4.3.3 Register Whole-Tissue Sections at Low Magnification

1. Extract the different layers of the NPDI pyramidal file using Plugins>NDPI tools>Extract to tiff. The plug-in will try to load the highest resolution layer. This usually fails because of the size of the image. As a result, a message error box will pop up. Close it and go on for the next step.
2. Load the required layer using NDPI tools>Open Tiff (not higher than 5× because 20× images are usually too big to be loaded).
3. Repeat the process (**steps 4** and **5**) for the different WSI to register (*see* **Note 8**).
4. Put the different images in one image stack using Image>Stacks>image to stack (copy center).
5. Plugins>Registration>Linear Stack Alignment with SIFT.
6. Save the registered image stack (File>Save as TIFF format).

4.3.4 Register Selected Areas at High Magnification

1. Load low-resolution preview of the WSI using NDPItools>PreviewNDPI.
2. Draw a region of interest (ROI) with the rectangle selection tool of the IJ menu bar (*see* **Note 9**).
3. Extract this region using NDPItools>Extract to TIFF format.
4. Repeat **step 1** with the next WSI to register.
5. Copy the ROI of interest on this preview image: Edit>Selection>restore Selection. Move the position of the ROI to the desired area (drag and drop the selection).
6. Repeat **steps 4** and **5** if other WSI have to be registered.
7. Close all the preview images.
8. Put the different images in one image stack using Image>Stacks>image to stack (copy center).
9. Plugins>Registration>linear Stack Alignment with SIFT.
10. Save the registered image stack (File>Save as TIFF format) (Fig. 2a–c).

Fig. 2 (continued) DC-LAMP/anti-human CD3 IHC, and (**c**) double anti-human CD20/anti-human PD-1 IHC. Regions of whole-slide image (WSI) were extracted at 20× resolution and registered, as described in Subheading 4.3.4. (**d–f**) An area containing a TLS was then cropped from these registered images. (**g–l**) Stainings were separated using the color deconvolution function of ImageJ, contrast inverted (**g–k**), and then overlaid (**l**). (**a–c**) Scale bar = 2.5 mm. (**d–l**) Scale bar = 250 μm. Abbreviation: *IHC* Immunohistochemistry

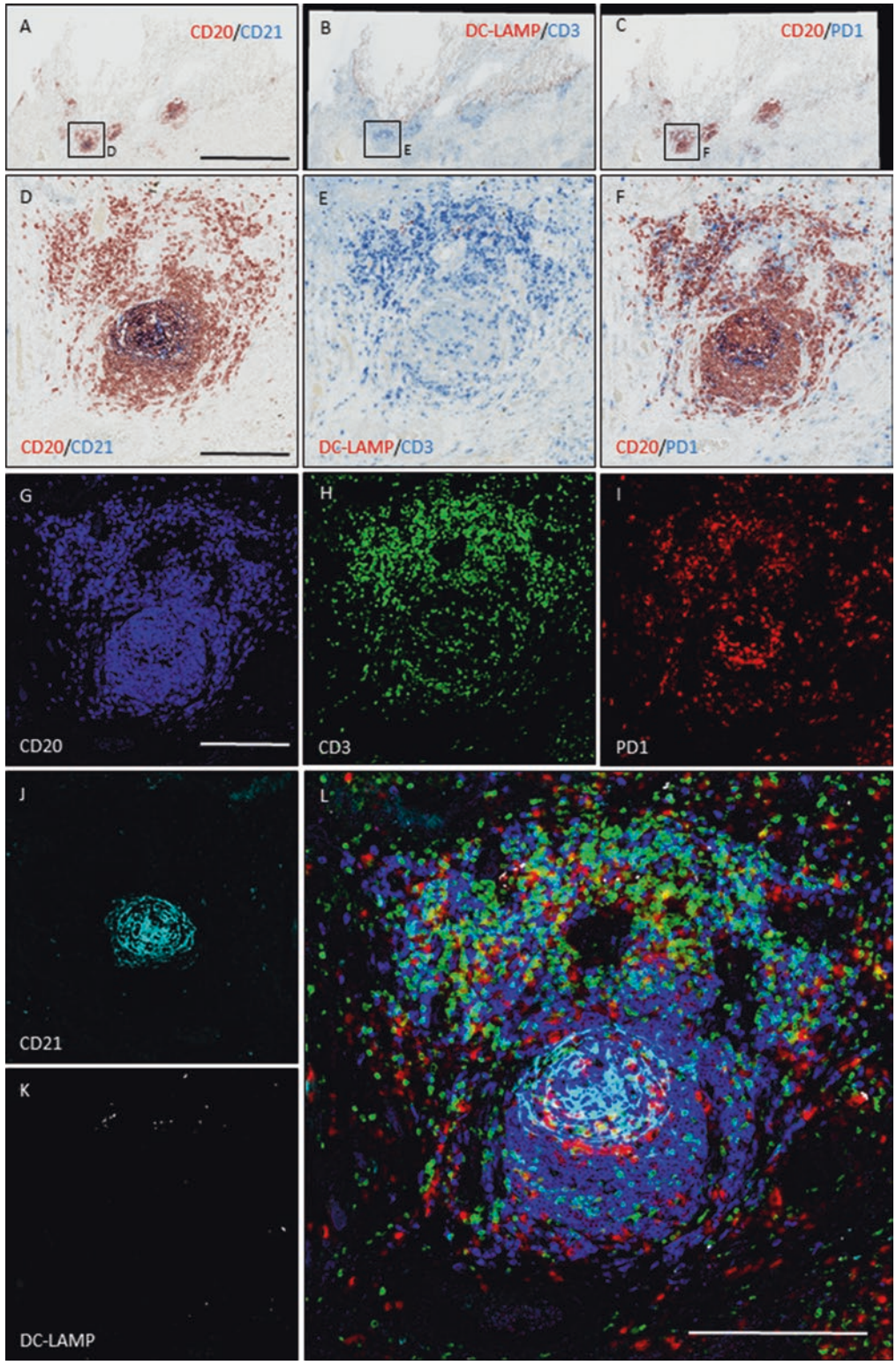

Fig. 2 Full TLS visualization after image registration of three serial tissue sections. (**a**–**c**) Registration of selected areas at high magnification, from (**a**) double anti-human CD20/anti-human CD21 IHC, (**b**) double anti-human

4.3.5 Overlay of the Registered Images

1. Draw a ROI corresponding to one TLS.
2. Crop the stack using Image>Crop.
3. Split the images from the stack using Image>Stacks>Stack to Images (Fig. 2d–f).
4. For each image, separate the stainings, using Image>Color>Color Deconvolution.
5. Keep only the useful images containing one labeling. Invert the contrast using Edit>Invert.
6. Apply the desired color map on each image: Image>Look Up Tables. Choose among Gray, Red, Green, Blue, Cyan, Magenta, and Yellow (Fig. 2g–k).
7. Create the overlay using Image Color>Merge Channels (Fig. 2l).

4.3.6 Registration of WSI at Full Resolution

Of course, the usefulness of the registration of WSI at low resolution or of small areas at full resolution is limited, except for demonstrative purpose. For analysis purpose, it is highly desirable to register full-resolution WSI. In this regard, open-source solutions have been proposed using "Elastix," a free software based on the ITK library [31, 32]. More recently, a plug-in was developed [33] for the open-source software "ICY" [34] as well as a stand-alone software named "Hyper-Stain inspector" [35]. However those solutions are still experimental and not well suited for the analysis of large-scale datasets containing several tenths of WSI images. At this time, the best solution is to use commercially available software such as the "Visiopharm Visiomorph" software and its WSI registration module "TISSUEALIGN." This module allows the registration of several WSI either automatically or thanks to landmarks manually defined by the user. This task is achieved with a good accuracy and speed. It is also possible to register IF images together with bright-field (IHC) images. Once registered, a stack of WSI is obtained. It is then possible to define ROIs on a reference slide, for example on a hematoxylin and eosin-stained tissue sections, and to report those ROIs on the other registered images for analysis in the same areas at full resolution, if required.

5 Notes

1. Anti-human DC-LAMP clone 1010E1.01 also displays a cross-reactivity with canine, feline, murine, and sheep DC-LAMP.
2. In each protocol, after antigen retrieval, it is possible to let the slides in a bath of 1× TBS overnight at room temperature before continuing the experiment (**step 5** in Subheadings 3.1, 3.2, and 3.3).
3. When removing the excess of buffer with absorbent papers, pay attention to the tissue.

4. Process the slides one by one: Do not let the slides dry for longer than 1 min before adding the following reagent, to avoid tissue alteration and staining background.
5. During the revelation steps (**steps 23–26** in Subheadings 3.1, 3.2, and 3.3), the substrate for HRP (AEC) is commonly added first. However, it is also possible to add first the substrate for AP (SAP).
6. For double IHC anti-human CD20/anti-human CD21, carefully check under the microscope CD21 staining. CD21 in blue must not be too dark for subsequent analysis on Calopix software (otherwise it can be confounded with black anthracosis in the lung).
7. During TLS-associated B-cell follicle quantification, red $CD20^+$ B-cell aggregates without the presence of blue $CD21^+$ FDCs are also considered as TLS-associated B-cell follicles (quantified) (Fig. 1a, b), provided that they display a minimum surface of 7000 μm^2 (the visualization or not of FDCs within B-cell follicles may strongly depend on the tissue section).
8. Instead of different IHC stainings performed on serial tissue sections, the different WSI to register may also correspond to sequential IHC stainings performed on the same tissue section, with steps of imaging and then erasing of the staining obtained between each labeling (multiplexed IHC). In that case, image registration is much less challenging.
9. For image registration, during the "registration of selected areas at high magnification," the selected areas have to be large enough to contain a sufficient amount of unambiguous features.

Funding

This work was supported by the "Institut National de la Santé et de la Recherche Médicale (INSERM), Sorbonne University, Paris-Descartes University, the Labex Immuno-Oncology (LAXE62_9UMRS872 Fridman), CARPEM (Cancer Research for PErsonalized Medicine), Fondation ARC pour la Recherche sur le Cancer. Priyanka Devi-Marulkar was supported by a grant from the Fondation ARC pour la Recherche sur le Cancer. Claire Germain was supported by a grant from MedImmune LLC.

References

1. Dieu-Nosjean M-C, Antoine M, Danel C et al (2008) Long-term survival for patients with non–small-cell lung cancer with intratumoral lymphoid structures. J Clin Oncol 26:4410–4417
2. Germain C, Gnjatic S, Tamzalit F et al (2014) Presence of B cells in tertiary lymphoid structures is associated with a protective immunity in patients with lung cancer. Am J Respir Crit Care Med 189:832–844

3. Thaunat O, Patey N, Morelon E et al (2006) Lymphoid neogenesis in chronic rejection: the murderer is in the house. Curr Opin Immunol 18:576–579
4. Cipponi A, Mercier M, Seremet T et al (2012) Neogenesis of lymphoid structures and antibody responses occur in human melanoma metastases. Cancer Res 72:3997–4007
5. Gottlin EB, Bentley RC, Campa MJ et al (2011) The Association of Intratumoral Germinal Centers with early-stage non-small cell lung cancer. J Thorac Oncol Off Publ Int Assoc Study Lung Cancer 6:1687–1690
6. Goc J, Germain C, Vo-Bourgais TKD et al (2014) Dendritic cells in tumor-associated tertiary lymphoid structures signal a Th1 cytotoxic immune contexture and license the positive prognostic value of infiltrating CD8+ T cells. Cancer Res 74:705–715
7. Teillaud J-L, Dieu-Nosjean M-C (2017) Tertiary lymphoid structures: an anti-tumor school for adaptive immune cells and an antibody factory to fight cancer? Front Immunol 8:830
8. Drayton DL, Liao S, Mounzer RH et al (2006) Lymphoid organ development: from ontogeny to neogenesis. Nat Immunol 7:344–353
9. Aloisi F, Pujol-Borrell R (2006) Lymphoid neogenesis in chronic inflammatory diseases. Nat Rev Immunol 6:205–217
10. Dieu-Nosjean M-C, Goc J, Giraldo NA et al (2014) Tertiary lymphoid structures in cancer and beyond. Trends Immunol 35:571–580
11. Neyt K, Perros F, GeurtsvanKessel CH et al (2012) Tertiary lymphoid organs in infection and autoimmunity. Trends Immunol 33:297–305
12. Baddoura FK, Nasr IW, Wrobel B et al (2005) Lymphoid neogenesis in murine cardiac allografts undergoing chronic rejection. Am J Transplant Off J Am Soc Transplant Am Soc Transpl Surg 5:510–516
13. Kerjaschki D, Regele HM, Moosberger I et al (2004) Lymphatic neoangiogenesis in human kidney transplants is associated with immunologically active lymphocytic infiltrates. J Am Soc Nephrol JASN 15:603–612
14. Thaunat O, Patey N, Caligiuri G et al (2010) Chronic rejection triggers the development of an aggressive intragraft immune response through recapitulation of lymphoid organogenesis. J Immunol Baltim Md 1950 185:717–728
15. Thaunat O, Field A-C, Dai J et al (2005) Lymphoid neogenesis in chronic rejection: evidence for a local humoral alloimmune response. Proc Natl Acad Sci U S A 102:14,723–14,728
16. Moyron-Quiroz JE, Rangel-Moreno J, Kusser K et al (2004) Role of inducible bronchus associated lymphoid tissue (iBALT) in respiratory immunity. Nat Med 10:927–934
17. Messina JL, Fenstermacher DA, Eschrich S et al (2012) 12-Chemokine gene signature identifies lymph node-like structures in melanoma: potential for patient selection for immunotherapy? Sci Rep 2:765
18. Coppola D, Nebozhyn M, Khalil F et al (2011) Unique ectopic lymph node-like structures present in human primary colorectal carcinoma are identified by immune gene array profiling. Am J Pathol 179:37–45
19. Gu-Trantien C, Loi S, Garaud S et al (2013) CD4+ follicular helper T cell infiltration predicts breast cancer survival. J Clin Invest 123:2873–2892
20. Wirsing AM, Rikardsen OG, Steigen SE et al (2014) Characterisation and prognostic value of tertiary lymphoid structures in oral squamous cell carcinoma. BMC Clin Pathol 14:38
21. Sautès-Fridman C, Lawand M, Giraldo NA et al (2016) Tertiary lymphoid structures in cancers: prognostic value, regulation, and manipulation for therapeutic intervention. Front Immunol 7:407
22. Glass G, Papin JA, Mandell JW (2009) SIMPLE: a sequential immunoperoxidase labeling and erasing method. J Histochem Cytochem Off J Histochem Soc 57:899–905
23. Potts S, Johnson T, Voelker F, et al (2014) Methods for feature analysis on consecutive tissue sections, http://www.freepatentsonline.com/8787651.html
24. Schneider CA, Rasband WS, Eliceiri KW (2012) NIH Image to ImageJ: 25 years of image analysis. Nat Methods 9:671–675
25. Schindelin J, Arganda-Carreras I, Frise E et al (2012) Fiji: an open-source platform for biological-image analysis. Nat Methods 9:676–682
26. Linkert M, Rueden CT, Allan C et al (2010) Metadata matters: access to image data in the real world. J Cell Biol 189:777–782
27. Deroulers C, Ameisen D, Badoual M et al (2013) Analyzing huge pathology images with open source software. Diagn Pathol 8:92
28. Lowe DG (2004) Distinctive image features from scale-invariant keypoints. Int J Comput Vis 60:91–110
29. Thévenaz P, Ruttimann UE, Unser M (1998) A pyramid approach to subpixel registration based on intensity. IEEE Trans Image Process Publ IEEE Signal Process Soc 7:27–41
30. Arganda-Carreras I, Sorzano COS, Marabini R et al (2006) Consistent and elastic registration

of histological sections using vector-spline regularization. In: Beichel RR, Sonka M (eds) Computer vision approaches to medical image analysis. Springer, Berlin, Heidelberg, pp 85–95

31. Mueller D, Vossen D, Hulsken B (2011) Real-time deformable registration of multi-modal whole slides for digital pathology. Comput Med Imaging Graph Off J Comput Med Imaging Soc 35:542–556
32. Moles Lopez X, Barbot P, Van Eycke Y-R et al (2015) Registration of whole immunohistochemical slide images: an efficient way to characterize biomarker colocalization. J Am Med Inform Assoc 22:86–99
33. Obando DFG, Frafjord A, Øynebråten I, et al (2017) Multi-staining registration of large histology images, In: 2017 IEEE 14th International Symposium on Biomedical Imaging (ISBI 2017), pp. 345–348
34. de CF, Dallongeville S, Chenouard N et al (2012) Icy: an open bioimage informatics platform for extended reproducible research. Nat Methods 9:690–696
35. Trahearn N, Epstein D, Cree I et al (2017) Hyper-stain inspector: a framework for robust registration and localised co-expression analysis of multiple whole-slide images of serial histology sections. Sci Rep 7:5641

Chapter 5

A Quantitative Pathology Approach to Analyze the Development of Human Cancer-Associated Tertiary Lymphoid Structures

Karīna Siliņa, Chiara Burkhardt, Ruben Casanova, Alex Solterman, and Maries van den Broek

Abstract

Tertiary lymphoid structures (TLS) develop in the human tumor microenvironment and correlate with prolonged survival in most cancer types. We recently demonstrated that TLS development follows sequential maturation stages and culminates in the generation of a germinal center (GC) reaction. This maturation process is crucial for the prognostic relevance of TLS in lung and colorectal cancer patients.

The mechanisms underlying TLS development in various inflammatory conditions or their functional relevance in tumor immunity are not fully understood. Investigating which cell types and soluble mediators orchestrate lymphoid neogenesis in human tissues requires a method that allows simultaneous detection of multiple markers.

Here, we describe a quantitative pathology approach to identify and quantify different TLS maturation stages in combination with other parameters. This approach consists of seven-color immunofluorescence protocol using tyramide signal amplification combined with multispectral microscopy and quantitative data acquisition from histological images.

Key words Germinal center, Tertiary lymphoid structure, Lymphoid organ neogenesis, Cancer, Quantitative pathology, Multispectral imaging, Multispectral microscopy, Vectra, Tyramide signal amplification, Immunofluorescence

1 Introduction

Lymphoid neogenesis resulting in the development of tertiary lymphoid structures (TLS) occurs under chronic inflammatory conditions and involves different cell types including perivascular stromal cells, B cells, high endothelial venules (HEVs), T cells, macrophages, and dendritic cells (DCs) (reviewed in [1, 2]). We recently demonstrated that TLS development in the microenvironment of lung and colorectal cancer follows sequential maturation stages [3, 4]. The process begins with the accumulation of

Marie-Caroline Dieu-Nosjean (ed.), *Tertiary Lymphoid Structures: Methods and Protocols*, Methods in Molecular Biology, vol. 1845, https://doi.org/10.1007/978-1-4939-8709-2_5,

lymphocytes in response to chemokine cues. Next, follicular dendritic cells (FDCs) differentiate to generate TLS that resemble primary follicles of the secondary lymphoid organs. Finally, a germinal center (GC) reaction develops resulting in TLS that resemble secondary follicles. The presence of TLS in human tumor microenvironment is often associated with improved patient outcome [2, 5, 6]. We showed that the generation of GCs was crucial for the prognostic power of TLS in untreated lung and colorectal cancer patients [4]. This suggests that TLS promote antitumor immunity. However, despite the frequent observation of GC-containing TLS in various human tissues, the molecular and cellular mechanisms that initiate TLS development and drive TLS maturation in different inflammatory contexts are incompletely understood.

The dissection of the interplay between different cell types and signaling molecules leading to TLS formation within the histological context requires the detection of multiple parameters on tissue sections. We focus here on immunofluorescence because it enables analysis of more markers simultaneously than bright-field imaging. Several intrinsic limitations must be considered when using immunofluorescent staining of multiple parameters on the same tissue section. First, the signal of tissue immunofluorescence has lower intensity when compared to flow cytometry, which often precludes the use of directly labeled primary antibodies. In such cases, signal amplification using labeled secondary antibodies is necessary. Second, the limited number of species in which most primary antibodies are produced thus restricts the number of markers one can analyze within the same tissue section. This obstacle can, however, be overcome by using tyramide signal amplification (TSA): Dye-conjugated tyramide molecules are activated by horseradish peroxidase (HRP), which initiates a radical chain reaction leading to the covalent binding of dye-tyramide residues to the antibody-bound protein [7]. Because of this permanent labeling, the detection antibodies can be removed by heating without losing the fluorescent signal of the target antigen. A second antigen can now be detected using primary antibodies raised in the same species as for the first antigen, followed by HRP-conjugated secondary antibody and a tyramide conjugated to a different dye. This detection/removal process can be repeated several times. TSA considerably increases the detection sensitivity of tissue immunostaining [7], thus allowing the detection of molecules that are present in low concentrations such as secreted cytokines.

Multispectral imaging (MSI) is a recent technological advancement that allows increasing the number of fluorescent colors that can be simultaneously detected by a conventional fluorescence microscope [8]. MSI also provides the possibility to separate tissue autofluorescence from the specific fluorophore signals. This involves the use of a multispectral camera for the acquisition of spectral profiles of each individual fluorophore as well as the spec-

tral profile of tissue autofluorescence using unstained tissue. Further, using a dedicated image-processing software, the spectral profiles present in each pixel can be assigned to specific fluorophores and/or autofluorescence through a process called spectral unmixing. Thus, the main factor limiting the number of parameters that can be detected simultaneously is the spectral overlap of fluorophores, which cannot be properly unmixed if their emission spectra overlap too much. The development of fluorophores with narrower emission spectra in combination with the multispectral imaging and TSA currently allows for robust seven-color immunofluorescence protocols. This number may still increase by development of new dyes.

Here, we describe a quantitative pathology approach for the analysis of TLS in different maturation stages and in combination with other relevant TLS-associated cell types including HEVs and conventional DCs. This method can be further adapted to other tissues or scientific questions. To distinguish the different TLS maturation stages, a minimal combination of CD20, CD21, and CD23 expression needs to be analyzed. The remaining three markers can be used to assess chemokine expression, vasculature, tissue-specific niche cells, or other parameters.

The method we developed and describe here consists of (i) immunostaining of formalin-fixed paraffin-embedded (FFPE) human tissues for the detection of six markers plus a nuclear staining, (ii) multispectral imaging using the Vectra 3.0™ automated microscopy system (PerkinElmer), and (iii) image data analysis using Inform™ (PerkinElmer) and RStudio software. We provide details on tissue slide preparation, staining procedure using tyramide-conjugated Opal™ dyes (PerkinElmer), multispectral image acquisition, and analysis of quantitative imaging data using tissue and cell segmentation algorithms of Inform™ software (PerkinElmer).

2 Materials

2.1 Preparation of FFPE Tissue Slides

1. Freshly cut FFPE tissue sections (2–5 μm) on routine pathology glass slides (*see* **Note 1**) including sections from secondary lymphoid organs.
2. 55 °C Incubator.
3. Pressure cooker (routine kitchen cooker, 5 L) and stove for antigen retrieval by autoclaving (*see* **Note 2**).
4. Metal forceps, at least 20 cm long.
5. Pretreatment and antigen retrieval buffer: 1× Trilogy™ solution (Cell Marque) (*see* **Note 3**).

6. Heat-resistant slide trays (glass jars with glass slide holders or plastic 50 mL tubes, depending on the number of slides being processed simultaneously) for antigen retrieval.
7. Regular slide trays for washing steps.
8. Washing buffer (WB): 1× Phosphate-buffered saline (PBS) containing 0.1% (v/v) Triton X-100.
9. Rocking platform.
10. PAP pen, for example ImmEdge Hydrophobic Barrier PAP Pen (Vector Laboratories) (*see* **Note 4**).
11. 3% H_2O_2 (v/v) in double-distilled water (ddW).
12. Wet chamber (a tray with a lid containing a support for holding slides and water).

2.2 Immunostaining of Human FFPE Tissues

1. Blocking buffer (BB): 4% Bovine serum albumin (w/v), 4% normal donkey serum (v/v) in WB.
2. 37 °C Incubator.
3. Antibody-dilution buffer (ADB): 1% Bovine serum albumin (w/v), 1% normal donkey serum (v/v) in WB.
4. Primary antibodies (Table 1): Rabbit anti-human CD3 (clone SP7), mouse anti-human CD20 (clone L26), rat anti-mouse/human PNAd (clone MECA-79), rat anti-mouse/human DC-LAMP (clone 1010E1.01), rabbit anti-human CD23 (clone SP23), mouse anti-human CD21 (clone 2G9) (*see* **Note 5**).
5. HRP-conjugated secondary antibodies (Table 1): Donkey anti-rabbit IgG (H+L), donkey anti-mouse IgG (H+L), donkey anti-rat IgG (H+L), goat anti-rat IgM (μ chain specific)

Table 1
Immunostaining reagents for the analysis of TLS in human tissues

Maker	Antibody clone	Antibody dilution	Producer, catalogue number	HRP-conjugated secondary antibody[a]
CD21	2G9	1:5000	Leica, NCL-L-CD21-2G9	Donkey anti-mouse IgG
DC-LAMP	1010E1.01	1:1000	Dendritics	Donkey anti-rat IgG
CD23	SP23	1:1000	Abcam, ab16702	Donkey anti-rabbit IgG
PNAd	MECA-79	1:5000	Biolegend, 120801	Goat anti-rat IgM
CD20	L26	1:5000	Dako	Donkey anti-mouse IgG
CD3	SP7	1:1000	Thermo Fisher	Donkey anti-rabbit IgG

[a]All HRP-conjugated secondary antibodies were purchased from Jacksons ImmunoResearch. The optimal working dilutions were 1:500 for anti-mouse IgG, anti-rat IgM, and IgG, and 1:1000 for anti-rabbit IgG

Table 2
The detection of each fluorescently stained marker by Vectra 3.0™

Maker	Fluorophore, dilution	Excitation (nm)	Emission (nm)	Detection filter
Nucleus	DAPI, 1:10	358	461	2
CD21	Opal-520, 1:100	494	525	3
DC-LAMP	Opal-540, 1:100	523	536	4
CD23	Opal-570, 1:100	550	570	4, 5
PNAd	Opal-620, 1:150	588	616	5
CD20	Opal-650, 1:150	627	650	6
CD3	Opal-690, 1:50	676	694	6

with minimal cross-reactivity to immunoglobulins from other species (*see* **Note 6**).

6. Tyramide-fluorophore conjugates: Opal™ 7-color Manual IHC Kit (PerkinElmer) (Table 2). This kit also contains the Amplification Diluent buffer necessary for generating the working dilutions of the tyramide-conjugated dyes. The kit contains an optimized combination of six modified fluorescent dyes with narrow emission spectra and the nuclear stain 4′,6-diamidino-2-phenylindole (DAPI). The use of such dyes is crucial for multispectral image processing to enable unmixing of the spectra from dyes that are detected with the same emission filter.
7. 95 °C Water bath (*see* **Note 7**).
8. Heat-resistant slide trays (glass jars with glass slide holders or plastic 50 mL tubes, depending on the number of slides being processed simultaneously) for antibody removal.
9. Regular slide trays for washing steps.
10. Antibody removal buffer (ARB): 10 mM Citric acid, pH 6.0.
11. WB, rocking platform, and wet chamber, as in Subheading 2.1.
12. Antifade mounting medium without DAPI like ProLong™ Diamond (Thermo Fisher) (*see* **Note 8**).
13. Glass coverslips.

2.3 Multispectral Imaging

1. Vectra 3.0™ multispectral imaging system (PerkinElmer).
2. Mounted tissue slides:
   (a) A fully unstained tissue section that has been subjected to the same processing protocol as the stained slides (antigen retrieval, blocking, washing, heating) but omitting all

fluorescent dyes. This slide is necessary to determine the spectral profile of autofluorescence of the tissue of interest (*see* **Note 9**).

(b) Tissue sections that have been stained with only one fluorescent dye, including a separate slide for the DAPI staining (*see* **Note 10**). These slides are necessary to determine the spectral profile of each dye used in the multiplex protocol.

(c) Slides stained with the seven-color protocol.

2.4 Image and Data Processing

1. Phenochart™ software (PerkinElmer).
2. Inform™ software (PerkinElmer).
3. RStudio software (*see* **Note 11**).

3 Methods

3.1 Immunostaining

The protocol described here has been optimized for the manual processing of up to 20 slides in parallel with the least possible number of heating steps for antibody removal to reduce the risk of tissue and epitope damage. If not indicated otherwise, all steps are performed at room temperature (RT). During all incubation steps the sections should be protected from light (i.e., washing containers and wet chambers covered with aluminum foil). Apart from the slides of interest, ten additional slides must be included (*see* above under **step 2** in Subheading 2.3): one slide that is not stained with any of the fluorophores, seven slides that are stained with each individual fluorophore only, one negative control slide where all primary antibodies are omitted, and one positive control slide (any of the secondary lymphoid organs). The single-color and unstained slides need to be included only once if the same combination of fluorescent dyes is used and the same tissue is analyzed. The single-stained slides are necessary for the generation of the spectral profile for each dye and the unstained slide is necessary to establish the autofluorescence profile of the tissue of interest. These spectral profiles are used for the unmixing of fluorophore signals in the multiplex-stained tissue sections using the Inform™ software. Of note, positive and negative control slides need to be included in every experiment.

3.1.1 Slide Pre-processing

1. Incubate FFPE tissue slides at 55 °C for 2–16 h.
2. Prepare two equal heat-resistant glass trays containing 1× Trilogy™ solution. Place slides in a glass slide holder and transfer it into one of the trays so that all tissues are fully immersed in the buffer without filling the tray to the brim. Leave the second tray with an equal amount of Trilogy™ solution without slides.

3. Fill the pressure cooker with 2 L of ddW, and place a heat-resistant platform (e.g., an autoclavable tip box) to prevent submersion of the slide trays inside the pressure cooker.
4. Cover both trays with loose lids and place them in the pressure cooker on a stove. Close the lid of the pressure cooker, turn the stove on, and wait until the pressure has reached its maximum, which is indicated by the fully lifted pressure nob on the pressure cooker's lid.
5. Autoclave the slides for 15 min, then remove the cooker from the heat, and release the pressure by keeping the pressure nob lifted using long forceps or other heat-resistant tool (*see* **Note 12**).
6. Immediately after opening the pressure cooker, carefully transfer the slides to the second tray containing the hot Trilogy™ solution. Do not shake any of the trays or the slides to avoid boiling retardation, which will damage the tissue.
7. Incubate slides in the second tray for 5 min to remove remaining paraffin residues.
8. Transfer the slides to another tray containing ddW and place it on a rocking platform for 5 min (*see* **Note 13**).
9. One by one, dry the glass area surrounding the tissue with a paper napkin and encircle the tissue with the PAP pen. Do not allow the tissue to dry at any time throughout the duration of the protocol.
10. Place slides in a wet chamber with tissue facing upwards, apply 3% H_2O_2 solution, and incubate for 15 min to block endogenous peroxidases. Depending on the size of the tissue section, 100–300 μL/slide is sufficient.
11. Decant the H_2O_2 solution and wash the slides in WB for 15 min on a rocking platform.
12. Continue with immunostaining or leave the slides in the WB at 4 °C until further use (*see* **Note 14**).

3.1.2 Immunostaining

1. Place slides in a wet chamber with tissue facing upwards, apply BB, and incubate for 15 min at 37 °C. Depending on the size of the tissue section, 100–300 μL/slide is sufficient.
2. Decant BB; place slides back in the wet chamber; apply the first primary antibody mix in ADB containing mouse anti-human CD21, rabbit anti-human CD23, and rat anti-mouse PNAd antibodies; and incubate at 4 °C overnight. Depending on the size of the tissue section, 50–150 μL/slide is sufficient (*see* **Notes 5** and **15**).
3. Decant the primary antibody mixture and wash in WB for 3 × 5 min on a rocking platform.

4. Place slides in a wet chamber with tissue facing upwards, apply the first HRP-conjugated secondary antibody (anti-mouse IgG in ADB), and incubate for 1 h (*see* **Note 6**). Depending on the size of the tissue section, 50–150 μL/slide is sufficient.
5. Decant the secondary antibody mix and wash in WB for 3 × 5 min on a rocking platform.
6. Place slides in a wet chamber with tissue facing upwards, apply the first tyramide-fluorophore conjugate Opal-520 diluted in the amplification diluent buffer, and incubate for 10 min to detect the CD21 antigen (*see* **Note 16**).
7. Decant the tyramide-dye mix and wash in WB for 5 min on a rocking platform.
8. Place slides in a wet chamber with tissue facing upwards, apply 3% H_2O_2, and incubate for 30 min to block the activity of the first HRP-conjugated secondary antibody (*see* **Note 17**).
9. Decant the H_2O_2 solution and wash the slides in WB for 15 min on a rocking platform.
10. Place slides in a wet chamber with tissue facing upwards, apply the second HRP-conjugated secondary antibody (donkey anti-rabbit IgG in ADB), and incubate for 1 h (*see* **Note 6**). Depending on the size of the tissue section, 50–150 μL/slide is sufficient.
11. Repeat **steps 5–9**, but use the tyramide-fluorophore conjugate Opal-570 to detect CD23 antigen.
12. Place slides in a wet chamber with tissue facing upwards, apply the third HRP-conjugated secondary antibody (goat anti-rat IgM in ADB), and incubate for 1 h (*see* **Note 6**). Depending on the size of the tissue section, 50–15 μL/slide is sufficient.
13. Repeat **steps 5–7**, but use the tyramide-fluorophore conjugate Opal-620 to detect PNAd antigen.
14. Place slides in a heat-resistant tray containing ARB such that tissues are covered and the tray is not filled to the brim.
15. Place the tray in a 95 °C water bath for 10 min to remove the bound antibodies.
16. Wash the slides in WB for 10 min on a rocking platform.
17. Place slides in a wet chamber with tissue facing upwards, apply BB, and incubate for 15 min at 37 °C. Depending on the size of the tissue section, 100–300 μL/slide is sufficient.
18. Decant BB; place slides back in the wet chamber; apply the second primary antibody mix in ADB containing mouse anti-human CD20, rabbit anti-human CD3, and rat anti-mouse DC-LAMP antibodies; and incubate overnight at 4 °C (*see*

Note 5). Depending on the size of the tissue section, 50–150 μL/slide is sufficient.

19. Repeat **steps 3–13**, but use donkey anti-mouse IgG, donkey anti-rabbit IgG, and donkey anti-rat IgG antibodies with tyramide-fluorophore conjugates Opal-650, Opal-690, and Opal-540 to detect CD20, CD3, and DC-LAMP antigens, respectively.
20. Place slides in a wet chamber with tissue facing upwards, apply the DAPI solution (2 drops/1 mL PBS), and incubate for 5 min. Depending on the size of the tissue section, 100–300 μL/slide is sufficient.
21. Decant the DAPI solution and wash slides in WB for 5 min on a rocking platform.
22. One by one, mount the coverslips using an antifade mounting medium that is suitable for the detection of fluorophores emitting also in the far-red spectrum (*see* **Note 8**).
23. Store slides at 4 °C until imaging as well as for long-term storage.

3.2 Multispectral Imaging

The process described below corresponds to the standard operating procedure of the Vectra 3.0™ multispectral imaging system with automated slide loading. This microscope is equipped with a LED white and UV light source, 1 bright-field (position 1) and 5 fluorescence excitation/emission filters (positions 2–6), and the Nuance™ multispectral camera (PerkinElmer). The excitation/emission data and the respective detection filters for each fluorophore/maker are depicted in Table 2.

3.2.1 Establishment of Imaging Protocol

For clarity, in the description of the use of the dedicated software, we have highlighted buttons and tabs in bold italics and the options of choice in italics.

1. Using the ***Edit Protocol*** tab of Vectra™ software, indicate the use of 10× objective for the whole-slide overview scan and 20× objective for the multispectral high-power field (HPF) acquisition. Determine the optimal exposure times for each of the five fluorescent channels for each of the objectives using slides that have been stained with only a single fluorophore. Exposure times between 50 and 100 ms are recommended. Set *DAPI* as the reference signal for finding the focal plane and choose the *Saturation Protection* option. Save the scanning protocol in the respective study folder.
2. Using the single-color-stained slides and the determined exposure times, find an optimal region of interest with the highest marker expression and acquire a multispectral HPF snapshot

for each individual fluorophore. Save these snapshots under the respective fluorophore name.

3. Using the unstained slide and the determined exposure times, acquire a multispectral HPF snapshot of a tissue area containing blood vessels, fibers, or other autofluorescent structures. Save this snapshot under the Autofluorescence name.

3.2.2 Slide Scanning

1. Using the ***Scan Slides*** tab of Vectra™ software, generate the task list containing the slide names with the respective positions in the slide-loading cassette, indicate the name of the generated scanning protocol, and choose the *Prescan* task, which will generate whole-slide overview scans.
2. Perform whole-slide scans of all slides of interest stained with the seven-color protocol.
3. Open whole-slide scan images using Phenochart™ software and select the regions of interest for multispectral HPF acquisition for all slides of interest, optimally containing one TLS per HPF.
4. In the ***Scan Slides*** tab of Vectra™ software, modify the task list by selecting the *Acquire MSI Fields* task, which will automatically find the position of the selected HPFs from the position annotations generated by Phenochart™ software for each slide.
5. Perform multispectral HPF acquisition.

3.3 Image Analysis

3.3.1 Spectral Unmixing

1. Generate the spectral library of the used fluorophores by choosing the ***Build Library*** tab in Inform™ software. Open the multispectral HPF snapshots of each individual fluorophore, extract, and save the respective spectral profiles (Fig. 1, top left).
2. Open 3–5 multispectral HPF images from each slide of interest and the Autofluorescence image in Inform software™. To perform spectral unmixing, select the seven fluorophores from the generated spectral library. Using the ***Autofluorescence Selection*** tool draw a line over the regions with most autofluorescent signal in the Autofluorescence image. By clicking on the ***Prepare Slides*** button, the software will perform unmixing of all indicated fluorophore and autofluorescence profiles, which can now be viewed as individual channels or in any combination assigning colors as necessary (Fig. 1, top right). Figure 2a depicts the detection of each individual marker and the marker combination in human tonsil. Figure 2b (left) depicts a GC-containing TLS in a human lung tumor section. Next, save the established image view settings as an Inform™ project file.

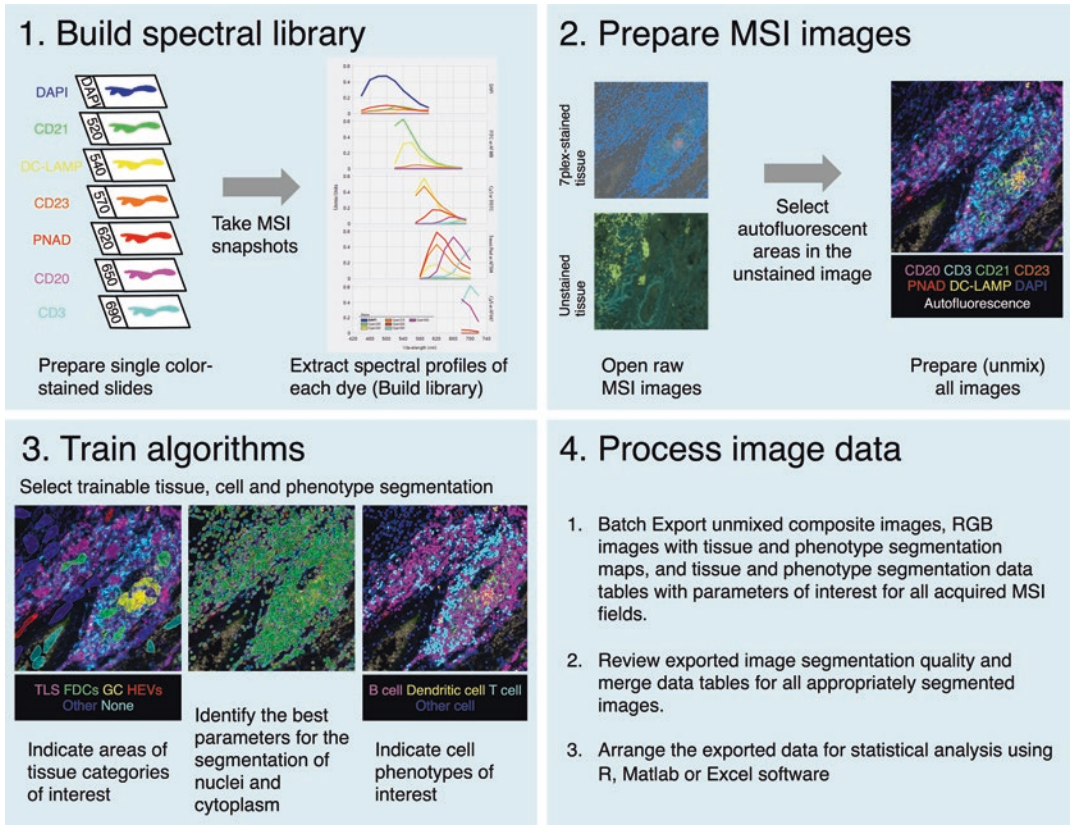

Fig. 1 Multispectral image analysis workflow. Schematic representation of the main four steps of multispectral image analysis using the Inform™ software. Representative images of lung cancer tissues undergoing each processing step are shown

3.3.2 Tissue and Cell Segmentation

1. ***Configure*** the Inform™ project by activating the *Trainable Tissue Segmentation*, *Cell Segmentation*, and *Phenotyping* options. Because FDCs and HEVs are cells with highly irregular shape, we recommend using tissue segmentation rather than cell segmentation for quantification of these cell types. The cell segmentation and phenotyping algorithms can be reliably trained to recognize T cells, DCs, and B cells.
2. In the ***Tissue Segmentation*** tab, generate tissue segmentation categories named Germinal Centre, Follicular Dendritic Cells, B Cell Cluster, High Endothelial Venule, Other, and Empty. Next, mark training areas corresponding to each of the generated tissue categories: (i) germinal centers that are positive for CD20, CD21, and CD23; (ii) areas with follicular dendritic cells that are positive for CD21 and CD20 but not CD23; (iii) areas containing dense B cell aggregates that are positive for CD20 but not CD21 and CD23; (iv) areas containing PNAd signal; (v) all other areas containing tissue; and (vi) empty spaces (Fig. 1, bottom left). Train tissue segmentation algo-

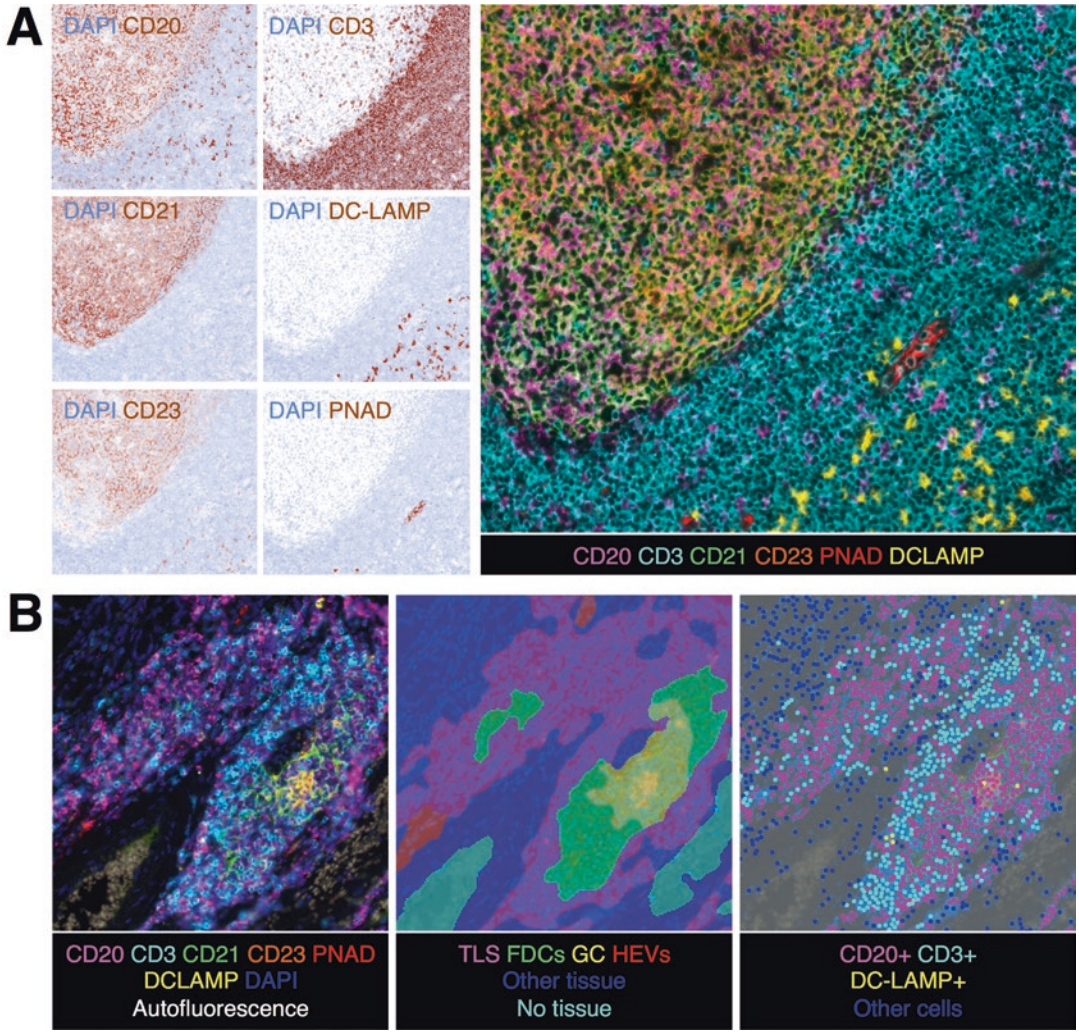

Fig. 2 MSI of seven-color immunostained human tissues for the analysis of TLS. Tissue sections were immunostained to detect B cells (CD20), T cells (CD3), mature dendritic cells (DC-LAMP), high endothelial venules (PNAd), follicular dendritic cells (CD21), and germinal centers (CD23) in combination with the nuclear stain DAPI using the Opal™ 7-color Manual IHC Kit (PerkinElmer). Multispectral images were acquired with the automated microscopy system Vectra 3.0™ (PerkinElmer). Autofluorescence profile was determined in unstained human lung tumor tissue and each individual marker signal was unmixed using Inform™ software (PerkinElmer). (**a**) Human tonsil tissue was used as a positive control, and each individual marker staining is displayed as a pseudo-bright-field image and the composite image depicting the tissue expression of all analyzed markers. (**b**) A representative image of a GC-positive TLS in human lung tissue from a lung cancer patient with autofluorescent erythrocytes (left); image overlaid with tissue segmentation map (middle) and cell phenotype map (right)

rithm using pattern scale *Large* and segmentation resolution *Fine* until the training indicator stops moving. Check the quality of the algorithm by segmenting all images in the project and retrain, as required. Figure 2b (middle) depicts an example of a segmentation map of human lung tissue containing TLS from a lung cancer patient.

3. Proceed with the ***Cell Segmentation*** tab and train the cell segmentation algorithm based on *Nuclear Counterstain DAPI*. Next, segment the cytoplasm as a 4-pixel band surrounding the nucleus (Fig. 1, bottom left).
4. Proceed with the ***Phenotyping*** tab and train the cell phenotyping algorithm. First, generate phenotype categories to be detected: T cell, mature dendritic cell, B cell, and other. Next, assign at least 30 cells corresponding to each category and train the algorithm. Test the performance of the algorithm by segmenting all images in the project and retrain, as required (Fig. 1, bottom left). Figure 2b (right) depicts an example of detected cell phenotypes in lung tissue containing TLS from a lung cancer patient.

3.3.3 Image Data Processing

1. **Export** the Composite images and RGB images with Tissue segmentation map and with Phenotype map and the Tissue segmentation and Cell segmentation Tables (Fig. 1, bottom right).
2. In the **Review and Merge** tab of Inform™ software, select the folder containing the exported data. This opens a review window where exported images can be verified and images with mistakes in segmentation or artifacts can be excluded from the final data file. After reviewing all images, click on the **Merge** button to generate a merged text file containing data from all approved images. This also creates a second file containing data from the rejected images (Fig. 1, bottom right).
3. Using RStudio, create an Excel file by arranging the data from the merged text file according to tissue categories for each patient, and generate a summary data table containing the information about the size of analyzed tissue categories and the number of each cell phenotype in the different tissue categories for each patient (Fig. 1, bottom right). The data can now be subjected to various statistical analyses. Specific R scripts are available upon request.

4 Notes

1. Cut FFPE tissue sections can be stored at 4 °C for up to 3 months without apparent decrease in signal for the described antigens.
2. A microwave, which allows for the regulation of power intensity, can be used instead of a pressure cooker (*see* the Opal™ 7-color Manual IHC Kit description for the requirements of the microwave).

3. We have compared the Trilogy™ solution pretreatment with the conventional pretreatment protocol (xylene deparaffinization, graded ethanol rehydration, and antigen retrieval by autoclaving in 10 mM citric acid pH 6.0, or Tris–EDTA buffer pH 9.0) and found that the immunostaining signal intensity was superior for all antibodies using the Trilogy™ solution.
4. We have tested several PAP pens and found that the ImmEdge pen from Vector Laboratories stays on the slides after multiple washing and heating rounds without the necessity to redraw the border, which saves a considerable amount of time especially when processing many slides in parallel.
5. The optimal dilution of the primary antibodies should be determined for your experimental setting and antibody manufacturer. As a rule of thumb, the use of TSA provides strong immunostaining signals using 5–10 times lower primary antibody concentrations than in conventional immunostaining protocols using fluorophore-labeled secondary antibodies.
6. It is important to use secondary antibodies with the least possible cross-reactivity due to the high sensitivity of the tyramide signal amplification approach. The dilutions will depend on the manufacturer.
7. A microwave (*see* **Note 2**) can be used instead of the water bath.
8. Not all antifade mountants are suitable for the detection of far-red dyes. Make sure to use one that is. In our experience, Prolong™ Diamond mounting medium provides reliable detection of all above-described fluorophores for up to 3 months.
9. Use a separate washing tray for the unstained slide to avoid any fluorescent dye transfer especially DAPI from the stained slides.
10. Use separate washing trays for the single Opal™ color-stained slides to avoid any fluorescent dye transfer especially DAPI from other stained slides. This is crucial for the identification of the pure spectral profiles for each dye, which is necessary for the spectral unmixing step by the Inform™ software.
11. Matlab, Excel, or other suitable software can be used instead of RStudio.
12. Protecting your hand with a towel keep the pressure nob lifted. Take care not to release the pressure too fast as this might cause boiling of the solution inside the slide trays causing tissue damage.
13. Using ddW instead of WB for this step makes it easier to dry the glass surface surrounding the tissue in order to draw the barrier.
14. Slides can be kept in the WB at 4 °C for up to 3 days.

15. The incubation time for all antibodies except anti-PNAd could be reduced to 2 h at RT.
16. The manufacturer recommends diluting the Opal™ tyramide-dyes 1:50. In our experience, 1:100 dilution is detected equally well, with the exception of Opal-690. Because Opal-650 and Opal-960 are detected through the same microscope filter (*see* Table 2), it is crucial to establish such antibody and tyramide-dye dilutions that are detected with the same exposure time. A recommended exposure time for all filters is 50–100 ms. In our experience, Opal-650 needs to be diluted 1:150 and Opal-690 1:50 to achieve the same exposure time and to obtain signals that can be reliably unmixed by Inform™ software.
17. Here, we have combined three primary antibodies raised in different species in the same incubation step. This allows to use TSA by sequential incubation of HRP-conjugated secondary antibodies (with minimal cross-reactivity) in combination with H_2O_2 treatment after each tyramide reaction. This quenches the HRP of the previous antibody before applying the next antibody followed by the next tyramide-dye conjugate. This way no heat-induced antibody removal is necessary, which decreases the chance of tissue and epitope destruction and considerably shortens the duration of the manual protocol. Antibody removal by heating is necessary only after all three secondary antibodies have been used in order to proceed with the next round of primary antibodies. If, however, most primary antibodies were raised in the same species, heat-induced antibody removal is necessary after each tyramide reaction. In this case, it is important to determine which epitopes are most sensitive to multiple heating rounds in order to establish the optimal staining order.

Funding

This work was supported by the Swiss National Science Foundation, the Sciex Foundation, the Science Foundation for Oncology, the Cancer League Zurich, the University Research Priority Program "Translational Cancer Research," and the Swiss Cancer League.

References

1. Jones GW, Hill DG, Jones SA (2016) Understanding immune cells in tertiary lymphoid organ development: it is all starting to come together. Front Immunol 7:401. https://doi.org/10.3389/fimmu.2016.00401
2. Silina K, Rulle U, Kalnina Z, Line A (2014) Manipulation of tumour-infiltrating B cells and tertiary lymphoid structures: a novel anti-cancer treatment avenue? Cancer Immunol Immunother 63:643–662. https://doi.org/10.1007/s00262-014-1544-9
3. Posch F, Silina K, Leibl S, Mündlein A, Moch H, Siebenhüner A, Samaras P, Riedl J, Stotz M, Szkandera J, Stöger H, Pichler M, Stupp R, van

den Broek M, Schraml P, Gerger A, Petrausch U, Winder T (2017) Maturation of tertiary lymphoid structures predicts the risk for recurrence in stage II and III colorectal cancer. Oncoimmunology 7(2):e1378844. https://doi.org/10.1080/2162402X.2017.1378844

4. Silina K, Soltermann A, Movahedian Attar F, Casanova R, Uckeley ZM, Thut H, Wandres M, Isajevs S, Cheng PF, Curioni Fontecedro A, Foukas P, Levesque MP, Moch H, Linē A, van den Broek M (2018) Germinal centers determine the prognostic relevance of tertiary lymphoid structures and are impaired by corticosteroids in lung squamous cell carcinoma. Cancer Res 78:1308–1320. https://doi.org/10.1158/0008-5472.CAN-17-1987
5. Dieu-Nosjean MC, Giraldo NA, Kaplon H et al (2016) Tertiary lymphoid structures, drivers of the anti-tumor responses in human cancers. Immunol Rev 271:260–275. https://doi.org/10.1111/imr.12405
6. Sautes-Fridman C, Lawand M, Giraldo NA et al (2016) Tertiary lymphoid structures in cancers: prognostic value, regulation, and manipulation for therapeutic intervention. Front Immunol 7:407. https://doi.org/10.3389/fimmu.2016.00407
7. Faget L, Hnasko TS (2015) Tyramide signal amplification for immunofluorescent enhancement. Methods Mol Biol 1318:161–172. https://doi.org/10.1007/978-1-4939-2742-5_16
8. Mansfield JR (2014) Multispectral imaging: a review of its technical aspects and applications in anatomic pathology. Vet Pathol 51:185–210. https://doi.org/10.1177/0300985813506918

Chapter 6

Multiplex Immunohistochemistry for Image Analysis of Tertiary Lymphoid Structures in Cancer

Keith E. Steele and Charles Brown

Abstract

Multiplex immunohistochemistry allows the demonstration of multiple protein antigens in individual histological sections of formalin-fixed paraffin-embedded tumors or other types of tissue. Carefully designed and optimized immunohistochemistry (IHC) assays not only maximize the information available from limited tissues, but also enable a higher level interpretation of that information by demonstrating the histoanatomical relationships among key cell types which express the included biomarkers. Programmable automated IHC instruments support the development and application of complicated multiplex IHC protocols, help save time and effort, and enhance immunostaining quality and reproducibility. Simple data can be extracted from immunostained tissues to include qualitative (descriptive) findings and semiquantitative analysis. The value of multiplex IHC can be increased further by the utilization of image analysis software either to better visualize multiple markers or by applying suitable digital scoring solutions to capture data (automated pathology).

Here, we describe a five-marker multiplex based on application of two individual assays to serial sections of non-small cell lung carcinoma (NSCLC). We use this assay to label PD1, PD-L1, CD3, CD68, and cytokeratins in relation to tertiary lymphoid structures (TLS) and other regions of the tumor microenvironment. We illustrate how visualization of the immunostaining results can be used to understand TLS organization and other aspects of the tumor microenvironment, and briefly consider means to further yield additional information.

Key words Multiplex immunohistochemistry, Tertiary lymphoid structure, Non-small cell lung carcinoma, Immuno-oncology, Tumor microenvironment, Immune checkpoint molecule, Digital transformation

1 Introduction

The immune response to cancer is fundamentally complex, with a variety of cell types and numerous proteins present in various regions of the tumor microenvironment. In the field of immuno-oncology, the relationships between such cells expressing one or another protein is a particular area for which our understanding seems limited. Tertiary lymphoid structures (TLS) exemplify a

Marie-Caroline Dieu-Nosjean (ed.), *Tertiary Lymphoid Structures: Methods and Protocols*, Methods in Molecular Biology, vol. 1845, https://doi.org/10.1007/978-1-4939-8709-2_6,

microcosm of this overall spatial complexity, and are important in that their presence indicates the existence of an active immune response to a number of cancers [1, 2]. Multiplex immunohistochemistry (IHC) or immunofluorescence (IF) to label multiple proteins in tissue sections is a useful means to get increased amounts of information out of limited available tissues or to demonstrate relationships among several key cell types expressing one or another protein. A number of multiplex IHC and IF methods have been reported, each with advantages and disadvantages [3–8]. As a practical solution suitable for use by most research histopathology laboratories currently, we find the use of multiplex IHC to provide substantial value in understanding the complexity of TLS in terms of the different cell types present and the key immune proteins they express. Further value can be gained when this approach is combined with image analysis.

Here, we demonstrate a single assay that combines two individual chromogenic IHC segments performed on two serial sections of formalin-fixed paraffin-embedded (FFPE) human lung cancer to demonstrate cells that express PD1, PD-L1, CD3, and CD68 in the context of cytokeratins. The complexity of performing this procedure should be obvious, as illustrated by the number of individual reagent steps involved (not counting wash steps). The use of automated immunostaining instruments is therefore almost a requirement to achieve quality results. Based on this combination of multiplex IHC, we illustrate the kinds of information evident in the tumor microenvironment and TLS. And to that, we add digital transformation of classified images to illustrate a "virtual IF"-like single image. This combination takes advantage of the relative simplicity of chromogenic IHC and bright-field digital scanning. It further takes advantage of image analysis to combine these markers to better understand the localization of individual cell types as well as the relationships among the different marker-positive cells within the TLS and other parts of the complex tumor microenvironment. We use this approach to also illustrate how additional data parameters can be generated from images processed in this way.

2 Materials

2.1 Histology

1. Positively charged glass slides, SuperFrost Plus® or equivalent.
2. Coverslips.
3. Coverslip-mounting medium.
4. Standard rotary microtome.
5. Standard heated histology water bath.
6. Research-grade microscope.

2.2 Immuno histochemistry

1. Anti-human PD1 antibody, rabbit (Rb) monoclonal antibody (MAB) (clone D3W4U), to dilute to 0.52 μg/mL in reaction buffer (DAKO, Agilent).
2. Anti-human PD-L1 antibody, Rb MAB (clone SP263), to dilute to 0.5 μg/mL in reaction buffer (Ventana).
3. Anti-human CD3 antibody, Rb MAB (clone 2GV6, Ventana), provided ready to use (RTU).
4. Anti-human CD68 antibody, mouse (Ms) MAB (clone KP-1, Ventana), provided RTU.
5. Anti-human pan-cytokeratin antibodies, Ms MAB (clones AE1/AE3/PCK26, Ventana), provided RTU.
6. Deparaffinization solution 1 (Leica Biosystems), provided RTU.
7. Deparaffinization solution 2 (Ventana), to dilute 1:10 with deionized water (dH_2O).
8. Antigen retrieval solution 1: Tris–EDTA, pH 9.0 (Leica), provided RTU.
9. Antigen retrieval solution 2: Tris–EDTA, pH 9.0 (Ventana), provided RTU (*see* **Note 1**).
10. Antigen retrieval solution 3: Citrate buffer, pH 6.0 (Ventana), provided RTU.
11. Peroxidase blocking solution 1 (Leica), provided RTU.
12. Peroxidase blocking solution 2 (Ventana), provided RTU.
13. Secondary antibody 1: Horseradish peroxidase (HRP), polymer-labeled anti-Rb Ig (Leica).
14. Secondary antibody 2: HRP, polymer-labeled anti-Rb Ig (Ventana).
15. Secondary antibody 3: HRP, polymer-labeled anti-Ms Ig (Ventana).
16. Secondary antibody 4: Alkaline phosphatase (AP), polymer-labeled anti-Ms Ig (Ventana).
17. Chromogen 1: 3,3′-Diaminobenzidine (DAB) (Leica).
18. Chromogen 2: HRP-reactive purple chromogen (Ventana), provided RTU.
19. Chromogen 3: DAB (Ventana).
20. Chromogen 4: AP-reactive yellow chromogen (Ventana).
21. Protease 3 (Ventana).
22. Hematoxylin II (Ventana).
23. Counterstain "bluing" reagent (Ventana), provided RTU.
24. Wash buffer A (Leica).
25. Wash buffer B (Ventana).

26. Wash solution containing detergent (original blue Dawn®): To dilute 2 mL detergent with 200 mL dH_2O.
27. 95% Ethanol.
28. 100% Ethanol.
29. 100% Xylene.
30. Distilled dH_2O.

2.3 Digital Slide Scanning and Image Analysis

1. Digital slide scanner Aperio AT™ turbo scanner (Leica Biosystems).
2. Image viewing and annotation software: Aperio ImageScope™ software version 12.1.0 (Leica Biosystems).
3. Research-grade computer with high-resolution monitor.
4. Interactive touch screen monitor: WACOM model Cintiq21UX (WACOM Co.).
5. Interactive pen (WACOM).

3 Methods

Prepare all bulk instrument reagent solutions according to the manufacturer's instructions, unless otherwise specified below. Follow all safety, hazardous material handling, and hazardous waste disposal procedures according to applicable regulations and institutional requirements. Follow all manufacturer's instructions for use of individual automated IHC instruments, unless otherwise specified below. Wash steps, omitted below, are also to be completed according to the manufacturer's instructions.

3.1 Histology

1. Prepare two serial sections of each test tissue, 4 μm thick.
2. Mount individual sections on positively charged glass slides.
3. Place slides on drying rack and air-dry at room temperature, overnight.

3.2 Immunohistochemistry PD1/PD-L1 (See Note 2)

1. Program the Leica Bond 2 (Leica Biosystems INC) autostaining instrument to complete **steps 2–13** in Subheading 3.2.
2. Load all test specimen slides onto the instrument.
3. Load all positive control tissue slides (*see* **Note 3**).
4. Apply deparaffinization solution 1. Incubate at 100 °C for 30 min.
5. Apply peroxidase blocking solution 1. Incubate at room temperature (RT) for 8 min.
6. Apply antigen retrieval solution 1. Incubate at 100 °C for 30 min.

7. Apply primary antibody 1, anti-PD1 (clone D3W4U). Incubate at RT for 30 min.
8. Apply secondary antibody 1. Incubate at RT for 8 min.
9. Apply chromogen 1 (DAB, Leica). Incubate at RT for 12 min.
10. Reapply antigen retrieval solution 1. Incubate at 95 °C for 12 min (*see* **Note 4**).
11. Apply primary antibody 2, anti-PD-L1 (clone SP263). Incubate at RT for 30 min.
12. Apply secondary antibody 2. Incubate at RT for 8 min.
13. Complete final wash step on the bond instrument.
14. Remove slides and place onto a slide rack in a container of reaction buffer (Ventana) at RT. Rinse two times, for 5 min each.
15. Program the Discovery Ultra (Ventana Medical Systems) autostaining instrument to complete **steps 16–19** in Subheading 3.2.
16. Remove the slides from the reaction buffer and place on the Discovery instrument.
17. Apply chromogen 2 (HRP-reactive purple). Incubate at 37 °C for 28 min (*see* **Note 5**).
18. Apply hematoxylin II nuclear counterstain. Incubate at RT for 16 min.
19. Apply bluing solution. Incubate at RT for 16 min.
20. Remove all slides from the instrument and place onto a slide rack in a solution containing detergent. Rinse for 2 min, two times (*see* **Note 6**).
21. Dehydrate and clear slides in successive solutions of 95% ethanol, 100% ethanol, and 100% xylene.
22. Apply coverslips.

3.3 Immunohistochemistry CD3/CD68/Cytokeratins (See Note 2)

1. Program the Discovery Ultra instrument to complete **steps 2–21** in Subheading 3.3.
2. Load all test specimen slides onto the instrument.
3. Load all positive control tissue slides (*see* **Note 3**).
4. Apply deparaffinization solution 2 per the manufacturer's instructions. Incubate at 69 °C, three changes, 8 min each.
5. Apply antigen retrieval solution 2 (Tris based). Incubate at 96 °C for 64 min.
6. Apply peroxidase blocking solution 2. Incubate at RT for 12 min.
7. Apply primary antibody 3, anti-CD3 (clone 2GV6). Incubate at 36 °C for 28 min.

8. Apply secondary antibody 2. Incubate at 37 °C for 8 min.
9. Apply chromogen 2 (HRP-reactive purple). Incubate at 37 °C for 24 min.
10. Apply antigen retrieval solution 3 (citrate based). Incubate at 92 °C for 8 min (*see* **Note 4**).
11. Reapply antigen retrieval solution 2 (Tris based). Incubate at 92 °C for 8 min (*see* **Note 4**).
12. Apply primary antibody 4, anti-CD68 (clone KP-1). Incubate at 36 °C for 16 min.
13. Apply secondary antibody 3. Incubate at 37 °C for 8 min.
14. Apply chromogen 3 (HRP-reactive DAB). Incubate at 37 °C for 12 min.
15. Reapply antigen retrieval solution 3 (citrate-based). Incubate at 93 °C for 8 min (*see* **Note 4**).
16. Apply protease 3. Incubate at 35 °C for 4 min (*see* **Note 4**).
17. Apply primary antibody 5, anti-pan-cytokeratins (clones AE1, AE3, and PCK26). Incubate at 36 °C for 16 min.
18. Apply secondary antibody 4. Incubate at 37 °C for 4 min.
19. Apply chromogen 4 (AP-reactive yellow). Incubate at 37 °C for 16 min.
20. Apply hematoxylin II nuclear counterstain. Incubate at RT for 16 min.
21. Apply bluing solution. Incubate at RT for 16 min.
22. Remove all slides from the instrument and place onto a slide rack in a solution containing detergent. Rinse for 2 min, three times (*see* **Note 6**).
23. Dehydrate and clear slides in successive solutions of 95% ethanol, 100% ethanol, and 100% xylene.
24. Apply coverslips.
25. Perform quality control of IHC assay performance by examining tonsil tissue positive and negative control slides microscopically to determine the suitability of staining results (*see* **Note 7**).

3.4 Digital Slide Scanning and Image Analysis

1. Program Aperio AT™ turbo scanner (Leica Biosystems) according to the manufacturer's instructions.
2. Load immunostained slides onto scanner.
3. Perform scanning using 20× objective (*see* **Note 8**).
4. View digital images using Aperio ImageScope™ software version 12.1.0 (Leica Biosystems) or alternate software (*see* **Note 9**).
5. Open images of paired serial sections and align side by side.

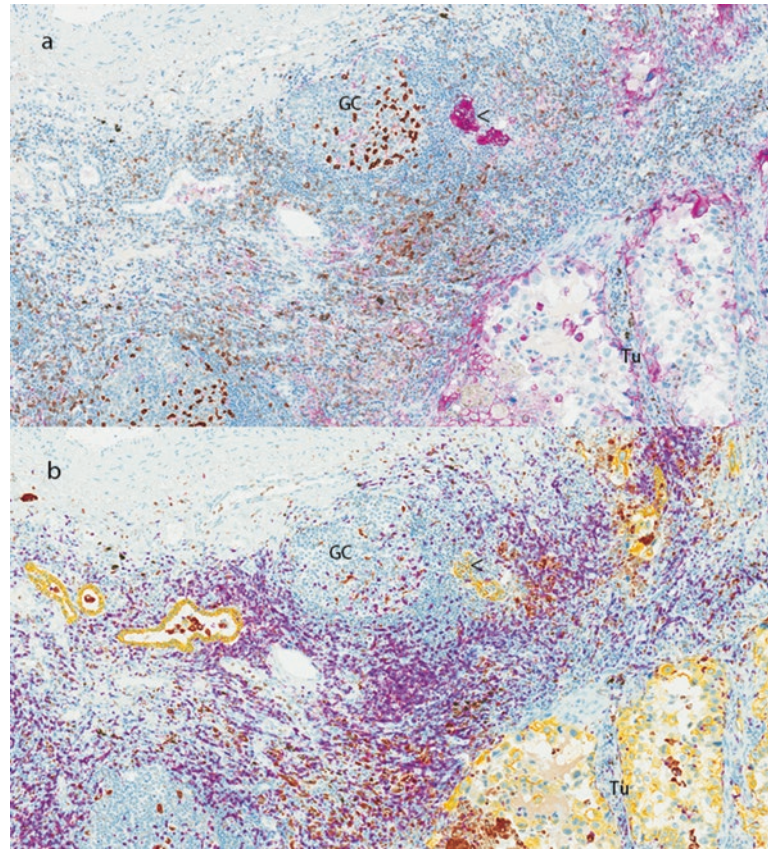

Fig. 1 Duplex (**a**) and triplex (**b**) IHC staining of serial sections of a non-small cell lung carcinoma with TLS. (**a**) PD1 (brown) is combined with PD-L1 (purple) and hematoxylin counterstaining. (**b**) CD3 (purple) is combined with CD68 (brown), pan-cytokeratins (yellow), and hematoxylin counterstaining. $PD1^+$ lymphocytes are intensely labeled in the germinal center (GC) of the TLS and are also present in the parafollicular zone of the TLS and in other regions of the tumor microenvironment. $PD\text{-}L1^+$ cells are co-localized with $PD1^+$ cells in the GC, but are more prominent in the tumor region (Tu), to include neoplastic cells and some infiltrating macrophages. Both $CD3^+$ lymphocytes and $CD68^+$ macrophages are present in the GC, parafollicular zone, and elsewhere in the tumor microenvironment, including a number of macrophages infiltrating tumor islands. A raft of intensely $PD\text{-}L1^+$ cells (arrowhead) is present in the TLS; in the serial section, these cells are also cytokeratin positive, demonstrating their epithelial origin. Original magnification: 200×

6. Perform qualitative and semiquantitative assessment of the numbers, locations, and spatial relationships among marker-positive cells (*see* Fig. 1 and **Note 10**).
7. Perform digital image analysis (*see* **Notes 11** and **12**).

4 Notes

1. Unless otherwise noted, seemingly similar reagents (e.g., Tris–EDTA buffer) are not used interchangeably between automated IHC stainers. We typically utilize the appropriate reagent supplied by each manufacturer for use on their instrument.
2. This combined "5-plex" assay requires two segments of 2 markers + 3 markers because the numbers of quality chromogens available commercially are limited and different chromogens may not have suitable spectral characteristics to combine for a given set of markers on a single tissue section. Thus, our assay represents a compromise approach that requires two tissue sections, to each of which is applied a single combination of markers. As explained subsequently (*see* **Note 12**), it is possible to combine all five markers visually or through the use of digital software that co-registers paired immunostained sections in order to form a single "virtual multiplex" of the combined markers.
3. The specific positive control tissues to be included are at the discretion of the user. Human tonsil contains cells expressing all five markers included in this assay, and is affordable and readily available as FFPE blocks. Human tonsil is therefore recommended. For positive control tissue, pairs of tonsil sections should be run in parallel. One section receives all primary antibodies, in proper sequence, while the second section receives isotype-matched (rabbit and mouse) immunoglobulins in place of the primary antibodies, also in sequence. Duplicate sections of test samples may be included for application of isotype antibodies. We typically do not include them in the assay described. Having optimized and tested these assays in a variety of tumor and normal tissues, we find their inclusion to rarely provide helpful information, that is, unexpected staining patterns (*see* also **Note 7**).
4. The application of these reagents combined with high heat serves as a denaturation step to strip the preceding primary antibody and polymer-labeled enzymes, but not the preceding chromogen. This prevents interference between these molecules and the subsequently applied reagents.
5. The HRP-reactive purple chromogen can currently only be applied on the Ventana autostaining instruments. We find the use of this particular purple chromogen to be very useful for combining with DAB and yellow chromogens. Thus, we feel the effort to transfer slides between instruments is of sufficient value to enable the performance of this and similar multiplex IHC stains done in our lab.

6. This step removes the "liquid coverslip" that is part of the Discovery autostaining instrument prior to dehydration and coverslipping.
7. Microscopic analysis of the positive control tissues is the primary quality control step for each IHC "run." FFPE sections of human tonsil should have all markers included in this multiplex assay present. The exact numbers and locations of cells expressing the five included markers may vary somewhat, however, from one tonsil specimen to another. $PD1^+$ lymphocytes are typically intensely labeled within germinal centers and should also be evident in other locations. $PD\text{-}L1^+$ intensely labeled epithelial cells should be evident in tonsillar crypts and other cells (e.g., macrophages in germinal centers) should also be labeled. $CD68^+$ macrophages should be evident in germinal centers and elsewhere. $CD3^+$ lymphocytes should be evident in T-lymphocyte-dependent regions such as the parafollicular zone, and elsewhere. Cytokeratin labeling should be evident in epithelial cells of the tonsil *per se*, or any adjacent epithelial tissue (e.g., salivary gland) that may also be present. It is important to utilize the same positive control tissue in the case that multiple "runs" of that assay are performed. And then, confirm that the staining qualities of immunostaining for each marker are consistent among the different runs. This quality control aspect is necessary to ensure that both the sensitivity and specificity of staining are appropriate for all runs from which data is generated. In addition, tonsil sections incubated with isotype control immunoglobulins (negative control) should be examined to assess appropriate (i.e., minimal) levels of nonspecific staining. Additional QC of the test slides is also required for general aspects of immunostaining because inappropriate staining of individual slides can occasionally happen, even for those stained on automated instruments.
8. Digital scanning at high magnification is slower and generates image files of greater size than at lower magnification. However, it also provides greater resolution of histological information for either visual inspection or potentially relevant to the quality of image analysis data. We typically scan using a 20× objective lens, but occasionally 40× scans are required. Each user should take these factors into account to determine the image resolution that meets the needs of their study.
9. We frequently use Aperio I ImageScope™ to view images scanned on the Aperio scanner. Other image visualization software may equally serve the needs of other users without access to ImageScope. We also use the proprietary Definiens VeriTrova™ software (Definiens AG, Munich, Germany) for image viewing and to perform other processes related to computational image analysis.

10. The initial value of the multiplexing approach described here is evident in the two separate images shown in Fig. 1 viewed adjacent to each other. Accordingly, PD1$^+$ lymphocytes (Fig. 1a, brown) are conspicuous in the germinal centers (GCs) of TLS of the lung cancer specimen shown. They are present as well in T-zone regions, where they co-localize with CD3$^+$ lymphocytes (Fig. 1b, purple), and also in the tumor microenvironment. Note the intensity of PD1 labeling in the GCs in particular *versus* other PD1$^+$ cells. CD68-positive macrophages (Fig. 1b, brown) are present mainly in GC (i.e., tingible-body macrophages), T-zone regions, and infiltrating tumor islands. A few PD-L1$^+$ cells (Fig. 1a, purple) are present in the GC; however most PD-L1$^+$ cells are neoplastic cells and macrophages of the tumor region (Tu), as well as small rafts of intensely positive epithelioid cells in TLS (arrowheads) that also express cytokeratins (Fig. 1b, yellow). The co-localization with cytokeratins identifies these rafts of PD-L1$^+$ cells as epithelial; however their origin is otherwise uncertain.
11. We use Definiens Developer XD™ software to perform image analysis, though other commercial and publicly available software can be used. We frequently apply regional tissue annotations manually to scanned images prior to image analysis. This serves to partition the subsequent data according to the specific tumor regions in which particular marker-positive cells reside. Manual annotations are done using Aperio ImageScope or Definiens VeriTrova software, and drawn either with a computer mouse or using an interactive pen tool and a touch screen display (e.g., Wacom Cintiq™). Examples of annotations appropriate to analysis of TLS are shown in Fig. 2, representing a larger field of view of the lung tumor shown in Fig. 1. Several TLS are annotated (blue). The tumor invasive margin is annotated separately (green) to mark a band of tissue approximately 500 μm wide and centered on the outermost neoplastic cells. The tumor center represents a third annotation (red) to include tumor inside the invasive margin. The use of suitable image analysis software to classify cells expressing one or another of the five markers included in this multiplex assay can therefore separate data according to these tumor regions.
12. The classification of marker-positive cells by image analysis software (Developer XD™) for individual tumor sections can be digitally overlaid to produce a pseudo-colorized virtual multiplex (*see* Fig. 3). Co-registration of the CD3/CD68/cytokeratins and PD1/PD-L1 images was performed, as previously described [9]. In this image, CD3$^+$ lymphocytes are colored green, PD1$^+$ lymphocytes yellow, CD68$^+$ macrophages blue, and PD-L1$^+$ cells red. Relationships among these various cells can therefore be understood visually in a more direct way. For

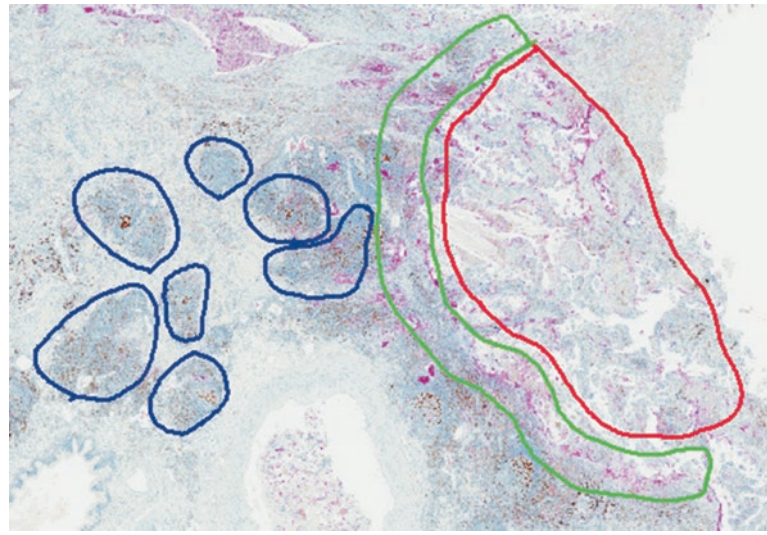

Fig. 2 Manual annotations of different tumor regions for a larger portion of the NSCLC shown in Fig. 1. Shown are several TLS (blue) in the tumor region beyond the invasive margin (green) and tumor center (red). Original magnification: 40×

example, the prevalence of PD1$^+$ cells in the T-lymphocyte-rich zone of the TLS, that is co-localized with CD3$^+$ lymphocytes, becomes more easily seen than in Fig. 1. A limitation of this approach, however, is that detection of co-expression of PD1 and CD3 is not possible, mainly because these two markers were performed on separate tissue sections. Another observation evident here, and one specifically relevant to immune oncology, is the spatial relationship between PD1 and PD-L1 in various regions of the tumor microenvironment. In this single image, a number of PD1$^+$ lymphocytes are nearby to PD-L1$^+$ cells, both in the GC and elsewhere. Such a proximity relationship between this important immuno-inhibitory receptor-ligand pair is relevant and has even previously been reported to correlate with therapeutic response to pembrolizumab in melanoma patients [10].

Acknowledgement

We thank Dr. Tze Heng Tan (Definiens AG, Munich, Germany) for providing the virtual IF rendering included, as Fig. 3.

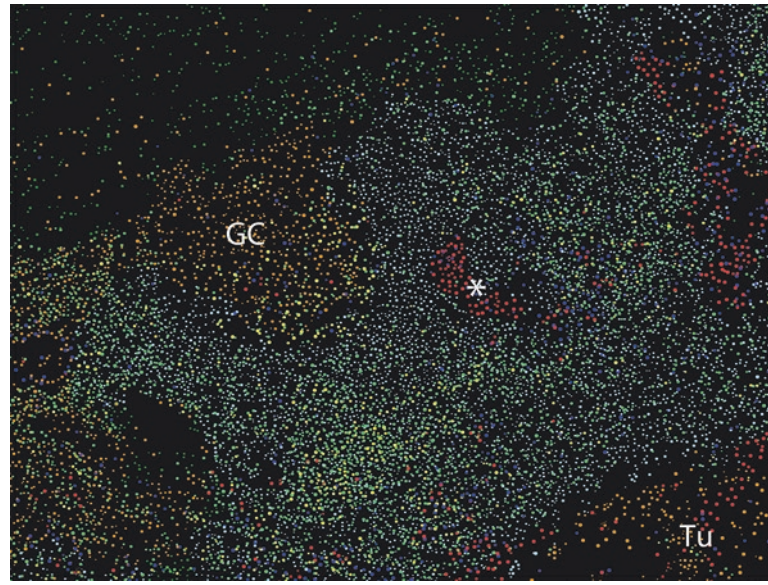

Fig. 3 A virtual immunofluorescence rendering of the combined multiplex IHC images shown in Fig. 1, produced by digital co-registration of the two images. This permits more direct identification of the spatial relationships between markers, for example, PD1$^+$ lymphocytes (yellow) *versus* PD-L1$^+$ cells (red, e.g., macrophages) in the germinal center (GC) and CD3$^+$ lymphocytes (green) and CD68$^+$ macrophages (blue) in multiple regions. A limitation of this approach is the determination of dual-positive cells when markers are applied to separate tissue sections (cytokeratin was intentionally left out of this virtual multiplex to permit visualization of PD-L1$^+$ cells in tumor islands (Tu) and TLS (*) also depicted in Fig. 1). Original magnification: 200×

References

1. Dieu-Nosjean M-C, Antoine M, Danel C et al (2008) Long-term survival for patients with non–small-cell lung cancer with intratumoral lymphoid structures. J Clin Oncol 26:4410–4417
2. Lutz ER, Wu AA, Bigelow E et al (2014) Immunotherapy converts nonimmunogenic pancreatic tumors into immunogenic foci of immune regulation. Cancer Immunol Res 2(7):616–631
3. Ramos-Vara JA, Miller MA (2014) When tissue antigens and antibodies get along: revisiting the technical aspects of immunohistochemistry—the red, brown, and blue technique. Vet Pathol 51(1):42–87
4. Gerdes MJ, Sevinsky CJ, Sood A et al (2013) Highly multiplexed single-cell analysis of formalin-fixed, paraffin-embedded cancer tissue. Proc Natl Acad Sci U S A 110(29):11,982–11,987
5. Remark R, Merghoub T, Grabe N et al (2016) In-depth tissue profiling using multiplexed immunohistochemical consecutive staining on single slide. Sci Immunol 1(1):aaf6925
6. Lawrence SM, Golubeva YG (2017) Optimization of immunostaining for prospective image analysis. In: Espina V (ed) Molecular profiling: methods in molecular biology, vol 1606. Humana, New York
7. Carstens JL, Correa de Sampaio P, Yang D, al BS (2017) Spatial computation of intratumoral T cells correlates with survival of patients with pancreatic cancer. Nat Commun 8:15095
8. Dixon AR, Bathany C, Tsuei M et al (2015) Recent developments in multiplexing techniques for immunohistochemistry. Expert Rev Mol Diagn 15:1171–1186
9. Brieu N, Pauly O, Zimmermann J, et al. (2016) Slide specific models for segmentation of differently stained digital histopathology whole slide images. Paper presented at the international society for optics and photonics, San Diego, CA, 27 Feb 2016
10. Tumeh PC, Harview CL, Yearley JH et al (2014) PD-1 blockade induces responses by inhibiting adaptive immune resistance. Nature 515:568–571

Chapter 7

Defining High Endothelial Venules and Tertiary Lymphoid Structures in Cancer

Emma Jones, Awen Gallimore, and Ann Ager

Abstract

High endothelial venules (HEVs) are structurally distinct blood vessels that develop during embryonic and neonatal life in all secondary lymphoid organs except the spleen. HEVs are critical for initiating and maintaining immune responses because they extract naïve and memory lymphocytes from the bloodstream, regardless of antigen receptor specificity, and deliver them to antigen-presenting cells inside lymph nodes under homeostatic conditions. HEVs also develop postnatally in nonlymphoid organs during chronic inflammation driven by autoimmunity, infection, allografts, and cancer. Extranodal HEVs are usually surrounded by dense lymphocytic infiltrates organized into lymph-node like, T- and B-cell-rich areas called tertiary lymphoid structures (TLS). HEV neogenesis is thought to facilitate the generation of tissue-destroying lymphocytes inside chronically inflamed tissues and cancers.

We are studying the mechanisms underpinning HEV neogenesis in solid cancers and the role of homeostatic T-cell trafficking in controlling cancer immunity. In this chapter we describe methods for identifying HEV in tissue sections of cancerous tissues in humans and mice using immunohistochemical staining for the HEV-specific marker peripheral lymph node addressin (PNAd). L-selectin binding to PNAd is a necessary first step in homeostatic lymphocyte trafficking which is the defining function of HEV. We also describe methods to measure L-selectin-dependent homing of lymphocytes from the bloodstream into lymphoid tissues and tumors in preclinical cancer models.

Key words High endothelial venule (HEV), Peripheral lymph node addressin (PNAd), Mucosal addressin cell adhesion molecule-1 (MAdCAM-1), Naïve T lymphocyte, Lymphocyte homing, L-selectin (CD62L), Tertiary lymphoid structure (TLS)

1 Introduction

High endothelial venules (HEVs) are structurally and antigenically distinct blood vessels especially adapted for lymphocyte trafficking [1]. HEVs develop in every secondary lymphoid organ except the spleen (i.e., lymph nodes (LN), tonsils, and Peyer's patches) during embryonic and neonatal life, and are fully integrated into the blood vasculature supplying these organs. The endothelial cells (EC) lining HEV in neonatal mice are immature and express the

Marie-Caroline Dieu-Nosjean (ed.), *Tertiary Lymphoid Structures: Methods and Protocols*, Methods in Molecular Biology, vol. 1845, https://doi.org/10.1007/978-1-4939-8709-2_7,

vascular addressin, mucosal addressin cell adhesion molecule (MAdCAM)-1. During the first weeks of neonatal life, HEVs mature into peripheral node addressin (PNAd) expressing HEV [2]. PNAd expression is induced by gut-derived dendritic cells in neonates [3] and maintained by lymphotoxin-β receptor (LTβR) signaling in HEV EC stimulated by LTαβ-expressing dendritic cells and lymphocytes [4, 5]. HEVs play a critical role in delivering naïve and memory T and B lymphocytes, regardless of antigen receptor specificity, from the bloodstream into lymphoid organs under homeostatic conditions. Here, lymphocytes scan dendritic cells and stromal networks for activating, tolerogenic, and homeostatic stimuli. HEVs, therefore, regulate the outcome of an immune response be it activation, tolerance, or homeostatic proliferation of lymphocytes. PNAd-expressing blood vessels that resemble structurally distinct HEV in LN develop postnatally in nonlymphoid organs during chronic inflammation driven by autoimmunity, infection, and allografts [6]. These extranodal HEVs are characteristically surrounded by dense lymphocytic infiltrates organized into lymph node-like structures with discrete T- and B-cell-rich areas and germinal centers and are called tertiary lymphoid structures (TLS). Extranodal HEVs facilitate entry of blood-borne lymphocytes and are therefore critical to the development and immune function of TLS. HEV-containing TLS also develop in solid, vascularized cancers and are receiving increasing attention because of their potential role in regulating immunity at the tumor site [7, 8]. The presence of TLS in resected solid cancers has been correlated with prolonged patient outcome in some cancers such as breast cancer [9, 10], melanoma [11, 12], and lung cancer [13]. In other cancers, TLS have been shown to either promote carcinogenesis such as virus-associated hepatocellular carcinoma [14] or accumulate with disease progression such as in primary breast carcinoma [15]. In colorectal cancer, TLS often containing germinal centers (Crohn's-like aggregates) develop in the surrounding peritumoral stroma as well as inside cancerous tissue. The number of TLS in colorectal cancer has been reported to correlate either with improved patient outcome or with disease progression depending on the stage of the disease [16–19].

In breast cancer and melanoma, the density of HEV correlated with improved patient outcome highlighting the important role that HEVs play in orchestrating anticancer immunity [20, 21]. HEV neogenesis correlates with regression of established tumors in preclinical mouse tumor immunotherapy models, such as depletion of Foxp3$^+$ regulatory T cells [22, 23] or combined checkpoint blockade inhibition and angiogenesis therapy [24]. HEV neogenesis and tumor regression are also seen when the TNF superfamily member LIGHT (TNSF14) (which signals via LTβR, an important driver of lymphoid organ development) is expressed by tumor cells or targeted to tumors or tumor blood vessels [25–27]. It is

thought that the antitumor effects are due to the generation of cancer cell-destroying lymphocytes from naïve T cells which have been recruited from the bloodstream into the cancer by newly formed HEV.

PNAd-expressing blood vessels lined by flat endothelial cells, rather than the cuboidal or plump endothelial morphology typical of mature HEV, are found inside cancer-induced ectopic lymphoid aggregates that are not organized into distinct T/B-cell areas [28]. These could represent immature HEV-containing structures in the process of forming TLS, or dedifferentiating HEV as found in reactive LN or following disruption of the LN microenvironment [5, 29]. Interestingly, PNAd-expressing blood vessels that form following depletion of $Foxp3^+$ regulatory T cells from methylcholanthrene-induced tumor-bearing mice are not generally associated with histologically distinct, TLS [22] which suggests that HEV neogenesis may occur independently of lymphoid neo-organogenesis. The development of HEV in the absence of full-blown TLS correlates with T-cell infiltration and cancer regression in this experimental model, highlighting the important role of HEV in controlling antitumoral immunity.

PNAd-expressing blood vessels have been reported in preclinical mouse tumor models particularly following immunotherapy. In tumor cell transplant models, PNAd expression is induced in tumor blood vessels by infiltrating $CD8^+$ T cells and NK cells [30]. In marked contrast to HEV development in LN, PNAd expression is not dependent on LTβR signaling but is stimulated instead by lymphotoxin α3 (LTα3). Although comprising <10% of the tumor vascular network and lined by flat endothelial cells PNAd-expressing tumor blood vessels are functional in that they recruit naïve, L-selectin-expressing T cells from the bloodstream into the tumor where they are activated to kill tumor tissue [30]. In methylcholanthrene-induced fibrosarcomas in mice, HEV neogenesis is also not dependent on LTβR but is driven mainly by T-cell-derived TNF-α and LTα3 [23]. However, HEV neogenesis during antiangiogenic/anti-PD-L1 therapy is dependent on LTβR signaling and in poorly infiltrated tumors where HEV neogenesis is low, such as glioblastomas, the combination of agonistic antibodies to LTβR alongside antiangiogenic/anti-PD-L1 therapy boosts HEV neogenesis [22]. Together, these findings suggest that TNFR and/or LTβR signaling in endothelial cells stimulates the development of PNAd-expressing HEV blood vessels that promote antitumor immunity by recruiting naïve T cells into cancerous tissues.

We are studying the role of homeostatic T-cell trafficking *via* HEV and the mechanisms underpinning HEV neogenesis in controlling local immunity inside mouse tumors and human cancers. We use immunohistochemistry to identify HEV in clinical and murine tissues by detection of PNAd, a specific marker of HEV (Fig. 1). We measure L-selectin-dependent recruitment of naïve T

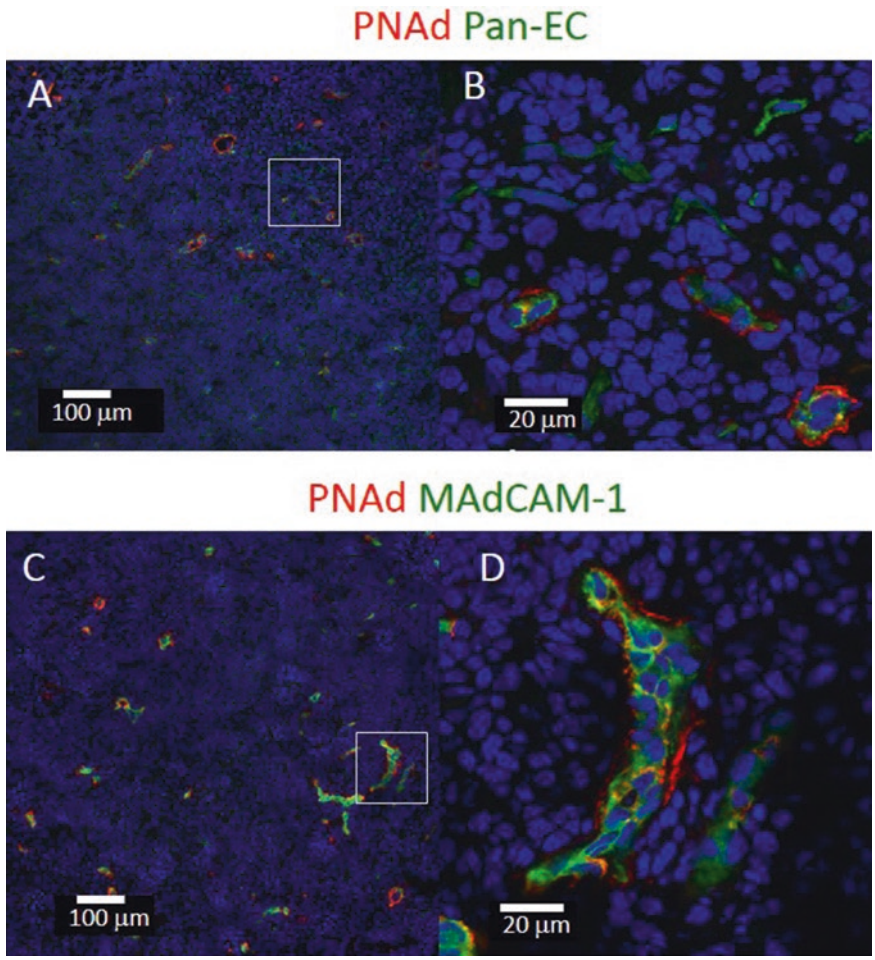

Fig. 1 HEV can be detected in mouse fibrosarcomas after regulatory T-cell depletion in FoxP3^{DTR} mice using diphtheria toxin. Frozen tumor sections were stained with anti-PNAd (MECA-79, red) + anti-pan-EC (MECA-32, green) antibodies (**A** and **B**) and anti-PNAd (MECA-79, red) + anti-MAdCAM-1 (MECA-367, green) antibodies (**C** and **D**). Cell nuclei were counterstained with DAPI (blue). Low-power images are shown in panels **A** and **C**, and high-power images of boxed regions are shown in panels **B** and **D**. Scale bars are shown in white

lymphocytes from the bloodstream into tissues, *via* mature, PNAd-expressing HEV, in mice using short-term homing assays and analyze tissue-infiltrating T cells by flow cytometry (Fig. 2) [31–33] and immunohistochemistry to colocate infiltrating T cells and HEV (Fig. 3) [31, 34].

2 Materials

All reagents which are not commercially available should be prepared with deionized, sterile water. All reagents are stored at +4 °C unless otherwise specified by the manufacturer. Tissues should be

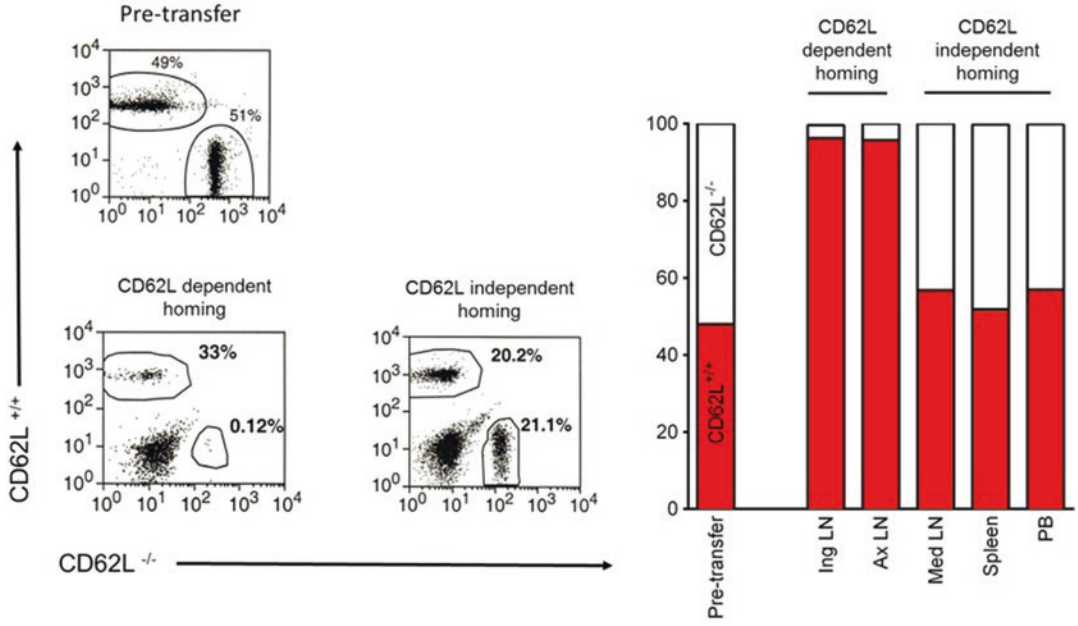

Fig. 2 L-selectin-dependent homing of T cells in mice. L-selectin-sufficient ($CD62L^{+/+}$) and L-selectin-deficient ($CD62L^{-/-}$) donor T cells were labeled with either CFSE or CMTMR and mixed 1:1 (pre-transfer). 1–3 h following intravenous administration to recipient mice, organs were analyzed for $CD62L^{+/+}$ and $CD62L^{-/-}$ T cells and T cell homing identified as either CD62L dependent or CD62L independent. Bar chart shows relative percentages of $CD62L^{+/+}$ and $CD62L^{-/-}$ T cells pre-transfer and recruited into inguinal (Ing), axillary (Ax), and mediastinal (Med) LN, spleen, and peripheral blood (PB). T-cell homing to peripheral LN such as inguinal and axillary is L-selectin dependent. In contrast, T-cell homing to the mucosal associated mediastinal LN is not exclusively dependent on L-selectin. HEVs are not found in the spleen so not dependent on L-selectin for T-cell entry. Peripheral blood is analyzed to determine whether changes in the ratio of T-cell populations inside tissues result from a change in the ratio in the bloodstream

collected into sterile phosphate-buffered saline, and lymphocytes isolated in growth media and resuspended in saline for injection into mice. All procedures apart from tissue collection and injections into mice should be performed in a biological safety cabinet. The following reagents are used in all methods: calcium- and magnesium-free phosphate-buffered saline (PBS), complete RPMI 1640 growth media supplemented with penicillin and streptomycin (RPMI), heat-inactivated (30 min at 56 °C) fetal calf serum (FCS), and 70% alcohol for sterilization. The antibodies used for immunofluorescence staining of frozen or paraffin-embedded tissue sections and flow cytometry of T cells are listed in Table 1.

2.1 Immunolabeling HEV and TLS in Murine Tumor Cryosections

1. Tissue-Tek plastic base molds (Thermo Fisher Scientific).
2. Optimum cutting temperature (OCT) compound.
3. Dry ice with or without ethanol for snap freezing murine tissue in OCT.
4. Cryostat capable of cutting cryosections.

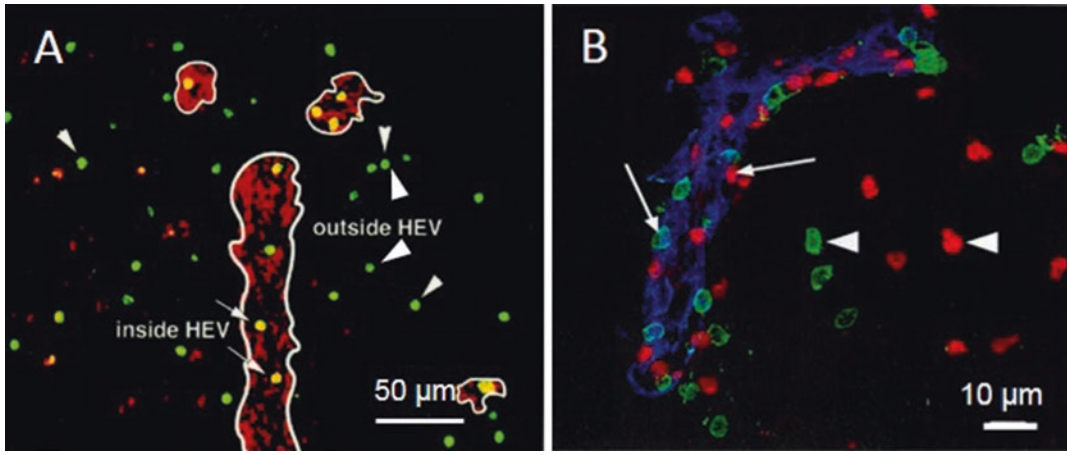

Fig. 3 Localization of homed T lymphocytes in HEV-containing tissues. (**A**) CFSE-labeled naïve T lymphocytes were injected into naïve mice and after 60 min peripheral lymph nodes analyzed for infiltrating T cells (green) and HEVs stained using MECA-79 (red). Representative image showing CFSE-labeled (green) T lymphocytes in the process of transmigration and inside HEV (arrows) and CFSE-labeled T lymphocytes which have completed transmigration and outside HEV (arrow heads). Bar, 50 μm. (**B**) Naïve T lymphocytes were split into two and labeled with either CFSE or CMTMR, mixed 1:1, and injected into naïve mice. After 60 min, peripheral lymph nodes were stained for HEV using MECA-79 (blue) and the ratios of CFSE (green) to CMTMR (orange) T cells inside HEV (white arrows) and outside HEV (arrowheads) determined

5. Hydrophobic pen for creating a hydrophobic barrier around tissue section (e.g., Pap pen, Vector).
6. Humidified chamber containing wet paper towel to prevent evaporation of staining reagents.
7. PBS for washing steps.
8. Fixative of choice (*see* **Note 1**): For example:
   (a) Acetone stored in glass Pyrex bottle at −20 °C.
   (b) Fresh 4% formaldehyde: Dilute 16% formaldehyde in PBS and adjust pH to 7.4; 16% formaldehyde can be either bought in ampules (Thermo Fisher Scientific) or prepared from paraformaldehyde powder (Sigma) and stored at −20 °C. Limit exposure to paraformaldehyde by preparing in a fume hood. Store 4% formaldehyde at 4 °C and use within 1 week.
   (c) Periodate-lysine-paraformaldehyde fixative (PLP; 0.075 M lysine, 0.37 M sodium phosphate (pH 7.2), 2% formaldehyde, and 0.01 M $NaIO_4$): Mix the following to create a buffered lysine solution: 0.36 g lysine (Sigma), 7.5 mL NaH_2PO_4 (0.1 M, pH 7.2; Sigma), 2.5 mL Na_2HPO_4 (0.1 M, pH 7.2; Sigma), and 10 mL H_2O. Immediately before use, add 15 mL of the buffered lysine solution to the following: 5 mL 8% formaldehyde and 50 mg sodium meta-periodate ($NaIO_4$; Sigma). It is not necessary to pH the final solution.

Table 1
Antibodies used for immunofluorescence staining and flow cytometry

Antigen	Conjugate	Clone	Isotype	Company	Working concentration (μg/mL)
Primary antibodies for immunolabeling frozen sections					
PNAd	Purified	MECA-79	Rat IgM, κ	Biolegend	2.5
Pan-endothelial cell (pan-EC)	Biotinylated	MECA-32	Rat IgG2a, κ	Biolegend	2
MAdCAM-1	Biotinylated	MECA-367	Rat IgG2a, κ	Biolegend	2
CD3	Purified	–	Rabbit polyclonal	DAKO	2
CD45R/B220	Biotinylated	RA3-6B2	Rat IgG2a, κ	Biolegend	2
Follicular dendritic cell (FDC)	Purified	FDC-M1	Rat IgG2c, κ	BD Biosciences	2
Secondary antibodies/reagents for immunolabeling frozen sections					
Anti-rat IgM	Alexa Fluor 594	–	Goat polyclonal	Invitrogen	1
Streptavidin	Alexa Fluor 488	–	–	Invitrogen	1
Streptavidin	Alexa Fluor 647	–	–	Invitrogen	1
Anti-rabbit	Alexa Fluor 594	–	Goat polyclonal	Invitrogen	1
Anti-rat IgG2c	Alexa Fluor FITC	MARG2c-5	Mouse IgG2a	Invitrogen	1
Isotype control antibodies for immunolabeling frozen sections					
Rat IgM κ	Purified	RTK2118	Rat IgM, κ	Biolegend	2
Rat IgG2a, κ	Biotinylated	RTK2758	Rat IgG2a, κ	Biolegend	2
Rabbit polyclonal	Purified	–	Rabbit polyclonal	Abcam	2
Rat IgG2c, κ	Purified	RTK4174	Rat IgG2c, κ	Biolegend	2
Primary antibodies for immunolabeling paraffin sections					
PNAd	Purified	MECA-79	Rat IgM, κ	Biolegend	2.5
CD45R/B220	Purified	RA3-6B2	Rat IgG2a, κ	Biolegend	2
CD3	Purified	–	Rabbit polyclonal	DAKO	2
Secondary reagents for immunolabeling paraffin sections					
Immpress anti-rat	HRP	–	Goat	Vector	–
Immpress anti-rabbit	HRP	–	Horse	Vector	–

(continued)

Table 1
(continued)

Antigen	Conjugate	Clone	Isotype	Company	Working concentration (μg/mL)
Isotype control antibodies for immunolabeling paraffin sections					
Rat IgM κ	Purified	RTK2118	Rat IgM, κ	Biolegend	2
Rat IgG2a, κ	Purified	RTK2758	Rat IgG2a, κ	Biolegend	2
Rabbit polyclonal	Purified	–	Rabbit polyclonal	Abcam	2
Primary antibodies for flow cytometry of T lymphocytes					
CD62L/L-selectin	PE	MEL-14	Rat IgG2a, κ	Biolegend	0.2
TCR	FITC	H57-597	Armenian hamster IgG	BD Pharmingen	0.2
CD44	APC-Cy7	IM7	Rat IgG2b, κ	Biolegend	0.2

9. If using formaldehyde or PLP to fix sections then prepare 0.3 M glycine (Thermo Fisher Scientific) in PBS, pH 7.4, to quench free aldehydes.
10. *Optional*: Avidin/biotin blocking kit if a biotinylated primary or secondary antibody is used.
11. Serum blocking solution to block nonspecific binding of antibodies. 2.5–5% serum of the species in which the secondary antibody is raised is often used. Other sera, for example horse or mouse serum, may also be used.
12. Primary antibodies diluted in 1% bovine serum albumin (BSA, Sigma) in PBS: Rat anti-mouse PNAd antibody (clone MECA-79, rat IgM) is used at a working concentration of 2.5 μg/mL to detect HEV (*see* **Notes 2** and **3**). Alternatively, MECA-79 hybridoma supernatant can be prepared in-house and titrated on LN sections before staining HEV in tumor sections. Additional antibodies can be used simultaneously to detect other cells or structures such as TLS. Example 1: Biotinylated rat anti-mouse pan-EC antigens (clone MECA-32, rat IgG2a, used at a working concentration of 2 μg/mL, Biolegend) can be used to confirm that MECA-79 stains endothelial structures (Fig. 1) (*see* **Note 4**). Example 2: Biotinylated rat anti-mouse MAdCAM-1 (clone MECA-367, rat IgG2a, used at a working concentration of 2 μg/mL, Biolegend) can be used to detect immature HEV in tumors (Fig. 1). Example 3: The presence of TLS in tumor tissue, characterized by T/B-cell segregation and follicular dendritic cell (FDC) networks, may

be revealed using antibodies to T cells (e.g., rabbit anti-human CD3, which also detects mouse CD3, DAKO A0452, used at 2 μg/mL), B cells (biotinylated rat anti-mouse/human CD45R/B220, clone RA3-6B2, rat IgG2a, used at a working concentration of 2 μg/mL, Biolegend), and FDC (rat anti-mouse FDC, clone FDC-M1, rat IgG2c, used at a working concentration of 2 μg/mL, BD Biosciences).

13. For every antibody used, an isotype control antibody should be used at the same working concentration, in parallel on another section to check the staining is specific. A rat IgM isotype control antibody is used to check MECA-79 staining is specific. Biotinylated rat IgG2a is used to check pan-EC antigen (clone MECA-32), MAdCAM-1 (clone MECA-367), and B cell (clone RA3-6B2) staining is specific (Fig. 1). Rat IgG2c is used to check FDC (clone FDC-M1) staining is specific and rabbit IgG polyclonal isotype control is used to check CD3 (DAKO A0452) staining is specific.
14. Fluorescently conjugated secondary reagents diluted in 1% BSA in PBS: To detect MECA-79, a fluorescently conjugated anti-rat IgM may be used. Other primary antibodies can be detected with fluorescently conjugated species-specific secondary antibodies or fluorescently conjugated streptavidin reagents. The fluorochromes chosen should be compatible with the specific capabilities of the microscope being used to analyze the tissues, that is, the laser systems and detectors. The Alexa Fluor dyes are excellent conjugates since they are very bright and resistant to photobleaching; Alexa Fluor 488, 594, and 647 emission spectra are sufficiently separated to provide minimal overlap between fluorochromes and are compatible with most standard wide-field and confocal fluorescent microscopes.
15. Optional: Nuclear counterstain. Example Hoechst or DAPI (Sigma) diluted in PBS.
16. Mounting media: Example: Vectashield (Vector) or Prolong gold (Thermo Fisher Scientific).
17. Glass coverslips (thickness #1.5 coverslips should be used in fluorescence microscopy to obtain the brightest images with minimal spherical aberration; Thermo Fisher Scientific).

2.2 Immunolabeling HEV and TLS in Paraffin-Embedded Murine Tumor Sections

1. Tissue-Tek plastic base molds (Thermo Fisher Scientific).
2. Neutral buffered formal saline (NBFS).
3. Paraffin wax (Shandon Histoplast, Thermo Fisher Scientific).
4. Microtome capable of cutting paraffin sections (e.g., Thermo Fisher Scientific).
5. Blades (MX35, Thermo Fisher Scientific).
6. Hydrophobic pen for creating a hydrophobic barrier around tissue section (e.g., Pap pen, Vector).

7. Humidified chamber containing wet paper towel to prevent evaporation of staining reagents.
8. 100% Xylene.
9. Graded alcohols: 100, 95, 90, 80, and 70% ethanol.
10. PBS for washing steps.
11. Peroxidase blocking solution: Either 1% hydrogen peroxide/methanol or a commercial blocking reagent (e.g., Bloxall; Vector) (*see* **Note 7**).
12. Serum blocking solution to block nonspecific binding of antibodies: Often 2.5–5% serum of the species in which the secondary antibody is made is used. Other sera for example horse or mouse serum may also be used.
13. Primary antibody diluted in 1% BSA in PBS: Rat anti-mouse PNAd antibody (MECA-79, rat IgM, used at a working concentration of 2.5 μg/mL) can be used to detect HEV.
14. A rat IgM isotype control antibody should be used at the same working concentration in parallel on another section to check MECA-79 staining is specific.
15. Enzyme-conjugated secondary antibody complexes to detect primary antibody. Example: Immpress anti-rat horseradish peroxidase (HRP) kit (Vector).
16. Enzyme substrate to visualize immunolabeled target. Example: DAB, Impact VIP, or Impact SG (Vector).
17. Optional: Nuclear counterstain. Example: Hematoxylin (Sigma).
18. Mounting media: Example: Distyrene, plasticizer, and xylene (DPX; Raymond Lamb).
19. Glass coverslips (Menzel; Thermo Fisher Scientific).

2.3 L-Selectin-Dependent Homing of Naïve T Lymphocytes in Mice

1. The following equipment are required: 0.001 g Balance in animal unit for weighing tissues, humidified CO_2 incubator at 37 °C, refrigerated benchtop centrifuge, trypan blue solution and Neubauer chamber or other equipment for cell counts and viability, 2 mL plastic syringes, 70 μm cell strainers, 50 mL polypropylene tubes. T-cell donor mice: 8–12-week-old, sex-matched, and syngeneic to experimental mice.
2. Experimental mice with HEV-containing cancers as recipients of donor T cells.
3. Sterilized instruments (dissecting scissors, forceps, and scalpel).
4. Labeled tubes containing 1 mL ice-cold PBS for collection of spleens from T-cell donor mice.
5. Labeled tubes containing 1 mL ice-cold PBS for collection of cancerous tissues, lymph nodes, and spleens from experimen-

tal mice after injection of donor T cells (labeled with mouse number (e.g., 1–5) and organ (e.g., cancer, spleen, LN)).

6. Red blood cell lysis buffer.
7. Naïve T-cell isolation kits using negative selection.
8. Cell tracker dye: Carboxyfluorescein diacetate-succinimidyl ester (CFSE, Molecular Probes).
9. Fluorescently conjugated antibodies to TCR (clone H57-597, Armenian hamster IgG), L-selectin/CD62L (clone MEL-14, rat IgG2a), and CD44 (clone IM7, rat IgG2b). Low endotoxin, azide-free antibodies to L-selectin (MEL-14, rat IgG2a) and rat IgG2a isotype control for T cell homing studies in mice.
10. Rat-anti mouse PNAd (clone MECA 79, rat IgM), fluorescently conjugated or biotinylated anti-rat IgM to detect MECA79 in tissue sections.
11. Fixative: 2% Formaldehyde/5% sucrose in PBS, 20% sucrose in PBS.
12. Freezing and storing tissues: Liquid nitrogen.

3 Methods

3.1 Immunolabeling HEV and TLS in Murine Tumor Cryosections

1. Collect tumor tissue and place immediately in optimal cutting temperature compound (OCT) in a plastic mold. Add sufficient OCT to completely cover the tissue.
2. Snap-freeze in dry ice and store blocks in small plastic ziplock bags at −80 °C until needed.
3. Cut 5–10 μm sections on a cryostat and mount sections on glass slides. Typically, we mount two sections per slide.
4. Allow slides to dry for approximately 1 h at room temperature (RT) and store in a slide box at −80 °C until needed.
5. Remove slides from freezer, allow them to warm up to RT, and wipe away any residual moisture, taking care not to touch the tissue section.
6. Fix sections in ice-cold 100% acetone, 4% formaldehyde, or PLP fixative for 10 min (*see* **Note 1**). Wash slides three times in PBS over 5 min at RT.
7. Drain slides and carefully wipe off excess liquid before next step. Be careful not to let the section dry out.
8. Draw a circle around each section with a hydrophobic marker.
9. *Optional*: If fixed in 4% formaldehyde or PLP quench free aldehydes with 0.3 M glycine in PBS for 10 min at RT and then wash slides three times in PBS over 5 min at RT.

10. *Optional*: If using a biotinylated antibody block endogenous biotin with avidin/biotin block and then wash slides three times in PBS over 5 min at RT.
11. Block nonspecific protein binding with serum-blocking solution for 30 min at RT.
12. Drain slides (no need to wash the slides).

    Incubate with MECA-79 antibody or rat IgM isotype control in 1% BSA/PBS overnight at 4 °C or for 1 h at RT in a humidified chamber. *Optional*: Include other antibodies such as MECA-367 to identify immature HEV, MECA-32, to confirm that MECA-79 is detected on EC (*see* Fig. 1) or T-cell, B-cell, and FDC antibodies (Table 1) to determine if TLS are present.
13. Wash slides three times in PBS over 5 min at RT.
14. Incubate with fluorescently conjugated secondary antibodies in 1% BSA/PBS for 30–60 min at RT (*see* **Note 5**). Counterstain with nuclear dye for 10 min at RT (e.g., Hoechst or DAPI).
15. Wash slides three times in PBS over 5 min at RT.
16. Mount slides in mounting media and coverslip.
17. Slides should be stored in the dark at +4 °C until analysis and image acquisition by fluorescence microscopy. Staining may be preserved for at least 2 months if Alexa Fluor dyes are used and slides are stored correctly.

3.2 Immunolabeling HEV and TLS in Paraffin-Embedded Murine Tumor Sections

1. Collect tumor tissue and fix in neutral buffered formal saline (NBFS) for 24–48 h.
2. Process in tissue processor (Leica) as follows:
   (a) 70% Ethanol—1 h at 45 °C
   (b) 80% Ethanol—1 h at 45 °C
   (c) 95% Ethanol—1 h at 45 °C
   (d) 100% Ethanol—1 h at 45 °C
   (e) 100% Ethanol—1 h at 45 °C
   (f) 100% Ethanol—1 h at 45 °C
   (g) 100% Xylene—1.5 h at 45 °C
   (h) 100% Xylene—2 h at 45 °C
   (i) 100% Xylene—2 h at 45 °C
   (j) Wax—1.5 h at 65 °C
   (k) Wax—2 h at 65 °C
   (l) Wax—2.5 h at 65 °C
   (m) Embed in wax and cool
3. Store tissue blocks in a cool dry place until ready to cut.

4. Precool tissue blocks on ice or on a cold plate (Leica).
5. Cut 5–10 μm sections on a microtome and mount on glass slides.
6. Place slides in a slide rack at 60 °C for 1 h to overnight to melt off wax.
7. Hydrate sections in a slide chamber with 3× 100% xylene washes, 5 min each, and then descending alcohols (100, 100, 90, and 70%) for 3 min each. Wash in running water for 5 min and then rinse in dH_20.
8. Use either Tris/EDTA (10 mM Tris base, 1 mM EDTA solution, 0.05% Tween 20, pH 9.0) or sodium citrate (10 mM sodium citrate, 0.05% Tween 20, pH 6.0) antigen retrieval buffer for heat-induced epitope retrieval (*see* **Note 6**).
9. Wash slides three times in PBS over 5 min.
10. Drain slides and carefully wipe off excess water before next step. Be careful not to let the section dry out.
11. Draw a circle around each section with a hydrophobic marker.
12. Neutralize endogenous peroxidase activity with 1% hydrogen peroxide/methanol for 10 min at RT or alternatively use a commercial blocking reagent (e.g., Bloxall, Vector; *see* **Note 7**).
13. Wash slides three times in PBS over 5 min.
14. Block nonspecific protein binding with blocking solution for 30 min at RT.
15. Drain slides (no need to wash).
16. Incubate with MECA-79 antibody or rat IgM isotype control in 1% BSA/PBS overnight at 4 °C or for 1 h at RT in a humidified chamber.
17. Wash slides three times in PBS over 5 min.
18. Incubate with anti-rat Immpress reagent (Vector) or other HRP conjugated secondary antibody and incubate at RT for 30 min.
19. Wash slides three times in PBS over 5 min.
20. Incubate with freshly prepared DAB Chromogen solution and monitor under a microscope until color develops.
21. Rinse with deionized H_2O and then wash in fresh deionized H_2O.
22. *Optional*: It is possible to sequentially stain the same tissue section with other antibodies in order to identify other cells and structures using different colored chromogens (*see* **Note 8**). For example, the presence of TLS-containing organized B- and T-cell zones can be verified with rat anti-mouse CD45R/B220 (Biolegend) detected with anti-rat Immpress

reagent (Vector) and Vector-VIP (purple; Vector) followed by rabbit anti-mouse CD3 (DAKO) detected with anti-rat Immpress reagent (Vector) and Vector-SG (grey; Vector).

23. Counterstain in hematoxylin (10–20 s) and blue in Scott's tap water (10 s) (*see* **Note 9**).
24. Dehydrate in ascending alcohols (70, 90, 100, and 100%) for 3 min each and 3× 100% xylene washes for 5 min each.
25. Mount in mounting media and coverslip.

3.3 L-Selectin-Dependent Homing of Naïve T Lymphocytes in Mice

1. Cull T-cell donor mice by CO_2 inhalation and/or cervical dislocation and pin out on dissecting board ventral side up. Swab ventral surface with 70% alcohol to sterilize and wet fur, and open abdominal cavity by midline incision using scalpel. Remove spleen carefully using forceps and scissors and avoid damaging the surface. Collect spleen into PBS in labeled tubes and transport on ice to biological safety cabinet (*see* **Notes 10** and **11**).
2. Place cell strainer in the neck of a labeled 50 mL polypropylene tube in a tube rack and pour spleen and PBS through cell strainer.
3. Split open paper covering of 2 mL plastic syringe, and remove plunger using paper covering to maintain sterility of flat end (not rubber seal end). Mash spleen using flat end of plunger. Wash strainer using 5 mL of PBS; repeat if necessary to completely disaggregate tissue; discard strainer.
4. Seal tubes and collect splenocytes by centrifugation at 250 g for 5 min at +4 °C. Aspirate or remove PBS by pouring.
5. Tap the bottom of the tube to dislodge cell pellet, carefully resuspend in 2 mL red cell lysis buffer using 10 mL strippette, make up to 5 mL with red cell lysis buffer, and incubate for 5 min on ice. Add 10 mL PBS, collect cells by centrifugation, and repeat PBS wash once.
6. Isolate naïve T cells by negative selection using commercially available kits according to the manufacturer's instructions (*see* **Note 12**).
7. Resuspend T cells to 5×10^7/mL in FCS-free PBS for labeling with CFSE (*see* **Note 13**) and remove 1×10^5 cells for staining to check naïve T-cell purity (*see* **Note 14**).
8. Label T cells in 2 μM CFSE in FCS-free PBS in the dark for 15 min at 37 °C, wash twice in 5–10 mL PBS containing 1% FCS, resuspend to 2.5×10^7 cells/mL in saline, and split into two equal aliquots. Collect cells by centrifugation and preincubate one aliquot with 100 μg/mL rat anti-mouse L-selectin (clone MEL-14, rat IgG2a) and the second aliquot with

100 μg/mL isotype control (clone MAC193, rat IgG2a) for 30 min at 4 °C (*see* **Note 13**).

9. Inject 0.2 mL of T cells plus antibody (5×10^6 cells) intravenously into experimental mice (*see* **Notes 10**, **15**, and **16**).
10. Cull mice after 1, 4, or 24 h (*see* **Note 17**) by CO_2 inhalation and/or cervical dislocation. Collect blood by cardiac puncture from the left ventricle using a 1 mL syringe with 27G needle into 1.5 mL heparinized Eppendorf tubes containing 100 μL of 10 units/mL heparin or citrate-EDTA. Store carcasses on ice and prepare for dissection, as described in **step 1**.
11. Collect tumor, spleen, peripheral (axillary, brachial, and inguinal) LN, and mucosal (mesenteric or mediastinal) LN, and process as follows: cut tumor, spleen, and mucosal LN into two halves, one half to analyze infiltrating T cells by histology and the other half to isolate infiltrating T cells for flow cytometric analysis. Pool right peripheral LN and use to isolate infiltrating T cells. Collect left peripheral LN separately for immunolocalization of infiltrating T cells. Fix LN, spleen, and tumor in 2% formaldehyde/5% sucrose in PBS for 2 h, transfer to 20% sucrose in PBS for 2 h, snap-freeze in liquid nitrogen, and store at −80 °C for up to 2 years. Collect lymphocytes from one half of a tumor, one half of spleen, and pooled right peripheral LN, as described in **steps 2–5** above (*see* **Notes 18** and **19**).
12. Lyse red blood cells in spleen, tumor, and peripheral blood, as described in **step 5**.
13. Analyze CFSE-labeled lymphocytes on a flow cytometer analyzer using the fluorescein isothiocyanate filter. Data on 2×10^5 viable cells in spleen and blood, and $5–10 \times 10^5$ viable cells for LN, is acquired and the data analyzed using FlowJo software. The percentage of CFSE-labeled cells recovered in the spleen, blood, and each group of LN is determined and compared between control and treatment groups. If L-selectin-deficient T cells are available label using CMTMR, mix them 1:1 with CFSE-labeled L-selectin-sufficient T cells, and inject a total of 20×10^6 cells into a single group of experimental mice. In tissues with mature HEV, L-selectin-sufficient T cells are highly enriched over L-selectin-deficient T cells (Fig. 2).
14. Cryostat sections of 8 μm are cut from fixed, frozen tissues (*see* **step 11**), HEV stained using MECA-79 and red fluorescence-conjugated secondary antibody, as described in Subheading 3.1, **step 12**, but without additional fixation (step 6). The presence of TLS in fixed tumor tissue may be revealed using antibodies that detect T and B cells in formalin-fixed paraffin-embedded tissues (Table 1). The position of CFSE-labeled lymphocytes (green) in relation to HEVs (red) is determined

by fluorescence microscopy using a confocal laser scanning microscope. For each tissue, 10–15 images containing complete cross sections through 30–55 HEVs (average total HEV area 2500 μm^2) are collected and analyzed using Image J-NIH software. The total cross-sectional area of HEVs and the remaining area within each image are calculated. CFSE-labeled cells "inside HEVs" are those attached to the luminal surface of the vessel wall and within the HEV wall (Fig. 3a; arrows). The remaining CFSE-labeled cells are scored as "outside HEVs" (Fig. 3a; arrowheads). Total lymphocytes counts range from 200 to 500 cells. The numbers of CFSE-labeled cells inside and outside HEVs are not significantly different in inguinal and brachial LN of individual mice or between animals in the same experimental group [31]. Results are pooled from inguinal and brachial LN of mice within each experimental group and expressed as means ± SEM CFSE-labeled cells/mm^2 inside and outside HEVs [34].

4 Notes

1. Fixation is required to maintain tissue morphology. The choice of fixative depends on the antigen and antibody used to detect it. Formaldehyde is a cross-linking fixative and maintains good tissue architecture; however, some antigens cannot easily be detected after formaldehyde fixation (e.g., mouse CD4). Acetone removes lipids, dehydrates cells, and precipitates proteins so cell structure is poorly preserved but may allow better detection of some antigens (e.g., mouse CD4). PLP can be prepared with varying concentrations of formaldehyde and was designed to primarily cross-link carbohydrates to maintain antigenic sites on proteins. Since membranes are rich in glycoproteins and glycolipids, PLP provides good preservation of membrane antigens of the immune system. HEVs are detected well with all of these fixation methods; however if other cells of the immune system are also immunolabeled then different fixation protocols should be tested.
2. MECA-79 is a rat IgM and can precipitate over time resulting in speckled staining at which point the antibody needs to be discarded.
3. MECA-79 can detect HEV in both mouse and human cryosections or paraffin sections. However other antibodies, for example, clones MECA-32 and MECA-367, are mouse specific so alternative human-specific antibodies would be needed.
4. When two rat primary antibodies are used simultaneously (e.g., clones MECA-79 and MECA-367 or MECA-32) fluorescently or biotin-conjugated primary antibodies or isotype-

specific secondary antibodies should be used so that anti-rat secondaries are avoided.

5. Since MECA-79 is a rat IgM antibody, it can be detected with an anti-rat IgM secondary antibody. However this secondary antibody will cross-react to endogenous mouse IgM, which can be detected in plasma cells in mouse tissue. Plasma cells can be identified by co-staining with anti-mouse CD138 or alternatively MECA79 staining of HEV can be positively identified by morphology or co-staining with a pan-EC marker.
6. Either Tris/EDTA or sodium citrate antigen retrieval methods are both suitable for detecting HEV in paraffin tissue sections. The choice of antigen retrieval is determined by other antibodies used to sequentially stain tissue sections.
7. Hydrogen peroxide/methanol will quench endogenous peroxidase that would otherwise react with the HRP substrate (e.g., DAB) resulting in undesirable background. Some proteins may be sensitive to methanol or hydrogen peroxide treatment and may reduce staining of the antigen; in this case quenching with hydrogen peroxide/methanol may be performed after the primary antibody incubation step or alternatively a commercial blocking reagent such as Bloxall may used.
8. It is difficult to distinguish by eye two colocalized stains on a single structure or cell by immunohistochemistry, for example, MECA-79 and an EC marker. If this is required immunofluorescence is recommended. However, spatially separated antigens can be detected by immunohistochemistry.
9. Light staining with hematoxylin for 10–20 s is usually sufficient. However, if sections are stained sequentially with multiple antibodies, it may be unnecessary to counterstain with hematoxylin since the antibody staining might be obscured.
10. Each mouse receives 5–10 $\times$ 10^6 labeled donor T cells and two groups of 5 mice are required per experiment, one group receiving naïve T cells pretreated with control antibody and the second pretreated with anti-L-selectin antibody to inhibit binding of naïve T cells to HEV. The total number of naïve T cells per experiment is therefore 50–100 $\times$ 10^6 T cells. The yield of T cells is 30–50 $\times$ 10^6 cells per spleen so 2–3 donor mice will provide sufficient T cells for each experiment. If donor mice are limiting, T cells can be isolated from peripheral (axillary, brachial, and inguinal) and mesenteric LN and pooled with splenic T cells.
11. Dissecting instruments are sterilized by autoclaving in sealed bags or by submerging in 70% alcohol.
12. We have used kits for isolating T cells and $CD8^+$ T cells from Miltenyi Biotec and Stem Cell Technologies.

13. We have used carboxyfluorescein diacetate-succinimidyl ester (CFSE, Molecular Probes) 5-(and 6)-([{4-chloromethyl}benzoyl]amino) tetramethylrhodamine (CMTMR; Cell Tracker Orange; Molecular Probes), PKH26 (Molecular Probes), or SNARFJ-1 dye (Molecular Probes) to label naïve T cells for short-term homing of wild-type L-selectin-expressing T cells and In Vivo MAb anti-mouse L-selectin from BioXCell. Instead of blocking L-selectin on donor T cells, PNAd-dependent homing can be tested by injecting CFSE-labeled naïve T cells into groups of recipient mice injected either with 100 μg MECA-79 or 100 μg isotype control antibody immediately before donor T cells are injected.
14. Naïve T cells are CD62L positive and CD44 negative/low.
15. Where L-selectin-deficient T cells are available we have used CMTMR to label L-selectin-deficient T cells, mixed them 1:1 with CFSE-labeled L-selectin-sufficient T cells, and injected a total of 20×10^6 cells into a single group of experimental mice. In tissues with functional HEV, L-selectin-sufficient T cells are highly enriched over L-selectin-deficient T cells (Fig. 2). Cell tracker dyes need to be reversed to check for effects of cell tracker dyes on T-cell recruitment from the bloodstream *via* HEV in wild-type mice (Fig. 3b).
16. To avoid using cell tracker dyes, we have injected unlabeled T cells isolated from CD90.2 (Thy.1.2) mice and injected in CD90.1 (Thy.1.1) cancer-bearing mice and used antibodies to CD90.2 to detect donor T cells by flow cytometry and immunohistochemistry.
17. To measure recruitment directly from the bloodstream into tissues time points of 1–3 h are preferred since this is before T cells exit third-party organs such as the spleen or LN. However, the level of T-cell recruitment into cancerous tissues may be low and longer time points of 24–48 h are required [30, 35].
18. Collect peripheral (axillary, brachial, inguinal) LN as positive controls for L-selectin/CD62L-dependent T cell homing. Organs and tissue compartments that do not shown L-selectin/CD62L dependent T cell homing include mediastinal LN, mesenteric LN, spleen, and peripheral blood (Fig. 2).
19. Tissue disaggregation using enzymes may increase the yield of infiltrating T cells from fibrotic tissues and cancers over mechanical disaggregation; this needs to be determined empirically for each type of tumor.FundingEJ and AG are supported by a program grant from Cancer Research UK (C16731/A21200). AA is supported by project grants from the Medical Research Council UK (MR/L008742/1) and Cancer Research UK C42412/A24416.

References

1. Ager A, May MJ (2015) Understanding high endothelial venules: Lessons for cancer immunology. Oncoimmunology 4(6):e1008791
2. Mebius RE, Streeter PR, Michie S, Butcher EC, Weissman IL (1996) A developmental switch in lymphocyte homing receptor and endothelial vascular addressin expression regulates lymphocyte homing and permits CD4+ CD3− cells to colonize lymph nodes. Proc Natl Acad Sci U S A 93:11,019–11,024
3. Zhang Z, Li J, Zheng W, Zhao G, Zhang H, Wang X et al (2016) Peripheral lymphoid volume expansion and maintenance are controlled by gut microbiota via RALDH+ dendritic cells. Immunity 44:330–342
4. Moussion C, Girard JP (2011) Dendritic cells control lymphocyte entry to lymph nodes through high endothelial venules. Nature 479:542–546
5. Liao S, Ruddle NH (2006) Synchrony of high endothelial venules and lymphatic vessels revealed by immunization. J Immunol 177:3369–3379
6. Drayton DL, Liao S, Mounzer RH, Ruddle NH (2006) Lymphoid organ development: from ontogeny to neogenesis. Nat Immunol 7:344–353
7. Dieu-Nosjean MC, Giraldo NA, Kaplon H, Germain C, Fridman WH, Sautes-Fridman C (2016) Tertiary lymphoid structures, drivers of the anti-tumor responses in human cancers. Immunol Rev 271:260–275
8. Colbeck EJ, Ager A, Gallimore A, Jones G (2017) Tertiary lymphoid structures in cancer: drivers of anti-tumor immuity, immunosuppression or bystander sentinels in disease. Front Immunol 8:1830 doi.org/10.3389/fimmu.2017.01830
9. Gu-Trantien C, Loi S, Garaud S, Equeter C, Libin M, de Wind A et al (2013) CD4(+) follicular helper T cell infiltration predicts breast cancer survival. J Clin Invest 123:2873–2892
10. Lee HJ, Park IA, Song IH, Shin SJ, Kim JY, Yu JH et al (2016) Tertiary lymphoid structures: prognostic significance and relationship with tumour-infiltrating lymphocytes in triple-negative breast cancer. J Clin Pathol 69:422–430
11. Ladanyi A, Kiss J, Somlai B, Gilde K, Fejos Z, Mohos A et al (2007) Density of DC-LAMP(+) mature dendritic cells in combination with activated T lymphocytes infiltrating primary cutaneous melanoma is a strong independent prognostic factor. Cancer Immunol Immunother 56:1459–1469
12. Messina JL, Fenstermacher DA, Eschrich S, Qu X, Berglund AE, Lloyd MC et al (2012) 12-Chemokine gene signature identifies lymph node-like structures in melanoma: potential for patient selection for immunotherapy? Sci Rep 2:765
13. Dieu-Nosjean MC, Antoine M, Danel C, Heudes D, Wislez M, Poulot V et al (2008) Long-term survival for patients with non-small-cell lung cancer with intratumoral lymphoid structures. J Clin Oncol 26:4410–4417
14. Finkin S, Yuan D, Stein I, Taniguchi K, Weber A, Unger K et al (2015) Ectopic lymphoid structures function as microniches for tumor progenitor cells in hepatocellular carcinoma. Nat Immunol 16:1235–1244
15. Figenschau SL, Fismen S, Fenton KA, Fenton C, Mortensen ES (2015) Tertiary lymphoid structures are associated with higher tumor grade in primary operable breast cancer patients. BMC Cancer 15:101
16. Di Caro G, Bergomas F, Grizzi F, Doni A, Bianchi P, Malesci A et al (2014) Occurrence of tertiary lymphoid tissue is associated with T-cell infiltration and predicts better prognosis in early-stage colorectal cancers. Clin Cancer Res 20:2147–2158
17. Bento DC, Jones E, Junaid S, Tull J, Williams GT, Godkin A et al (2015) High endothelial venules are rare in colorectal cancers but accumulate in extra-tumoral areas with disease progression. Oncoimmunology 4(3): e974374
18. Coppola D, Nebozhyn M, Khalil F, Dai H, Yeatman T, Loboda A et al (2011) Unique ectopic lymph node-like structures present in human primary colorectal carcinoma are identified by immune gene array profiling. Am J Pathol 179:37–45
19. McMullen TP, Lai R, Dabbagh L, Wallace TM, de Gara CJ (2010) Survival in rectal cancer is predicted by T cell infiltration of tumour-associated lymphoid nodules. Clin Exp Immunol 161:81–88
20. Martinet L, Garrido I, Filleron T, Le Guellec S, Bellard E, Fournie JJ et al (2011) Human solid tumors contain high endothelial venules: association with T- and B-lymphocyte infiltration and favorable prognosis in breast cancer. Cancer Res 71:5678–5687
21. Martinet L, Le Guellec S, Filleron T, Lamant L, Meyer N, Rochaix P et al (2012) High endothelial venules (HEVs) in human melanoma lesions: major gateways for tumor-infiltrating lymphocytes. Oncoimmunology 1:829–839
22. Hindley JP, Jones E, Smart K, Bridgeman H, Lauder SN, Ondondo B et al (2012) T-cell trafficking facilitated by high endothelial venules is required for tumor control after reg-

ulatory T-cell depletion. Cancer Res 72:5473–5482
23. Colbeck EJ, Jones E, Hindley JP, Smart K, Schulz R, Browne M et al (2017) Treg depletion licenses T cell-driven HEV neogenesis and promotes tumor destruction. Cancer Immunol Res 5:1005–1015
24. Allen E, Jabouille A, Rivera LB, Lodewijckx I, Missiaen R, Steri V et al (2017) Combined antiangiogenic and anti-PD-L1 therapy stimulates tumor immunity through HEV formation. Sci Transl Med 9:eaak9679
25. Yu P, Lee Y, Liu W, Chin RK, Wang J, Wang Y et al (2004) Priming of naive T cells inside tumors leads to eradication of established tumors. Nat Immunol 5:141–149
26. Johansson-Percival A, He B, Li ZJ, Kjellen A, Russell K, Li J et al (2017) De novo induction of intratumoral lymphoid structures and vessel normalization enhances immunotherapy in resistant tumors. Nat Immunol 18:1207–1217
27. Tang H, Wang Y, Chlewicki LK, Zhang Y, Guo J, Liang W et al (2016) Facilitating T cell infiltration in tumor microenvironment overcomes resistance to PD-L1 blockade. Cancer Cell 29:285–296
28. Avram G, Sanchez-Sendra B, Martin JM, Terradez L, Ramos D, Monteagudo C (2013) The density and type of MECA-79-positive high endothelial venules correlate with lymphocytic infiltration and tumour regression in primary cutaneous melanoma. Histopathology 63:852–861
29. Mebius RE, Streeter PR, Breve J, Duijvestijn AM, Kraal G (1991) The influence of afferent lymphatic vessel interruption on vascular addressin expression. J Cell Biol 115:85–95
30. Peske JD, Thompson ED, Gemta L, Baylis RA, Fu YX, Engelhard VH (2015) Effector lymphocyte-induced lymph node-like vasculature enables naive T-cell entry into tumours and enhanced anti-tumour immunity. Nat Commun 6:7114
31. Galkina E, Tanousis K, Preece G, Tolaini M, Kioussis D, Florey O et al (2003) L-selectin shedding does not regulate constitutive T cell trafficking but controls the migration pathways of antigen-activated T lymphocytes. J Exp Med 198:1323–1335
32. Galkina E, Florey O, Zarbock A, Smith BR, Preece G, Lawrence MB et al (2007) T lymphocyte rolling and recruitment into peripheral lymph nodes is regulated by a saturable density of L-selectin (CD62L). Eur J Immunol 37:1243–1253
33. Mohammed RN, Watson HA, Vigar M, Ohme J, Thomson A, Humphreys IR et al (2016) L-selectin is essential for delivery of activated CD8(+) T cells to virus-infected organs for protective immunity. Cell Rep 14:760–771
34. Faveeuw C, Preece G, Ager A (2001) Transendothelial migration of lymphocytes across high endothelial venules into lymph nodes is affected by metalloproteinases. Blood 98:688–695
35. Ondondo B, Colbeck E, Jones E, Smart K, Lauder SN, Hindley J et al (2015) A distinct chemokine axis does not account for enrichment of Foxp3(+) CD4(+) T cells in carcinogen-induced fibrosarcomas. Immunology 145:94–104

Chapter 8

Development of Methods for Selective Gene Expression Profiling in Tertiary Lymphoid Structure Using Laser Capture Microdissection

Claudia Gutierrez-Chavez, Samantha Knockaert, Marie-Caroline Dieu-Nosjean, and Jérémy Goc

Abstract

Tertiary lymphoid structures (TLS) are de novo lymphoid formations that are induced within tissues during inflammatory episodes. TLS have been reported at various anatomic sites and in many different contexts like cancer, infections, autoimmunity, graft rejection, and idiopathic diseases. These inducible, ectopic, and transient lymphoid structures exhibit the prototypical architecture found within secondary lymphoid organs (SLO) and have been recently appreciated as a major driver of the local adaptive immune reaction. As TLS emerge within tissues, the isolation in situ and the molecular characterization of these structures are challenging to operate. Laser capture microdissection (LCM) is a powerful tool to isolate selective structural components and cells from frozen or paraffin-embedded tissues. We and other groups previously applied LCM to decipher the molecular network within TLS and uncover their intrinsic connection with the local microenvironment. In this chapter, we describe a detailed LCM method for selecting and isolating TLS in situ to perform comprehensive downstream molecular analyses.

Key words Tertiary lymphoid structure, Laser capture microdissection, Gene expression profiling, RNA analysis, Lymphocyte, Frozen tissue, Lung cancer

1 Introduction

Tertiary lymphoid structures (TLS) have been described in mammalians at various anatomical sites and in many inflammatory contexts, comprising cancer, autoimmune diseases, graft rejection, idiopathic diseases, and viral and bacterial infections [1–5]. TLS share most of the structural characteristics found within canonical secondary lymphoid organs (SLO) such as lymph nodes, including a T-cell zone infiltrated with mature dendritic cells [6–8], and a germinal center with a network of follicular dendritic cells and proliferating B cells [9–12], surrounded by lymphatic vessels and high endothelial venules that express peripheral node addressin (PNAd) [11, 13].

Marie-Caroline Dieu-Nosjean (ed.), *Tertiary Lymphoid Structures: Methods and Protocols*, Methods in Molecular Biology, vol. 1845, https://doi.org/10.1007/978-1-4939-8709-2_8,

The immunological function of TLS is the center of intense investigations as these structures have been recently appreciated as major drivers of the local adaptive immune reaction within various types of inflamed tissues [1, 3, 5]. For example, in autoimmunity or graft rejection, the presence of TLS has been associated with the aggravation of the disease and thus a deleterious effect [3, 4]. Conversely, TLS presence in tumors or at sites of infection has been mainly associated with a better control of the disease and, most of the time, a favorable prognosis [1, 7, 14, 15]. Thus, TLS are a newly appreciated driver of the local adaptive immune reaction that can have harmful or beneficial impact depending on the pathological context.

A number of methods that are described in this issue, like immunohistochemistry, flow cytometry, cell sorting, and deep gene analyses, are powerful approaches to deeply investigate the organization, composition, and immune function of TLS in various anatomical sites and pathological contexts. Nevertheless, interrogating the role of TLS in situ and deciphering their cellular and molecular interactions within the local microenvironment remain a major challenge, especially in humans, as these nonencapsulated structures spontaneously emerge within and/or adjacent to nonlymphoid tissue under inflammatory condition. To comprehensively interrogate the in vivo interactions between TLS and their environmental tissue, specific approaches allowing the molecular characterization of TLS in situ, that is, within the context of their intrinsic tissue microecology, are needed.

Laser capture microdissection (LCM) offers a relatively rapid and accurate method to isolate and routinely analyze tissue regions of interest from their native tissue microenvironment under direct microscopic visualization. LCM can be used to isolate precise anatomical regions of tissue, single cells, or in the present case a concentrated and organized population of lymphocytes from frozen or embedded tissue sections on a microscope slide for various downstream applications like RNA, DNA, protein, or metabolite analyses [16–18]. As a testimony of the effectiveness of this method and proof of applications for TLS investigations, we previously applied LCM to successfully isolate TLS from a cohort of primary lung cancer patients [11]. Using RNA transcript profiling, we demonstrated that lung tumor-associated TLS exhibit a specific chemoattractant molecular signature within the tumor microenvironment, including a network of chemoattractant molecules (CCL19, CCL21, CXCL13, CCL17, CCL22, and IL-16), adhesion molecules (ICAM-2, ICAM-3, VCAM-1, and MAdCAM-1), and integrins (αL, α4, and αD) [11]. This specific molecular signature was confirmed at proteic level and is associated with the selective presence of high endothelial venules and T-cell infiltration within TLS [11]. Thus, LCM combined with RNA transcript profiling allowed to identify the molecular network mediating the migration of

tumor-infiltrating T cells into tumor-associated TLS [11]. LCM is a powerful tool to decipher TLS functions in various tissues and inflammatory contexts, and has been recently applied to inform the role of TLS in lung and skin tumors [12, 19], colitis [20], pulmonary hypertension [21], experimental autoimmune encephalomyelitis [22], aortic aneurysm [23], atherosclerosis [24, 25], and uveitis [26].

A variety of downstream applications from LCM exist, including DNA genotyping, RNA transcript or signal pathway profiling, cDNA library generation, proteomics or biomarker discovery, and metabolomics analyses. With the emergence of next-generation sequencing technologies [27], LCM now represents a practical and very efficient method to conduct deep molecular analyses of TLS in various pathological contexts. In addition to TLS, LCM can also be applied to simultaneously isolate distinct components of the tumor microenvironment, like tumor nests, stroma, blood, or lymphatic vessels, to further conduct molecular comparisons. In this chapter, we describe a detailed and straightforward method for the isolation of TLS and RNA extraction by LCM from human or murine frozen tissues to perform a comprehensive downstream RNA analysis.

2 Materials

2.1 Preparation of Frozen Tissue Sections for Laser Capture Microdissection

1. Solid frozen tissue sample pre-screened for a high density of TLS and a good RNA quality (RIN ≥8).
2. Cryostat microtome (e.g., Leica or other manufacturers) with glass anti-roll preset to −20 °C.
3. Dry ice.
4. Dry ice container with lid.
5. RNase*Zap*® (Applied Biosystems) for RNase removal.
6. Clean tweezers and brushes for cryostat cleaning.
7. Cryostat O-ring chucks.
8. Disposable microtome blades HP35n non-coated (Thermo Fisher Scientific).
9. Leica LMD slides (e.g., 0.2 μm PEN membrane).
10. Cryomatrix optimal cutting temperature (OCT) embedding medium (Thermo Fisher Scientific).
11. 1000 and 100 μL pipets dedicated for RNA work.
12. Filter pipet tips (for 1000 and 100 μL pipets).
13. Nuclease-free water.
14. 100% Ethanol.

15. 70% Ethanol (100% ethanol diluted in ultrapure nuclease-free distilled water).
16. RNase-free 0.01% toluidine blue (diluted in 100% ethanol).
17. 100% Xylene.
18. 50 mL RNase-free Falcon tubes.
19. Centrifuge for tubes.
20. Absorbent paper.
21. Pencil for slide labeling.
22. Staining rack for slide.
23. Slide box.

2.2 Laser Capture Microdissection of TLS from Frozen Tissues

1. Leica Microsystems AS LMD Laser Microdissection Systems (or LCM system from other manufacturers).
2. 0.2 mL RNase-free PCR tubes with flat cap suitable for the LCM-stage collection holder.
3. Buffer RLT (Qiagen) for lysis of cells and tissues before RNA isolation.
4. 14.3 M ß-mercaptoethanol.
5. 100 µL Pipet dedicated for RNA work.

2.3 RNA Extraction from Microdissected TLS

1. RNeasy Micro Kit (Qiagen).
2. DNase I (1500 Kunitz units, Qiagen).
3. Microcentrifuge ($\geq$13,000 $\times g$).
4. 80% Ethanol prepared with ethanol (96–100%) diluted with nuclease-free distilled water.
5. RNase-free 50 mL Falcon tube.
6. Ice.

2.4 Assessing RNA Integrity

1. Agilent RNA 6000 Pico kit (Agilent Technologies).
2. Agilent 2100 Bioanalyzer with Chip priming station and IKA vortex mixer (Agilent Technologies).
3. Heating block.
4. Microcentrifuge ($\geq$13,000 $\times g$).
5. RNase*ZAP*® (Applied Biosystems).
6. Nuclease-free water.
7. 0.5 mL RNase-free microcentrifuge tubes.
8. Pipet 1000 and 10 µL dedicated for RNA work.
9. Ice.

2.5 Reverse Transcription for cDNA Generation

1. High-Capacity cDNA Reverse Transcription Kit (Applied Biosystems).
2. Pipet 200, 10, and 2 μL dedicated for RNA work.
3. PCR thermal cycler.

2.6 Quantitative Real-Time Polymerase Chain Reaction Assays

1. Applied Biosystems quantitative real-time PCR system (or compatible real-time PCR system from other suppliers).
2. MicroAmp Optical 96-Well Reaction Plate for quantitative Real-Time PCR (Thermo Fisher Scientific).
3. 96-Well MicroAmp Optical Adhesive Film (Applied Biosystems).
4. Compression pad to seal the quantitative real-time PCR plate.
5. TaqMan Universal PCR Master Mix (Applied Biosystems).
6. TaqMan Gene Expression Assays (Applied Biosystems).
7. Pipet 200, 10, and 2 μL dedicated for RNA work.

3 Methods

This section describes the successive steps that should be conducted for TLS isolation by LCM, RNA extraction, and gene expression analyses from frozen tissue samples. The protocol provided is a general method for LCM that has been successfully applied for TLS RNA profiling on human lung tumor tissues [11]. The experiments are described in the following order: frozen tissue preparation, LCM isolation, RNA extraction, RNA integrity assessment, reverse transcription cDNA generation, quantitative real-time (qRT) PCR, and analysis. This method is intended to be a starting point for extensive LCM and molecular analyses of TLS on various types of mammalian tissues. Thus, conditions should be tested and optimized by the users for the application on other types of human or murine tissues before proceeding.

3.1 Preparation of Frozen Tissue Sections for Laser Capture Microdissection

The frozen tissue sample has been snap-frozen by immersion into liquid nitrogen immediately after surgery or organ sample to preserve RNA integrity and was stored in liquid nitrogen or at −80 °C before the experiment (*see* **Note 1**). Frozen tissues must be transported in an appropriate container containing dry ice for further cryosection (*see* **Note 2**). When possible, it is highly recommended to first screen the frozen tissue of interest to confirm preservation of the histological architecture, the presence of TLS, and a good RNA quality (RIN ≥8) before proceeding to the LCM.

1. Set the temperature of the cryostat to −20 °C. Clean the workstation, the cryostat chamber, and the knife holder (not the knife blade) and treat the tweezers and brushes that will be used to handle the tissue sections with RNase*Zap* (*see* **Note 3**).

2. Place the frozen tissue sample into the cryostat, and let it equilibrate for at least 10 min at −20 °C (*see* **Note 4**).
3. Add one drop of Cryomatrix OCT embedding medium on the surface of a cold chuck serving as the "glue" at the interface (*see* **Note 5**), and quickly attach the frozen tissue with the help of the tweezers before the OCT hardens. Apply just the minimal amount of OCT needed to finely cover the surface of the chuck and securely mount the tissue (*see* **Note 6**).
4. Wait for 10 min for the OCT to solidify at −20 °C (the OCT will turn from translucent to white when frozen). Assure that the tissue is solidly stuck and mount the chuck in the specimen holder orienting the tissue to expose the region of interest.
5. Gently bring the tissue section near to the blade. Using a fresh disposable blade, shave OCT (set the cutting thickness from 5 to 10 μm) from the tissue block until the tissue becomes visible. If necessary, start with successive cuttings of 30 μm until a decent amount of tissue has been sectioned giving access to a large region of interest. At the end of this step, the investigator should obtain a clear and well-oriented plan section of the tissue.
6. Set the thickness of the tissue section at 5–14 μm (depending on the nature and the hardness of the tissue to be microdissected) and start cutting gently. Manipulate the newly cut tissue section onto the glass anti-roll plate and use a small brush to straighten out the section (*see* **Note 7**).
7. Collect the tissue section on a PEN membrane LMD glass slide (that investigator has labeled using the pencil) by carefully placing the slide (with the membrane side facing down) against the tissue section and pressing quickly and gently. The tissue section should stick immediately on the membrane. During this step, the tissue section must be handed with extra careful precautions to preserve the native architecture of the tissue (*see* **Note 8**). This will be critical to facilitate the detection and the successful microdissection of TLS during the LCM step.
8. To maximize resources per slide and the potential number of TLS to be microdissected, proceed to cut several tissue sections (as described in **steps 6**–**7**) and collect them sequentially on the same PEN membrane LMD glass slide to load a total of 4–10 samples (depending on the nature and the size of the tissue) per slide (*see* **Notes 9** and **10**).
9. Remove the PEN membrane LMD glass slide from the cryostat and immediately apply a 70% ethanol fixative solution for 1 min on the tissue sections (*see* **Note 11**). The fixation and staining steps should then be performed under a hood dedicated for RNA work.

10. Drain the 70% ethanol and gently rinse with nuclease-free water for 10 s.
11. Drain the water and start the coloration by gently applying RNase-free 0.01% toluidine blue (≈100 μL) onto the slide to completely cover the tissue sections and let the slide stain for 90 s (*see* **Note 12**).
12. Gently wash the slide with 70% ethanol for 30 s and then with 100% ethanol for 30 s. Additionally, the slide may also be rinsed in xylene for a maximum of 5 min to enhance dehydration before proceeding with LCM (*see* **Note 13**). Blot the slide on an absorbent paper in between the different solution washes, to prevent carryover from the previous solution (*see* **Note 14**).
13. Allow the slide to air-dry for 5 min before loading on the microscope platform. When the tissue section is dry, the slide is ready to proceed to LCM.

3.2 Laser Capture Microdissection of TLS

1. Turn on power for the microscope and laser control box. Let the laser warm up during approximately 10 min (*see* **Note 15**).
2. Use a cover-slipped toluidine blue-stained section of the tissue to pre-analyze the tissue and estimate the number of TLS before starting the LCM. This step will help the investigator to estimate the number of LCM sessions required to yield sufficient RNA quantity for downstream analyses. This step will also avoid losing time analyzing the tissue and risking potential RNA degradation when performing the LCM on the PEN membrane glass slide.
3. Pipet 35 μL of lysis buffer (RLT + 1% ß-mercaptoethanol) for OCT-embedded tissues into the cap of a clean 0.2 mL RNase-free collection tube with flat cap. Load the tube in the collection for tube caps on the holder apparatus of the LCM system under the microscope platform.
4. Place the PEN membrane glass slide on the microscope stage with the membrane and the stained tissue sections facing down.
5. Calibrate the laser (*see* **Note 16**) and adjust the laser parameters (power, aperture, speed, frequency, and focus) appropriately according to the type of tissue to be microdissected (*see* **Note 17**).
6. Make sure that the cap is aligned with the objective on the microscope (it should be visible through the aperture in the stage) before starting the LCM. Focus the microscope with the 20× objective to get a clear view of the tissue. Locate all the TLS-enriched regions of interest by moving the tracking beam.
7. Using the drawing tool, draw an area that surrounds the TLS, proceed to fire the laser (if a specific number of TLS is desired

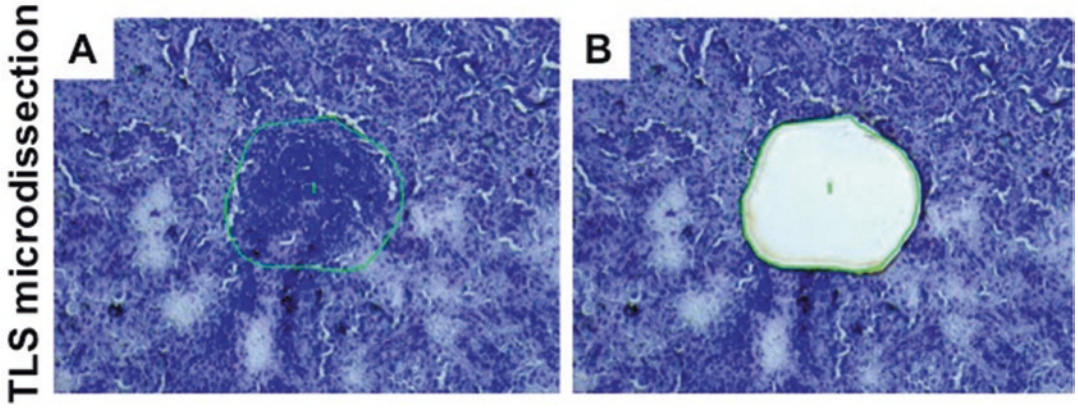

Fig. 1 Laser capture microdissection of TLS. TLS from a frozen human lung tumor before (**a**) and after (**b**) the laser capture microdissection. The microdissected area is designated by the green line. Tissue section was fixed and stained with 0.01% toluidine blue before performing the LCM

to collect, then investigator can optionally locate and assign all the areas where TLS are present and then proceed to the LCM), and drop the microdissected TLS in the RLT buffer. A clear and confident detection of TLS is critical for this step; thus TLS microdissection should always be performed by an investigator who is well trained to identify and confidently distinguish TLS among the tissue complexity. We define TLS as an aggregate of more than 50 cells with lymphocyte morphology and demonstrating nodular formation with close cell-to-cell contact within the structure (Fig. 1).

8. After completing the LCM, unload the collection tube, carefully close the cap, and briefly spin down the dissectates (*see* **Note 18**).
9. Gently open the lid and rinse the cap surface with another 40 μL of lysis buffer (total final volume = 75 μL). Carefully close the cap to avoid any loss of material and mix gently by inverting the tube so that the lysis buffer rinses the cap (*see* **Note 19**).
10. Keep the collection tube at −20 °C inside the cryostat until the end of the LCM session (*see* **Note 20**).

3.3 RNA Extraction of Microdissected TLS

We recommend using the RNeasy Micro kit (Qiagen) for RNA extraction that is adapted for RNA purification from small amounts of tissues or cells (maximum 45 μg of RNA per sample). Investigators should work quickly at room temperature (15–25 °C) and in an RNA work-dedicated area during all the RNA extraction process.

1. Vortex the tubes for 30 s and add 1 volume of 70% ethanol to the homogenized lysate. Mix well by pipetting up and down and

immediately transfer the lysate (including any precipitate that might have formed after ethanol addition) to the RNeasy MinElute spin column placed in an RNase-free 2 mL collection tube.

2. Gently close the lid and centrifuge for 1 min at 100 × *g* and then centrifuge for 1 additional minute at 10,000 × *g*.
3. Discard the effluent present in the collection tube (*see* **Note 21**) and briefly wipe the tube on an absorbent paper before replacing the filter.
4. Add 350 μL of RW1 buffer inside the RNeasy MinElute spin column.
5. Gently close the lid and centrifuge for 1 min at 10,000 × *g*. Discard the effluent present in the collection tube and briefly wipe the tube on an absorbent paper before replacing the filter.
6. Prepare the DNase I incubation mix by pipetting 10 μL of DNase I stock solution to 70 μL of RDD buffer. Mix gently by inverting the tube (*see* **Note 22**).
7. Add 80 μL of the DNase I incubation mix by gently pipetting directly on the middle of the silica membrane (be extra careful not to disrupt the membrane during this step) of the column and let incubate at room temperature (20–30 °C) for 15 min (*see* **Note 23**).
8. Add 350 μL of RW1 buffer inside the RNeasy MinElute spin column and centrifuge for 1 min at 10,000 × *g*. Discard the effluent and the collection tube and transfer the column to a new RNase-free 2 mL collection tube.
9. Add 500 μL of RPE buffer (*see* **Note 24**) and centrifuge for 1 min at 10,000 × *g*. Discard the effluent present in the collection tube and briefly wipe the tube on an absorbent paper before replacing the filter.
10. Add 500 μL of 80% ethanol to the RNeasy MinElute spin column. Close the lid gently, and centrifuge for 2 min at 10,000 × *g* to wash the spin column membrane. Discard the effluent present in the collection tube and briefly wipe the tube on an absorbent paper before replacing the filter.
11. Centrifuge for 1 min at 10,000 × *g* with the lid open to allow the silica membrane to dry.
12. Place the RNeasy MinElute spin column in a new and labeled RNase-free 1.5 mL tube, and add 14 μL of nuclease-free water into the middle of the column membrane.
13. Centrifuge for 1 min at 1000 × *g* and then centrifuge for 1 min a 10,000 × *g* to collect total RNA. Discard the column.
14. Transfer 1.3 μL of the RNA sample to a new 0.2 mL tube for further evaluation of RNA quality and quantity. Store the samples immediately at −80 °C.

3.4 Assessing RNA Integrity

1. Allow all reagents from the Agilent RNA 6000 Pico kit (Agilent Technologies): Pico Gel Matrix, Pico Dye Concentrate, Pico Conditioning Solution, and Pico Marker to equilibrate at room temperature and protected from light for at least 30 min before use (*see* **Note 25**). Remove an aliquot of the Pico RNA Ladder from the freezer and let it thaw on ice (*see* **Note 26**).
2. Pipet 550 μL of the RNA 6000 Pico gel matrix (red tube) into the top of receptacle of a spin filter. Place the spin filter in the microcentrifuge and centrifuge at 1500 × *g* for 10 min at room temperature. Aliquot 65 μL of filtered gel into 0.5 mL RNase-free microcentrifuge tubes. The filtered gel can then be stored at 4 °C for up to 4 weeks.
3. Pipet 1.3 μL of each RNA samples into an RNase-free 0.5 mL tube. Heat denature the RNA samples for 2 min at 70 °C with a heat block. Keep then the RNA on ice until further utilization. Before further use, briefly centrifuge the tube to collect the RNA at the bottom of the tube.
4. Vortex the RNA dye concentrate (blue tube) for 10 s and spin down briefly. Add 1 μL of dye concentrate into a 65 μL aliquot of filtered gel (previously equilibrated at room temperature). Vortex well for 10 s and centrifuge for 10 min at 13,000 × *g*. The gel-dye mix must then be used within 1 day and one tube can be used to run two chips.
5. Start the 2100 Expert Software and turn on the Bioanalyzer. To wash the electrodes of the Bioanalyzer, place an electrode cleaner containing 350 mL of nuclease-free water in the instrument, close the lid, and let it wash for 5 min. In the meantime, select "Assays," "Electrophoresis," "RNA," and finally "Eukaryotic Total RNA Pico Series" on the instrument menu. Then define the number of samples (from 1 to 11 per chip) to be assayed and enter the corresponding sample information. After cleaning, remove the electrode cleaner and allow the remaining water to evaporate for 30 s before closing the lid of the Bioanalyzer (*see* **Note 27**).
6. Prepare the chip priming station and insert a new RNA Pico Chip within the station. Pipet 9 μL of the gel-dye mix into the well marked with an encircled "G" (*see* **Note 28**). Make sure that the syringe is positioned back to 1 mL and then close the chip priming station until you hear a click confirming that the priming station is closed properly. Press the plunger down until it is secured beneath the syringe clip. Wait for exactly 30 s and then release the plunger with the clip-release mechanism. Wait for 5 s and then slowly pull back the syringe to the 1 mL position.
7. Open the chip station and pipet 9 μL of the gel-dye mix into the two remaining wells marked "G." Then, add 9 μL of the RNA 6000 Pico Conditioning Solution (white tube) to the well marked "CS."

8. Pipet 5 μL of the RNA 6000 Pico Marker (green tube) into the ladder well and in all wells containing RNA samples. Add 6 μL of Pico RNA Marker to any empty sample wells.
9. Add 1 μL of aliquoted and heat-denatured RNA 6000 Pico Ladder to the ladder well and 1 μL of RNA sample to the appropriate sample wells. After loading all wells, vortex the chip using the manufacturer-supplied IKA vortexer for 1 min at 2400 rpm. Within the next 5 min, place the Pico Chip on the Agilent 2100 Bioanalyzer and start the run (*see* **Note 29**).

If investigators are working on single cells isolated within TLS and/or for specific applications, like RNA-seq, requiring an important quantity of material, it may be necessary to first amplify the RNA [28] before proceeding to downstream applications.

3.5 Reverse Transcription for cDNA Generation

The RNA yielded from LCM will be reverse transcribed using the High-Capacity cDNA Reverse Transcription Kit (Applied Biosystems). The reagents supplied per kit are sufficient for 200 reactions (20 μL/reaction). Use up to 2 μg of total RNA per 20 μL of reactions. Define the volume of master mix required for your experiment before starting the reverse transcription PCR. Work on ice during all the process.

1. Allow the High-Capacity cDNA Reverse Transcription Kit (Applied Biosystems) to thaw on ice. Then, prepare the 2× reverse transcription master mix (in 10% excess) still on ice. Each 2× 10 μL master mix reaction requires combining:
   (a) 2 μL 10× RT buffer
   (b) 0.8 μL 25× dNTP mix (100 mM)
   (c) 2 μL 10× RT random primers
   (d) 1 μL MultiScribe reverse transcriptase
   (e) 1 μL RNase inhibitor
   (f) 3.2 μL Nuclease-free water

   Mix gently and centrifuge briefly. Pipet 10 μL of the 2× RT master mix into each well of a 96-well reaction plate or in individual PCR tubes.
2. Pipet 10 μL of RNA sample into each well or tube, mixing by pipetting up and down two times. Centrifuge briefly to spin down the content at the bottom of the tube and to eliminate any air bubbles.
3. Load the plate or tubes into the thermal cycler and let incubate using the following program: 10 min at 25 °C, 2 h at 37 °C, 5 min at 85 °C, and then hold at 4 °C.

4. When the reverse transcription reaction is complete, add nuclease-free water to adjust the concentration of the samples to 5 ng/μL.
5. Mix the diluted samples well and centrifuge briefly. Place on ice for proceeding qRT-PCR or store at −20 °C for further applications.

3.6 Quantitative Real-Time Polymerase Chain Reaction Assays

A variety of techniques for deep molecular analyses exist, including next-generation sequencing or microarrays [27]. Each of them comes with its own advantages and limitations in terms of signal sensitivity, specificity, and stability. Quantitative RT-PCR quantification of mRNA molecules remains a reliable and routine method, even in combination with few microdissected cells for sensitive gene expression analyses or target gene confirmation. For the following protocol description, we describe a qRT-PCR method based on TaqMan Gene Expression Assays (*see* **Note 30**). To generate accurate and reproducible results from qRT-PCR, be careful and precise when performing each step in the protocol, especially for pipetting.

1. Turn the TaqMan Real-Time PCR instrument on and allow it to warm up for at least 20 min. We used TaqMan2900HD (Applied Biosystems) for this step, but note that TaqMan assays can also be run on a variety of real-time PCR instruments from other constructors. In the meantime, prepare your experiment settings and load the appropriate target genes and fluorophores (FAM™, VIC® dye-labeled MGB probe, or SYBR Green) in your experiment file and save the file.
2. Perform the qRT-PCR using the TaqMan Gene Expression Assay of interest. qRT-PCR reactions should be performed at least in duplicate, but if sufficient material is available we recommend performing the assay with triplicate or quadruplicate reactions. The following protocol is based on 10 ng of cDNA per gene analysis for a total volume of 20 μL per reaction (*see* **Note 31**). First, prepare a master mix containing the following per reaction (*see* **Note 32**):
   (a) 10 μL of 2× TaqMan Gene Expression Master Mix
   (b) 7 μL of nuclease-free water
   (c) 1 μL of 20× TaqMan Gene Expression Assay
3. Pipet 18 μL of the master mix per well of a qRT-PCR plate and then add 2 μL of cDNA (5 ng/μL) into the appropriate wells. Be extremely careful not to generate air bubbles in the wells when pipetting.
4. Seal the plate with the appropriate cover adhesive film and apply a compression pad all over the plate to confirm the sealing. Centrifuge the plate briefly.

5. Load the reaction plate into the real-time PCR system. In the instrument settings, set the volume of reaction to 20 μL and set the following cycles:
   (a) Cycle 1: 10 min at 95 °C
   (b) Cycle 2: 15 s at 95 °C for 40 cycles
   (c) Cycle 3: 1 min at 60 °C for 40 cycles
   (d) Cycle 4: hold at 4 °C
6. Start the run.
7. Calculate the Ct values for each sample and the reference housekeeping genes and average the value per replicates. Calculate the expression level of each specific target (gene) between the different samples by using the relative standard curve or the comparative Ct methods [29].

4 Notes

1. Frozen sections are the best choice for RNA analyses. Prompt freezing of the sample limits RNA and protein degradation due to nuclease and protease activity. For a long-term storage (i.e., more than 6 months), it is recommended to conserve the samples in liquid nitrogen as it offers the best preservation of proteins and RNA. Conservation at −80 °C is adequate for short-term storage (i.e., less than 6 months). Alternatively, formalin-fixed paraffin-embedded (FFPE) tissue can also be used, as it has been referenced in the literature [17, 18]. Nevertheless, it is more challenging obtaining acceptable RNA quality from FFPE tissues after LCM. For these reasons, we recommend to always favor LCM on frozen tissue when possible. Frozen tissue should be tested for RNA quality before proceeding to LCM (we recommend only using tissue with a RIN ≥8).
2. The investigators should observe universal precautions when manipulating human tissue samples. Use standard personal protective equipment (latex, gloves, lab coat, and safety glasses if required) and manipulate all biological material as potential biohazard. Dispose all biohazardous materials in appropriate container. Tissues from mice must be used in accordance with the Care and Use of Laboratory Animals, and the study protocol must have been approved by the appropriate Institutional Animal Care and Use Committee.
3. For robust RNA analyses, it is critical to obtain RNA of the highest possible quality by preventing RNase contamination and degradation during tissue collection, cryosection, LCM, RNA extraction, and downstream applications. Standard lab

precautions for RNA manipulation must be applied during all these steps. A specific clean area for RNA work should have been designated in the lab. All equipment and laboratory benches should have been cleaned with RNase*Zap* or 100% ethanol before starting the procedure (carefully wash all the surfaces, supports, and tools in the cryostat). RNase-free material must be used at all stages of work with RNA. Gloves should be worn at all times and changed frequently, especially after contact with liquids or surfaces that may be contaminated with RNases. Filter pipet tips should be used and changed each time you pipet to avoid potential cross-contamination between samples and to prevent RNase contamination. For most procedures, it is advisable to use nuclease-free, hydrophobic, nonstick tubes to minimize loss of sample that may otherwise adhere to the tube walls.

4. Make sure that the tissue sample has equilibrated at cryostat temperature before starting cutting. This will avoid undesirable folds in the section and sticking to the membrane slide during the cut collection.
5. Cover the chuck's flat surface with a piece of wet towel paper and let it dry in the cryostat at −20 °C before pasting the tissue section with OCT medium on the chuck. This will facilitate the disassembly of the tissue section from the chuck at the end of the cryosection. Investigator will simply need to remove the towel paper to detach the tissue from the chuck.
6. Be quick when pasting the frozen tissue with OCT on the chuck. The OCT medium generally takes less than 1 min to solidify. As an indication, the OCT will turn white in color when completely frozen and solid. Investigator should use a tissue less than 1.5 cm size to facilitate cutting. It is recommended adjusting the angle of the tissue block before the medium hardens so that the region of interest of the tissue is facing up and aligned in parallel with the chuck surface. This will then facilitate getting a proper orientation of the tissue section with the microtome blade after loading the chuck in the specimen holder of the cryostat.
7. It is critical to avoid tissue carryover during cutting procedure. Carryover contamination of one specimen from another will results in false or non-reproducible results. Thus, the blade used to cut sections should be kept clean during the experiment, and every excess tissue fragments should be systematically wiped from the area with the brush. A fresh microtome blade should be used for each new specimen, and disposable blades used if possible. If LCM is performed for downstream RNA analyses, it is recommended cleaning the stage of the

microtome, which contacts the sectioned tissue, with the brush and RNase*Zap* between each specimen.

8. If investigator encounters difficulty to maintain original structure of the tissue, due to friability of the section or difficulty in cutting, the tissue may be too cold. Therefore, the temperature of the cryostat should be adjusted until finding the optimal temperature point for the cutting. Optimal temperature point will depend on the nature and the thickness of the tissue.
9. Keep the membrane PEN slides at room temperature before applying a tissue section. Tissues don't adhere well on cold membrane slides. Work gently and as quickly as possible. If the investigator wants to include multiple tissue sections on a slide to maximize resources, keep the slide in the cryostat and warm the area of the slide where the tissue will be deposited by pressing your thumb to the reverse side.
10. PEN membrane slide loaded with tissue sections can be conserved 1 month at −80 °C for further microdissection. Nevertheless, please note that the duration for RNA preservation can vary depending on the nature of the tissue. When possible, we always recommend performing the LCM immediately after the tissue cryosection.
11. It is mandatory to prevent the slide from drying or thawing before the contact with 70% ethanol to avoid loss of tissue adherence to the PEN membrane of the glass slide and/or to prevent RNA degradation.
12. Since tissue section on PEN membrane slide is not coverslipped, the microscopic visualization of the tissue is often darker than first expected when starting the LCM. Optimizing the time of staining and diluting the colorant with nuclease-free water will produce lighter staining and will help finding the best staining conditions for each specific type of tissue.
13. A complete dehydration of the tissue is critical to minimize the adhesive forces between the tissue section and the slide and optimize the LCM efficiency. Increasing the incubation time up to 2 min for the 100% ethanol and up to 5 min for xylene will enhance dehydration and increase the efficiency of the microdissection. These steps can be repeated if the investigator encounters issue with the tissue transfer during LCM. Optionally, after fixation, staining, and dehydrating steps, the slides can be gently heated on a heating block for a maximum of 5 min to ensure full dehydration.
14. There are many alternatives to toluidine blue coloration, like hematoxylin and eosin or methylene blue, that can be tested and preferred depending on the type of tissue to be microdissected [17]. Further, immunohistochemistry procedure for

staining of specific cell subtypes within TLS (like dendritic cells, B cells, or T cells) can also be applied and combined with LCM [18]. This procedure should be set up and optimized by the user for each specific antibody combination.

15. Various methods of LCM exist that can be divided into contact and noncontact methods in reference to the process used to isolate and extract the targeted cells or structures from the native tissue [18]. For this protocol, we are referencing to a Leica LMD system using a noncontact gravity-assisted microdissection method.
16. Move the microscope objective until finding an empty "white area" (without tissue section) on the slide when calibrating the laser parameters for testing its accuracy.
17. The setting up of the laser parameters (power, aperture, speed, frequency, and focus) is critical for the success of the experiment. These parameters are strongly dependent on the nature and the thickness of the tissue as well as the size of the structures to be microdissected. Thus, laser parameters must systematically be optimized depending on the tissue and the experiment. It is also strongly recommended testing the settings of the laser on a control tissue before starting a LCM session on a precious tissue sample.
18. As a confirmation of a proper collection of the microdissected TLS, the RLT lysis solution within the flat cap should progressively turn blue during the LCM step due to the accumulation of toluidine blue-stained tissue within the lysis buffer. Absence of blue coloration should raise concern about the RNA concentration or the proper collection of the tissue during the LCM. It is recommended collecting the microdissected TLS in at least two PCR tubes for recovering enough quantity of material for posterior RNA extraction.
19. The steps in Subheading 3.2 should be carried out as quickly as possible. Tissue staining and LCM of TLS should require a maximum of 60 min (depending on the number of microdissected tissue sections per slide) to prevent RNA degradation.
20. Tissue lysates can be extracted for RNA immediately after the LCM session or alternatively stored at −80 °C for up to 6 months. When possible, we recommend performing the RNA extraction the same day after performing the LCM.
21. To avoid ß-mercaptoethanol odors in the lab, discard the RLT buffer eluent in a closed 50 mL Falcon tube during Subheading 3.3, **step 3**, of the RNA extraction.
22. DNase I is highly sensitive to physical degradation and risk denaturation if vortexed.

23. It is important to assure that the DNase I incubation mix is in contact with the membrane; otherwise the digestion will be incomplete.
24. Qiagen supplies the buffer RPE as a concentrate in the kit. Investigator must have prepared a working solution, that is, by adding 4 volumes of 100% ethanol to the concentrate RPE buffer, before starting.
25. Dyes are light sensitive and must be kept covered while equilibrating at room temperature. The total RNA concentration for use with the Agilent RNA 6000 Pico kit must be between 500 and 5000 pg/μL. If concentration of the sample is above this range, dilute it with nuclease-free water.
26. To avoid repetitive/thaw cycles, the Pico RNA Ladder must have been prepared and aliquoted upon kit arrival. The ladder needs to be denatured by warming for 2 min at 70 °C on a heat block before cooling on ice. Add 90 μL of nuclease-free water, mix well before aliquoting in 0.5 mL RNase-free vials, and store at −80 °C.
27. For periodic washing or when you suspect a RNA contamination on the Bioanalyzer electrodes, remove the pin set on the Bioanalyzer and proceed to wash the electrodes with RNase*Zap*. Then rinse thoroughly with nuclease-free water.
28. Never use the blowout function of the pipet when loading the Pico chip. This may generate air bubbles within the chip that will interfere with the RNA analysis during the chip run.
29. RNA extracted from TLS should have a concentration of ≥7 ng/μL and a RNA integrity number (RIN) ≥7 for posterior gene expression analysis. A RIN number <5 may raise major concerns about nonspecific amplification during the reverse transcription and the real-time PCR steps, and thus should not be used for downstream analyses. A low RIN number can be due to incorrect snap-freezing of the native tissue or due to a too long session (>60 min) of LCM that has resulted in RNA degradation, or can alternatively come from problems occurred during RNA extraction. If the investigator has confirmed that the initial frozen tissue has a good RNA quality (RIN ≥8), it is recommended repeating the LCM and RNA isolation steps.
30. In addition to TaqMan, there are several detection methods available that can be used for performing qRT-PCR from microdissected tissue, including SYBR Green.
31. In our experience, 10 ng of cDNA material usually allows good gene detection. Nevertheless, when working with low-abundance transcripts gene targets, the starting amount of cDNA needs to be increased to achieve an appropriate range of

detection. In this case, the volume of water in the master mix will need to be adjusted, accordingly.

32. TaqMan assay materials are light sensitive and must be kept in the freezer, away from light, until you are ready to use them. Excessive exposure to light may degrade the fluorescent probes and impact the results.

Acknowledgments

We thank all present and past members of the Laboratory "Cancer, Immune control and Escape" (UMRS1138 INSERM, Cordeliers Research Center), pathologists, and clinicians who have participated in these studies, for their help and valuable discussions. We are grateful to lung cancer patients involved in this research performed in our laboratory.

Funding: This work was supported by the Institut National de la Santé et de la Recherche Médicale (INSERM), Pierre and Marie Curie University, Paris-Descartes University, the Labex Immuno-Oncology (LAXE62_9UMRS872 Fridman), CARPEM (Cancer Research for PErsonalized Medicine), Fondation ARC pour la Recherche sur le Cancer. Jeremy Goc was supported by a grant from the Fondation ARC pour la Recherche sur le Cancer.

References

1. Dieu-Nosjean M-C, Goc J, Giraldo NA et al (2014) Tertiary lymphoid structures in cancer and beyond. Trends Immunol 35:571–580
2. Goc J, Fridman WH, Sautès-Fridman C et al (2013) Characteristics of tertiary lymphoid structures in primary cancers. OncoImmunology 2:e26836
3. Pitzalis C, Jones GW, Bombardieri M et al (2014) Ectopic lymphoid-like structures in infection, cancer and autoimmunity. Nat Rev Immunol 14:447–462
4. Koenig A, Thaunat O (2016) Lymphoid neogenesis and tertiary lymphoid organs in transplanted organs. Front Immunol 7:646
5. Engelhard VH, Rodriguez AB, Mauldin IS et al (2018) Immune cell infiltration and tertiary lymphoid structures as determinants of antitumor immunity. J Immunol Baltim Md 1950 200:432–442
6. Dieu-Nosjean M-C, Antoine M, Danel C et al (2008) Long-term survival for patients with non-small-cell lung cancer with intratumoral lymphoid structures. J Clin Oncol Off J Am Soc Clin Oncol 26:4410–4417
7. Goc J, Germain C, Vo-Bourgais TKD et al (2014) Dendritic cells in tumor-associated tertiary lymphoid structures signal a Th1 cytotoxic immune contexture and license the positive prognostic value of infiltrating CD8+ T cells. Cancer Res 74:705–715
8. Remark R, Alifano M, Cremer I et al (2013) Characteristics and clinical impacts of the immune environments in colorectal and renal cell carcinoma lung metastases: influence of tumor origin. Clin Cancer Res Off J Am Assoc Cancer Res 19:4079–4091
9. Germain C, Gnjatic S, Tamzalit F et al (2014) Presence of B cells in tertiary lymphoid structures is associated with a protective immunity in patients with lung cancer. Am J Respir Crit Care Med 189:832–844
10. Gu-Trantien C, Loi S, Garaud S et al (2013) CD4+ follicular helper T cell infiltration predicts breast cancer survival. J Clin Invest 123:2873–2892
11. de CL, Goc J, Damotte D et al (2011) Characterization of chemokines and adhesion

molecules associated with T cell presence in tertiary lymphoid structures in human lung cancer. Cancer Res 71:6391–6399

12. Cipponi A, Mercier M, Seremet T et al (2012) Neogenesis of lymphoid structures and antibody responses occur in human melanoma metastases. Cancer Res 72:3997–4007
13. Ruddle NH (2016) High endothelial venules and lymphatic vessels in tertiary lymphoid organs: characteristics, functions, and regulation. Front Immunol 7:491
14. Moyron-Quiroz JE, Rangel-Moreno J, Kusser K et al (2004) Role of inducible bronchus associated lymphoid tissue (iBALT) in respiratory immunity. Nat Med 10:927–934
15. Di Caro G, Bergomas F, Grizzi F et al (2014) Occurrence of tertiary lymphoid tissue is associated to T cell infiltration and predicts better prognosis in early stage colorectal cancers. Clin Cancer Res Off J Am Assoc Cancer Res 20:2147–2158
16. Decarlo K, Emley A, Dadzie OE et al (2011) Laser capture microdissection: methods and applications. Methods Mol Biol Clifton NJ 755:1–15
17. Espina V, Wulfkuhle JD, Calvert VS et al (2006) Laser-capture microdissection. Nat Protoc 1:586–603
18. Frost AR, Eltoum I-E, Siegal GP et al (2015) Laser microdissection. Curr Protoc Mol Biol 112:25A.1.1–25A.130
19. Johansson-Percival A, He B, Li Z-J et al (2017) De novo induction of intratumoral lymphoid structures and vessel normalization enhances immunotherapy in resistant tumors. Nat Immunol 18:1207–1217
20. Lochner M, Ohnmacht C, Presley L et al (2011) Microbiota-induced tertiary lymphoid tissues aggravate inflammatory disease in the absence of RORγt and LTi cells. J Exp Med 208:125–134
21. Colvin KL, Cripe PJ, Ivy DD et al (2013) Bronchus-associated lymphoid tissue in pulmonary hypertension produces pathologic autoantibodies. Am J Respir Crit Care Med 188:1126–1136
22. Lehmann-Horn K, Wang S-Z, Sagan SA et al (2016) B cell repertoire expansion occurs in meningeal ectopic lymphoid tissue. JCI Insight 1:e87234
23. Spear R, Boytard L, Blervaque R et al (2015) Adventitial tertiary lymphoid organs as potential source of microRNA biomarkers for abdominal aortic aneurysm. Int J Mol Sci 16:11276–11293
24. Srikakulapu P, Hu D, Yin C et al (2016) Artery tertiary lymphoid organs control multilayered territorialized atherosclerosis B-cell responses in aged ApoE−/− mice. Arterioscler Thromb Vasc Biol 36:1174–1185
25. Hu D, Mohanta SK, Yin C et al (2015) Artery tertiary lymphoid organs control aorta immunity and protect against atherosclerosis via vascular smooth muscle cell lymphotoxin β receptors. Immunity 42:1100–1115
26. Kielczewski JL, Horai R, Jittayasothorn Y et al (2016) Tertiary lymphoid tissue forms in retinas of mice with spontaneous autoimmune uveitis and has consequences on visual function. J Immunol 196:1013–1025
27. Goodwin S, McPherson JD, McCombie WR (2016) Coming of age: ten years of next-generation sequencing technologies. Nat Rev Genet 17:333–351
28. Kube DM, Savci-Heijink CD, Lamblin A-F et al (2007) Optimization of laser capture microdissection and RNA amplification for gene expression profiling of prostate cancer. BMC Mol Biol 8:25
29. Schmittgen TD, Livak KJ (2008) Analyzing real-time PCR data by the comparative C(T) method. Nat Protoc 3:1101–1108

Chapter 9

Quantifying Tertiary Lymphoid Structure-Associated Genes in Formalin-Fixed Paraffin-Embedded Breast Cancer Tissues

Chunyan Gu-Trantien, Soizic Garaud, Edoardo Migliori, Cinzia Solinas, Jean-Nicolas Lodewyckx, and Karen Willard-Gallo

Abstract

Tertiary lymphoid structures (TLS) have been detected in several types of human solid tumors. These structures are thought to regulate local adaptive immune responses that can promote or antagonize tumor progression. Despite positive prognostic values associated with a TLS presence in several studies, discrepancies still exist. TLS are structurally organized entities composed of varying numbers of multiple cell types making their assessment in tumor tissues, particularly biopsies, challenging. Immunohistochemical staining of TLS-related cell populations is the most frequently used method for identifying and scoring them; however, TLS-related gene expression has also been explored. The protocols described are detailed to allow the user to quantify TLS-related gene expression on formalin-fixed paraffin-embedded human breast tumor tissues.

Key words Tertiary lymphoid structure, Gene expression, qPCR, Formalin-fixed paraffin-embedded tissue, Breast cancer

1 Introduction

Secondary lymphoid organs (SLOs), including lymph nodes, spleen, Peyer's patches, and mucosal associated lymphoid tissues (MALT; the largest being tonsils), are highly sophisticated structures designed to optimize antigen capture and presentation so that rare antigen-specific circulating T and B cells encounter their cognate antigens and initiate an adaptive immune response [1]. SLOs are essential for systemic protection of our body from viral infection and pathogen invasion. Areas of SLOs are divided into distinct T-cell zones and B-cell follicles to separate priming and activation of naïve T and B cells, respectively. Naïve T cells ($CD4^+$ and smaller numbers of $CD8^+$) interact with dendritic cells (DCs) and other professional antigen-presenting cells (APCs) in the T-cell

Marie-Caroline Dieu-Nosjean (ed.), *Tertiary Lymphoid Structures: Methods and Protocols*, Methods in Molecular Biology, vol. 1845, https://doi.org/10.1007/978-1-4939-8709-2_9,

zone. Germinal center (GC) formation, induced in the B-cell follicle during a primary immune response, provides as a controlled microenvironment for activated B cells to undergo clonal expansion and affinity maturation. This process is helped by their interactions with follicular helper T (T_{FH}) cells and follicular dendritic cells (FDCs), which lead to selection of antigen-specific high-affinity B cells for memory B cell or antibody-secreting plasma cell differentiation and maturation. These processes are a crucial element of humoral immune response in adaptive immunity.

Tertiary lymphoid structures (TLS) develop postnatally and occur in response to chronic inflammation at nonlymphoid anatomical locations. These SLO-like entities are generally small in size and situated in or near the affected tissues in diseases including chronic infection, autoimmunity, and, more recently, cancer. Similar to SLOs, T- and B-cell-predominant areas are observed in well-formed TLS, with mature DCs found in the T-cell zone and GCs apparent in the B-cell area that contains proliferating B cells, T_{FH} cells, and a dense FDC network [2, 3]. High endothelial venules (HEVs), blood vessels adapted for lymphocyte trafficking into SLOs, also form in the T-cell zones of many TLS [4], providing efficient movement of peripheral lymphocytes (including naïve cells) to and from the tissue [5].

In autoimmunity, TLS are often associated with the more aggressive forms of disease [6]. Recent studies have also correlated their presence with improved survival in several human solid tumors although some investigations found the inverse [7]. TLS are thought to provide a site that facilitates immune cell interactions leading to local antigen-specific T- and B-cell priming, activation, and differentiation into memory and/or effector cells. These activities produce adaptive immune responses that either exacerbate (autoimmunity) or help combat (infection and cancer) the disease.

Accurate TLS detection normally requires examination of specific markers expressed on key cellular components using immunohistochemistry (IHC) [2, 8]. These markers can however change because TLS are dynamic sites that can arise or dissipate longitudinally during disease progression. Their level of organization extends from lymphoid aggregates to mature TLS with GCs. Several studies propose that these different structures represent developmental stages of TLS. The least frequent but highest level of organization is considered the GC-containing TLS, which can coexist with suboptimally organized smaller T- and B-cell aggregates [9]. Alternatively, the aggregates could be part of a fully formed TLS detectable on a different tissue plane [10]. Whether the more abundant, sub-organized structures evolve to GC during tumor progression in patients is not currently known but suggested to be possibly true by our recent study [11].

Alternative methods for detecting TLS, such as gene expression analysis, likely capture the molecular basis underlying TLS activities and/or formation. Specific genes have been proposed as markers for these morphologically distinct structures, which are commonly associated with them in human autoimmune diseases and cancer. A set of 12 chemokine genes were correlated with a TLS presence in colorectal cancer and subsequently confirmed in melanoma [12, 13]. Lung cancer TLS differentially express many chemokines and adhesion molecules compared to the tumor nests (usually lacking TLS) [14]. Consistent with this is that important factors involved in T- and B-cell recruitment to SLOs, *CCL19/CCL21* and *CXCL13* (T- and B-cell chemoattractants, respectively), are the most specific TLS genes found to date. These signals together with FDC-specific marker genes (e.g., *CD21L*) and early mediators of SLO development [lymphotoxins α and β (*LTA* and *LTB*)] are specifically associated with a GC presence in rheumatoid synovitis and melanoma metastases [15, 16]. Our studies have identified PD-1^{hi}CD200^{hi}ICOS^{int}CXCR5^{-} T_{FH}X13 cells as the major CXCL13 producers in human breast cancer (BC) with these specialized helper cells appearing to promote local TLS formation at the tumor site [3, 11].

Formalin-fixed paraffin-embedded (FFPE) blocks are the most frequent source of human tumor material that is available from tumor banks and pathology departments today. These samples are used for routine diagnostic analyses including IHC. RNA extracted from these samples frequently exhibits high levels of degradation. Recent advances have improved the quality of gene expression quantification from FFPE tumor tissues and this has increased the material available for molecular analysis in human cancer. The following protocol details the steps for using FFPE breast tumor tissues to quantify TLS-related gene expression, using *CXCL13* and *LTB* as examples, and preparing dual CD3/CD20 IHC for parallel TLS scoring by experienced pathologists.

2 Materials

2.1 Preparation of Tissue Sections from FFPE Tumor Blocks

1. 1.5 or 2 mL RNase-free microcentrifuge tubes.
2. Microtome and new blade.
3. RNase decontamination solution (e.g., RNaseZap RNase Decontamination Solution, Ambion).

2.2 RNA Extraction from FFPE Tumor Tissues

1. RNeasy FFPE kit (Qiagen): This kit contains Buffer PKD, DNase Booster Buffer, Buffer RBC, Buffer RPE (to be mixed with four volumes of 96–100% ethanol), proteinase K, DNase I (lyophilized 1500 Kunitz units; to be reconstituted in 550 μL RNase-free water), and RNeasy MinElute spin columns. Store

DNase I and RNeasy MinElute spin columns at 4 °C and the other components at room temperature (proteinase K can be stored either at room temperature or at 4 °C).

2. 100% Xylene.
3. 96–100% Ethanol.
4. Sterile, RNase-free micropipette tips.
5. 1.5 or 2 mL Microcentrifuge tubes.
6. Heating block stable at 80 °C.
7. NanoDrop spectrophotometer.

2.3 Reverse Transcription of RNA to cDNA

1. High-Capacity RNA-to-cDNA kit (Applied Biosystems): This kit contains RT Buffer Mix and RT Enzyme Mix. Store at −20 °C.
2. RNase-free water.
3. 0.2 mL PCR tubes.
4. Sterile, RNase-free micropipette tips.
5. Thermal cycler (e.g., Veriti 96-well Thermal Cycler, Applied Biosystems).

2.4 Pre-amplification and Real-Time PCR Quantification of Gene Expression

All of the specific products used in our laboratory for this step were provided by Applied Biosystems (currently Thermo Fisher Scientific).

1. TaqMan PreAmp Master Mix: Store at 4 °C and protect from light.
2. TaqMan Universal Master Mix II with UNG: Store at 4 °C and protect from light.
3. TaqMan Gene Expression Assays: Store at −20 °C and protect from light.
4. Nuclease-free water.
5. 1.5 mL Microcentrifuge tubes.
6. Micropipette tips, sterile, filtered.
7. MicroAmp Fast Optical 96-Well Reaction Plate with Barcode or equivalent.
8. MicroAmp Optical Adhesive Film.
9. Veriti 96-well Thermal Cycler (Applied Biosystems) or equivalent.
10. 7900HT Fast Real-Time PCR System (Applied Biosystems) or equivalent.

2.5 Immunohistochemical Staining of FFPE Tumor Tissues

1. Water bath (for 40 °C incubation).
2. Microtome and blade.

3. Oven (for 37 °C incubation).
4. Superfrost Plus microscope slides.
5. Rabbit anti-human CD3 polyclonal antibody (Dako).
6. Mouse anti-human CD20 monoclonal antibody (clone L26).
7. UltraView Universal 3,3′-diaminobenzidine (DAB) Detection Kit (Ventana Medical Systems): This kit contains *ultra*View Universal DAB Inhibitor, *ultra*View Universal Horseradish Peroxidase (HRP) Multimer containing a cocktail of HRP-labeled secondary antibodies, *ultra*View Universal DAB Chromogen, *ultra*View Universal DAB H_2O_2, and *ultra*View Universal Copper. Store at 4 °C.
8. UltraView Universal Alkaline Phosphatase (AP) Red Detection Kit (Ventana Medical Systems): This kit contains *ultra*View Universal AP Red Multimer containing a cocktail of AP-labeled secondary antibodies, *ultra*View Universal AP Red Enhancer, *ultra*View Universal AP Red Fast Red A, *ultra*View Universal AP Red Naphthol, and *ultra*View Universal AP Red Fast Red B. Store at 4 °C.
9. Automated IHC slide staining system (e.g., BenchMark XT platform, Ventana Medical Systems).
10. Hematoxylin counterstain reagent (e.g., Hematoxylin, Ventana Medical Systems).
11. Bluing reagent (e.g., Bluing Reagent, Ventana Medical Systems).
12. Mild liquid dishwashing soap.
13. 96–100% Ethanol.
14. 100% Isopropanol.
15. 100% Xylene.
16. Film coverslipper (e.g., Tissue-Tek Prisma & Coverslipper HQ Plus, Sakura).
17. Coverslipping films (e.g., Tissue-Tek Coverslipping Film, Sakura).

2.6 Correlation Between TLS-Related Gene Expression and IHC-Scored TLS

1. SDS software (Applied Biosystems) or equivalent.
2. Bright-field microscope.
3. GraphPad Prism software or equivalent.

3 Methods

3.1 Preparation of Tissue Sections from FFPE Tumor Blocks

Always work with clean gloves for RNA and avoid touching the inside of any containers (*see* **Note 1**).

1. Before tissue sectioning, chill FFPE blocks on ice for 20 min (*see* **Note 2**).
2. Fix the FFPE block to the microtome and ensure, as much as possible, that the tissue surface is vertical to the blade (*see* **Note 3**).
3. Set the section thickness at 5 μm (*see* **Note 4**).
4. Use a new blade to avoid any possibility of contamination by RNase.
5. Adjust the distance of the block surface to progressively reach the blade.
6. Start cutting and verify that the sections contain the entire tissue area.
7. Throw out the two first sections that might be oxidized (*see* **Note 5**).
8. Continue to cut three sections of 5 μm each (*see* **Note 6**).
9. Use a clean forceps (*see* **Note 7**) to put the sections immediately into a clean, RNase-free 1.5 mL microcentrifuge tube.
10. Close the lid and keep the tissue sections at 4 °C until RNA extraction, or proceed immediately to RNA extraction (*see* **Note 8**).

3.2 RNA Extraction from FFPE Tumor Tissues

The following RNA extraction protocol largely follows the manufacturer's instructions for the RNeasy FFPE kit (Qiagen) with some adaptations.

1. De-paraffinization Using 100% Xylene (*see* **Note 9**)

   A1: Add 1 mL 100% xylene. Vortex vigorously for 10 s, hold at room temperature for 5 min, and then centrifuge at full speed (*see* **Note 10**) for 2 min.

   A2: Carefully remove the supernatant with a micropipette without disturbing the pellet (*see* **Note 11**).

   A3: Add 1 mL of 96–100% ethanol to the pellet, mix by vortexing, and centrifuge at full speed (*see* **Note 10**) for 2 min.

   A4: Carefully remove the supernatant with a micropipette without disturbing the pellet. Carefully remove any residual ethanol using a fine micropipette tip.

   A5: With the lid open incubate at room temperature until all the residual ethanol has evaporated (about 15 min).
2. Add 150 μL (*see* **Note 12**) Buffer PKD and mix by vortexing.
3. Add 10 μL proteinase K. Mix gently by pipetting up and down.
4. Incubate at 56 °C for 15 min, and then at 80 °C for 15 min.
5. Incubate on ice for 3 min. Then centrifuge for 15 min at 20,000 × *g* at room temperature.

6. Transfer the supernatant to a new microcentrifuge tube without disturbing the pellet. **Steps 7–16** are carried out at room temperature.
7. Add 16 µL (*see* **Note 12**) DNase Booster Buffer and 10 µL DNase I (reconstituted solution). Mix by inverting the tube. Centrifuge briefly to collect residual liquid from the sides of the tube.
8. Incubate at room temperature for 15 min.
9. Add 320 µL (*see* **Note 12**) Buffer RBC to adjust binding conditions and mix the lysate thoroughly.
10. Add 1200 µL (*see* **Note 12**) of 96–100% ethanol on the sample and mix well by pipetting. *Do not centrifuge.*
11. Transfer 700 µL of the sample, including any precipitate that may have formed, to an RNeasy MinElute spin column placed in a 2 mL collection tube. Close the lid gently and centrifuge for 20 s at ≥8000 × *g*. Discard the flow-through.
12. Repeat the previous step until the entire sample has passed through the RNeasy MinElute spin column.
13. Add 500 µL of Buffer RPE to the RNeasy MinElute spin column. Close the lid gently and centrifuge for 15 s at ≥8000 × *g*. Discard the flow-through.
14. Again, add 500 µL of Buffer RPE to the RNeasy MinElute spin column. Close the lid gently and centrifuge for 2 min at ≥8000 × *g*. Discard the collection tube with the flow-through.
15. Place the RNeasy MinElute spin column in a new 2 mL collection tube. Open the lid of the spin column and centrifuge at full speed (*see* **Note 10**) for 5 min. Discard the collection tube with the flow-through.
16. Place the RNeasy MinElute spin column in a new 1.5 mL collection tube. Add 14 µL (*see* **Note 13**) of RNase-free water to the spin column membrane (eject water just above the center of the membrane). Close the lid gently and centrifuge for 1 min at full speed (*see* **Note 10**) to elute total RNA.
17. Put the RNA on ice.
18. Quantify RNA using a NanoDrop or equivalent spectrophotometer using 1 µL per sample (*see* **Note 14)**.
19. Store the remaining RNA at −80 °C.

3.3 cDNA Preparation

Currently, several commercial cDNA synthesis kits are of high efficiency. The High-Capacity RNA-to-cDNA kit is composed of two easy-to-use fractions: one tube containing a 2× RT Buffer Mix and another tube containing a 20× RT Enzyme Mix.

1. Before starting, thaw the RT Buffer Mix tube at room temperature (*see* **Note 15**). After completely thawing, mix by inverting several times, then spin down, and keep on ice.
2. Thaw the RNAs in a refrigerator (4 °C). Move them to ice after they are completely thawed.
3. Up to 2 μg of total RNA can be reverse transcribed per reaction.
4. One reaction contains 10 μL of 2× RT Buffer Mix, 1 μL of 20× RT Enzyme Mix, and 9 μL of RNA (adjust with RNase-free water if sample volume is less than 9 μL of RNA) in a 0.2 mL PCR tube.
5. Prepare a mixture of RT Buffer Mix and RT Enzyme Mix for the total number of reactions (*see* **Note 16**).
6. Add suitable volumes of RNase-free water (if required) to the bottom of each PCR tube. Add suitable volumes of total RNA, and briefly mix with water (if applicable) by pipetting once.
7. Distribute 11 μL of the mixture (RT Buffer Mix + RT Enzyme Mix) into each PCR tube, just above the RNA. Mixing by pipetting is permitted but not necessary. **Steps 6** and **7** can be reversed.
8. Centrifuge briefly if all the liquid is not at the bottom of the tube.
9. Run the incubation program at 37 °C for 60 min, and 95 °C for 5 min, and then hold at 4 °C on a thermal cycler.
10. Store the cDNA at −20 °C.

3.4 Pre-amplification and Real-Time PCR Quantification of Gene Expression

Due to high levels of RNA degradation (segmentation; *see* **Note 17**) in FFPE samples, detectable and quantifiable segments of the gene transcripts are at very low copy numbers. To use a reasonable quantity of RNA from the FFPE extract to detect a satisfactory number of gene targets, an intermediate step called pre-amplification (also by PCR) is necessary before the final step of real-time PCR for mRNA quantification. To ensure linearity (*see* **Note 18**) of the pre-amplification step, all investigated genes are amplified together with low concentrations (0.05× of the normal concentrations) of the PCR primers and the TaqMan probes (included in commercial TaqMan Gene Expression Assays). Work on ice and avoid exposure to light with the TaqMan Gene Expression Assays.

1. Thaw the TaqMan Gene Expression Assays and the cDNA in the refrigerator (4 °C). Move them to ice once they are completely thawed.
2. In a 1.5 mL microcentrifuge tube, combine equal volumes of each 20× TaqMan Gene Expression Assay (up to a total of 100 assays depending upon the study design) (*see* **Note 19**).

3. Dilute the pooled TaqMan assays using RNase-free water (*see* **Note 20**) so that each assay is at a concentration of 0.2× [the volume of the diluted pooled assays (typically 12.5 μL/reaction) accounts for 1/4 of the final volume of the pre-amplification reaction (typically 50 μL)] (*see* **Note 19**).
4. For 50 μL reactions, mix 25 μL of TaqMan PreAmp Master Mix (2×), 12.5 μL of the diluted pooled TaqMan assays, and 12.5 μL of cDNA in 0.2 mL PCR tubes. We use an amount of cDNA that corresponds to 100 ng of initial total RNA (*see* **Note 21**).
5. Cap the microcentrifuge tubes.
6. Mix the reactions by gently inverting the tubes, and then centrifuge briefly.
7. Perform the pre-amplification PCR reaction on a thermal cycler using the following program: 95 °C for 10 min, then 10 cycles at 95 °C for 15 s, and 60 °C for 4 min (*see* **Note 22**).
8. Dilute fivefold (*see* **Note 23**) the pre-amplification product using RNase-free water (*see* **Note 20**).
9. Use 5 μL of pre-amplified, diluted cDNA for each 20 μL PCR reaction of real-time quantification of individual target and housekeeping gene expression (*see* **Note 24**).
10. In addition to the cDNA, each 20 μL PCR reaction contains 1 μL of a specific 20× TaqMan Gene Expression Assay, 10 μL of TaqMan Universal Master Mix II with UNG, and 4 μL of nuclease-free water.
11. For each gene, prepare a mixture of the latter three components for the total number of reactions foreseen (*see* **Note 16**).
12. Fill the 96-well plates with 5 μL of cDNA and 15 μL of the mixture, in triplicate (*see* **Note 25**).
13. Seal the plates with MicroAmp Optical Adhesive Film.
14. Centrifuge the plates for 2 min at 200 × *g* (*see* **Note 26**).
15. Run the plate on a 7900HT Fast Real-Time PCR System or equivalent using the following program: 50 °C for 2 min, 95 °C for 10 min, then 40 cycles at 95 °C for 15 sec, and 60 °C for 1 min.

3.5 TLS Scoring on IHC-Stained Tumor Sections

IHC is a commonly used technique to monitor protein expression and localization in the context of tissue morphology. IHC uses antibodies to detect and analyze protein expression while maintaining the composition, cellular characteristics, and structure of the native tissue. Chemical fixation secures cellular and molecular interactions in complex tissues. Tissue samples can be embedded in paraffin before being cut into thin sections that are mounted on slides for staining and analysis. To visualize TLS in BC, we devel-

oped a dual-CD3/CD20 IHC staining that clearly reveals dense aggregates of B cells adjacent to a T-cell zone [8] (Fig. 1a, b). Dual-CD3/CD20 IHC is performed by an automated IHC slide staining system (Ventana Benchmark XT; **steps 11–22**) at our institute that delivers consistent and high-quality results. Dehydration and slide mounting (**steps 25** and **26**) are performed by the Tissue-Tek Prisma & Coverslipper HQ Plus.

1. Chill FFPE blocks on ice before sectioning, as in Subheading 3.1, **step 1** (*see* **Note 2**).
2. Fill a water bath with ultrapure water and heat to 40 °C (*see* **Note 27**).
3. Place the blade in the holder and insert the paraffin block.
4. Carefully, wind the block to approach the blade and cut a few thin sections to ensure that the positioning is correct.
5. Trim the block to expose the tissue surface at a thickness of 10–15 μm.
6. Cut sections for staining at a thickness of about 4–5 μm.
7. Using a brush, pick up the ribbon sections and float them on the surface of the water in the water bath so they flatten out.
8. Use a dissecting needle to separate the sections.
9. Use microscope slides to pick the sections out of the water bath and store upright in a slide rack.
10. Dry slides overnight at 37 °C in an oven (*see* **Note 28**).
11. De-paraffinize and rehydrate the section (*see* **Note 29**).
12. Unmask antigen by following antibody-specific recommendations (*see* **Note 30**).
13. Apply *ultra*View Universal DAB Inhibitor to the slide and incubate for 4 min at room temperature.
14. Incubate anti-human CD3 antibody for 32 min at 37 °C.
15. Apply *ultra*View Universal HRP Multimer to the slide and incubate for 8 min at room temperature.
16. Visualize CD3 staining by incubation with *ultra*View Universal DAB Chromogen and *ultra*View Universal DAB H_2O_2 for 8 min at room temperature, which produces a brown precipitate.
17. Incubate with *ultra*View universal Copper for 4 min at room temperature to enhance the CD3 detection signals.
18. Incubate anti-human CD20 antibody for 32 min at 37 °C.
19. Apply *ultra*View Universal AP Red Multimer to the slide and incubate for 12 min at room temperature.
20. Incubate with *ultra*View Universal AP Red Enhancer for 4 min at room temperature to enhance the CD20 detection signals.

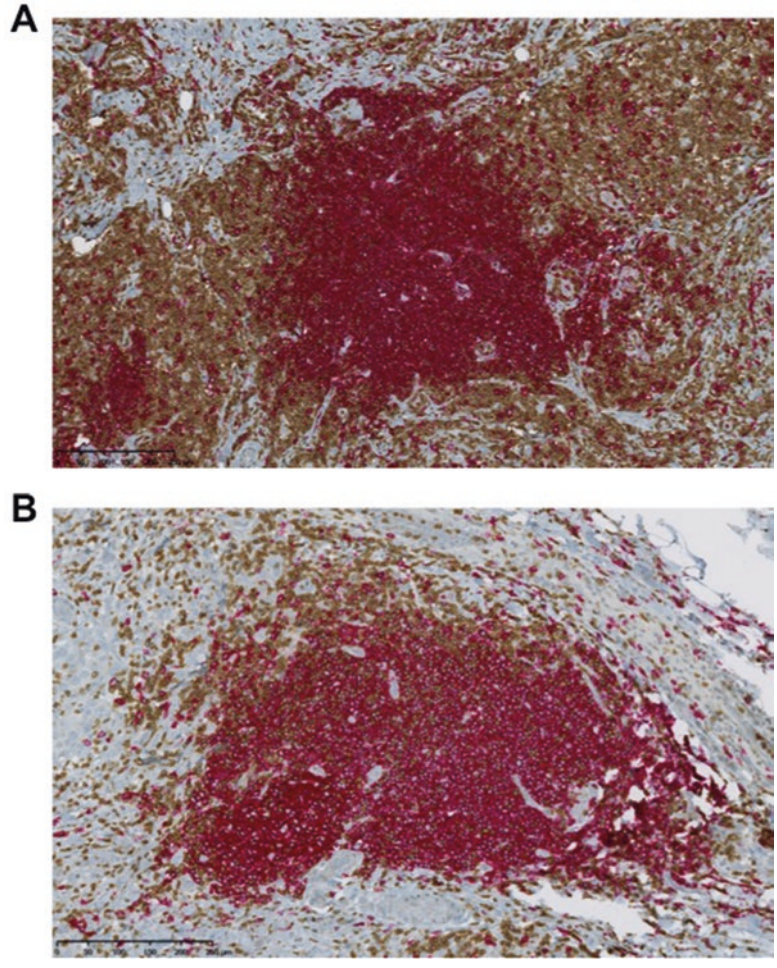

Fig. 1 Representative TLS in human BC tissue. FFPE tumor sections were dual-IHC-stained for CD3 (T cells in brown) and CD20 (B cells in red). TLS are characterized by a dense, compact B-cell zone (similar to B-cell follicles in SLOs) adjacent to a more expansive T-cell zone (variable in cell density). (**a**) A TLS containing a large T-cell zone. (**b**) A TLS with more B cells than T cells. Images are at ×400 magnification

21. Visualize CD20 staining by incubation with *ultra*View Universal AP Red Fast Red A and *ultra*View Universal AP Red Naphthol for 8 min followed by incubation with *ultra*View Universal AP Red Fast Red B for 8 min, all at room temperature. **Steps 20** and **21** produce an enhanced red precipitate.
22. Counterstain sections with hematoxylin and a bluing reagent, which stains the cell nuclei blue to better visualize the tissue morphology.
23. Wash slides in a mild liquid dishwashing soap.

24. Rinse slides thoroughly in distilled water to remove all of the detergent.
25. Dehydrate sections in successive baths of alcohol (70% ethanol, 96–100% ethanol, then 100% isopropanol) and two baths of 100% xylene.
26. Mount the coverslip using Tissue-Tek Coverslipping Film, a resin-coated plastic film that eliminates the need for cover glasses and liquid mounting media.
27. Examine the stained tissue sections with a microscope.
28. TLS counting is restricted to a B-cell follicle surrounded or adjacent to a T-cell zone in the invasive tumor area (including the tumor bed and peri-tumoral stroma). Regions of in situ carcinoma, normal glandular epithelium, and necrosis are excluded from evaluation. The TLS score is expressed as the number of TLS per tumor surface area in mm^2 (*see* **Note 31**).

3.6 Correlation Between TLS-Related Gene Expression and IHC-Scored TLS

1. We quantified *CXCL13* and *LTB* gene expression on a series of 80 BC tumors using *POLR2A*, *TBP*, and *TMBIM4* as housekeeping genes (*see* **Note 24**). The TaqMan Gene Expression Assays are listed in Table 1 with the amplicon length (base pairs or bp) (*see* **Note 17**) indicated.
2. The C_T values of the real-time qPCR results are calculated using the SDS software with the option "Manual C_T" and a threshold of 0.2 (*see* **Note 32**).
3. To compare gene expression across samples, we consider ΔC_T values that correspond to the difference between the C_T values of each target gene and the mean C_T values of all the housekeeping genes ($\Delta C_T = C_{T(\text{target gene})} - C_{T(\text{mean of all housekeeping genes})}$). ΔC_T values are inversely proportional to the quantity of the specific mRNA in a given sample (*see* **Note 33**).
4. The $-\Delta C_T$ values (positively proportional to gene expression) of the *CXCL13* and *LTB* genes were then correlated with the TLS score (no. of TLS/mm^2 breast tumor surface scored on CD3/CD20 IHC-stained tissue sections) for each individual patient (Fig. 2a, b).

4 Notes

1. Human body (including hands) is a rich source of RNase.
2. The small amount of moisture that penetrates the paraffin from the melting ice will make the tissue easier to cut.
3. The goal is to quickly get the first section that covers the entire tissue area to avoid wasting material.

Table 1
TaqMan gene expression assays used for FFPE samples

Gene name	Company	Assay ID	Amplicon length (bp)
POLR2A	Applied Biosystems	Hs00172187_m1	61
TMBIM4	Applied Biosystems	Hs00211390_m1	63
TBP	Applied Biosystems	Hs00427621_m1	65
CXCL13	Applied Biosystems	Hs00757930_m1	70
LTB	Applied Biosystems	Hs00242739_m1	78

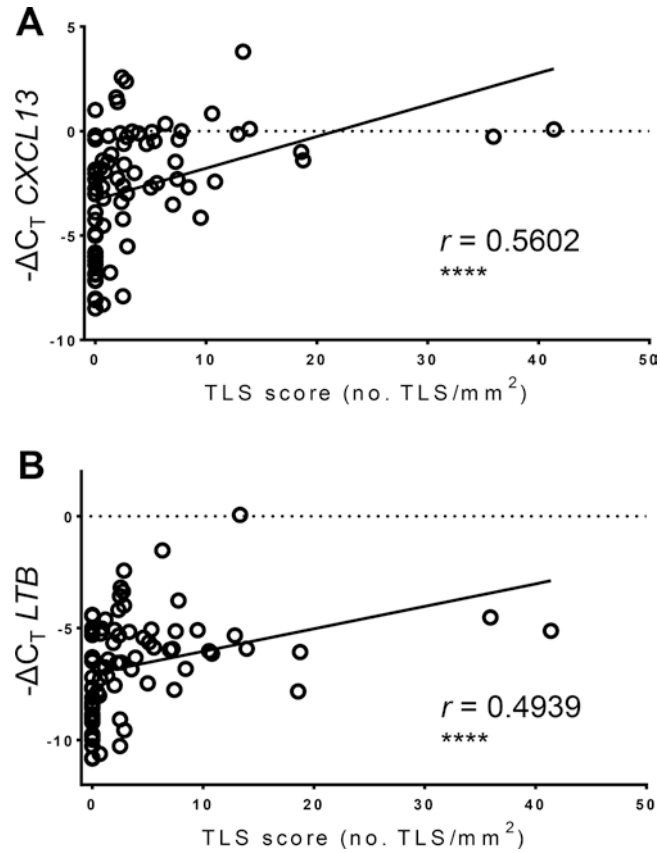

Fig. 2 Spearman correlations between ***CXCL13*** (**a**) or ***LTB*** (**b**) gene expression and TLS scores on dual-CD3/CD20 IHC-stained BC tissue sections. Gene expression levels were quantified using qPCR following cDNA pre-amplification. Data are from a series of 80 FFPE BC samples. ***P***-values (two-tailed) <0.05 are considered significant. Degrees of significance: $P < 0.05$ (*), $P < 0.01$ (**), $P < 0.001$ (***), and $P < 0.0001$ (****)

4. The maximum allowable thickness is 20 μm for the RNeasy FFPE kit (Qiagen). We prefer to use 5 μm sections to ensure complete de-paraffinization.
5. Alternatively one of the first sections could be counterstained with hematoxylin to have an idea about the cellular composition (e.g., lymphocytes, tumor cells) of the tissue sections extracted.
6. The RNeasy FFPE kit (Qiagen) can handle up to four 10 μm sections with a surface area up to 250 mm^2 in a single extraction by using the larger reagent volumes proposed in the standard protocol (cf. Qiagen RNeasy FFPE Handbook). FFPE tumor blocks prepared in routine pathology laboratories contain variable surface sizes depending on the size of the tumor. Breast tumors are usually small and the embedded tissue areas vary from 25 to 200 mm^2. In general, 3 × 5 μm sections are suitable for a single extraction using the smaller volumes of reagents proposed in the standard protocol.
7. The forceps can be cleaned using an RNase decontamination solution (e.g., RNaseZAP, Ambion). After applying RNaseZAP, wipe thoroughly with a paper towel, rinse with water, and dry with a clean paper towel.
8. To minimize further RNA degradation, the cut tissue needs to be extracted within 24 h of sectioning.
9. The first step of de-paraffinization can be achieved using several methods including De-paraffinization Solution (Qiagen); organic solvents such as heptane, xylene, limonene, and CitriSolv; or melting. We use xylene at our laboratory, which is economical and can be used in large volumes to ensure thorough de-paraffinization.
10. The microcentrifuge that we used allows a maximum speed of 25,000 × *g*.
11. The pellet is not very solid. Avoid touching the pellet. If necessary, leave a small volume of xylene that will be washed by the ethanol. **Steps A1** and **A2** can be repeated if the de-paraffinization seems incomplete (the solution is turbid in this case).
12. We used the smaller volumes for all reagents and followed the standard protocol for the RNeasy FFPE kit (Qiagen), except for ethanol (**step 10**), which is available in unlimited quantities.
13. We used a minimal volume of RNase-free water for RNA elution to obtain the highest possible concentrations.
14. RNAs extracted from FFPE samples are generally significantly degraded. The RNA integrity number (RIN) is not informative for the utility of the RNA extracted from FFPE tissues

[17]. Typically, we obtain a RIN around 2.2–2.3 but have no problems with the downstream analysis. The final qPCR results are evaluated for all samples, but when the housekeeping genes are detected at low levels (e.g., $C_T > 30$) and the genes of interest are undetectable ($C_T > 36$), samples need to be considered with caution or excluded from the analysis (also *see* Subheading 3.6).

15. The RT Enzyme Mix remains liquid at −20 °C so it does not need to be thawed.
16. The total number of reactions should contain 2–4 (depending on the number of effective reactions) more than required to compensate for the volume loss caused by repeated pipetting.
17. Mean sizes of the RNA fragments extracted from FFPE samples are about 100–200 nucleotides. To achieve accurate quantification of fragmented mRNA expression, the most important thing is to choose primers amplifying small amplicons (the amplified region of the cDNA) that are preferentially less than 70 bp. We use commercial TaqMan Gene Expression Assays (Applied Biosystems). When choices are limited, assays that generate amplicons longer than 70 bp may also be tested. Each assay needs to be validated first using a series of control samples (similar tissues but not part of the study) that are of the same quality as those included in the research study.
18. Increase proportionally the number of cDNA copies for each gene in each sample so the initial relative quantities of individual genes across samples will remain the same in the final products after pre-amplification.
19. Each TaqMan assay is 20× concentrated (to be diluted 20-fold in the final classical PCR reaction). For pre-amplification, a final concentration of 0.05× is required, so the assay needs to be diluted 400-fold for this step. For example, for a 50 μL pre-amplification reaction, we need 12.5 μL of a diluted TaqMan assay mixture (0.125 μL of a 20× assay each; this volume is too small to be pipetted, so we need an intermediate dilution). For different cDNA samples, the same TaqMan assay mixture will be used, so we prepare a sufficient amount of this mixture by simply mixing equal volumes of each assay before diluting them together to a concentration of 0.2×.
20. RNase-free water is suitable for replacing the Tris–EDTA (TE) buffer proposed in the standard protocol for the TaqMan PreAmp Master Mix kit (Applied Biosystems).
21. For one 50 μL of pre-amplification, the allowable quantity of cDNA (corresponding to initial RNA) is 1–250 ng, which needs to be adapted according to the quality and the total available amounts of the RNA. For FFPE tumor samples, we determined 100 ng to be a good compromise between the

RNA quantity variations (obtained from a single extraction) across samples and the quality of gene quantification using pre-amplified cDNA.

22. The number of pre-amplification cycles can be adjusted depending upon the number of genes to be quantified. Ten cycles produce sufficient material for 50 × 20 μL or 20 × 50 μL final PCR reactions. Fourteen cycles produce material for 200 × 20 μL or 80 × 50 μL PCR reactions. We used 10 cycles in our experiments for quantifying less than 15 genes.
23. Dilute 5-fold for 10 cycles and 20-fold for 14 cycles, respectively. The diluted, pre-amplified cDNA can be stored at −20 °C in aliquots by minimizing freeze-thaw cycles.
24. Universal housekeeping genes are hard to identify with exceptions to uniform expression often detected in large data sets. To minimize the risk, it is recommended that no less than three housekeeping genes are used for gene expression analysis in total tumor tissues that contain a mixture of cell types. In addition, the extent of RNA degradation can vary between individual FFPE blocks, which may differentially affect gene detection in each sample. We selected our housekeeping genes [*POLR2A*, *TMBIM4* (="*CGI-119*" in ref. 18) and *TBP*] from publications [18, 19] and commercially available TaqMan Gene Expression Assays designed for housekeeping genes (Applied Biosystems). The homogeneity of their natural expression levels was validated in a series of 88 frozen BC samples (with high-quality RNA) from a microarray data set [20] (Fig. 3a). The combination (mean values) of the three housekeeping genes further improved the homogeneity. We analyzed 60 BC with available FFPE samples using qPCR after pre-amplification. Exceptionally, reduced detection levels (inversely proportional to C_T values) were found in 4 out of 60 (6.7%) samples for the mean of housekeeping genes (Fig. 3b, blue frame). Nevertheless, a linear correlation was obtained for the genes of interest (e.g., *CXCL13*) between the microarray data analyzing frozen samples and qPCR results from FFPE samples (*CXCL13* was normalized to the mean of the housekeeping genes in FFPE samples) (Fig. 3c). It is possible that including other reliable housekeeping genes would improve these results.
25. Due to the large number of samples in these studies, it is better to include the maximum number of samples (rather than genes) on the same plate. This avoids errors coming from preparation of different mixtures for each gene and improves inter-experimenter reproducibility. Typically, we organize our experiments so that one or two (maximum) genes in triplicate are run on a single plate.

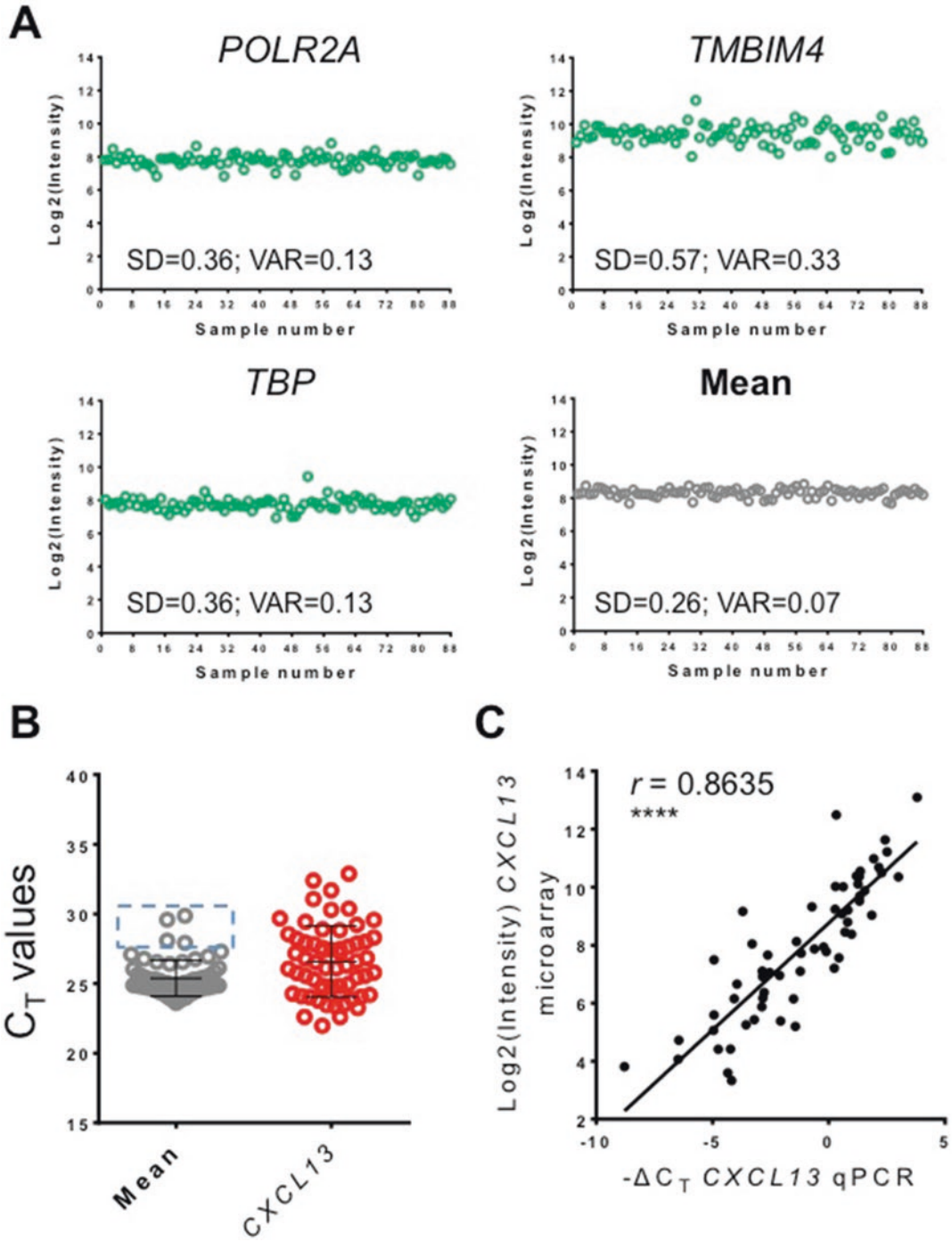

Fig. 3 Gene expression in frozen and FFPE BC tissues. (**a**) Expression levels of individual and mean values for three housekeeping genes (***POLR2A***, ***TMBIM4***, and ***TBP***) in frozen BC samples from a microarray data set ($n = 88$) [20]. ***SD*** standard deviation and ***VAR*** variance. (**b**) qPCR C_T values for the mean of these housekeeping genes in FFPE BC samples from 60 patients in (**a**) [11]. The ***CXCL13*** gene is shown for comparison. (**c**) Pearson correlation between frozen microarray and FFPE qPCR data for the ***CXCL13*** gene ($n = 60$). *P*-values (two-tailed) <0.05 are considered significant. Degrees of significance: $P < 0.05$ (*), $P < 0.01$ (**), $P < 0.001$ (***), and $P < 0.0001$ (****)

26. Centrifugation at high speed could affect enzyme efficiency. This speed is sufficient to push the drops to the bottom of the well.
27. A Section-Transfer-System with an integrated water bath and a disposable blade system optimizes the paraffin ribbon retrieval process. The sections are gently transferred by a permanent laminar water flow into the water bath providing more useable sections from less material.
28. Dried FFPE sections can be stored at 4 °C for 1 week.
29. Incomplete removal of paraffin can lead to poor staining of the tissue section. From this point onwards, *at no time* should the tissue sections be allowed to dry. Drying will cause nonspecific antibody binding and therefore high background staining.
30. Most formalin-fixed tissues require an antigen retrieval step due to the formation of methylene bridges during fixation, which cross-link proteins and therefore mask antigen epitopes including those recognized by antibodies used for IHC. The two methods of antigen retrieval are heat mediated using sodium citrate buffer or EDTA, and enzymatic reagents. For the dual-CD3/CD20 staining, sodium citrate buffer is used.
31. TLS were scored by two experienced immunopathologists in our institute examining CD3/CD20 IHC-stained full-face breast tumor sections.
32. The PCR amplification curves are carefully examined. The threshold can be adjusted based on the data obtained but generally 0.2 is optimal in our laboratory. It is important to use the same threshold for analyzing data from different plates that quantify the same gene. Occasionally, obviously imperfect results showing artifact amplification curves should be deleted before data analysis. If this occurs in more than one of the triplicates for the same gene and the same sample, this data will need to be verified by redoing a PCR reaction. For sample exclusion, also *see* **Note 14**.
33. The expression level of housekeeping genes should ideally be proportional to the total RNA amount and/or the total number of cells of a given sample.

Acknowledgements

The authors thank the Department of Anatomical Pathology, Institut Jules Bordet, Brussels, Belgium, for use of the IHC staining equipment and Mrs. Anais Boisson for excellent technical assistance.

References

1. Willard-Mack CL (2006) Normal structure, function, and histology of lymph nodes. Toxicol Pathol 34:409–424
2. Dieu-Nosjean MC, Antoine M, Danel C et al (2008) Long-term survival for patients with non-small-cell lung cancer with intratumoral lymphoid structures. J Clin Oncol 26:4410–4417
3. Gu-Trantien C, Loi S, Garaud S et al (2013) CD4(+) follicular helper T cell infiltration predicts breast cancer survival. J Clin Invest 123:2873–2892
4. Martinet L, Garrido I, Filleron T et al (2011) Human solid tumors contain high endothelial venules: association with T- and B-lymphocyte infiltration and favorable prognosis in breast cancer. Cancer Res 71:5678–5687
5. Ager A (2017) High endothelial venules and other blood vessels: critical regulators of lymphoid organ development and function. Front Immunol 8:45. https://doi.org/10.3389/fimmu.2017.00045
6. Neyt K, Perros F, GeurtsvanKessel CH et al (2012) Tertiary lymphoid organs in infection and autoimmunity. Trends Immunol 33:297–305
7. Sautès-Fridman C, Lawand M, Giraldo NA et al (2016) Tertiary lymphoid structures in cancers: prognostic value, regulation, and manipulation for therapeutic intervention. Front Immunol 7:407. https://doi.org/10.3389/fimmu.2016.00407
8. Buisseret L, Desmedt C, Garaud S et al (2017) Reliability of tumor-infiltrating lymphocyte and tertiary lymphoid structure assessment in human breast cancer. Mod Pathol 30:1204–1212
9. Kroeger DR, Milne K, Nelson BH (2016) Tumor-infiltrating plasma cells are associated with tertiary lymphoid structures, cytolytic T-cell responses, and superior prognosis in ovarian cancer. Clin Cancer Res 22:3005–3015
10. Wirsing AM, Rikardsen OG, Steigen SE et al (2014) Characterisation and prognostic value of tertiary lymphoid structures in oral squamous cell carcinoma. BMC Clin Pathol 14:38. https://doi.org/10.1186/1472-6890-14-38
11. Gu-Trantien C, Migliori E, Buisseret L et al (2017) CXCL13-producing TFH cells link immune suppression and adaptive memory in human breast cancer. JCI Insight 2(11). https://doi.org/10.1172/jci.insight.91487
12. Coppola D, Nebozhyn M, Khalil F et al (2011) Unique ectopic lymph node-like structures present in human primary colorectal carcinoma are identified by immune gene array profiling. Am J Pathol 179:37–45
13. Messina JL, Fenstermacher DA, Eschrich S et al (2012) 12-Chemokine gene signature identifies lymph node-like structures in melanoma: potential for patient selection for immunotherapy? Sci Rep 2. https://doi.org/10.1038/srep00765
14. de Chaisemartin L, Goc J, Damotte D et al (2011) Characterization of chemokines and adhesion molecules associated with T cell presence in tertiary lymphoid structures in human lung cancer. Cancer Res 71:6391–6399
15. Takemura S, Braun A, Crowson C et al (2001) Lymphoid neogenesis in rheumatoid synovitis. J Immunol 167:1072–1080
16. Cipponi A, Mercier M, Seremet T et al (2012) Neogenesis of lymphoid structures and antibody responses occur in human melanoma metastases. Cancer Res 72:3997–4007
17. Abramovitz M, Ordanic-Kodani M, Wang Y et al (2008) Optimization of RNA extraction from FFPE tissues for expression profiling in the DASL assay. BioTechniques 44:417–423
18. Lee S, Jo M, Lee J et al (2007) Identification of novel universal housekeeping genes by statistical analysis of microarray data. J Biochem Mol Biol 40:226–231
19. Vandesompele J, De Preter K, Pattyn F et al (2002) Accurate normalization of real-time quantitative RT-PCR data by geometric averaging of multiple internal control genes. Genome Biol 3:RESEARCH0034
20. Dedeurwaerder S, Desmedt C, Calonne E et al (2011) DNA methylation profiling reveals a predominant immune component in breast cancers. EMBO Mol Med 3:726–741

Chapter 10

Generation of Recombinant Monoclonal Antibodies from Single B Cells Isolated from Synovial Tissue of Rheumatoid Arthritis Patients

Elisa Corsiero, Lucas Jagemann, Michele Bombardieri, and Costantino Pitzalis

Abstract

Ectopic lymphoid structure (ELS) can form in the target tissues of patients with chronic inflammatory autoimmune diseases such as rheumatoid arthritis (RA) and Sjögren's syndrome (SS). Although it is still not clear why ELS form only in a subset of patients, it is well known that these structures can acquire features of ectopic germinal centers and contribute actively to the production of autoantibodies. Here, we describe a method to generate recombinant monoclonal antibodies from single ELS$^+$ synovial tissue B cells obtained from RA patients. This chapter gives a detailed description of the method beginning from the mononuclear cell preparation from RA synovial tissue, single-cell sort of B cells by flow cytometry, amplification of the immunoglobulin (Ig) genes (both heavy- and light-chain genes) by PCR, and subsequent Ig gene expression vector cloning for full recombinant IgG1 monoclonal antibody (rmAb) production in vitro. The recombinant mAbs generated can be then characterized for (1) analysis of the Ig gene repertoires for clonal studies, (2) immunoreactivity profile, and (3) functional studies both in vitro and in vivo.

Key words Synovial tissue, Single B cell, Single-cell-nested PCR, Cloning, Monoclonal antibody, Ectopic lymphoid structure, Rheumatoid arthritis

1 Introduction

Immunoglobulins (Ig) or antibodies are a central component of the immune system. They consist of two identical heavy chains (IgH) and two identical light chains (Igκ or Igλ), each of which contains a variable domain for antigen recognition and a constant region for the effector functions. The IgH locus consists of variable (V), diversity (D), and joining (J) gene segments. The Igκ/λ locus consists only of V and J gene segments. Assembly of V(D)J gene segments by V(D)J recombination process is the central mechanism that leads to Ig antigen receptor diversity. The Ig variable domain consists of three short regions, named complementarity-determining regions (CDR), which are embedded into four

Marie-Caroline Dieu-Nosjean (ed.), *Tertiary Lymphoid Structures: Methods and Protocols*, Methods in Molecular Biology, vol. 1845, https://doi.org/10.1007/978-1-4939-8709-2_10,

conserved framework regions (FR). Starting from the amino terminus of both VH and VL, the CDR are called CDR1, CDR2, and CDR3. The FR1, 2, and 3 together with the CDR1 and CDR2 are encoded by the V gene segments. The FR4 is encoded by the J gene segment. Additional diversity in the Ig antigen receptor is introduced in structures called germinal centers (GCs) where somatic hypermutation and affinity-based selection take place bringing to the generation of memory and plasma cells which produce high-affinity antibodies. In healthy individuals, GCs form in secondary lymphoid organs (lymph nodes, spleen, mucosal associated lymphoid tissues). During infection, autoimmune diseases, cancer, transplant rejection, and ectopic lymphoid structures (ELS), also called tertiary lymphoid structures, resembling GCs can form at the site of inflammation supporting the local production of autoantibodies [1, 2]. For instance, 40% of patients with rheumatoid arthritis (RA), an inflammatory autoimmune disease, develops in their joint ELS which can acquire features of secondary lymphoid organs supporting a GC response [3, 4]. Interestingly, these structures have been shown to support locally antibody diversification, and thus production of autoreactive B cells [1, 5]. However, the nature and fine specificities of (auto)antigens driving B-cell autoimmunity and the exact pathogenic role of autoantibodies in RA but also other autoimmune diseases such as Sjögren's syndrome (SS) have not been elucidated yet.

One of the limitations in order to address these important aspects is the technical challenge of analyzing the fine specificity of autoreactive B cells isolated from the inflammatory milieu. Moreover, the possibility to analyze B-cell autoreactivity from lesional B cells of autoimmune patients at single-cell level is a good tool to better understand the frequency and Ig gene repertoire underlying the development of autoimmunity.

Here, we describe a method which allows the cloning and expression of recombinant monoclonal antibodies (rmAbs) from single lesional B cells isolated from RA synovial tissue characterized by functional ELS [1, 6]. This technique is a modified version of the strategy developed some years ago in the Nussenzweig's laboratory [7–9]. The protocol gives a detailed guide of all the steps involved in the generation of rmAbs from single B cells obtained from RA synovial tissue, applicable to other inflammatory tissues (e.g., salivary glands of SS patients), starting from isolation of mononuclear cells, single-B-cell sort by flow cytometry, amplification of the Ig genes, cloning, and in vitro expression of full IgG1 rmAbs (Fig. 1). The rmAbs generated can then be used for downstream analysis including (1) analysis of the Ig gene repertoires for clonal studies, (2) immunoreactivity profile, and (3) functional studies both in vitro and in vivo.

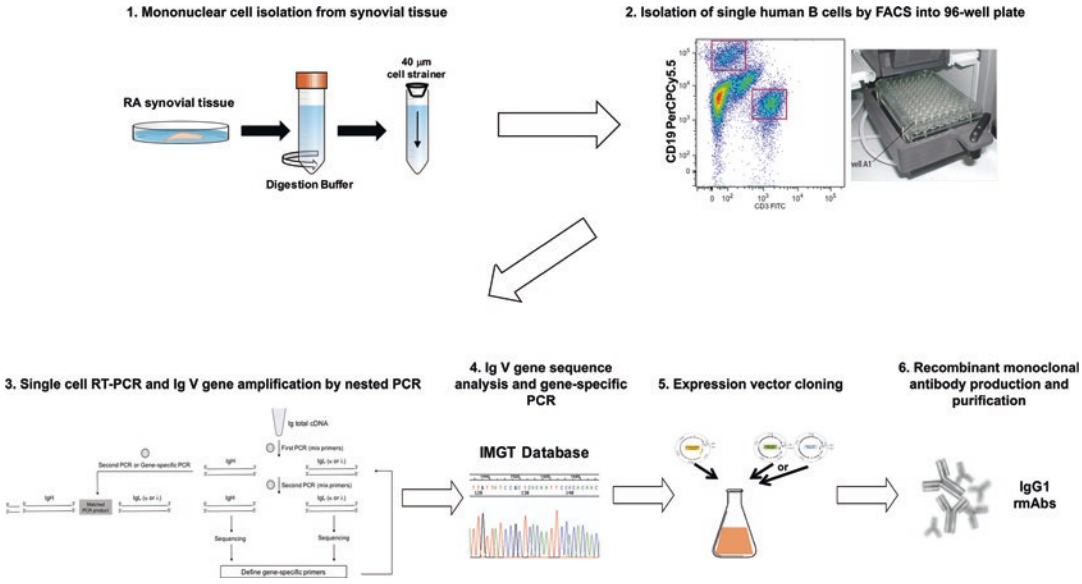

Fig. 1 Summary of the strategy to generate RA synovial recombinant monoclonal antibodies. The method starts from (*1*) mononuclear cell preparation from synovial tissue followed by (*2*) isolation of single B cells by flow cytometry, (*3*, *4*) Ig V gene amplification, (*5*) expression vector cloning, and (*6*) monoclonal antibody production

2 Materials

2.1 Mononuclear Cell Isolation from Synovial Tissue

1. Hot plate.
2. Glass beaker.
3. Synovial tissue obtained from joint replacement or biopsy (*see* **Note 1**).
4. Petri dishes 100 mm Ø × 15 mm H.
5. 5 mL Polypropylene round-bottom tubes.
6. Forceps and tweezers.
7. 40 and 70 µm nylon mesh cell strainers.
8. 5 mL Syringe plungers.
9. Magnetic stirring bars, micro (5 mm × 2 mm).
10. 1× Phosphate-buffered saline (PBS) without calcium and magnesium (pH 7.3–7.5).
11. Ultrapure 0.5 M EDTA, pH 8.0 (sterile filtered solution).
12. Tissue digestion buffer: Roswell Park Memorial Institute (RPMI)-1640 Medium supplemented with 2% heat-inactivated fetal bovine serum (FBS), collagenase D (from *Clostridium histolyticum*), deoxyribonuclease I (DNase I) from bovine pancreas (*see* **Note 2**)
13. Trypan blue solution 0.4%: Use at a final concentration of 0.2%, diluted in 1× PBS.

2.2 Isolation of Single Human B Cells

1. Flow cytometry facility with cell sorters with capacity for single-cell sorting into 96-well plates.
2. Refrigerated microcentrifuge suitable for 1.5 mL tubes.
3. 1.5 mL Tubes.
4. 96-Well plates, skirted (*see* **Note 3**).
5. Reservoir reagent 100 mL sterile polystyrene.
6. DNase- and RNase-free adhesive aluminum foil.
7. 1× PBS.
8. Purified mononuclear cells.
9. FACS buffer staining solution: Cold 1× PBS with 2% FBS and fluorescent-labeled anti-human antibodies at the final working concentration (*see* **Note 4**).
10. DAPI (4′,6-Diamidino-2-phenylindole, dihydrochloride): Store protected from light at −20 °C. Prepare according to the manufacturer's instruction.
11. Single-cell lysis solution: Ice-cold 0.5× PBS, 100 mM dithiothreitol (DTT), 40 U/μL RNasin ribonuclease inhibitor. Keep on ice.

2.3 Single-Cell RT-PCR and Gene Amplification by Nested PCR

1. PCR thermal cycler suitable for 96-well PCR plates skirted and half-skirted.
2. Hot plate suitable for 96-well PCR plates.
3. Gel tank for DNA agarose gel.
4. PCR cooler suitable for 96-well PCR plates.
5. 96-Well plates, half-skirted.
6. Reservoir reagent 100 mL sterile polystyrene.
7. Adhesive plate seals and adhesive PCR seals suitable for high-temperature incubations.
8. Ethanol, RNase, and DNase Away decontamination solution.
9. Nuclease-free water.
10. Random hexamer primer (RHP) mix: 300 ng/μL Random hexamer primers, 10% NP-40 for molecular biology, 40 U/μL RNasin (*see* **Note 5**). Keep on ice.
11. Reverse transcription (RT) mix: 5× First-strand buffer, 25 mM dNTP mix prepared from 100 mM dNTP set, 100 mM DTT, 40 U/μL RNasin, 200 U/mL Superscript III Reverse Transcriptase (*see* **Note 6**). Keep on ice.
12. PCR mix: 25 mM dNTP mix, 5′ primer mix and 3′ primer mix (*see* **Note 7,** Tables 1 and 2), 5 U/μL HotStart Taq DNA polymerase (*see* **Note 8**).
13. Agarose.

Table 1
Complete list of primers for IgV gene amplification (Parts I and II)

Primer	Sequence
Part I	
First nested PCR HC	**Forward 5′ to 3′**
5′ L-VH 1	ACAGGTGCCCACTCCCAGGTGCAG
5′ L-VH 3	AAGGTGTCCAGTGTGARGTGCAG
5′ L-VH 4/6	CCCAGATGGGTCCTGTCCCAGGTGCAG
5′ L-VH 5	CAAGGAGTCTGTTCCGAGGTGCAG
	Reverse 3′ to 5′
3′ Cμ CH1 ext	GGAAGGAAGTCCTGTGCGAGGC
3′ Cγ CH1 ext	GGAAGGTGTGCACGCCGCTGGTC
3′ Cα CH1 ext	TGGGAAGTTTCTGGCGGTCACG
Second nested PCR HC and specific PCR	**Forward 5′ to 3′**
5′ AgeI VH1	CTGCAACCGGTGTACATTCCCAGGTGCAGCTGGTGCAG
5′ AgeI VH1/5	CTGCAACCGGTGTACATTCCGAGGTGCAGCTGGTGCAG
5′ AgeI VH 1-18	CTGCAACCGGTGTACATTCCCAGGTTCAGCTGGTGCAG
5′ AgeI VH 1-24	CTGCAACCGGTGTACATTCCCAGGTCCAGCTGGTACAG
5′ AgeI VH3	CTGCAACCGGTGTACATTCTGAGGTGCAGCTGGTGGAG
5′ AgeI VH3-23	CTGCAACCGGTGTACATTCTGAGGTGCAGCTGTTGGAG
5′ AgeI VH3-33	CTGCAACCGGTGTACATTCTCAGGTGCAGCTGGTGGAG
5′ AgeI VH 3-9	CTGCAACCGGTGTACATTCTGAAGTGCAGCTGGTGGAG
5′ AgeI VH4	CTGCAACCGGTGTACATTCCCAGGTGCAGCTGCAGGAG

(continued)

Table 1
(continued)

Primer	Sequence
5′ AgeI VH 4-34	CTGCAACCGGTGTACATTCCCAGGTGCAGCTACAGCAGTG
5′ AgeI VH4-39	CTGCAACCGGTGTACATTCCCAGCTGCAGCTGCAGGAG
5′ AgeI VH 6-1	CTGCAACCGGTGTACATTCCCAGGTACAGCTGCAGCAG
	Reverse 3′ to 5′
3′ Cμ CH1 int	GGGAATTCTCACAGGAGACGA
3′ Cγ IgG int	GTTCGGGGAAGTAGTCCTTGAC
3′ Cα CH1-2 int	GTCCGCTTTCGCTCCAGGTCACACT
Specific PCR	**Reverse 3′ to 5′**
3′ SalI 1/2/4/5	TGCGAAGTCGACGCTGAGGAGACGGTGACCAG
3′ SalI 3	TGCGAAGTCGACGCTGAAGAGACGGTGACCATTG
3′ SalI 6	TGCGAAGTCGACGCTGAGGAGACGGTGACCGTG
Part II	
First nested PCR λ LC	**Forward 5′ to 3′**
5′ L Vλ1	GGTCCTGGGCCCAGTCTGTGCTG
5′ L Vλ2	GGTCCTGGGCCCAGTCTGCCCTG
5′ L Vλ3	GCTCTGTGACCTCCTATGAGCTG
5′ L Vλ4/5	GGTCTCTCTCSCAGCYTGTGCTG
5′ L Vλ6	GTTCTTGGGCCAATTTTATGCTG
5′ L Vλ7	GGTCCAATTCYCAGGCTGTGGTG
5′ L Vλ8	GAGTGGATTCTCAGACTGTGGTG

	Reverse 3′ to 5′
3′ Cλ	CACCAGTGTGGCCTTGTTGGCTTG
Second nested PCR λ LC	**Forward 5′ to 3′**
5′ AgeI Vλ1	CTGCTACCGGTTCCTGGGCCCAGTCTGTGCTGACKCAG
5′ AgeI Vλ2	CTGCTACCGGTTCCTGGGCCCAGTCTGCCCTGACTCAG
5′ AgeI Vλ3	CTGCTACCGGTTCTGTGACCTCCTATGAGCTGACWCAG
5′ AgeI Vλ4/5	CTGCTACCGGTTCTCTCTCSCAGCYTGTGCTGACTCA
5′ AgeI Vλ6	CTGCTACCGGTTCTTGGGCCAATTTTATGCTGACTCAG
5′ AgeI Vλ7/8	CTGCTACCGGTTCCAATTCYCAGRCTGTGGTGACYCAG
	Reverse 3′ to 5′
3′ XhoI Cλ	CTCCTCACTCGAGGGYGGGAACAGAGTG
First nested PCR κLC	**Forward 5′ to 3′**
5′ L Vκ1/2	ATGAGGSTCCCYGCTCAGCTGCTGG
5′ L Vκ3	CTCTTCCTCCTGCTACTCTGGCTCCCAG
5′ L Vκ4	ATTTCTCTGTTGCTCTGGATCTCTG
	Reverse 3′ to 5′
3′ Cκ543	GTTTCTCGTAGTCTGCTTTGCTCA
Second nested PCR κ LC	**Forward 5′ to 3′**
5′ Pan Vκ	ATGACCCAGWCTCCABYCWCCCTG
	Reverse 3′ to 5′
3′ Cκ494	GTGCTGTCCTTGCTGTCCTGCT
Specific PCR k LC	**Forward 5′ to 3′**

(continued)

Table 1
(continued)

Primer	Sequence
5′ AgeI Vκ1-5	CTGCAACCGGTGTACATTCTGACATCCAGATGACCCAGTC
5′ AgeI Vκ1-9	TTGTGCTGCAACCGGTGTACATTCAGACATCCAGTTGACCCAGTCT
5′ AgeI Vκ1D-43	CTGCAACCGGTGTACATTGTGCCATCCGGATGACCCAGTC
5′ AgeI Vκ2-24	CTGCAACCGGTGTACATGGGGATATTGTGATGACCCAGAC
5′ AgeI Vκ2-28	CTGCAACCGGTGTACATGGGGATATTGTGATGACTCAGTC
5′ AgeI Vκ2-30	CTGCAACCGGTGTACATGGGGATGTTGTGATGACTCAGTC
5′ Age Vκ3-11	TTGTGCTGCAACCGGTGTACATTCAGAAATTGTGTTGACACAGTC
5′ Age Vκ3-15	CTGCAACCGGTGTACATTCAGAAATAGTGATGACGCAGTC
5′ Age Vκ3-20	TTGTGCTGCAACCGGTGTACATTCAGAAATTGTGTTGACGCAGTCT
5′ Age Vκ4-1	CTGCAACCGGTGTACATTCGGACATCGTGATGACCCAGTC
	Reverse 3′ to 5′
3′ BsiWI Jκ1/4	GCCACCGTACGTTTGATYTCCACCTTGGTC
3′ BsiWI Jκ2	GCCACCGTACGTTTGATCTCCAGCTTGGTC
3′ BsiWI Jκ3	GCCACCGTACGTTTGATATCCACTTTGGTC
3′ BsiWI Jκ5	GCCACCGTACGTTTAATCTCCAGTCGTGTC

Table 2
Reverse primers used to amplify IgH and IgL chain gene transcripts

B-cell population	IgH PCR reverse primer	Igκ reverse primer	Igλ reverse primer
$CD19^{+}CD3^{-}$ B cells	First PCR: C μ CH1 ext	First PCR: C κ 543	First PCR: C λ
	Second PCR: C μ CH1 int	Second PCR: C κ 494	Second PCR: XhoI Cλ
	First PCR: Cγ CH1 ext		
	Second PCR: Cγ IgG int		
	First PCR: Cα CH1 ext		
	Second PCR: Cα CH1-2 int		

14. Tris/borate/EDTA (TBE) running buffer: 1 M Tris base, 0.9 M boric acid, and 0.01 M EDTA.
15. GelRed Nucleic Acid gel stain (*see* **Note 9**).
16. Loading dye for DNA agarose gel: 40% w/v Sucrose, 0.25% bromophenol blue (6× solution) (*see* **Note 10**).
17. 100 bp DNA ladder ranging from 100 to 1517 bp.
18. 3′ Primers for sequencing: 3' Cμ CH1 int, 3' Cμ IgG int, 3' Cμ CH1–2 int (Table 1).

2.4 Gene Sequence Analysis and Gene-Specific PCR

1. Sequencing service company.
2. International ImmunoGeneTics (IMGT) free online database (www.imgt.org/vquest).
3. PCR cooler suitable for 96-well PCR plates.
4. PCR thermal cycler suitable for 96-well PCR plates skirted and half-skirted.
5. Gel tank for DNA agarose gel.
6. 96-Well plates, half-skirted.
7. Reservoir reagent 100 mL sterile polystyrene.
8. Adhesive plate seals and adhesive PCR seals suitable for high-temperature incubations.
9. Nuclease-free water.
10. Ethanol, RNase, and DNase Away decontamination solution.

11. Gene-specific primers (Table 3) (*see* **Note 12**).
12. PCR master mix: 29.2 μL Nuclease-free water, 4 μL PCR buffer, 0.4 μL dNTP mix, and 0.2 μL HotStart Taq DNA polymerase.
13. PCR cleanup kit for purification of PCR products.

2.5 Expression Vector Cloning

1. PCR thermal cycler suitable for 96-well PCR plates.
2. UV spectrophotometer.
3. Water bath (with floating tube racks); 37 °C incubator with shaker.
4. 0.2 mL PCR tubes; 14 mL round-bottom polypropylene tubes.
5. Petri dishes 100 mm Ø × 15 mm H; disposable bacteria cell spreaders and inoculating loops.
6. Nuclease-free water.
7. AgeI-HF (20 U/mL) restriction endonuclease with 10× CutSmart buffer (*see* **Note 13**).
8. SalI-HF (20 U/mL) restriction endonuclease with 10× CutSmart buffer (*see* **Note 13**).
9. BsiWI (10 U/mL) restriction endonuclease with 10× NEBuffer 3.1.
10. XhoI (20 U/mL) restriction endonuclease with 10× CutSmart buffer (*see* **Note 13**).
11. Human IgH γ1 linearized plasmid vector (50 ng/μL) with cloning sites for AgeI and SalI (*see* **Note 14**).
12. Human IgL κ1 linearized plasmid vector (50 ng/μL) with cloning sites for AgeI and BsiWI (*see* **Note 14**).
13. Human IgL λ2 linearized plasmid vector (50 ng/μL) with cloning sites for AgeI and XhoI (*see* **Note 14**).
14. T4 DNA ligase with 10× reaction buffer.
15. LB agar plates with ampicillin: 5 g Yeast extract, 15 g agar, 5 g NaCl, 10 g tryptone in 1000 mL of distilled water + 100 μg/mL (final) ampicillin. Autoclave LB agar before use (*see* **Note 15**).
16. LB medium: 5 g Yeast extract, 5 g NaCl, 10 g tryptone in 1000 mL of distilled water + 100 μg/mL (final) ampicillin. Autoclave LB medium before use.
17. DH10B chemically competent *Escherichia coli* (*E. coli*) cells (*see* **Note 16**).
18. 5′ Ab-sense primer and 3′ primer (3' IgG internal, 3' Cκ 494, 3' Cλ) (*see* **Note 17**).
19. Nucleic acid purification plasmid kit.

Table 3
Gene-specific PCR primers for IgH and IgL (κ/λ) (see Note 11)

IgH V	5′ Primer	IgH J	3′ Primer	IgκV	5′ Primer	IgκJ	3′ Primer	IgλV	5′ Primer	IgλJ	3′ Primer
1-18	5′ Age VH1-24	1	3′ SalI JH1/2/4/5	1-12	5′ Age Vκ1-5	1	3′ BsiWI Jκ 1/4	1	5′ AgeI Vλ1	1	3′ XhoI Cλ
1-2	5′ Age VH1-24	2	3′ SalI JH1/2/4/5	1-16	5′ Age Vκ1-5	2	3′ BsiWI Jκ 2	2	5′ AgeI Vλ2	2	3′ XhoI Cλ
1-24	5′ Age VH1-24	3	3′ SalI JH3	1-17	5′ Age Vκ1-5	3	3′ BsiWI Jκ 3	3	5′ AgeI Vλ3	3	3′ XhoI Cλ
1-3	5′ Age VH1-24	4	3′ SalI JH1/2/4/5	1-27	5′ Age Vκ1-5	4	3′ BsiWI Jκ 1/4	4	5′ AgeI Vλ4/5	4	3′ XhoI Cλ
1-45	5′ Age VH1-24	5	3′ SalI JH1/2/4/5	1-33	5′ Age Vκ1-5	5	3′ BsiWI Jκ 6	5	5′ AgeI Vλ4/5	5	3′ XhoI Cλ
1-46	5′ Age VH1-24	6	3′ SalI JH6	1-37	5′ Age Vκ1-9			6	5′ AgeI Vλ6	6	3′ XhoI Cλ
1-58	5′ Age VH1-24			1-39	5′ Age Vκ1-5			7	5′ AgeI Vλ7/8	7	3′ XhoI Cλ
1-69	5′ Age VH1-24			1-5	5′ Age Vκ1-5			8	5′ AgeI Vλ7/8		
1-8	5′ Age VH1-24			1-8	5′ Age Vκ1D-43						
2-26	5′ Age VH2-26			1-9	5′ Age Vκ1-9						
2-5	5′ Age VH2-5			1-NL1	5′ Age Vκ1-5						
2-70	5′ Age VH2-70			1/OR2-0	5′ Age Vκ1-5						
3-11	5′ Age VH3-33			1D-12	5′ Age Vκ1-5						
3-13	5′ Age VH3-9			1D-16	5′ Age Vκ1-5						
3-15	5′ Age VH3-9			1D-33	5′ Age Vκ1-5						
3-16	5′ Age VH3-9			1D-39	5′ Age Vκ1-5						
3-20	5′ Age VH3-9			2-24	5′ Age Vκ2-24						
3-21	5′ Age VH3-9			2-28	5′ Age Vκ2-28						

(continued)

Table 3
(continued)

IgH V	5′ Primer	IgH J	3′ Primer	Igκ V	5′ Primer	Igκ J	3′ Primer	Igλ V	5′ Primer	Igλ J	3′ Primer
3-23	5′ Age VH3-23			2-29	5′ Age Vκ2-24						
3-30	5′ Age VH3-33			2-30	5′ Age Vκ2-30						
3-33	5′ Age VH3-33			2-40	5′ Age Vκ2-24						
3-35	5′ Age VH3-9			2D-24	5′ Age Vκ2-24						
3-38	5′ Age VH3-9			2D-26	5′ Age Vκ3-15						
3-43	5′ Age VH3-9			2D-28	5′ Age Vκ2-28						
3-48	5′ Age VH3-9			2D-29	5′ Age Vκ2-24						
3-49	5′ Age VH3-9			2D-30	5′ Age Vκ2-30						
3-53	5′ Age VH3-9			2D-40	5′ Age Vκ2-24						
3-64	5′ Age VH3-9			3-11	5′ Age Vκ3-11						
3-66	5′ Age VH3-9			3-15	5′ Age Vκ3-15						
3-7	5′ Age VH3-9			3-20	5′ Age Vκ3-11						
3-72	5′ Age VH3-9			3-7	5′ Age Vκ3-15						
3-73	5′ Age VH3-9			3-NL1/2/3/4/5	5′ Age Vκ3-11						
3-74	5′ Age VH3-9			3/OR2-268	5′ Age Vκ3-15						
3-9	5′ Age VH3-9			3D-11	5′ Age Vκ3-11						
4-28	5′ Age VH4			3D-15	5′ Age Vκ3-15						
4-30-2	5′ Age VH4-39			3D-20	5′ Age Vκ3-11						
4-30-4	5′ Age VH4			3D-7	5′ Age Vκ3-15						

4-31	5′ Age VH4	4-1	5′ Age Vκ2-28
4-34	5′ Age VH4-34	6-21	5′ Age Vκ3-11
4-39	5′ Age VH4-39	6D-21	5′ Age Vκ3-11
4-4	5′ Age VH4	6D-41	5′ Age Vκ2-30
4-59	5′ Age VH4		
4-61	5′ Age VH4		
4-b	5′ Age VH4		
5-51	5′ Age VH1/5		
5-a	5′ Age VH1/5		
6-1	5′ Age VH6-1		
7-4-1	5′ Age VH1-24		
7-81	5′ Age VH1-24		

2.6 Recombinant Monoclonal Antibody Production

1. Cell culture incubator.
2. Orbital shaker.
3. 125 mL Polycarbonate, disposable, sterile, vent-cap Erlenmeyer shaker flasks.
4. 0.2 μm Syringe filter.
5. Expi293F™ cells, Expi293™ Expression Medium, ExpiFectamine™ Reagent, ExpiFectamine™ Transfection Enhancer 1 and ExpiFectamine™ Transfection Enhancer 2, Opti-MEM® Reduced-Serum Medium (all from Thermo Fisher Scientific) (*see* **Note 18**).
6. Plasmid DNA: 15 μg for IgH plasmid and 15 μg for IgL (κ or λ) plasmid (*see* **Note 19**).

2.7 Purification of Recombinant Monoclonal Antibodies

1. UV spectrophotometer.
2. Glass Chromatography Column (BioRad) (*see* **Note 20**).
3. 1.5 mL Tubes; spectrophotometer cuvettes.
4. Protein gel electrophoresis tank.
5. 1× PBS.
6. Protein A Sepharose beads (GE Healthcare Life Science) (*see* **Note 21**).
7. Elution buffer: 0.1 M Glycine-HCl, pH 3.0.
8. Neutralization buffer: 1 M Tris base, pH 9.0.
9. 4–20% SDS polyacrylamide gel: Reducing and nonreducing loading buffer for SDS-PAGE gel.
10. Color protein standard broad range (11–245 kDa).

3 Methods

3.1 Mononuclear Cell Isolation from Synovial Tissue

Mononuclear cells are isolated from synovial tissue specimens obtained from joint replacement surgery or biopsy characterized by the presence of lymphocytic infiltration. The extracellular matrix in animal tissues is made by collagens and other extracellular matrix proteins such as glycoproteins and proteoglycans. To isolate single cells without disrupting the cellular structure a combination of proteolytic enzymes is necessary to dissociate the tissue (*see* **Note 22**). All steps are performed under a tissue culture laminar hood.

1. Put the synovial tissue into a petri dish with RPMI-1640 (Fig. 2) (*see* **Notes 23** and **24**).
2. Cut the synovial tissue into small pieces using scissors (*see* **Note 25**).
3. Prepare 5 mL round-bottom tube(s) containing the digestion buffer (*see* **Notes 26** and **27**).

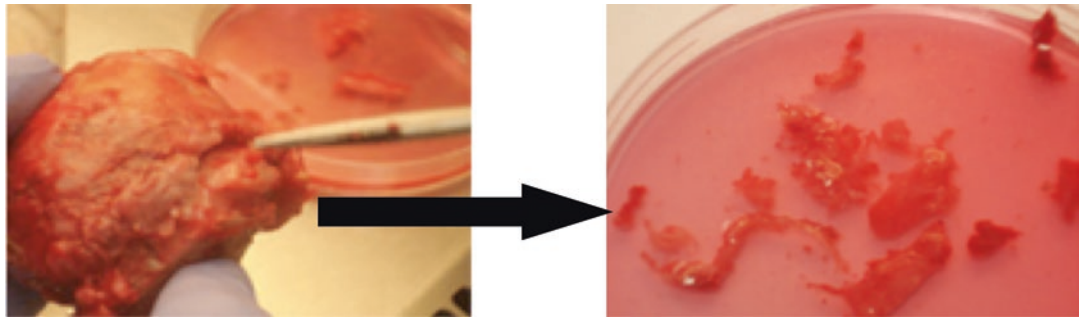

Fig. 2 Representative picture showing synovial tissue dissected out from a joint. The image shows an example of synovial tissue before and after the cutting out from an RA joint

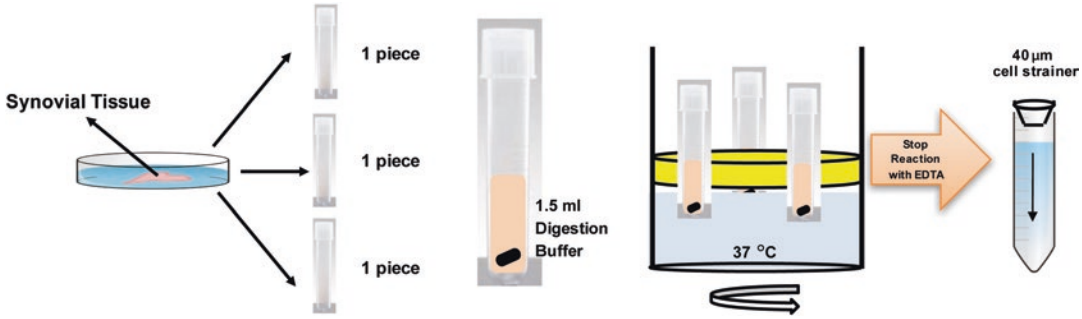

Fig. 3 Preparation of mononuclear cells from synovial tissue. Schematic representation of synovial tissue digestion used to isolate mononuclear cells in order to sort single $CD19^+$ $CD3^-$ B cells by FACS

4. Transfer the cut synovial tissue into 5 mL round-bottom tubes with the digestion buffer (*see* **Note 28**).
5. Add one magnetic stirring bar to each 5 mL round-bottom tube using tweezers.
6. Start the digestion for 1 h at 37 °C under shaking in a water bath (Fig. 3) (*see* **Note 29**).
7. Add 15 µL of 0.5 M EDTA to each tube to stop the reaction.
8. Filter each sample through 40 µm cell strainer to remove undigested tissue and centrifuge for 10 min at 400 × *g*. The filtered solution contains the mononuclear cells (Fig. 3).
9. Resuspend the mononuclear cells in RPMI-1640 and count the cells.
10. Proceed to the immunofluorescence labeling for flow cytometry for single-cell sorting (*see* **Note 30**).

3.2 Isolation of Single Human B Cells by Fluorescence-Activated Cell Sorting (FACS) into 96-Well Plates

Purified mononuclear cells isolated from synovial tissues are stained with fluorescent-labeled anti-human CD19 and anti-human CD3, in order to isolate single $CD19^+$ $CD3^-$ B cells (Fig. 4) (*see* **Note 31**).

1. Aliquot purified mononuclear cells into 1.5 mL tubes and centrifuge at 400 × *g* for 4 min at 4 °C.

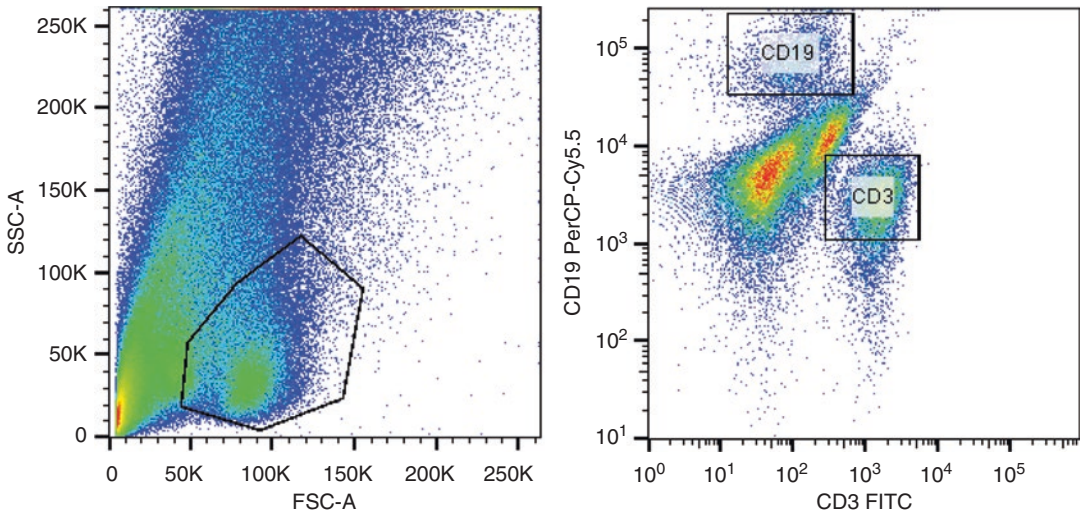

Fig. 4 Sorting gating strategy example. Mononuclear cells are surface labeled with fluorochrome-coupled anti-CD19 and anti-CD3 antibodies. The sorting gate strategy for single $CD19^+$ $CD3^-$ B cell is shown

2. Wash cells with 1× PBS.
3. Resuspend the cell pellet in 100 µL of FACS buffer staining solution containing all the antibodies at the appropriate final concentration.
4. Incubate the cells for at least for 30 min in the dark at 4 °C.
5. Wash the cells with 1 mL FACS buffer and resuspend in FACS buffer at a final concentration of 10^7 cells/mL.
6. Add DAPI to exclude dead cells.
7. Keep samples on ice until single-cell sorting is performed.
8. Sort the cells into 96-well PCR skirted plates containing 4 µL of single-cell lysis solution per each well (*see* **Note 32**). Immediately after the sorting, seal the plate with the adhesive aluminum foil and put on dry ice. If not immediately used for the steps described below, store the plates at −80 °C (*see* **Note 33**).

3.3 Single-Cell RT-PCR and Immunoglobulin V Gene Amplification by Nested PCR

3.3.1 Single-Cell RT-PCR

Complementary DNA is synthesized in a total volume of 14.5 µL per well in the original 96-well sorting plate. Before starting all steps in this section, it is important to clean the PCR hood or the laboratory bench and laboratory pipettes with ethanol, RNase Away, and DNase Away decontamination solution in order to work in RNase/DNase-free conditions. Perform all the steps on ice or on a PCR cooler.

1. Thaw a plate of single-sorted B cells on ice and spin down before removing the adhesive aluminum foil.

2. Add 3.5 μL RHP mix to each well. Cover the plate with adhesive plate seal and spin down.
3. Transfer the plate on a hot plate for 1 min at 68 °C and put back on ice or onto the PCR-cooler.
4. Remove cautiously the adhesive PCR seal and add 7 μL RT mix to each well. Cover the plate with adhesive PCR plate seal and spin down.
5. Perform the reverse transcription at 42 °C for 5 min, 25 °C for 10 min, 50 °C for 60 min, and 94 °C for 5 min.
6. cDNA can be stored at −20 °C before performing the immunoglobulin gene amplification PCR.

3.3.2 Immunoglobulin V Gene Amplification by Nested PCR

For each cell, IgH and corresponding IgL chain (Igκ and Igλ) gene transcripts are amplified independently by nested PCR starting from 2 μL of cDNA as template. For the IgH gene, three independent nested PCR are performed in order to discriminate between IgH constant regions Cμ, Cγ, and Cα. The nested PCR is a modification of the common PCR in which two sets of primers are used in two consecutive rounds of PCR. The second set of primers bind the first PCR product internally ensuring that the product from the second PCR has little contamination, thus increasing the sensitivity and specificity of the PCR. All PCR reactions are performed in 96-well half-skirted plates in a total volume of 40 μL per well.

1. Prepare a PCR master mix for the ***first*** round of nested PCR (or first PCR), as shown below.

Reagent—PCR master mix 1	1-Well (μL)	96-Wells (μL) (see Note 34)
Nuclease-free water	32.16	3647.6
PCR buffer	4.00	440.0
5′ Primer mix	0.13	14.3
3′ Primer mix	0.13	14.3
dNTP	0.40	44.0
HotStart Taq	0.18	19.8

2. Add 38 μL of PCR master mix 1 and 2 μL of cDNA to each well of a new 96-well plate. Cover with adhesive PCR seal plate and spin down.
3. Perform the first PCR at 94 °C for 15 min; for 50 cycles at 94 °C for 30 s, 58 °C (IgH/Igκ) or 60 °C (Igλ) for 30 s, 72 °C for 55 s; 72 °C for 10 min.

4. Prepare a PCR master mix for the ***second*** round of nested PCR (or second PCR), as shown below.

Reagent—PCR master mix 2	1-Well (μL)	96-Wells (μL) (see Note 34)
Nuclease-free water	31.66	3482.6
PCR buffer	4.00	440.0
5′ Primer mix	0.13	14.3
3′ Primer mix	0.13	14.3
dNTP	0.40	44.0
HotStart Taq	0.18	19.8

5. Add 36.5 μL of PCR master mix 2 and 3.5 μL of first nested PCR product to each well of a new 96-well plate. Cover with adhesive PCR seal plate and spin down.
6. Perform the second PCR at 94 °C for 15 min; for 50 cycles at 94 °C for 30 s, 58 °C (IgH/Igκ) or 60 °C (Igλ) for 30 s, 72 °C for 45 s; 72 °C for 10 min.
7. Check the size of the second PCR products by running a 2% agarose gel. Expected sizes of the second PCR are IgH = 450 bp, Igκ = 510 bp, and Igλ = 405 bp. Load 5 μL of the PCR product mixed with 5 μL of loading dye into the agarose gel containing GelRed and run for 30 min at 120 V. Visualize the DNA bands using a UV transilluminator.
8. Send the second PCR product of the expected size (IgH, Igκ, and/or Igλ) for sequencing with the respective 3′ primer.

3.4 Ig V Gene Sequence Analysis and Gene-Specific PCR

Ig nucleotide sequences are analyzed using the IMGT/V-QUEST database in order to identify the V, D, and J genes and alleles in rearranged V-J and V-D-J sequences by alignment with germline Ig gene and allele sequences of the IMGT directory. It defines the FR and CDR regions and provides a detailed characterization of the query sequence. The algorithm used to identify the closest V, D, and J genes and alleles is based on global pairwise alignment followed by a similarity evaluation. Determining the Ig gene usage is essential for performing the gene-specific PCR (Fig. 5).

1. Determine for each PCR product (IgH and IgL (κ/λ)) the Ig-V and Ig-J gene usage in order to set up the gene-specific second nested PCR.
2. Define the gene-specific primer using Table 3.
3. Clean the PCR hood or the laboratory bench and laboratory pipettes with ethanol, RNase Away, and DNase Away decontamination solution.

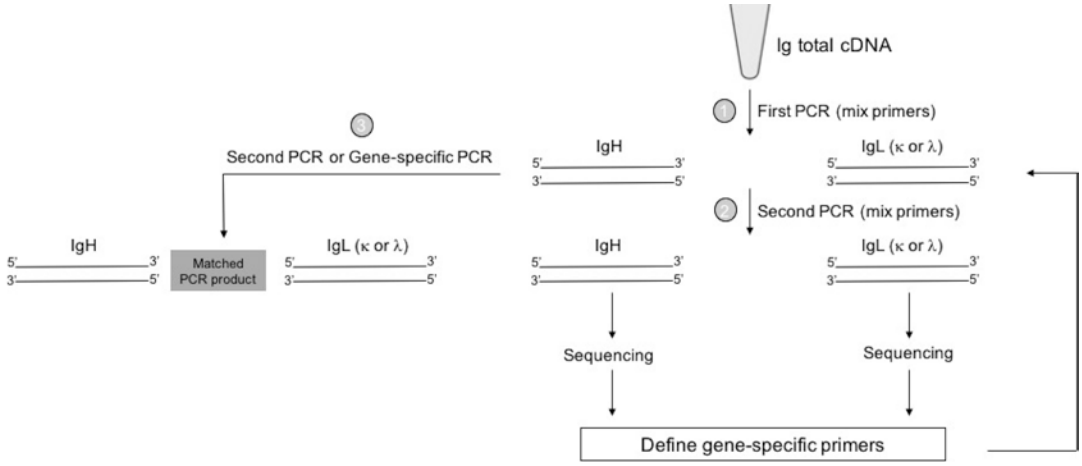

Fig. 5 Schematic representation of the first, second, and gene-specific PCR. (1) First round of nested PCR starting from total Ig cDNA and using a mix of primers. (2) Second round of nested PCR starting from the first PCR product and using a mix of primers. (3) Gene-specific PCR starting from the first PCR product and using gene-specific primers

4. Dilute gene-specific primers to a working concentration of 5 μM in nuclease-free water.
5. In a 96-well plate deposit 2 μL of the matched 5′ and 3′ primers for one PCR product into the same well. Cover the plate with adhesive plate seal and spin down.
6. In the same plate with the primers, add 33.8 μL of PCR master mix in each well.
7. In a new 96-well PCR plate, add 4.2 μL of unpurified first PCR into the correct well corresponding to the matched primers. Add the mix containing the PCR master mix and primers. Spin down and seal the plate with adhesive PCR plate.
8. Perform the second round of nested PCR at 94 °C for 15 min; for 50 cycles at 94 °C for 30 s, 58 °C (IgH/Igκ) or 60 °C (Igλ) for 30 s, 72 °C for 45 s; 72 °C for 10 min.
9. Check the size of the gene-specific PCR products by running a 2% agarose gel. Expected sizes are IgH = 450 bp, Igκ = 510 bp, and Igλ = 405 bp. Load 5 μL of the PCR product mixed with 5 μL of loading dye into the agarose gel containing GelRed and run for 30 min at 120 V. Visualize the DNA bands using a UV transilluminator.
10. Purify gene-specific PCR products using a PCR cleanup kit following the manufacturer's instruction. Elute the PCR products in nuclease-free water in a final volume of 60 μL.
11. PCR products can be stored at −20 °C before performing the expression vector cloning.

Table 4
Enzyme digestion mix for IgH, Igκ, and Igλ PCR product

	IgH PCR product	Igκ PCR product	Igλ PCR product
Mix 1	5.9 μL Nuclease-free water	3.95 μL Nuclease-free water	5.9 μL Nuclease-free water
	0.05 μL AgeI-HF	0.05 μL AgeI-HF	0.05 μL AgeI-HF
	0.05 μL SalI-HF		0.05 μL XhoI
Mix 2		1.7 μL Nuclease-free water	
		0.2 μL NEBuffer 3.1	
		0.1 μL BsiWI	

3.5 Expression Vector Cloning: PCR Product Restriction Enzyme Digestion, Ligation, and Bacteria Cell Transformation

Restriction enzyme digestion is used to generate compatible ends on the PCR product that can be ligated into a specific expression vector DNA. In order to generate compatible ends, all the primers used in the gene-specific PCR are characterized by the presence of restriction sites which are compatible with the expression vector that will be used to express the rmAbs.

3.5.1 PCR Product Restriction Enzyme Digestion

1. Prepare enzyme digestion mixes 1 and 2 for IgH, Igκ, and Igλ following Table 4 (*see* **Note 35**).
2. Use 30 μL purified PCR product, add 4 μL CutSmart buffer, and 6 μL of the digestion mix 1 for IgH/Igλ or 4 μL of the digestion mix 1 for Igκ (*see* **Note 36**). Incubate for 2 h at 37 °C (*see* **Note 37**).
3. Only for Igκ add 2 μL of the digestion mix 2. Incubate for 2 h at 55 °C (*see* **Note 37**).
4. Purify the digested PCR products using a PCR cleanup kit following the manufacturer's instruction. Elute the digested PCR products in nuclease-free water in a final volume of 60 μL.
5. Digested PCR products can be stored at −20 °C before performing the ligation and transformation step.

3.5.2 Ligation

1. Set up the following reaction in a 0.2 mL PCR tube on ice (*see* **Note 38**).

Reagent	10 μL Final volume
T4 DNA ligase buffer 10×	1 μL
Vector DNA (50 ng/μL) (*see* **Note 39**)	0.5 μL
PCR product	8 μL
T4 DNA ligase	0.5 μL

2. Incubate for 1 h at room temperature or overnight at 16 °C.

3.5.3 Bacteria Cell Transformation

1. Thaw competent cells on ice. Mix gently and transfer 5 μL of cells into a 0.2 mL tube on ice (*see* **Notes 40** and **41**).
2. Add 3 μL of ligation product to the cell mixture and leave on ice for 30 min.
3. Heat shock at 42 °C in a water bath for 20 s and place the tubes back on ice for 5 min.
4. Add 200 μL of LB medium and place for 1 h at 37 °C under shaking (200 rpm) (*see* **Note 42**).
5. Warm LB agar plates at 37 °C or room temperature, spread 200 μL of the mixture onto the plate, and incubate overnight at 37 °C leaving the plate upside down. Label each plate with the corresponding PCR product name in order to distinguish between the IgH, Igκ, and Igλ individual clones (*see* **Note 43**).
6. Set up the following insert check PCR reaction on ice (*see* **Note 44**).

Reagent	25 μL Final volume
Nuclease-free water	19.1 μL
10× PCR buffer	2.5 μL
dNTP 1.25 mM	2.5 μL
5′ Ab sense	0.2 μL
3′ Primer (IgG internal/Cκ 494/Cλ)	0.2 μL
Taq DNA polymerase	0.5 μL

7. Pick up three individual colonies with 10 μL pipette tips, transfer into a backup LB agar plate, and then place the same pipette tips each in a different well of a 96-well PCR plate containing the PCR insert check mix. Perform the PCR at 94 °C for

15 min; for 27 cycles at 94 °C for 5 min, 94 °C for 30 s, 58 °C for 30 s, 72 °C for 60 s; 72 °C for 10 min.

8. Check the size of the insert, check PCR products by running a 2% agarose gel. Expected sizes are Igγ1 vector = 650 bp, Igκ1 vector = 700 bp, and Igλ2 vector = 590 bp. Load 5 μL of the PCR product mixed with 5 μL of loading dye into the agarose gel containing GelRed and run for 30 min at 120 V. Visualize the DNA bands using a UV transilluminator.
9. Sequence the insert check PCR product using the 5′ Ab sense primer as sequencing primer to confirm the identity with the second PCR product. Check also that the PCR product is in frame within the plasmid. Pick up the colonies with 100% of identity from the backup plate using an inoculating loop and inoculate 4 mL LB medium containing 100 μg/mL ampicillin in 14 mL round-bottom tube. Loosely close the tube and incubate at 37 °C overnight under vigorous shaking (250 rpm) (*see* **Note 45**).
10. After incubation, check for growth which is characterized by a cloudy medium appearance (*see* **Note 46**).
11. Use some of the inoculating medium for preparing a glycerol stock for long-term storage of the bacteria before starting the plasmid mini-prep (*see* **Note 47**).
12. Isolate plasmid using a nucleic acid purification plasmid kit (plasmid mini-prep) following the manufacturer's instruction. Elute DNA plasmid in 75 μL nuclease-free water.
13. Measure the concentration of the DNA plasmid with a spectrophotometer at A260nm. Determine the purity of the DNA plasmid by the ratio 260/280 nm (*see* **Note 48**).

3.6 Recombinant Monoclonal Antibody Production

Recombinant monoclonal antibodies are expressed using the Expi293F™ Expression System that allows a rapid and high-yield protein production in mammalian cells. Expi293F cells are specifically adapted to grow in suspension at high density and exhibit higher protein production compared to classical 293 cells. The medium used in this system is chemically defined and serum- and protein free that, in combination with the Expi293 Transfection Reagent, enables a high-efficiency transfection.

1. Add 7.5×10^7 Expi293F cells to 25.5 mL of Expi293 Expression medium in a 125 mL Erlenmeyer flask (8% CO_2 incubator at 37 °C and 125 rpm on an orbital shaker) (*see* **Notes 49** and **50**).
2. Dilute 30 μg of plasmid DNA (15 μg IgH plasmid and 15 μg IgL (κ or λ) plasmid) in Opti-MEM to a total volume of 1.5 mL. Mix gently.

3. Dilute 81 μL of ExpiFectamine Reagent in Opti-MEM to a total volume of 1.5 mL. Mix gently and incubate for 5 min at room temperature.
4. Add the diluted DNA to the diluted ExpiFectamine Reagent for a total volume of 3 mL. Mix gently.
5. Incubate the mixture for 20 min at room temperature.
6. Add 3 mL mixture to the flask. Put flask back to the incubator.
7. After 20 h, add 150 μL of ExpiFectamine Transfection Enhancer 1 and 1.5 mL of Enhancer 2 to the flask.
8. Six days after transfection, sediment cells by centrifugation for 10 min at 800 × *g* at 4 °C.
9. Filter the supernatant through 0.2 μm syringe filter and store at 4 °C (*see* **Note 51**).

3.7 Purification of Recombinant Monoclonal Antibodies Using Protein A Beads

Recombinant monoclonal antibodies are purified from the culture supernatant by affinity chromatography using Protein A Sepharose beads.

1. Equilibrate 100 mg of Protein A Sepharose beads with cold 1× PBS. Centrifuge for 10 min at 4000 × *g* at 4 °C. Aspirate supernatant and resuspend beads in 1 mL of 1× PBS.
2. Add the equilibrated Protein A beads into the culture supernatant and incubate overnight at 4 °C under rotation.
3. Separately, add 0.5 M NaOH into the chromatography column and leave the solution overnight to clean and sanitize the column (*see* **Notes 52** and **53**).
4. Discard the NaOH solution. Rinse and equilibrate the column with abundant cold 1× PBS.
5. Load culture supernatant/Protein A beads onto the chromatography column and discard flow-through (*see* **Note 54**).
6. Wash the beads with 2 × 50 mL of cold 1× PBS and discard the flow-through (*see* **Note 54**).
7. Elute recombinant antibody adding elution buffer. Collect three fractions of 500 μL in microcentrifuge tubes containing 50 μL of neutralization buffer (*see* **Note 55**).
8. Measure antibody concentration at A_{280nm} using a UV spectrophotometer.
9. Purified antibody may be stored at 4 °C. Sodium azide may be added for long-term storage (*see* **Note 56**).
10. Analyze purity and integrity of recovered immunoglobulin by loading 500 ng/lane in a SDS-PAGE followed by a protein staining technique (*see* **Note 57**).

4 Notes

1. The synovial membrane or synovium is a loose connective tissue which is found between the joint capsule and the joint cavity of arthrodial joints. The normal synovium is composed mainly by two distinct layers: the intimal lining layer and the synovial sub-lining layer. The intimal lining layer is mainly composed by fibroblast-like synoviocytes and macrophages. The sub-lining layer is made of connective tissue containing blood vessels, fibroblasts, adipocytes, and some resident immune cells like macrophages and mast cells [10]. During chronic inflammation, the intimal lining layer is characterized by marked hyperplasia, whereas the sub-lining layer is the site of massive infiltration of immune cells. In order to generate recombinant monoclonal antibodies, only synovial tissue with infiltration of lymphoid cells is used.
2. Prepare a stock concentration at 100 mg/mL and 10 mg/mL in 1× PBS for collagenase D and DNase I, respectively. Aliquot and store at −20 °C. Use heat-inactivated FBS throughout all the protocol.
3. It is important to use skirted PCR plates to avoid tilting of the plates during the single-cell FACS sorting.
4. This protocol has been designed to isolate single $CD19^+$ $CD3^-$ B cells but the sorting strategy can be modified accordingly to the cell population of interest: CD19 antibody (clone SJ25C1) and CD3 antibody (clone HIT3a).
5. Random hexamer primers and NP-40 are diluted at their final concentration in nuclease-free water.
6. The 100 mM dNTP set consists of four deoxynucleotides (dATP, dCTP, dGTP, dTTP), each at a concentration of 100 mM. Prepare aliquots of dNTP mix adding 50 μL dATP, 50 μL dCTP, 50 μL dGTP, and 50 μL dTTP from the 100 mM dNTP set. Store aliquots at −20 °C.
7. Prepare each primer to a working dilution of 50 μM. For the primer mix, combine equal volume of each primer. Primer mixes can be prepared in advance and stored at −20 °C. All the primers used are the same as previously published with the exception in the use of the Cμ internal primer (GGGAATTCTCACAGGAGACGA) in the second round of the nested PCR [7, 8].
8. The HotStart Taq DNA polymerase has an error rate of 2×10^{-5}/nucleotide and cycle and it has been chosen instead of high-fidelity enzymes which introduce less error because the HotStar Taq DNA polymerase has a high amplification efficiency for low-copy templates when starting from single cell.

9. GelRed is a safe and ultrasensitive fluorescent nuclei acid dye which is used to replace the toxic ethidium bromide for staining the dsDNA in agarose gels. Use according to the manufacturer's instruction.
10. Dilute the loading dye to a working dilution of 1× in distilled water before use.
11. For Igλ 3′ primer, use the primer 3' XhoI Cλ for all the PCR products.
12. Use the following primers for sequencing: for IgH = 3' Cμ CH1 int or Cγ IgG int or Cα CH1–2 int; for Igκ = 3' Ck494; for Igλ = 3' XhoI Cλ.
13. 10× NEB CutSmart buffer includes already BSA.
14. IgH γ1, IgL κ1, and IgL λ2 expression vectors are characterized by the ampicillin-resistant gene. The original vectors are from Dr. Hedda Wardemann's group, as published in [7, 8]. Human IgG heavy- and light-chain expression vectors are also commercially available. Please check that the cloning sites are compatible with the primers containing restriction sites in use in this protocol.
15. Cool autoclaved LB agar medium to below 50 °C (when you can hold it easily) before adding ampicillin which is a heat-sensitive antibiotic. Pour LB agar medium into a 100 mm petri dish next to a Bunsen burner. Dry plates by leaving them upside down with lids on at room temperature overnight. Store plates inverted at 4 °C in a darkroom or wrapped in aluminum foil to preserve light-sensitive ampicillin. Do not store for longer than 1 month as ampicillin may degrade.
16. Genotype DH10B *E. coli* cells: Δ(ara-leu) 7697 araD139 ΔlacX74 galK16 galE15 e14-ϕ80dlacZΔM15 recA1 relA1 endA1 nupG rpsL (StrR) rph spoT1 Δ(mrr-hsdRMS-mcrBC). Competent cells are supplied with a control vector pUC19 used as positive control during the transformation reaction.
17. Prepare each primer to a working dilution of 50 μM: 5′ Absense primer (GCTTCGTTAGAACGCGGCTAC); 3′ IgG internal (GTTCGGGGAAGTAGTCCTTGAC) for IgH γ1 vector; 3′ Cκ 494 (GTGCTGTCCTTGCTGTCCTGCT) for IgL κ1 vector; and 3′ Cλ (CACCAGTGTGGCCTTGTT GGCTTG) for IgL λ2 vector.
18. Standard adherent HEK293T cells can also be used for the production of the recombinant monoclonal antibodies together with alternative transfection reagents such as polyethylenimine (PEI), as reported in the section "Recombinant Antibody Production" in [8].

19. To produce lower amount of recombinant antibodies, it is possible to reduce the quantity of plasmids. In this case, scale down all required solutions.
20. For smaller volume, disposable polypropylene spin columns (1.2 mL bed volume) can be used.
21. Alternatively, protein G beads can also be used.
22. Collagenase is an enzyme which is used for the dissociation of tissues since it breaks down the native collagen that holds tissues together. In particular, collagenase D is used to preserve functionality and integrity of cell-surface proteins. Enzyme activity is inhibited by the addition of EDTA.
23. Synovial tissue is the pink layer on the fat tissue and once it is in the medium it forms telltale fronds-like structure (Fig. 2). Do not (1) use tissue that has been burnt during cauterization which is indicated by black coloration and (2) take materials from around the artery entrance.
24. Add the RPMI-1640 medium as much as you need to cover the synovial tissue in order not to dry out the tissue during the cutting.
25. Be aware that the synovial tissue is a quite gluey and elastic tissue.
26. The number of 5 mL round-bottom tubes depends on the amount of synovial tissue pieces prepared.
27. For one tube = 1.5 mL RPMI-1640, 2% FBS, 37 μL collagenase D, and 2 μL DNase I.
28. 1–2 Pieces for tube.
29. Set the water bath at 37 °C before starting all the steps.
30. Be aware that single-cell sorting is associated with considerable cell loss up to 95%. Therefore, it is better starting the sorting from at least 1×10^6 cells.
31. From the total cell number, depending on the final yield, use $0.5/1 \times 10^6$ cells for each of the following controls.

    Control 1: Use single staining for setting up the flow cytometer and to perform fluorescence compensation. Use compensation beads, according to the manufacturer's instruction.

    Control 2: Use the fluorescence minus one (FMO) controls to set appropriately the cell population gates.
32. Prepare the PCR sorting plate(s) in advance and keep at 4 °C. After the addition of the lysis buffer, spin down the plate and seal with adhesive plate seal.
33. Transferring the PCR plate on dry ice quickly is a critical step for maintaining a high RNA integrity.

34. For one plate, prepare a master mix for 110 wells in order to have a surplus of reagents.
35. Preparing an enzyme digestion master mix is necessary to avoid loss of enzyme due to small pipetting volumes.
36. Depending on the number of PCR products to digest, this step can be performed in single-PCR 0.2 mL tubes or into 96-well PCR plate.
37. Digestion can be performed either in a water bath or in a PCR cycler.
38. T4 DNA ligase should be added last.
39. For the IgH PCR product use the human IgHγ1 linearized plasmid vector; for Igκ PCR product use the human IgLκ1 linearized plasmid vector; for Igλ PCR product use the human IgLλ2 linearized plasmid vector.
40. Do not vortex the tubes. For maximum transformation efficiency, the mixture should be incubated at least for 30 min. Reducing the incubation time decreases the transformation efficiency.
41. Normally, the manufacturer's instruction suggests to use 50 μL for each transformation. However, scaling down of 1:10 for each transformation is also possible bringing to a good transformation efficiency.
42. Incubate for at least 1 h. Reducing the incubation time decreases the transformation efficiency.
43. LB agar plates can be used warm or cold, wet or dry, without affecting the transformation efficiency. However, working with warm plates is easier and allows a more rapid colony formation.
44. Set up also a positive and negative control mix.

Reagent	Positive control	Negative control
Nuclease-free water	3 μL	3 μL
Expression plasmid vector	–	5 μL
pUC19	5 μL	–

45. 4 mL Inoculation volume is used for preparing mini-prep. For larger preps, bigger volumes of LB inoculating medium are necessary.
46. Use as control LB media with ampicillin without any bacteria inoculated. In this tube, you should not see the appearance of a cloudy medium after inoculation overnight.

47. Prepare a glycerol stock: Add 500 μL of the overnight bacteria culture to 500 μL of 60% glycerol in a cryovial tube and gently mix. Make 60% glycerol solution by diluting 100% glycerol in deionized water and autoclave before use. Freeze the glycerol stock tube at −80 °C.
48. A good purity ranges from 1.80 to 2.00.
49. Expi293F cells are grown according to the manufacturer's instructions. Cells should be passaged every 3–4 days when the density reaches 3–5 × 10^6 cells/mL, and split to 0.3–0.5 × 10^6 cells/mL.
50. Transfection of Expi293F cells is also possible in smaller volume. In this case, scale down all required solutions.
51. Collect and filter the supernatant under the tissue culture hood to keep the supernatant on sterile conditions, particularly if you need to use the antibodies for in vivo assays.
52. Sodium hydroxide is effective in removing proteins and nucleic acids. It is also effective for inactivating most viruses, bacteria, yeasts, and endotoxins.
53. For smaller supernatant volumes, more suitable chromatography columns can be used, like spin disposable chromatography columns (BioRad).
54. The flow-through can be collected to check if the binding capacity of the Protein A Sepharose beads has not been saturated, and thus for residual presence of antibody in the supernatant.
55. Fractions may be pooled after determining protein concentration.
56. Alternatively, use a desalting column or dialysis to exchange the purified antibody into a more suitable buffer.
57. In parallel, sample can be prepared using a nonreducing loading buffer to check the integrity of the antibody. Molecular weight Ig in reducing condition: HC (each chain) = 50 kDa; LC (each chain) = 25 kDa. Molecular weight Ig in nonreducing condition = 150 kDa.

References

1. Corsiero E, Bombardieri M, Carlotti E et al (2016) Single cell cloning and recombinant monoclonal antibodies generation from RA synovial B cells reveal frequent targeting of citrullinated histones of NETs. Ann Rheum Dis 75:1866–1875. https://doi.org/10.1136/annrheumdis-2015-208356
2. Pitzalis C, Jones GW, Bombardieri M, Jones SA (2014) Ectopic lymphoid-like structures in infection, cancer and autoimmunity. Nat Rev Immunol 14:447–462. https://doi.org/10.1038/nri3700
3. Humby F, Bombardieri M, Manzo A et al (2009) Ectopic lymphoid structures support ongoing production of class-switched autoantibodies in rheumatoid synovium. PLoS Med 6:e1. https://doi.org/10.1371/journal.pmed.0060001

4. Manzo A, Bombardieri M, Humby F, Pitzalis C (2010) Secondary and ectopic lymphoid tissue responses in rheumatoid arthritis: from inflammation to autoimmunity and tissue damage/remodeling. Immunol Rev 233:267–285. https://doi.org/10.1111/j.0105-2896.2009.00861.x
5. Scheel T, Gursche A, Zacher J et al (2011) V-region gene analysis of locally defined synovial B and plasma cells reveals selected B cell expansion and accumulation of plasma cell clones in rheumatoid arthritis. Arthritis Rheum 63:63–72. https://doi.org/10.1002/art.27767
6. Corsiero E, Sutcliffe N, Pitzalis C, Bombardieri M (2014) Accumulation of self-reactive naive and memory B cell reveals sequential defects in B cell tolerance checkpoints in Sjogren's syndrome. PLoS One 9:e114575. https://doi.org/10.1371/journal.pone.0114575
7. Tiller T, Meffre E, Yurasov S et al (2008) Efficient generation of monoclonal antibodies from single human B cells by single cell RT-PCR and expression vector cloning. J Immunol Methods 329:112–124. https://doi.org/10.1016/j.jim.2007.09.017
8. Wardemann H, Kofer J (2013) Expression cloning of human B cell immunoglobulins. Methods Mol Biol 971:93–111. https://doi.org/10.1007/978-1-62703-269-8_5
9. Wardemann H, Yurasov S, Schaefer A et al (2003) Predominant autoantibody production by early human B cell precursors. Science 301:1374–1377. https://doi.org/10.1126/science.1086907
10. Arnett FC, Edworthy SM, Bloch DA et al (1988) The American Rheumatism Association 1987 revised criteria for the classification of rheumatoid arthritis. Arthritis Rheum 31:315–324

Chapter 11

Designed Methods for the Sorting of Tertiary Lymphoid Structure-Immune Cell Populations

Priyanka Devi-Marulkar, Hélène Kaplon, Marie-Caroline Dieu-Nosjean, and Myriam Lawand

Abstract

The tumor microenvironment is a complex network of interacting cells composed of immune and nonimmune cells. It has been reported that the composition of the immune contexture has a significant impact on tumor growth and patient survival in different solid tumors. For instance, we and other groups have previously demonstrated that a strong infiltration of T-helper type 1 (Th1) or memory $CD8^+$ T cells is associated with long-term survival of cancer patients. Nevertheless, the prognostic value of the other immune populations, namely regulatory T cells (Treg), B cells, and gamma delta (γδ) T cells, remains a matter of debate. Herein, we describe novel flow cytometry-based strategies to sort out these different immune populations in order to evaluate their role in non-small cell lung cancer (NSCLC).

Key words Tumor microenvironment, Lung cancer, Tumor-infiltrating B cell, Regulatory T cell, Gamma delta T cell, Flow cytometry, Tertiary lymphoid structure, Tumor immunology

1 Introduction

During the last decades, the immune microenvironment has been extensively characterized by immunohistochemistry in many solid tumors [1]. It has been shown that T lymphocytes are able to infiltrate the stroma and tumor islets [2], whereas B lymphocytes are mainly located at the invasive margin of the tumor, in ectopic lymphoid aggregates called tertiary lymphoid structures (TLS), displaying a similar architectural organization to secondary lymphoid organs [3]. They are composed of a B-cell zone adjacent to a T-cell zone. The prognostic value of TLS was reported for the first time in NSCLC patients [4].

Given that T cells are the key players in immunosurveillance, many studies have been conducted to deeply characterize their phenotype and function within the tumor microenvironment. Indeed, a high density of T lymphocytes and more particularly cytotoxic and memory $CD8^+$ T cells was shown to be correlated

Marie-Caroline Dieu-Nosjean (ed.), *Tertiary Lymphoid Structures: Methods and Protocols*, Methods in Molecular Biology, vol. 1845, https://doi.org/10.1007/978-1-4939-8709-2_11,

with a favorable clinical outcome in the most frequent solid tumor types [5]. However, the clinical impact of other T-cell subpopulations, such as conventional $CD4^+$ T cell and regulatory T cells (Treg), or unconventional T cells, such as γδ T cells, remains a matter of debate. For instance, in ovarian cancer, it has been demonstrated that a high Treg infiltrate was correlated with a poor clinical outcome [6], in opposition to head and neck cancer [7], follicular lymphoma [8], and colorectal cancer [9], for which the increased density of Tregs was associated with a good clinical outcome. Surprisingly, in some cases, such as anal carcinoma, glioma, and glioblastomas, the Treg infiltrate was not correlated with any clinical outcome [10–12]. Therefore, in order to better elucidate the function of Tregs in cancer, we developed an optimized method, which permits the sorting of $CD4^+$ T-cell subsets, i.e., Tregs and non-Treg $CD4^+$ T cells (mainly conventional $CD4^+$ T cells), from the lung tumor, non-tumoral distant lung, and blood of NSCLC patients. The method is designed to obtain highly pure T cells (purity 98–100%), which can be used for further cellular and molecular biology applications such as functional assays or gene expression analysis. This in particular allows a better understanding of the potential suppressive activities of Tregs in NSCLC patients.

Another population of unconventional T lymphocytes, called gamma delta (γδ) T cells, is also a key player in the antitumor immune response. γδ T cells express a particular T-cell receptor (TCR) composed of a γ chain and a δ chain [13]. In opposition to conventional T cells ($CD4^+$ and $CD8^+$ T cells), γδ T cells are able to recognize a broad range of antigens independently of the classical major histocompatibility (MHC) molecules. In human, there are two major subsets of γδ T cells: $V\delta2^+$ cells that are mainly present in the circulation and $V\delta2^-$ cells (among which $V\delta1^+$ cells) mainly present in epithelial tissues with a wider TCR diversity and less known antigen specificity. $V\delta2^+$ T cells always associate to the Vγ9 chain in adults and mainly recognize phosphorylated nonpeptidic molecules called phosphoantigens that are metabolic intermediates of the isoprenoid biosynthesis, and could be produced by tumor cells [14]. It has been shown that Vδ1 T lymphocytes from human lung tumors are able to selectively lyse autologous malignant cells ex vivo [15]. Furthermore, the administration of $V\gamma9V\delta2^+$ T cells at suitable intervals after chemotherapy and zoledronate treatment was demonstrated to increase the cytotoxic function and IFN-γ production by γδ T cells followed by a complete lysis of tumor cells in different malignancies [16]. Therefore, these cells seem to be a promising treatment tool. But their physiopathological relevance is not well known and different parameters concerning human γδ T-cell function and phenotype within

tissues are still not well understood. For this aim, a deeper characterization of γδ T-cell-associated biomarkers and function is required to better understand their prognostic value and their contribution to the antitumor immune response in NSCLC patients. Given that these cells are rare and could be activated by anti-TCR antibodies added during the classical cell sorting, their isolation for further assays is challenging. The techniques described in this chapter are useful to obtain "untouched" γδ T cells for functional assays but also to sort Vδ2$^+$ and Vδ2$^-$ T-cell subsets for gene expression analysis. Using these strategies, the sorting of γδ T-cell subsets could be optimized, undesired activation prior to functional assays avoided, and other cellular contaminants such as other immune cells, dead cells, and tumor cells eliminated. This will permit a better understanding of the contribution of intra-tumoral γδ T cells in the development of the antitumor immune response and ultimately may reconcile some studies in which results seemed contradictory.

Finally, the role of tumor-infiltrating B cells (TIL-B) in the tumor microenvironment is still controversial. On the one hand, the pro- and antitumor functions of B cells were reported in various studies and on the other hand the manipulation of B cells seems to be a promising therapeutical approach, as reviewed in [17]. The first studies have shown that the depletion of B cells in several mouse models could decelerate the tumor progression [18–20]. In another study in mice, it has been shown that B cells were recruited among leukocytes into the tumor [21]. These cells were able to produce lymphotoxins, thus promoting the proliferation and survival of cancer cells [21]. However more recent studies have reported an antitumor role of B cells in several human cancers such as in ovarian cancer [22], breast cancer [23], and hepatocellular carcinoma [24] and revealed that patients having high density of tumor-infiltrating B cells have a better clinical outcome than patients having few B-cell infiltrate. These cells are mainly located at the invasive margin of the tumor, more precisely in TLS. Our team has previously demonstrated that a high density of TLS-B cells is correlated with a higher overall survival in NSCLC patients [25, 26]. Furthermore, it has been shown that germinal center (GC)-B-cell formation and TLS density are reduced by corticosteroid treatment in lung squamous cell carcinoma [27]. These findings highlight the prognostic importance of GC-B in TLS during tumor development and treatment. Given these observations, we hypothesize that TLS-B cells may be key players in the antitumor immune response generated in NSCLC cancer and aimed to better characterize their phenotype and functional relevance. To address this question, we developed a novel flow cytometry-based approach to isolate untouched B cells from the tumor tissues, too.

2 Materials

2.1 NSCLC Sample Preparation

1. Petri dishes.
2. Scalpels.
3. Forceps.
4. Cell strainers.
5. 50 mL Falcon tubes.
6. 10 mL Syringes.
7. Cell Recovery Solution (Corning).
8. Dulbecco's phosphate-buffered saline (PBS).
9. Ethylenediaminetetraacetic acid (EDTA).
10. Heat-inactivated fetal calf serum (FCS).
11. Heat-inactivated human AB^+ serum (HS).
12. Washing buffer: 1× PBS, 5% FCS, 0.5 mM EDTA.
13. Lymphocyte separation medium (PAA).
14. Trypan blue.
15. 30 μm Individual filters (CellTrics, PARTEC).

2.2 Isolation of Untouched $CD4^+$ T Cells and γδ T Cells

1. EasySep™ Human $CD4^+$ T Cell Enrichment kit (StemCell Technologies).
2. Gamma/Delta T cell Isolation Kit (StemCell Technologies).
3. Magnet.
4. Washing buffer.
5. 5 mL FACS tubes with caps.

2.3 Cell Surface Staining for T- and B-Cell Sorting

1. Blocking buffer: 1× PBS, 2% HS, 0.5 mM EDTA.
2. Primary antibodies (*see* Tables 1, 2, 3, 4, 5, and 6).
3. Washing buffer.

2.4 Collection of Sorted Cells for Gene Expression Analysis

1. RLT buffer (Qiagen).
2. 98% β-Mercaptoethanol (98%) (Sigma Aldrich).
3. Eppendorf tubes and freezing vials.
4. Liquid nitrogen.

2.5 Collection of Sorted Cells for Cell Culture Assays

1. FCS.
2. Washing buffer.

2.6 mL FACS Tubes with Caps

1. RPMI 1640 medium (Gibco).
2. HS.

2.6.1 γδ T Cell Culture

Table 1
Antibodies for human Tregs and non-Treg CD4+ T-cell sorting for gene expression analysis

Specificity	Clone	Conjugate	Supplier	Volume (μL/10^6 cells)
CD3	UCHT1	AF700	BD Biosciences	1.5
CD4	OKT4	BV605	BioLegend	2
CD8	RPA-T8	FITC	BD Biosciences	1.5
CD25	BD+	PE-cy7	BD Biosciences	2
CD127	A019D5	BV650	BioLegend	3
CD62L	DREG-56	APC	BD Biosciences	2
DAPI (viability marker)				1 μL/mL cells

The table shows the different antibodies used for human Tregs and non-Treg CD4+ T-cell sorting, with their specificity, conjugates, clones, supplier, and volumes for gene expression analysis

Table 2
Antibodies for human Tregs and non-Treg CD4+ T-cell sorting for functional assays

Specificity	Clone	Conjugate	Supplier	Volume (μL/10^6 cells)
CD2	S5.2	APC	BD Biosciences	5
CD4	OKT4	BV605	BioLegend	2
CD8	RPA-T8	FITC	BD Biosciences	1.5
CD25	BD+	PE-Cy7	BD Biosciences	2
CD127	A019D5	BV650	BioLegend	3
LDCY (viability marker)			Thermo Fisher	0.6

Table 3
Antibodies for human γδ T-cell isolation for functional assays

Specificity	Clone	Conjugate	Supplier	Volume (μL/10^6 cells)
CD2	S5.2	APC	BD Biosciences	5
LDCY (viability marker)			Thermo Fisher	0.6

Table 4
Antibodies for human γδ T-cell isolation for gene expression analysis

Specificity	Clone	Conjugate	Supplier	Volume (μL/10^6 cells)
CD45	J.33	Pacific Blue	Beckman Coulter	1.5
CD3	UCHT1	AF700	BioLegend	1.5
Pan-γδ	IMMU510	PE	Beckman Coulter	5
Vδ2	IMMU389	AF 647	Beckman Coulter	2
LDCY (viability marker)			Thermo Fisher	0.6

Table 5
Antibodies to check human γδ T-cell isolation purity by flow cytometry

Specificity	Clone	Conjugate	Supplier	Volume (μL/10^6 cells)
CD227	HMPV	FITC	BD Biosciences	1
Epithelial antigen	Ber-EP4	FITC	DAKO	1
CD3	UCHT1	AF700	BioLegend	1.5
Pan-γδ	IMMU510	PE	Beckman Coulter	5
CD2	S5.2	APC	BD Biosciences	5
LDCY (viability marker)			Thermo Fisher	0.6

Table 6
Antibodies for negative selection of human B cells for functional assays

Specificity	Clone	Conjugate	Supplier	Volume (μL/10^6 cells)	Excluded cell types
CD14	HCD14	PercP	BioLegend	3	Macrophages, monocytes
CD2	RPA	APC-H7	BD Biosciences	2.5	T cells
CD16	3G8	APC-H7	BD Pharmingen	2	Neutrophils
CD56	NCAM16.2	APC	BD Pharmingen	1	NK, NKT cells
CD66b	80H3	FITC	Beckman Coulter	20	Neutrophils
CD227	Ber-EP4	FITC	Dako	1	Epithelial cells
CD11c	KB90	FITC	Dako	10	Dendritic cells
CD36	FA6.152	FITC	Beckman Coulter	10	Endothelial cells, macrophages, monocytes
CD43	DFT1	FITC	Immunotech	10	Leukocytes
CD45	HI30	PE-Cy7	BD Pharmingen	4	Nonimmune cells
DAPI (viability marker)				1 μL/mL of cells	Dead cells

3. Penicillin (10,000 U/mL)/streptomycin (10,000 μg/mL) (Gibco).
4. L-Glutamine (200 mM) (Gibco).
5. Sodium pyruvate (100 mM) (Gibco).
6. β-Mercaptoethanol (50 mM) (Gibco).
7. HEPES (1 M) (Gibco).

8. Prepare complete cell culture medium as follows: RPMI 1640 medium containing 100 U/mL penicillin and 100 μg/mL streptomycin, 2 mM L-glutamine, 5 mM sodium pyruvate, 1 mM HEPES, 50 μM β-mercaptoethanol, and 10% heat-inactivated HS (filtered and maintained in sterile conditions).
9. 96-Well plates for cell culture, round and flat bottom.
10. Mouse IgG1 anti-human Pan-γδ (clone IMMU510, Beckman Coulter).
11. Dynabeads™ Human T-Activator CD3/CD28 for T Cell Expansion and Activation (Invitrogen).
12. 1× PBS.
13. Cytometric Bead Array (CBA) Human Th1/Th2/Th17 Cytokine Kit (BD Biosciences).

3 Methods

3.1 Obtainment of a Cell Suspension from Non-tumoral Distant Lung, Tumor Tissue, and Peripheral Blood of NSCLC Patients

1. Place the tumor and non-tumoral distant lung (NTDL) in a petri dish using a forceps and keep the complete RPMI medium used for tumor collection (*see* medium composition in Subheading 2.6).
2. Dilacerate the tumor using a scalpel and a forceps (make pieces as small as possible).
3. Pour the tumor pieces directly from the petri dish to a 50 mL Falcon.
4. Rinse the petri dish with 20 mL of Cell Recovery Solution, close well the Falcon (surround the cap with "parafilm"), mix well (by inversion), and incubate for 1 h at 4 °C under gentle agitation.
5. After incubation, filter the suspension on a cell strainer placed onto a 50 mL Falcon; use a 10 mL syringe plunger to crush the pieces.
6. Rinse the filter first with the complete RPMI medium in which the tumor was collected, and then with 8–10 mL of washing buffer.
7. Spin the filtered suspension for 10 min at 300 × *g* at room temperature (along with available blood tubes).
8. After spinning, collect the plasma from blood samples (make aliquots of 500 μL in Eppendorf tubes and store them at −80 °C).
9. Resuspend blood cells, tumor, and NTDL pellets in 30 mL of washing buffer.
10. Load each sample suspension on 15 mL of lymphocyte separation medium.

11. Spin for 20 min at 800 × *g*, at room temperature, without acceleration and break.
12. Collect the ring of peripheral blood mononuclear cells (PBMCs) and tumor-infiltrating lymphocytes (TILs) in a 50 mL Falcon; take an aliquot of 20 µL of each sample for cell counting.
13. Count the cells; dilute the 20 µL aliquot (1/10) in trypan blue, and load 10 µL on a Kova slide.
14. Fill up the tubes containing the collected cells to 50 mL with washing buffer and centrifuge for 10 min, at 300 × *g*, and at 4 °C.
15. After the centrifugation, resuspend the cells in the washing buffer to get a final concentration of 50×10^6 cells/mL. Keep a 20 µL aliquot to analyze γδ T cells infiltration among cells recovered from blood, NTDL, and tumor tissues by flow cytometry.

3.2 Enrichment of CD4⁺ T Cells and γδ T Cells Using Negative Selection Kits

3.2.1 Enrichment of CD4⁺ T-Cell Populations

1. Prepare cell suspension at a concentration of 5×10^7 cells/mL in the washing buffer solution. Cells must be placed in a 5 mL tube to properly fit into the magnet.
2. Use the EasySep™ Human CD4⁺ T Cell Enrichment kit (StemCell Technologies) to negatively sort CD4⁺ T cells from the PBMCs or the TILs obtained previously. Add the EasySep™ Human CD4⁺ T Cell Enrichment Cocktail (cocktail contains antibodies against human CD8, CD14, CD16, CD19, CD20, CD36, CD56, CD66b, CD123, TCRγ/δ, and glycophorin A) at 50 µL/mL of total cells (e.g., for 1 mL of cells, add 50 µL of the antibody cocktail). Mix well and incubate at room temperature (15–25 °C) for 10 min.
3. Vortex the EasySep™ D Magnetic Particles for 30 s. Ensure that the particles are in a uniform suspension with no visible aggregates and use them directly without any washing step.
4. Add the EasySep™ D Magnetic Particles at 100 µL/mL cells. The magnetic bead suspension is prepared of magnetic dextran iron particles in Tris buffer. Mix well and incubate at room temperature for 5 min.
5. Fill up to a total volume of 2.5 mL by adding the washing buffer to the cell suspension.
6. Mix the cells in the tube by gently pipetting up and down 2–3 times.
7. Place the tube (without cap) in front of the magnet.
8. Incubate for 5 min at room temperature. The magnetically labeled unwanted cells will remain bound inside the original tube.

9. Use sterile pipette to gently take out the unlabeled cells in suspension. Transfer the cells to the 50 mL Falcon tube for further processing.
10. Wash the untouched cells twice by filling up the tube with 50 mL of washing buffer, and centrifuge for 10 min, at 300 × *g*, and at 4 °C.

3.2.2 Enrichment of Total γδ T Cells

1. Use the EasySep™ Human Gamma/Delta T cell Isolation Kit (StemCell Technologies, catalog #19255) for immunomagnetic isolation of untouched γδ T cells (follow the manufacturer's instructions).
2. Collect the negative fraction of each sample (i.e., tumor, NTDL, and blood) in new 5 mL FACS tubes with caps.
3. Count the cells.
4. Fill up the tube with washing buffer and centrifuge for 10 min at 300 × *g*, at 4 °C.
5. After centrifugation, collect the negative fraction pellet.
6. Check the purity of the isolated population by flow cytometry (*see* Table 5 for the antibodies) or proceed to a further cell sorting with the appropriate antibodies (*see* **Notes 1** and **2**) (*see* Table 3 to sort γδ T cells for functional assays and Table 4 to sort cells for gene expression analysis of γδ T cells).

3.3 Stainings for the Sorting of T- and B-Cell Subsets

1. Resuspend the isolated negative fraction enriched of $CD4^+$ T cells (*see* Subheading 3.2.1) or γδ T cells (*see* Subheading 3.2.2) in the appropriate volume of blocking buffer for FcR blocking to a final concentration of 10×10^6 cells/mL, and incubate for 30 min at 4 °C. To sort B cells, use the total TILs or PBMCs recovered from Subheading 3.1.
2. Without washing out the blocking buffer, add the appropriate antibodies recognizing the cell surface antigens (according to Tables 1, 2, 3, 4, 5, and 6) with or without CD62L staining (as a specific TLS marker), and based on the application (cell culture, gene expression analysis, phenotypic analysis). A previous titration should determine the optimal volume of antibody to be added to the cell suspension.
3. Vortex the antibodies and incubate with the cells for 30 min at 4 °C in the dark.
4. Fill up with 10 mL of washing buffer, mix, and centrifuge at 400 × *g* for 10 min at 4 °C to eliminate unfixed antibody.
5. Aspirate the supernatant and resuspend the cells in 1 mL of washing buffer.
6. Filter the cell suspension with 30 μm filter.
7. Add 1 μL/mL of DAPI to the cell suspension in order to exclude dead cells during the cell sorting.

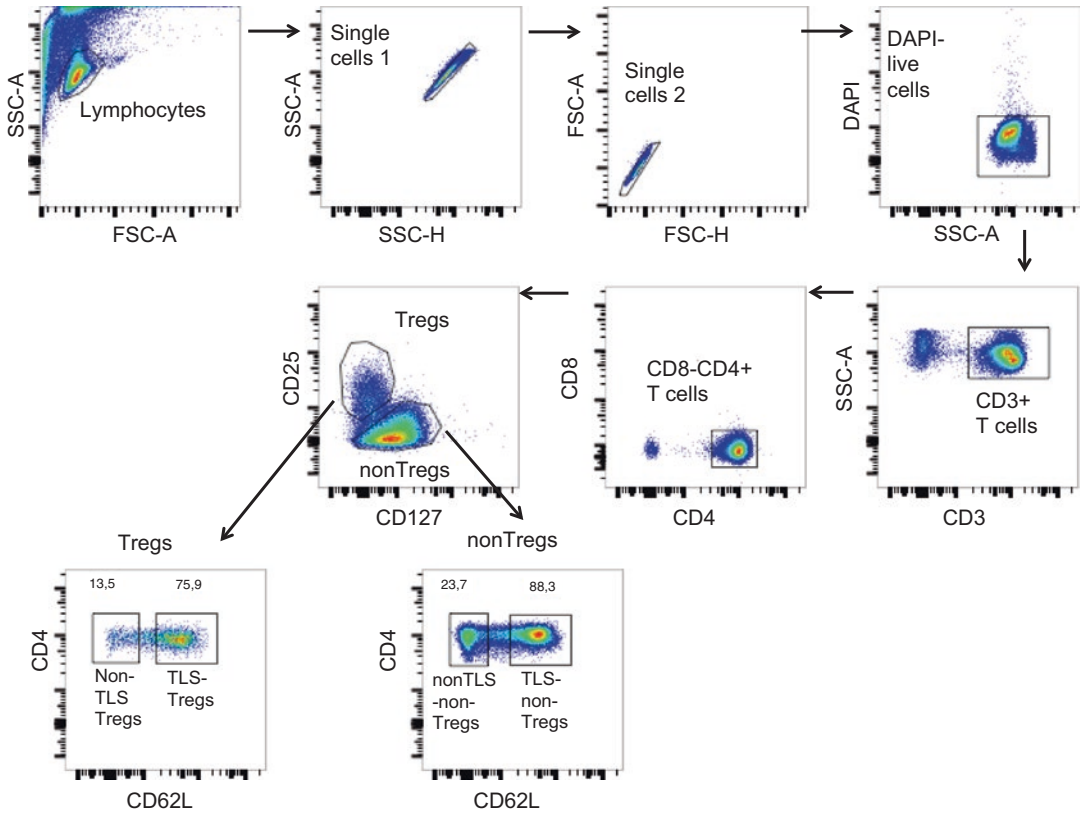

Fig. 1 Gating strategy to sort Tregs and non-Treg CD4⁺ T-cell subsets for gene expression analysis. Human CD4⁺ T-cell subsets sorted from the tumor, non-tumoral lung tissue, and blood of NSCLC patients. The gating strategy shows initial selection of live, single CD3⁺ CD4⁺ CD8⁻ T lymphocytes. Tregs and non-Treg CD4⁺ T cells defined according to the differential expression of CD25 and CD127 are further sorted as TLS and non-TLS cells based on the CD62L expression. The dot plots are representative of the sorting of the cells from one patient

8. Keep the cells on ice (or at 4 °C) in the dark before the flow cytometry analysis and/or the cell sorting (*see* **Notes 1–3**).

3.4 Gating Strategy for B- and T-Cell Subset Isolation

3.4.1 For CD4⁺ Treg and Non-Treg Populations

1. When you proceed to cell sorting, gate on lymphocytes according to SSC and FSC values and exclude the doublets (Fig. 1).
2. Options: For gene expression analysis, gate on live cells (DAPI⁻) expressing both CD3 and CD4 to select CD3⁺ CD4⁺ T cells. For functional immunosuppression assays, gate on live cells (LDCY⁻) expressing both CD4 and CD2 in order to avoid undesired activation through the binding of anti-CD3 antibody on T cells. LDCY is a viability marker and refers to LIVE/DEAD™ Fixable Yellow Dead Cell Stain Kit, for 405 nm excitation (Thermo Fisher).
3. The sorting of CD4⁺ Treg and non-Treg populations among total CD4⁺ T cells will be based on the differential expression

of CD25 and CD127. Indeed, gate on $CD4^+CD25^{hi}CD127^{-/lo}$ cells for the sorting of the $CD4^+$ T Treg population, and on $CD4^+CD25^{+/-}CD127^+$ cells for conventional $CD4^+$ T non-Treg cells.

4. The sorting of lymphocytes infiltrating TLS and non-TLS areas of the tumor will be performed based on the differential expression of CD62L molecule. TLS-T cells selectively express the CD62L marker whereas non-TLS T cells do not [2, 28]. Thus, four populations could be sorted in this case from fresh tumor and non-tumoral tissue specimens and blood, namely $CD62L^+$ TLS Tregs, non-TLS $CD62L^-$ Tregs, $CD62L^+$ TLS conventional $CD4^+$ non-Treg cells, and $CD62L^-$ non-TLS conventional $CD4^+$ non-Treg cells (Fig. 1).

3.4.2 For Total B Cells

1. Gate on the lymphocyte population according to SSC and FSC values.
2. Select live $DAPI^-$ cells.
3. Gate on live cells expressing the CD45 marker.
4. Gate on $CD45^+CD14^-CD56^-$ cells.
5. Then, gate on cells negative for epithelial, CD66b, CD11c, CD36, CD43, CD2, and CD16 markers.
6. Remove cell doublets.
7. Check the B-cell purity by adding an anti-CD19 antibody to an aliquot of the B-cell fraction (Fig. 2).

3.4.3 For Total γδ T Cell

1. Gate on the lymphocyte population based on SSC and FSC parameters.
2. Exclude the doublets.
3. Sort the $CD2^+LDCY^-$ γδ T-cell population (Fig. 3) for cell culture assay (*see* Subheading 3.7).

3.5 Collection of Sorted Cells for Gene Expression Analysis

1. Collect the sorted cells for gene expression per 2 mL freezing vials containing 300 μL of RLT and 1% β-mercaptoethanol.
2. Directly freeze the cells in a vial in a small container of liquid nitrogen, and then store them at −80 °C.

3.6 Collection of Sorted Cells for Functional Assays

1. For cell culture, collect the cells in Eppendorf tubes containing 200 μL of washing buffer (γδ T cells) or 500 μL of the pure filtered FCS ($CD4^+$ T-cell subsets and B cells).
2. After sorting, centrifuge the collected cells at 300 × *g* for 5 min at 4 °C.
3. Discard carefully the supernatant.
4. Resuspend the pellet in the appropriate volume of cell culture medium.

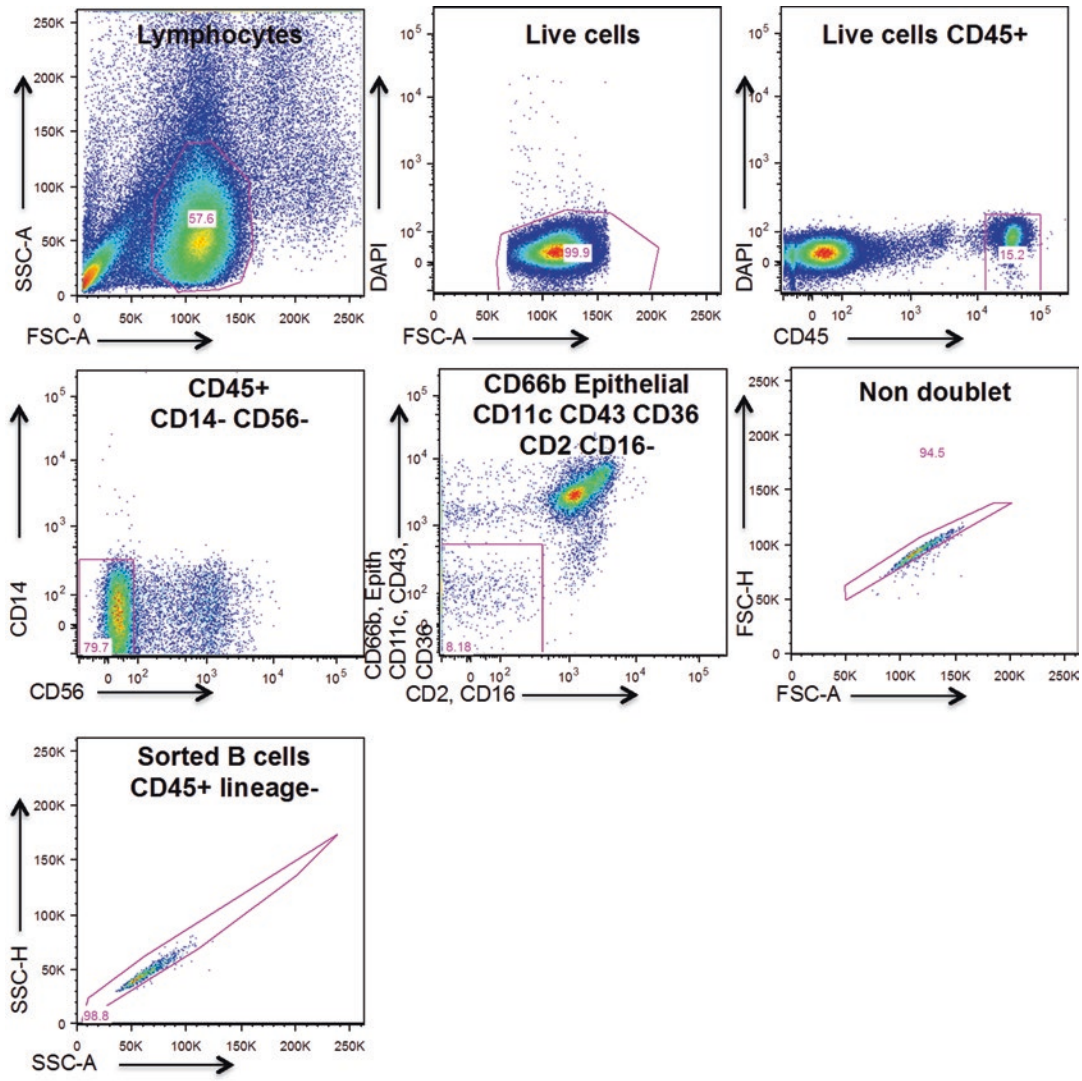

Fig. 2 Untouched tumor-infiltrating B-cell sorting strategy. The dot plots show the gating strategy for isolation of human B cells from blood of healthy donor. The same strategy was used for the tumor tissue

3.7 γδ *T-Cell Culture Assay*

1. For γδ-TCR-based cell activation, prepare a 96-well flat-bottom plate coated with unconjugated anti-Pan-γδ (clone IMMU510, Beckman Coulter) antibody (10 μL of antibody in 50 μL of 1× PBS per well) for 2 h at 37 °C in the incubator (or overnight at 4 °C).
2. Wash the excess of antibody with 200 μL/well of PBS.

Fig. 3 (continued) (blood, panel (**b**) and tumor, panel (**c**)) negative selection. The FACS plots show a high percentage of tumor cells remaining in the cell suspension obtained from the tumor, indicating the necessity to perform the further cell sorting of $CD2^+$ $LDCY^-$ γδ T population

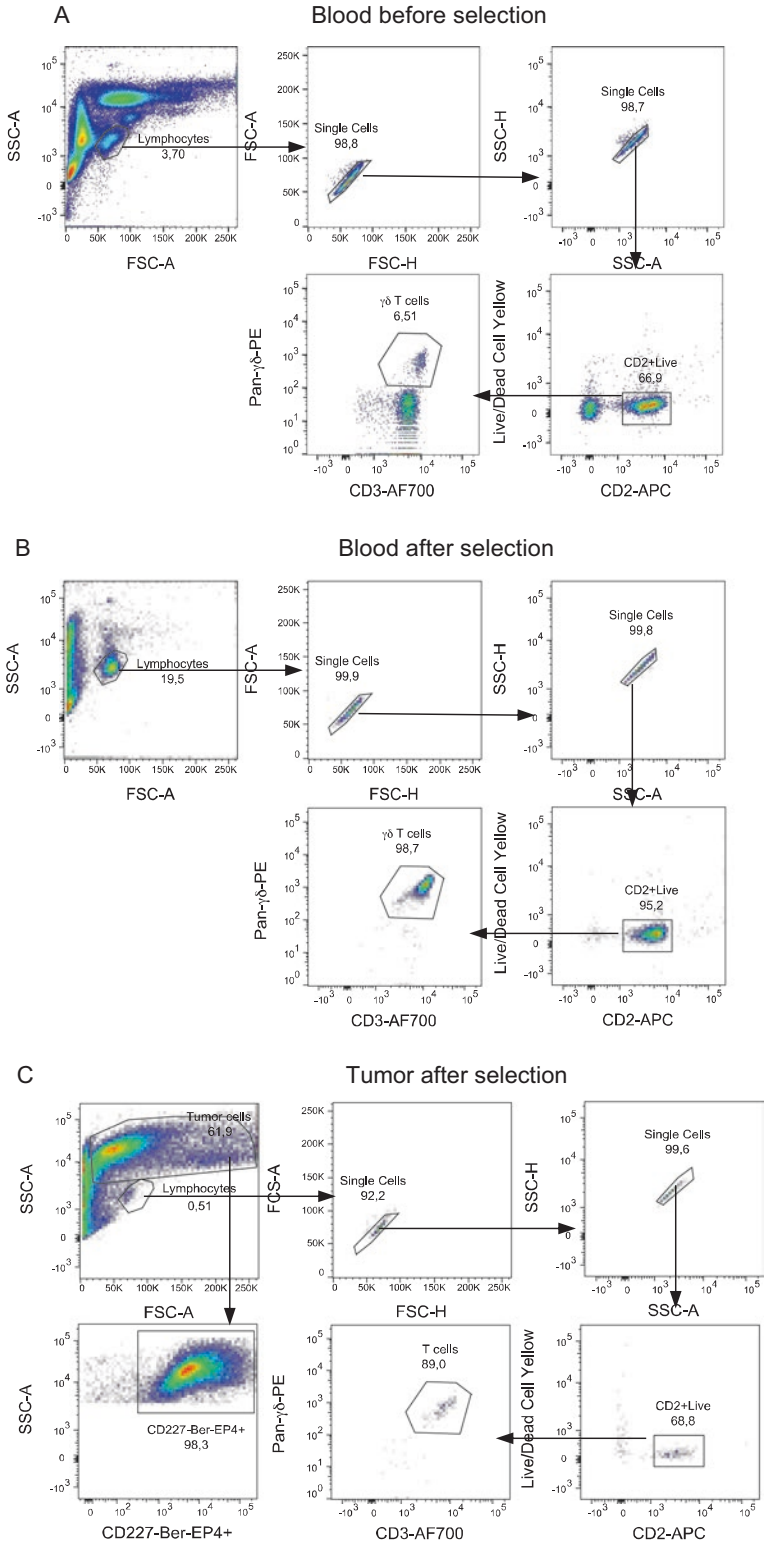

Fig. 3 γδ T-cell purity by flow cytometry after negative selection. Flow cytometry analysis on the isolated γδ T cells using EasySep™ Human Gamma/Delta T cell Isolation Kit (StemCell) before (blood, panel (**a**)) and after

3. Repeat **step 2** three times.
4. Add 100 μL of the γδ T-cell suspension to the anti-Pan-γδ-coated plate (10,000 cells/well).
5. Incubate the plate for 24 h at 37 °C in the incubator.
6. In the case of anti-CD3 stimulation, use a 96-well round-bottom plate. Directly add the anti-CD3/CD28 Dynabeads (Invitrogen) to γδ T cells (10,000 cells) (1 bead/10 cells). Also, incubate the plate for 24 h at 37 °C in the incubator.
7. 24 h later, spin the plates and collect the supernatant for cytokine production analysis with Cytometric Bead Array (CBA) Human Th1/Th2/Th17 Cytokine Kit (BD Biosciences, see the manufacturer's instructions).

4 Notes

1. The use of the magnetic bead-based enrichment kit is insufficient for achieving best purity of $CD4^+$ and γδ T cells from tissue because of the presence of epithelial contaminants. Thus, we added a further step of the cell sorting using appropriate antibodies (*see* Tables 1, 2, 3, and 4). This was useful to better study these immune cells in gene expression analysis and culture assays.
2. Do not use anti-CD3, anti-γδ TCR, or anti-CD19 antibodies to avoid cellular activation before cell culture. Anti-CD2 antibody can be used instead of anti-CD3 for the sorting of the T-cell subsets.
3. For some experiments as co-cultures, the positive selection of B cells is not recommended. Numerous research articles collected B cells using untouched isolation kits, which are very effective to collect human B cells from peripheral blood by negative selection (purity >95%). However, negative selection using these kits is not a good strategy to collect B cells from tissues such as tumors due to a strong presence of contaminating epithelial and stromal cells. Given the heterogeneity of tumors, it is infeasible to design and to modify these kits each time. Based on these results, the use of this negative selection strategy using a cell sorter seems to be more appropriate. The addition of anti-CD4 and anti-CD8 antibodies makes possible the sorting of not only untouched B lymphocytes but also T lymphocytes in order to perform a B-T co-culture assay.

Acknowledgments

We thank all present and past members of the Laboratory "Cancer, Immune control and Escape" (UMRS1138 INSERM, Cordeliers Research Center), pathologists, and clinicians who have participated in these studies, for their help and valuable discussions. We are grateful to lung cancer patients involved in this research performed in our laboratory.

Funding: This work was supported by the "Institut National de la Santé et de la Recherche Médicale (INSERM), Pierre and Marie Curie University, Paris-Descartes University, the Labex Immuno-Oncology (LAXE62_9UMRS872 Fridman), CARPEM (Cancer Research for PErsonalized Medicine), Institut National du Cancer (INCa-PLBio 2014-2017 GDSTRESS), and Fondation ARC pour la Recherche sur le Cancer. Priyanka Devi-Marulkar was supported by a grant from the Fondation ARC pour la Recherche sur le Cancer. Hélène Kaplon was supported by a grant from the Ligue Nationale contre le Cancer.

References

1. Fridman WH, Pagès F, Sautès-Fridman C et al (2012) The immune contexture in human tumours: impact on clinical outcome. Nat Rev Cancer 12:298–306
2. Goc J, Germain C, Vo-Bourgais TKD et al (2014) Dendritic cells in tumor-associated tertiary lymphoid structures signal a Th1 cytotoxic immune contexture and license the positive prognostic value of infiltrating CD8+ T cells. Cancer Res 74:705–715
3. Dieu-Nosjean M-C, Goc J, Giraldo NA et al (2014) Tertiary lymphoid structures in cancer and beyond. Trends Immunol 35:571–580
4. Dieu-Nosjean M-C, Antoine M, Danel C et al (2008) Long-term survival for patients with non-small-cell lung cancer with intratumoral lymphoid structures. J Clin Oncol Off J Am Soc Clin Oncol 26:4410–4417
5. Gentles AJ, Newman AM, Liu CL et al (2015) The prognostic landscape of genes and infiltrating immune cells across human cancers. Nat Med 21:938–945
6. Curiel TJ, Coukos G, Zou L et al (2004) Specific recruitment of regulatory T cells in ovarian carcinoma fosters immune privilege and predicts reduced survival. Nat Med 10:942–949
7. Badoual C, Hans S, Rodriguez J et al (2006) Prognostic value of tumor-infiltrating CD4+ T-cell subpopulations in head and neck cancers. Clin Cancer Res 12:465–472
8. Carreras J, Lopez-Guillermo A, Fox BC et al (2006) High numbers of tumor-infiltrating FOXP3-positive regulatory T cells are associated with improved overall survival in follicular lymphoma. Blood 108:2957–2964
9. Salama P, Stewart C, Forrest C et al (2012) FOXP3+ cell density in lymphoid follicles from histologically normal mucosa is a strong prognostic factor in early stage colon cancer. Cancer Immunol Immunother 61:1183–1190
10. Grabenbauer GG, Lahmer G, Distel L et al (2006) Tumor-infiltrating cytotoxic T cells but not regulatory T cells predict outcome in anal squamous cell carcinoma. Clin Cancer Res 12:3355–3360
11. Heimberger AB, Abou-Ghazal M, Reina-Ortiz C et al (2008) Incidence and prognostic impact of FoxP3+ regulatory T cells in human gliomas. Clin Cancer Res 14:5166–5172
12. Jacobs JFM, Idema AJ, Bol KF et al (2010) Prognostic significance and mechanism of Treg infiltration in human brain tumors. J Neuroimmunol 225:195–199
13. Lawand M, Déchanet-Merville J, Dieu-Nosjean M-C (2017) Key features of Gamma-Delta T-cell subsets in human diseases and their immunotherapeutic implications. Front Immunol 8:761
14. Constant P, Davodeau F, Peyrat MA et al (1994) Stimulation of human gamma delta T

cells by nonpeptidic mycobacterial ligands. Science 264:267–270

15. Zocchi MR, Ferrarini M, Rugarli C (1990) Selective lysis of the autologous tumor by delta TCS1+ gamma/delta+ tumor-infiltrating lymphocytes from human lung carcinomas. Eur J Immunol 20:2685–2689
16. Mattarollo SR, Kenna T, Nieda M et al (2007) Chemotherapy and zoledronate sensitize solid tumour cells to Vgamma9Vdelta2 T cell cytotoxicity. Cancer Immunol Immunother 56:1285–1297
17. Siliņa K, Rulle U, Kalniņa Z et al (2014) Manipulation of tumour-infiltrating B cells and tertiary lymphoid structures: a novel anti-cancer treatment avenue? Cancer Immunol Immunother 63:643–662
18. Qin Z, Richter G, Schüler T et al (1998) B cells inhibit induction of T cell-dependent tumor immunity. Nat Med 4:627–630
19. de Visser KE, Korets LV, Coussens LM (2005) De novo carcinogenesis promoted by chronic inflammation is B lymphocyte dependent. Cancer Cell 7:411–423
20. Tadmor T, Zhang Y, Cho H-M et al (2011) The absence of B lymphocytes reduces the number and function of T-regulatory cells and enhances the anti-tumor response in a murine tumor model. Cancer Immunol Immunother 60:609–619
21. Ammirante M, Luo J-L, Grivennikov S et al (2010) B-cell-derived lymphotoxin promotes castration-resistant prostate cancer. Nature 464:302–305
22. Kroeger DR, Milne K, Nelson BH (2016) Tumor-infiltrating plasma cells are associated with tertiary lymphoid structures, cytolytic T-cell responses, and superior prognosis in ovarian cancer. Clin Cancer Res 22:3005–3015
23. Mahmoud SMA, Lee AHS, Paish EC et al (2012) The prognostic significance of B lymphocytes in invasive carcinoma of the breast. Breast Cancer Res Treat 132:545–553
24. Shi J-Y, Gao Q, Wang Z-C et al (2013) Margin-infiltrating CD20(+) B cells display an atypical memory phenotype and correlate with favorable prognosis in hepatocellular carcinoma. Clin Cancer Res 19:5994–6005
25. Germain C, Gnjatic S, Tamzalit F et al (2014) Presence of B cells in tertiary lymphoid structures is associated with a protective immunity in patients with lung cancer. Am J Respir Crit Care Med 189:832–844
26. Germain C, Gnjatic S, Dieu-Nosjean M-C (2015) Tertiary lymphoid structure-associated B cells are key players in anti-tumor immunity. Front Immunol 6:67
27. Silina K, Soltermann A, Movahedian Attar F et al (2018) Germinal centers determine the prognostic relevance of tertiary lymphoid structures and are impaired by corticosteroids in lung squamous cell carcinoma. Cancer Res 78(5):1308–1320
28. de CL, Goc J, Damotte D et al (2011) Characterization of chemokines and adhesion molecules associated with T cell presence in tertiary lymphoid structures in human lung cancer. Cancer Res 71:6391–6399

Chapter 12

Identification of Tertiary Lymphoid Structure-Associated Follicular Helper T Cells in Human Tumors and Tissues

Coline Couillault, Claire Germain, Bertrand Dubois, and Hélène Kaplon

Abstract

Follicular helper T (Tfh) cells are major components of the humoral immune response due to their pivotal role in germinal center formation and antibody affinity maturation following B-cell isotype switching. This $CD4^+$ T-cell subtype is mainly found in the B-cell zone of secondary lymphoid organs as well as in tertiary lymphoid structures (TLS), which are highly organized structures composed of T and B cells, occasionally found at the invasive margin in the tumor microenvironment.

We describe here how to perform immunofluorescence staining of tumor tissue sections and multicolor flow cytometry on tumor cell suspensions to identify and visualize these TLS-associated Tfh cells within the tumor microenvironment of various human cancers. These assays take advantage of combinations of markers and molecules involved in Tfh differentiation and function.

Key words Tumor, Paraffin-embedded tissue, Follicular helper T cell, Tertiary lymphoid structure, Immunofluorescence, Flow cytometry, Multiplex, PD-1, CXCR5, Bcl-6

Abbreviations

Bcl-6	B-cell lymphoma 6
CXCL13	C-X-C motif chemokine 13
CXCR5	C-X-C chemokine receptor type 5
FBS	Fetal bovine serum
FDC	Follicular dendritic cell
FFPE	Formalin-fixed paraffin-embedded
GC	Germinal center
HCC	Hepatocellular carcinoma
HS	Human serum
ICOS	Inducible costimulator
IF	Immunofluorescence
LN	Lymph node
mDC	Mature dendritic cell
NSCLC	Non-small cell lung cancer

Marie-Caroline Dieu-Nosjean (ed.), *Tertiary Lymphoid Structures: Methods and Protocols*, Methods in Molecular Biology, vol. 1845, https://doi.org/10.1007/978-1-4939-8709-2_12,

PBS	Phosphate-buffered saline
PC	Plasma cell
PD-1	Programmed death-1
RT	Room temperature
SLO	Secondary lymphoid organ
Tfh	Follicular helper T cell
TLS	Tertiary lymphoid structure

1 Introduction

Follicular helper T (Tfh) cells constitute a $CD4^+$ T-cell subset dedicated to provide T-cell help to B cells and mainly found within germinal centers (GC) of B-cell follicles. Tfh cells support GC reactions and provide critical signals to B cells allowing antibody isotype switching, antibody affinity maturation, and B-cell differentiation into memory B cells and plasma cells (PC) [1]. GC Tfh cells are characterized by high surface expression of CXCR5 (C-X-C chemokine receptor type 5), PD-1 (programmed death-1), and inducible costimulator (ICOS); expression of the transcription factor Bcl-6 (B-cell lymphoma 6) in the nucleus; and secretion of IL-21, IL-4, and CXCL13 (C-X-C motif chemokine 13). The expression of CXCR5 by Tfh cells allows their homing to the B-cell follicle in response to gradients of CXCL13.

In solid tumors, Tfh cells are detected in lymph node-like structures with segregated T- and B-cell zones, called tertiary lymphoid structures (TLS) [2, 4]. The presence of these cells in tumor-associated TLS may suggest an ongoing local B-cell activation process leading to the differentiation of specific memory B cells and PC, whose presence predicts better patient survival in many solid cancer types [2–5]. Recent studies highlighted that the presence of a Tfh gene signature was associated with better clinical outcome in several cancer types, including breast cancer [6], colorectal cancer [7], and non-small cell lung cancer (NSCLC) [8]. Consistently, a higher risk of relapse has been observed in patients with CXCL13 deletion in colorectal cancer, probably due to lower densities of Tfh cells and B cells [7]. These findings strongly suggest that B-cell differentiation supported by tumor-infiltrating Tfh cells is a critical component of efficient antitumor immunity.

If the presence of TLS has been clearly correlated with a better prognosis in terms of survival in many solid tumors [9], the mechanisms of TLS neogenesis however are still unclear. Several factors seem to regulate their formation such as TNF family members (lymphotoxin [10, 11], LIGHT [12], BAFF [13]), cytokines (IL-17 [14], IL-6 [15], IL-22 [16]), and chemokines (CCL19/CCL21 [17, 18], CXCL13 [19, 20]). In this context, Tfh cells

may participate in TLS formation and maintenance through their capacity to secrete CXCL13, sustaining a local microenvironment controlling tumor growth [21, 22].

In this chapter, we describe complementary multiplex methods, i.e., two methods of immunofluorescence (IF) tissue staining (three- and five-color) on formalin-fixed paraffin-embedded (FFPE) tissue sections, and one method of flow cytometry analysis of cell suspensions prepared from fresh tumor samples, to efficiently detect in situ TLS-associated Tfh using NSCLC and hepatocellular carcinoma (HCC) as examples.

2 Materials

2.1 Samples

1. Five-µm-thick FFPE TLS-associated NSCLC tumor and lymph node (LN) sections.
2. Fresh HCC tumor samples.

2.2 Buffers

2.2.1 Visualization of TLS-Associated Tfh on FFPE Tumor Tissue by Triple-CD20/CD3/PD-1 Immunofluorescence Staining

1. 100% Xylene or Clearene (Leica).
2. 100% Absolute ethanol.
3. Distilled water.
4. Ethanol solutions at 90, 70, and 50%.
5. 10× TBS: 47.4 g Trizma® hydrochloride + 263 g sodium chloride, in 3 L of distilled water; pH adjusted to 7.4.
6. 1× TBS: 1 Volume of 10× TBS + 9 volumes of distilled water.
7. TBS-T: 1× TBS + 0.04% Tween 20.
8. Phosphate-buffered saline (PBS).

2.2.2 Detection of TLS-Associated Tfh on FFPE Tumor Sections by Multiplex CD3/CD4/CD20/Bcl6 IF Staining

1. 10× EZ Prep (deparaffinization solution) (Ventana): Needs to be reconstituted in type 2 pure water.
2. Pre-diluted Cell Conditioner #1 (CC1) solution: Tris–EDTA buffer pH 8.5 for antigen retrieval (Ventana).
3. 10× Reaction Buffer (Ventana): Needs to be reconstituted in type 2 pure water.
4. Discovery Inhibitor (Ventana): Peroxidase blocking solution containing hydrogen peroxide between 1 and 5%.
5. 10× TBS: 47.4 g Trizma® hydrochloride + 263 g sodium chloride in 3 L distilled water; pH adjusted at 7.4.
6. 1× TBS: 1 Volume of 10× TBS + 9 volumes of distilled water.

2.2.3 Tfh Identification by Multiparametric Flow Cytometry from Fresh Tumor Tissue

1. Complete RPMI: RPMI medium supplemented with 1% L-glutamine, 1% penicillin-streptomycin, and 10% heat-inactivated fetal bovine serum (FBS).

2. Complete RPMI medium without FBS: RPMI medium supplemented with 1% L-glutamine and 1% penicillin-streptomycin.
3. Phosphate-buffered saline (PBS).
4. Staining buffer: PBS supplemented with 5 mM EDTA.

2.3 Reagents

2.3.1 Visualization of TLS-Associated Tfh on FFPE Tumor Tissue by Triple-CD20/CD3/PD-1 Immunofluorescence Staining

1. Antigen retrieval solution: Target Retrieval Solution pH 6 (TRS, Dako, 10×; 1 volume + 9 volumes of distilled water, pH adjusted to 6).
2. 5% HS: 5% Decomplemented human serum diluted in PBS.
3. Antibody diluent (Dako REAL™, Dako).
4. Primary antibodies: Mouse anti-human CD20 (clone L26), rabbit anti-human CD3 (polyclonal IgG), and mouse anti-human PD-1 (clone NAT105) antibodies (*see* Table 1).
5. Secondary antibodies: Goat anti-mouse IgG2a-FITC, donkey anti-rabbit IgG-Cy3 ($F(ab')_2$), and goat anti-mouse IgG1-biotin ($F(ab')_2$) antibodies (*see* Table 1).
6. Streptavidin-AF647.
7. Mounting Medium with DAPI (ProLong® Gold Antifade Reagent with DAPI, Life Technologies).

2.3.2 Detection of TLS-Associated Tfh on FFPE Tumor Sections by Multiplex CD3/CD4/CD20/Bcl6 IF Staining

1. Primary antibodies: Mouse anti-human Bcl6 (clone GI191E/A8), rabbit anti-human CD4 (clone SP35), rabbit anti-human CD3 (clone 2GV6), mouse anti-human CD20 (clone L26) antibodies (*see* Table 1).
2. Secondary antibodies: OmniMap goat anti-rabbit coupled to HRP (ready to use) and OmniMap goat anti-mouse coupled to HRP (ready to use) (*see* Table 1).
3. Antibody diluent (Dako REAL™, Dako).
4. 9% Hydrogen peroxide.
5. Tyramide-fluorophore conjugates: Alexa Fluor AF546 tyramide reagent (Thermo Fisher), Alexa Fluor AF594 tyramide reagent (Thermo Fisher), Alexa Fluor AF647 tyramide reagent (Thermo Fisher), Alexa Fluor AF488 tyramide reagent (Thermo Fisher) (*see* Table 1).
6. DAPI solution (initial concentration 1 mg/mL, Thermo Fisher).
7. ProLong® Mounting medium without DAPI (Thermo Fisher).

2.3.3 Tfh Identification by Multiparametric Flow Cytometry from Fresh Tumor Tissue

1. Enzymes: Collagenase IA (Sigma Aldrich) and DNase I (Sigma Aldrich) endotoxin-free.
2. Türk's solution (EMD Millipore).
3. Zombie Yellow viability marker (BioLegend).

Table 1
List of reagents used to detect Tfh by immunofluorescence and flow cytometry

Antibody or reagent	Conjugate	Host	Clone	Source	Reference	Working dilution
IHC/IF						
CD20	UC	Mouse IgG2a	L26	Agilent/Dako	M0755	1/250
CD3	UC	Rabbit IgG	Polyclonal	Agilent/Dako	A0452	1/80
PD-1	UC	Mouse IgG1	NAT105	Roche	760-4895	Ready to use
Mouse IgG2a	FITC	Goat IgG	Polyclonal	JIR	115-545-206	1/100
Rabbit IgG	Cy3	Donkey IgG	Polyclonal	JIR	711-165-152	1/100
Mouse IgG1	Biotin	Goat IgG	Polyclonal	JIR	115-065-205	1/100
Streptavidin	AF647	NA	NA	JIR	016-600-084	1/100
Multiplex						
Bcl6	UC	Mouse IgG1	GI191E/A8	Ventana	760-4241	Ready to use
CD3	UC	Rabbit IgG	2GV6	Ventana	790-4341	Ready to use
CD4	UC	Rabbit	SP35	Ventana	790-4423	Ready to use
CD20	UC	Mouse IgG2a	L26	Agilent/Dako	M0755	1/250
OmniMap rabbit	HRP	Goat	NA	Ventana	760-4311	Ready to use
OmniMap mouse	HRP	Goat	NA	Ventana	760-4310	Ready to use
Tyramide	AF546	NA	NA	Thermo Fisher	B40954	1/100
Tyramide	AF594	NA	NA	Thermo Fisher	B40957	1/100
Tyramide	AF647	NA	NA	Thermo Fisher	B40958	1/100
Tyramide	AF488	NA	NA	Thermo Fisher	B40953	1/100
Flow cytometry						
CD45	AF700	Mouse IgG1	HI30	BD Biosciences		1/25
CD3	APC-H7	Mouse IgG1	SK7	BD Biosciences		1/25
CD4	FITC	Mouse IgG1	RPA-T4	BS Biosciences		1/25

(continued)

Table 1
(continued)

Antibody or reagent	Conjugate	Host	Clone	Source	Reference	Working dilution
PD1	BV605	Mouse IgG1	EH12.1	BD Biosciences		1/25
CXCR5	PE-Vio615	Recombinant human IgG	REA103	Miltenyi Biotech		1/10
ICOS	VioBLUE	Recombinant human IgG	REA1192	Miltenyi Biotech		1/10
Bcl6	PE	Mouse IgG1	H112.91	BD Biosciences		1/10
Mouse IgG1	BV605	Mouse IgG1	X40	BD Biosciences		1/25
Rea Control	PE-Vio615	Recombinant human IgG	REA293	Miltenyi Biotech		1/10
Rea Control	VioBlue	Recombinant human IgG	REA293	Miltenyi Biotech		1/10
Mouse IgG1	PE	Mouse IgG1	MOPC-21	BD Bioscience		1/25

The first two parts are dedicated to immunofluorescence. The last part described the characteristics of the primary antibodies used for flow cytometry. Abbreviations: *UC* unconjugated and *NA* not available

4. Foxp3/transcription factor staining buffer kit: Fixation/permeabilization buffer and permeabilization buffer (eBioscience).
5. Primary antibodies: Anti-human CD45-Alexa Fluor 700 (BD Biosciences), anti-human CD3-APC-H7 (BD Biosciences), anti-human CD4-FITC (BD Biosciences), anti-human PD1-BV605 (BD Biosciences), CXCR5-PE-Vio615 (Miltenyi Biotec), ICOS-VioBlue (Miltenyi Biotec), anti-human Bcl6-PE (BD Biosciences), mouse IgG1-BV605 (BD Biosciences), Rea Control-PE-Vio615 (Miltenyi Biotec), Rea Control-VioBlue (Miltenyi Biotec), mouse IgG1-PE (BD Biosciences) antibodies (*see* Table 1).

2.4 Specific Equipment

2.4.1 Visualization of TLS-Associated Tfh on FFPE Tumor Tissue by Triple-CD20/CD3/PD-1 Immunofluorescence Staining

1. Drying oven.
2. Laboratory fume hood.
3. Glass containers for slides.
4. Plastic containers for slides.
5. Water bath.
6. Absorbent papers.
7. Humidified chamber.

8. Glass coverslips.
9. Slide scanner: Axio Scan.Z1 fluorescence slide scanner, driven by Zen 2012 (blue edition) (Zeiss), or equivalent.

2.4.2 Detection of TLS-Associated Tfh on FFPE Tumor Sections by Multiplex CD3/CD4/CD20/Bcl6 IF Staining

1. Drying oven.
2. Plastic containers for slides.
3. Water bath.
4. Glass coverslips.
5. Ventana Discovery XT autostainer.
6. Confocal microscope LSM710 (Zeiss).

2.4.3 Tfh Identification by Multiparametric Flow Cytometry from Fresh Tumor Tissue

1. Sterile jars.
2. 50 mL Falcon tubes.
3. 10 mm Petri dishes.
4. Forceps.
5. Water bath.
6. 70 μm Cell strainers.
7. Magnetic stirrer.
8. Nonsterile V-bottom 96-well plates.
9. 1.2 mL Tubes (Micronic).
10. LSR Fortessa analyzer (BD Biosciences).
11. FlowJo© software (Tree Star).

3 Methods

3.1 Visualization of TLS-Associated Tfh on FFPE Tumor Tissue by Triple-CD20/CD3/PD-1 Immunofluorescence Staining

1. Dry the slides for a minimum of 30 min (or overnight) in a drying oven at 37 °C.
2. Deparaffinize the slides: Under a laboratory fume hood, immerse the slides in three successive baths of 100% xylene (or Clearene), for 5 min each, then in one bath of absolute ethanol for 5 min, one bath of 90% ethanol for 5 min, one bath of 70% ethanol for 5 min, one bath of 50% ethanol for 5 min, and one bath of distilled water for 5 min (use glass containers for slides) at room temperature (RT).
3. Retrieval of antigens: Immerse the slides in a bath of prewarmed antigen retrieval solution (TRS, pH 6) for 30 min at 97 °C (in a water bath; use a plastic container for slides).
4. Take out the plastic container from the water bath and let it cool for 30 min at RT, on the bench.
5. Wash the slides in 1 TBS for 5 min under gentle agitation at RT (use a glass container for slides) (*see* **Note 1**).

6. Dry the slides with absorbent papers (*see* **Note 2**).
7. Place the slides in a humidified chamber.
8. Cover the tissue with 5% HS, for 30 min at RT (for saturation of the receptors for the Fc portion of immunoglobulins). In general, 100–300 µL/tissue section is sufficient.
9. Simply remove the excess of HS (do not wash) and dry the slides with absorbent papers.
10. Cover the tissue with diluted primary antibodies: mouse anti-human CD20 (clone L26) + rabbit anti-human CD3 (polyclonal IgG) in the mouse anti-human PD-1 (clone NAT105); 100–300 µL/tissue section is sufficient (*see* Table 1). Incubate for 1.5 h at RT.
11. Wash the slides twice in TBS-T for 5 min under gentle agitation.
12. Dry the slides with absorbent papers.
13. Cover the tissue with diluted secondary antibodies: goat anti-mouse IgG2a-FITC + donkey anti-rabbit IgG-Cy3 + goat anti-mouse IgG1-biotin in TBS (*see* Table 1). Incubate for 30 min at RT.
14. Wash the slides twice in TBS-T for 5 min under agitation.
15. Dry the slides with absorbent papers.
16. Cover the tissue with streptavidin-AF647 in TBS, and incubate for 30 min at room temperature (*see* Table 1).
17. Wash the slides twice in TBS-T for 5 min under gentle agitation.
18. Wash the slides in 1× TBS for 5 min under gentle agitation.
19. Wash the slides in distilled water for 5 min under gentle agitation (*see* **Note 3**).
20. Mount the slides with glass coverslips using ProLong® with DAPI.
21. Let dry the slides at RT in the dark for a maximum of 1 h. Store the slides at 4 °C in the dark until scanning (or at −20 °C for a longer period of time).
22. Scan the slides with a fluorescence slide scanner (Axio Scan. Z1/Zen 2012, blue edition/Zeiss, or equivalent) (Fig. 1) (*see* **Notes 4** and **5**).

3.2 Detection of TLS-Associated Tfh on FFPE Tumor Sections by Multiplex CD3/CD4/CD20/Bcl6 IF Staining

1. Prior to the staining process, dry the slides for a minimum of 30 min (or overnight) in a drying oven at 37 °C.
2. In Ventana Discovery XT autostainer (*see* **Notes 6** and 7), select deparaffinization step, in EZ prep buffer 75 °C, 8 min.
3. Choose cell conditioning using Cell Conditioner #1 (CC1) for antigen retrieval step at 95 °C for 44 min (*see* **Note 8**).

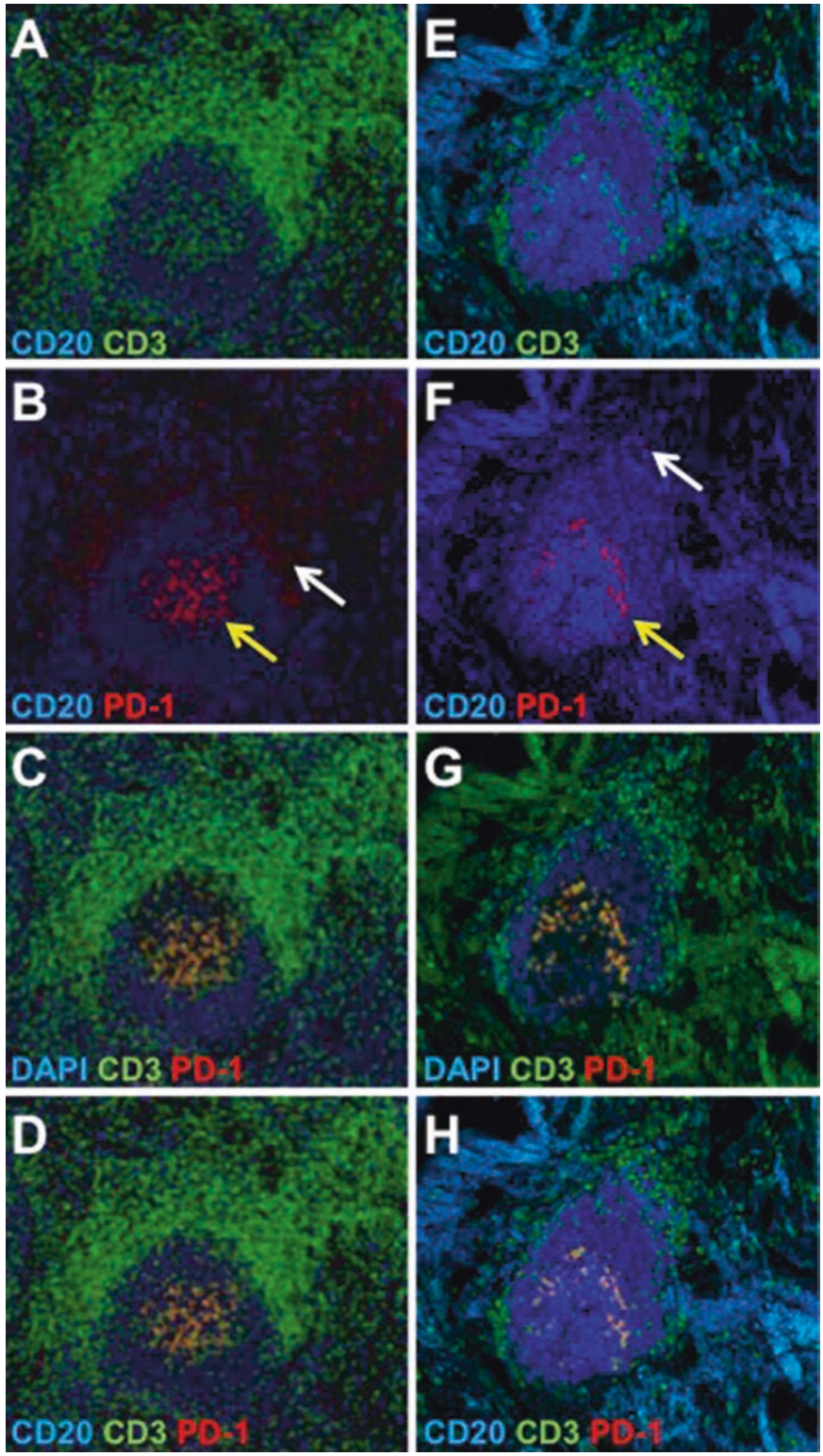

Fig. 1 Triple-IF stainings of FFPE sections from NSCLC-derived LN (**a**–**d**) or NSCLC tumor tissue (**e**–**h**) using antibodies against human CD20 (panels **a**–**b**, **d**, **e**–**f**, **h**), CD3 (panels **a**, **c**–**d**, **e**, **g**–**h**), PD-1 (panels **b**–**d**, **f**–**h**), and DAPI (panels **c** and **g**). (**e**–**h**) Focus on a TLS within NSCLC tissue. Yellow and white arrows (**b**, **f**) indicate PD-1^{bright} cells and PD-1$^{+/dim}$ cells, respectively. Magnification: ×200

4. Select blocking step to block endogenous peroxidases with one drop of Discovery Inhibitor, at RT for 8 min.
5. Select "primary antibody" to cover the tissue with 100 µL of ready-to-use mouse anti-human Bcl6 (clone GI191E/A8) for 32 min at 37 °C.
6. Select "multimer" to incubate the slides with 100 µL of ready-to-use secondary antibody (OmniMap mouse Ventana coupled to HRP) for 12 min.
7. Remove the slides from the Ventana autostainer and wash the slides extensively using a solution containing detergent.
8. Rinse for 2 min, three times.
9. Prepare hydrogen peroxide solution at 0.15% by diluting the stock 9% H_2O_2 in distilled water (solution A).
10. Dilute both tyramide component coupled to Alexa Fluor 546 (100×) and Solution A at 1/100 in 1× TBS to prepare Solution B (*see* **Note 9**).
11. Incubate each slide with 200 µL of Solution B at RT for 10 min.
12. Wash the slides twice in cold distilled water.
13. Put the slides in the Ventana autostainer.
14. Select dual sequence and apply antibody denaturation at 90 °C during 12 min (*see* **Note 10**).
15. Select "primary antibody" to cover the tissue with 100 µL of ready-to-use mouse anti-human CD3 (clone 2GV6) for 40 min at 37 °C.
16. As previously, select "multimer" to incubate the slides with 100 µL of ready-to-use OmniMap goat anti-rabbit coupled to HRP for 12 min.
17. Repeat **steps 7–9**.
18. Dilute both tyramide component coupled to Alexa Fluor 594 (100×) and Solution A at 1/100 in 1× TBS to prepare Solution C (*see* **Note 9**).
19. Incubate each slide with 200 µL of Solution C at RT for 10 min.
20. Wash the slides twice in cold distilled water.
21. Put the slides in the Ventana autostainer.
22. Select dual sequence and apply antibody denaturation at 90 °C during 12 min.
23. Select "primary antibody" to cover the tissue with 100 µL of ready-to-use mouse anti-human CD4 (clone SP35) at 37 °C for 12 min.

24. Select "multimer" to incubate the slides with 100 µL of ready-to-use OmniMap goat anti-rabbit coupled to HRP, at 37 °C for 16 min.
25. Repeat **steps 7–9**.
26. Dilute both tyramide component coupled to Alexa Fluor 647 (100×) and Solution A at 1/100 in 1× TBS to prepare Solution D (*see* **Note 9**).
27. Incubate each slide with 200 µL of Solution D at RT for 10 min.
28. Wash the slides twice in cold distilled water.
29. Put the slides in the Ventana Discovery XT autostainer.
30. Select dual sequence and apply antibody denaturation at 90 °C during 12 min.
31. Apply manually 100 µL of mouse anti-human CD20 (clone L26, diluted at 1/250 in antibody diluent) in the Ventana Discovery XT, at 37 °C for 60 min.
32. Apply secondary antibody: ready-to-use OmniMap goat anti-mouse coupled to HRP, at 37 °C for 12 min.
33. Repeat **steps 7–9**.
34. Dilute both tyramide component coupled to Alexa Fluor 488 (100×) and Solution A at 1/100 in TBS 1× to prepare Solution E (*see* **Note 9**).
35. Incubate each slide with 200 µL of Solution E at RT for 10 min.
36. Wash the slides twice in cold distilled water.
37. Apply 200 µL of DAPI solution (at 1 µg/mL in TBS 1×) for nucleus staining. Incubate at RT for 12 min (*see* **Note 11**).
38. Wash the slides twice in cold distilled water.
39. Mount the slides with glass coverslips using ProLong® Gold mounting medium without DAPI.
40. Scan some fields in the slides using a confocal microscope (LSM710 Zeiss or equivalent).
41. View digital images using the Zen (black) imaging software (Fig. 2) (*see* **Notes 12–14**).

3.3 Tfh Identification by Multiparametric Flow Cytometry from Fresh Tumor Tissue

1. Place the tissue in a petri dish using forceps.
2. Dilacerate the tumor tissue in pieces of up to 2 mm using a scalpel in complete RPMI medium without FBS (about 1 mL for 500 mg of tissue).
3. Transfer the tissue pieces with the medium into a sterile jar.
4. Add collagenase IA and DNase I to reach a final concentration of 1.25 mg/mL and 100 µg/mL, respectively, in a final

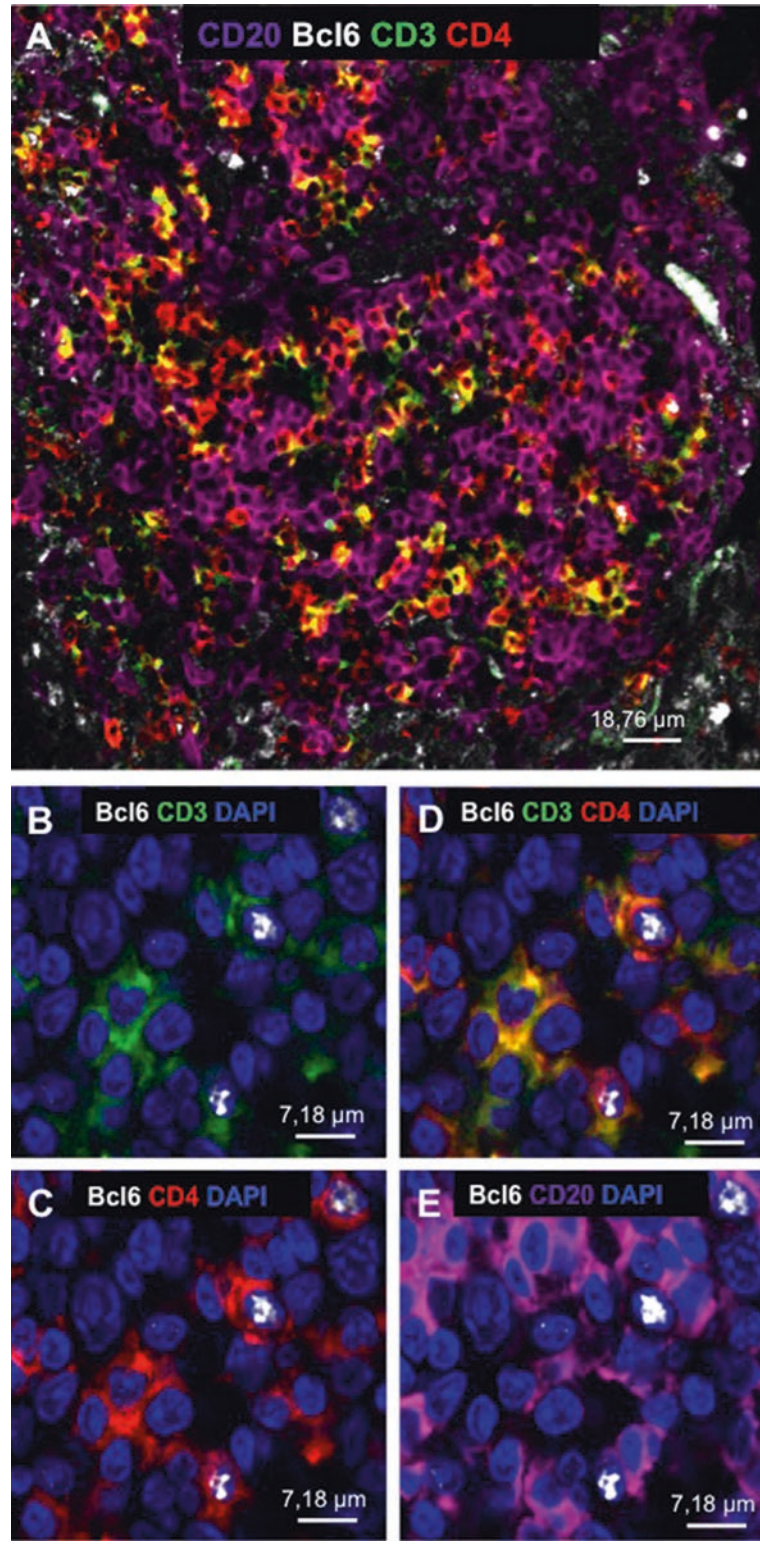

Fig. 2 Confocal imaging of a FFPE NSCLC tumor section using multiplex immunofluorescence. (**a**) Numerous $CD3^+$ (green) $CD4^+$ (red) T cells can be identified

volume of 10 mL of complete RPMI without FBS (*see* **Notes 15** and **16**).

5. Proceed to enzymatic digestion by incubating tissue pieces for 45 min at 37 °C under magnetic agitation in a cell incubator with 5% CO_2 (*see* **Note 17**).
6. Transfer the digested material in a 50 mL Falcon tube and centrifuge for 8 min at 350 *g*.
7. Remove the supernatant and resuspend the pellet in 10 mL of complete RPMI medium.
8. Filter the cell suspension through a 70 μm cell strainer and use a 10 mL syringe plunger to crush the remaining tumor fragments.
9. Rinse the cell strainer and complete with RPMI medium up to 50 mL.
10. Centrifuge for 8 min at 350 *g* at RT.
11. Resuspend the pellet in 1–10 mL of complete RPMI medium depending on pellet size.
12. Dilute 10 μL of cells in 90 μL of Türk's solution which destroys red blood cells to count them with a FastRead slide or equivalent.
13. Resuspend 6×10^6 of cells per tissue of interest in 5 mL of complete RPMI medium.
14. Incubate cells for a minimum of 1 h at 37 °C in a water bath to allow re-expression of CXCR5 on the cell surface (*see* **Note 18**).
15. Prepare the antibody mix and the corresponding isotype controls (*see* Table 1 and **Note 19**).
16. Centrifuge the cells for 8 min at 350 *g* at +4 °C.
17. Discard the supernatant and resuspend the cells in 150 μL of the viability marker solution (Zombie Yellow diluted in 1× PBS at 1/400).
18. Transfer 50 μL of the cell suspension in 96-well plate wells containing either antibody mix, isotype controls, or staining buffer only.
19. Incubate for 30 min at +4 °C.

Fig. 2 (continued) (in yellow) within the $CD20^+$ B-cell zone (purple) of TLS. (**b**–**e**) Visualization of Tfh cells within TLS. A higher magnification of Panel (**a**) enables the visualization of (**b**) $CD3^+$ (green) and (**c**) $CD4^+$ (red) cells. (**d**) Merge of (**b**)–(**c**) shows that some $CD3^+$ $CD4^+$ T cells (yellow) express Bcl6 (white), a master regulator of Tfh differentiation. (**e**) These $Bcl6^+$ cells (white) are visualized within the $CD20^+$ B-cell zone of TLS (purple), but do not express the B-cell marker CD20

20. Wash the cells with 100 µL of PBS in each well and centrifuge for 5 min at 400 *g* at +4 °C.
21. Discard the supernatant and resuspend the cells in 50 µL of fixation/permeabilization buffer per well.
22. Incubate for 10 min at +4 °C.
23. Centrifuge for 5 min at 400 *g* at +4 °C.
24. Remove the supernatant. Proceed to intranuclear staining by incubating the cells with antibody mix or isotype controls previously prepared in 50 µL of permeabilization buffer (Table 1).
25. Incubate for 20 min at 4 °C in the dark.
26. Wash the cells twice with 100 µL of permeabilization buffer at 400 *g* for 5 min.
27. Discard the supernatant.
28. Resuspend the cells with 150 µL staining buffer and transfer into Micronic tubes.
29. Rinse the tubes with 150 µL staining buffer and transfer into the same Micronic tubes.
30. Flow cytometry data are acquired with a Fortessa flow cytometer (BD Biosciences) within 2 days after staining and analyzed using the FlowJo software (Tree Star).

4 Notes

1. After antigen retrieval, it is possible to let the slides in a bath of 1× TBS overnight at RT before continuing the experiment.
2. When drying the slides with absorbent papers, pay attention to the tissue. Also, treat the slides one by one: do not let the slides dry for more than 2 min before adding the following reagent.
3. To better control DAPI intensity, it is possible (after **step 19**) to incubate the slides with a DAPI solution (working concentration: 50 µg/mL in 1× TBS, Life Technologies), for 2 min (or less) at RT, and then to perform step 20 using a mounting medium without DAPI (ProLong® Gold Antifade Reagent, Life Technologies).
4. Tfh cells correspond to PD-1^{bright} cells within CD20^{+} B-cell follicles of LN and TLS from NSCLC patients (Fig. 1b, f, yellow arrows). However, some PD-1$^{+/dim}$ cells can also be observed outside of the GC (Fig. 1b, f, white arrows).
5. Depending on the tissue, a lot of autofluorescence (collagen fibers) can be observed, especially in the FITC, and to a lesser extent in the Cy3, channel (Fig. 1e–h). For this reason, it is

advised to associate easily recognizable $CD20^+$ B-cell follicles and $CD3^+$ T cells with FITC and Cy3 channels, respectively, and to associate PD-1 with the AF647 channel.

6. Protocol can be performed on all Ventana machines (Ultra, Benchmark). However, optimizations may be necessary.
7. Multiplexing IF could be replaced by multiplexed immunohistochemistry with appropriate tyramide components. By IHC, the washing of the slides has to be completed with one bath of 50% ethanol followed by one bath of 70% ethanol, then one bath of 90% ethanol, one bath of absolute ethanol, and finally two baths of 100% xylene. This step is really important to remove residual paraffin which could interfere with staining analysis. Then, mount the slides with Cytoseal 60 toluene-based medium (Richard-Allan Scientific).
8. All antibodies work with Cell Conditioner #1 (CC1) in this case, but it is possible to perform another antigen retrieval step with CC2 (pH 6 citrate buffer).
9. Reconstitute prior to use tyramide coupled to Alexa Fluor reagent with 50 μL of DMSO (100× stock solution) according to the manufacturer's protocol.
10. The denaturation step is crucial to strip the preceding primary and secondary antibodies. Tyramides bind covalently to the tissue, so the denaturation step does not remove the signal.
11. Avoid using the ProLong® mounting medium with DAPI to get a better nucleus staining.
12. It is important to perform single staining for each fluorochrome to record reference emission spectra (library) in order to carry out spectra deconvolution. During image analysis, it is important to find an area with all stainings to avoid poor deconvolution.
13. Control tissues with expected positive staining for all markers must be included for each experiment. Human tonsil or LN is recommended to detect GC zones and Tfh cells, as a positive control of the staining.
14. The combination of CD3 and CD4 markers is essential to detect Tfh cells, as $CD4^+$ cells could also represent macrophages or dendritic cells.
15. **Steps 1–3** in Subheading 3.3 have to be carried out in RPMI without FBS to avoid the inhibition of enzyme action.
16. Collagenase 1A can be used to digest the extracellular matrix of different tissue with addition of DNase I to eliminate DNA of dead cells during the digestion. Timing and concentration might have to be adjusted depending on the tissue. The protocol described here works for breast, ovarian, hepatic, and NSCLC tumors.

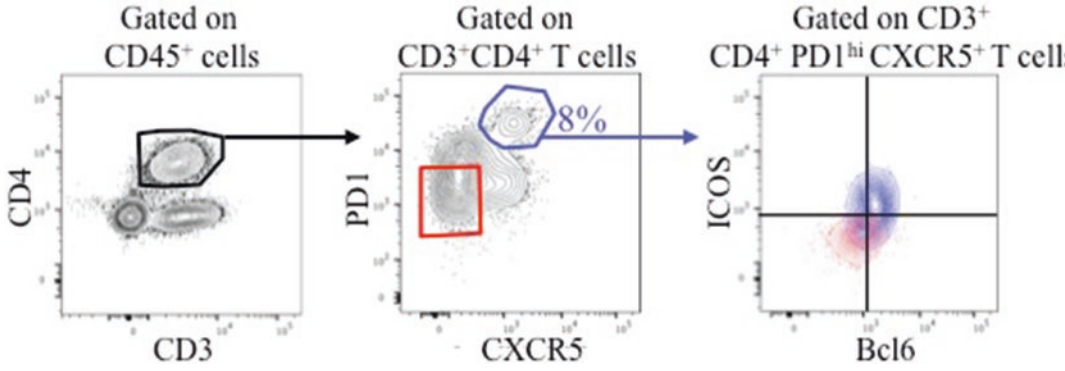

Fig. 3 Gating strategy for Tfh cell detection in hepatocellular carcinoma. After excluding debris and cell doublets, dead (Zombie Yellow$^+$) cells were gated out. Then, on the CD45$^+$ immune cell population, Tfh cells were identified as CD3$^+$CD4$^+$PD1^{hi}CXCR5$^+$ T cells (blue gate). Tfh cell phenotype was confirmed with Bcl6 and ICOS expression. PD1^{lo} cells were used as a negative internal control for Bcl6 and ICOS expression

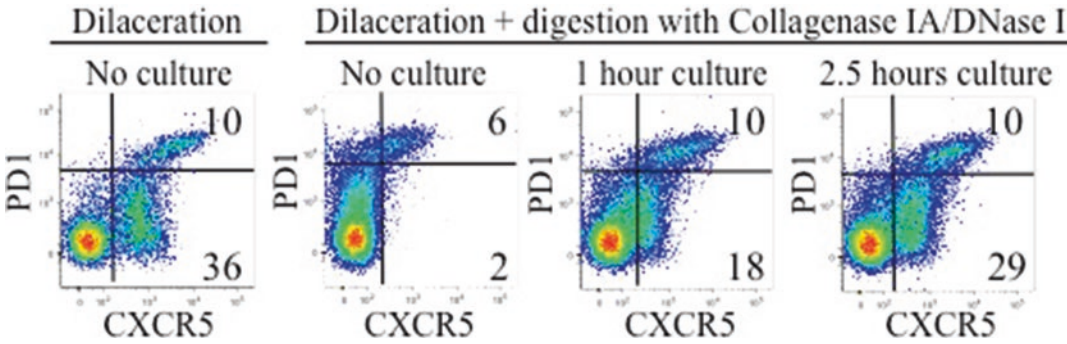

Fig. 4 Enzymatic digestion hampers surface CXCR5 detection by flow cytometry. Cells obtained by enzymatic digestion of tonsils were incubated at 37 °C in a water bath for 1 h and 2.5 h or were kept at 4 °C, and were then stained with the antibody mix (Table 1). Culture of cells prepared by enzymatic tissue digestion restores surface expression of CXR5 and allows identification of bona fide PD1^{hi}CXCR5^{hi} Tfh by flow cytometry at a frequency similar to that observed after mechanical dissociation alone (or in the absence of enzymatic digestion)

17. Use of a water bath is preferable to maintain, over a short period, a constant temperature in the tube.
18. Tissue digestion with Collagenase IA leads to the shaving of CXCR5 which is one of the main markers allowing Tfh identification (Fig. 3). Re-expression of surface CXCR5 is optimally obtained after 2.5 h of incubation at 37 °C, but 1 h is enough to identify Tfh cells (*see* Fig. 4).
19. A negative control tube contains all the antibodies with the exception of antibodies directed against PD-1, CXCR5, ICOS, and Bcl6 that are replaced by matched isotype controls.

Funding

Hélène Kaplon was supported by a grant from La Ligue contre le Cancer. The work developed by B. Dubois's group was supported by the Ligue Contre le Cancer Comité de Savoie, Fondation ARC pour la recherche sur le cancer, and INCa (PRT-K16).

References

1. Crotty S (2014) T follicular helper cell differentiation, function, and roles in disease. Immunity 41(4):529–542
2. Germain C, Gnjatic S, Tamzalit F et al (2014) Presence of B cells in tertiary lymphoid structures is associated with a protective immunity in patients with lung cancer. Am J Respir Crit Care Med 189(7):832–844
3. Schmidt M, Hellwig B, Hammad S et al (2012) A comprehensive analysis of human gene expression profiles identifies stromal immunoglobulin κ C as a compatible prognostic marker in human solid tumors. Clin Cancer Res 18(9):2695–2703
4. Lohr M, Edlund K, Botling J et al (2013) The prognostic relevance of tumour-infiltrating plasma cells and immunoglobulin kappa C indicates an important role of the humoral immune response in non-small cell lung cancer. Cancer Lett 333(2):222–228
5. Mohammed ZMA, Going JJ, Edwards J et al (2013) The relationship between lymphocyte subsets and clinico-pathological determinants of survival in patients with primary operable invasive ductal breast cancer. Br J Cancer 109(6):1676–1684
6. Gu-Trantien C, Loi S, Garaud S et al (2013) $CD4^+$ follicular helper T cell infiltration predicts breast cancer survival. J Clin Invest 123(7):2873–2892
7. Bindea G, Mlecnik B, Tosolini M et al (2013) Spatiotemporal dynamics of intratumoral immune cells reveal the immune landscape in human cancer. Immunity 39(4):782–795
8. Ma Q-Y, Huang D-Y, Zhang H-J et al (2016) Function of follicular helper T cell is impaired and correlates with survival time in non-small cell lung cancer. Int Immunopharmacol 41:1–7
9. Sautès-Fridman C, Lawand M, Giraldo NA et al (2016) Tertiary lymphoid structures in cancers: prognostic value, regulation, and manipulation for therapeutic intervention. Front Immunol 7:407
10. Drayton DL, Ying X, Lee J et al (2003) Ectopic LT alpha beta directs lymphoid organ neogenesis with concomitant expression of peripheral node addressin and a HEV-restricted sulfotransferase. J Exp Med 197(9):1153–1163
11. Lee Y, Chin RK, Christiansen P et al (2006) Recruitment and activation of naive T cells in the islets by lymphotoxin beta receptor-dependent tertiary lymphoid structure. Immunity 25(3):499–509
12. Johansson-Percival A, He B, Li Z-J et al (2017) De novo induction of intratumoral lymphoid structures and vessel normalization enhances immunotherapy in resistant tumors. Nat Immunol 18(11):1207–1217
13. Kang S, Fedoriw Y, Brenneman EK et al (2017) BAFF induces tertiary lymphoid structures and positions T cells within the glomeruli during lupus nephritis. J Immunol Baltim Md 1950 198(7):2602–2611
14. Rangel-Moreno J, Carragher DM, de la Luz Garcia-Hernandez M et al (2011) The development of inducible bronchus-associated lymphoid tissue depends on IL-17. Nat Immunol 12(7):639–646
15. Goya S, Matsuoka H, Mori M et al (2003) Sustained interleukin-6 signalling leads to the development of lymphoid organ-like structures in the lung. J Pathol 200(1):82–87
16. Barone F, Nayar S, Campos J et al (2015) IL-22 regulates lymphoid chemokine production and assembly of tertiary lymphoid organs. Proc Natl Acad Sci U S A 112(35):11024–11029

17. Chen S-C, Vassileva G, Kinsley D et al (2002) Ectopic expression of the murine chemokines CCL21a and CCL21b induces the formation of lymph node-like structures in pancreas, but not skin, of transgenic mice. J Immunol Baltim Md 1950 168(3):1001–1008
18. Marinkovic T, Garin A, Yokota Y et al (2006) Interaction of mature CD3+CD4+ T cells with dendritic cells triggers the development of tertiary lymphoid structures in the thyroid. J Clin Invest 116(10):2622–2632
19. Luther SA, Lopez T, Bai W et al (2000) BLC expression in pancreatic islets causes B cell recruitment and lymphotoxin-dependent lymphoid neogenesis. Immunity 12(5): 471–481
20. Magliozzi R, Columba-Cabezas S, Serafini B, Aloisi F (2004) Intracerebral expression of CXCL13 and BAFF is accompanied by formation of lymphoid follicle-like structures in the meninges of mice with relapsing experimental autoimmune encephalomyelitis. J Neuroimmunol 148(1–2):11–23
21. Pimenta EM, Barnes BJ (2014) Role of tertiary lymphoid structures (TLS) in anti-tumor immunity: potential tumor-induced cytokines/chemokines that regulate TLS formation in epithelial-derived cancers. Cancers 6(2):969–997
22. Hiraoka N, Ino Y, Yamazaki-Itoh R (2016) Tertiary lymphoid organs in Cancer tissues. Front Immunol 7:244

Chapter 13

Exploring the Role of Tertiary Lymphoid Structures Using a Mouse Model of Bacteria-Infected Lungs

Jean-Luc Teillaud, Lucile Regard, Clémence Martin, Sophie Sibéril, and Pierre-Régis Burgel

Abstract

Animal models can be helpful tools for deciphering the generation, maintenance, and role of tertiary lymphoid structures (TLS) during infections or tumor development. We describe here the establishment of a persistent lung infection in immune-competent mice by intratracheal instillation of agarose beads containing *Pseudomonas aeruginosa* or *Staphylococcus aureus* bacteria. After instillation, animals develop a chronic pulmonary infection, marked by the presence of TLS. This experimental setting allows the study of the function of TLS induced by bacteria encountered in patients with cystic fibrosis (CF) as *P. aeruginosa* and *S. aureus* are the two main bacterial strains that infect bronchi of adult CF patients. Additionally, we describe also how to manipulate the immune response in these infected animals by targeting immune cells involved in TLS function. Overall, this approach makes it possible to explore the role of chronic inflammation in the induction and maintenance of TLS in infected tissues.

Key words B cell, Chronic obstructive pulmonary disease, Cystic fibrosis, *Pseudomonas aeruginosa*, *Staphylococcus aureus*, Tertiary lymphoid structure

1 Introduction

Tertiary lymphoid structures (TLS) are ectopic lymphoid structures whose architecture is closely similar to that of secondary lymphoid structures (SLO) (i.e., spleen and lymph nodes). TLS were first depicted as lymphoid aggregates called bronchus-associated lymphoid tissue (BALT) in rabbit [1, 2] and then in humans [3]. They include a central B-cell zone that can be evidenced by labeling B-cell follicles with an anti-CD19 or anti-CD20 antibody and a marginal adjacent T-cell zone stained by an anti-CD3 antibody. In the latter zone, one can detect high endothelial venules (HEV) that are specialized blood vessels that allow peripheral lymphocyte transportation and recruitment into TLS. TLS contain germinal center (GC) in the B-cell follicles and follicular dendritic cells (FDC) that display antigens as immune complexes [4]. TLS are

Marie-Caroline Dieu-Nosjean (ed.), *Tertiary Lymphoid Structures: Methods and Protocols*, Methods in Molecular Biology, vol. 1845, https://doi.org/10.1007/978-1-4939-8709-2_13,

not detected in normal lungs in the absence of inflammation. These structures are present in the lungs of patients with chronic obstructive pulmonary disease (COPD), idiopathic pulmonary arterial hypertension, idiopathic pulmonary fibrosis, asthma, or pulmonary complications of rheumatoid arthritis [5–9]. Also, they have been found in patients with non-small cell lung cancer (NSCLC) [10] and then in a number of other tumor types (among which melanoma, bladder cancer, colorectal cancer, and in some breast cancers) [11]. In cancer patients, their presence has been associated with an improved survival and correlates with a more favorable clinical outcome. TLS have also been detected in the lungs of patients with cystic fibrosis (CF) [12]. Cystic fibrosis is a genetic disease due to mutations in the gene coding for the cystic fibrosis transmembrane conductance regulator (CFTR) protein, an ion channel expressed in epithelial cells. The CFTR dysfunction leads to an increase in mucus viscosity, persistent inflammation, and chronic bacterial infection, which contribute to the development of bronchiectasis. The prognosis of the disease depends on the respiratory impairment that is related to chronic bacterial infections. *Pseudomonas aeruginosa* (PA) and *Staphylococcus aureus* (SA) are the two main bacteria that infect bronchi of adult patients with cystic fibrosis. These chronic infections are associated with a strong airway inflammation and severe decline in pulmonary function of CF patients. In France, about 39% of CF patients are chronically infected with PA and 61% with SA [13]. In the USA, the CF Foundation Patient Registry indicates a 46% prevalence of PA infection and a 26% prevalence of methicillin-resistant SA (MRSA) and more than half of the patients having at least one culture positive for methicillin-sensitive SA (MSSA) in 2016 [14]. In mice, it has been shown that repeated nasal instillations of inactivated PA induce TLS [15] as well as acute infection of lungs with bacteria such as *Chlamydia pneumoniae* [16]. These experimental settings have made it possible to identify chemokines involved in the recruitment of immune cells that are present in TLS such as CXCL12, CXCL13, and CCL19 [15].

The role of TLS is still largely unknown. Although they appear beneficial in a large number of tumors [11] with one exception [17], whether their presence can be detrimental in diseases such as cystic fibrosis remains an open question. The precise cellular components of TLS could be essential in determining their role. This has been suggested by works showing that TLS represent a microniche for tumor progenitor cells in a genetically engineered mouse model of hepatocellular carcinoma [17] and that the presence of regulatory T cells (Treg) in TLS inhibits antitumor responses in a mouse model of lung adenocarcinoma [18]. Moreover, the persistent inflammatory tissue environment that is associated with TLS in most cases could impair the adaptive

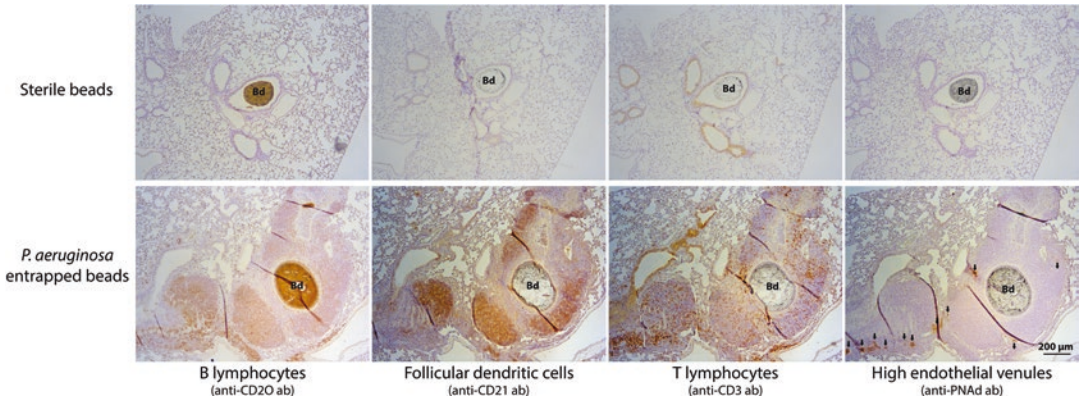

Fig. 1 Mouse instillation with bacterium-entrapped beads (here *Pseudomonas aeruginosa*) induces the neogenesis of peribronchial tertiary lymphoid structures (TLS) (detectable 10–14 days after instillation). Preparation and instillation of *Pseudomonas aeruginosa*-entrapped beads were performed as outlined in Subheadings 3.2 and 3.3. Representative photomicrographs of immunostainings (brown color) in lung tissues from mice sacrificed at day 14 after instillation with sterile (upper panels) and *Pseudomonas aeruginosa*-entrapped (lower panels) beads (Bd) are shown. *Pseudomonas aeruginosa*-infected mice (but not mice instillated with sterile beads) develop peribronchial TLS displaying from left to right segregated B-cell areas (anti-CD20 mAb, first panel) containing follicular dendritic cells (anti-CD21 Ab, second panel) as well as germinal centers (PNA, data not shown), and peripheral T-cell areas (anti-CD3 mAb, third panel) containing high endothelial venules (anti-PNAd Ab, fourth panel, marked with arrows)

responses against cancer cells or pathogens and provoke the destruction and remodeling of tissues, such as lungs.

Clearly, the development of animal models making it possible to study TLS induction and maintenance and their relationship with chronic inflammation, tumor control and escape, and acute and chronic infection is therefore needed. We describe below a technique to explore a murine model of chronic infection, where *P. aeruginosa* or *S. aureus* strains are used as inducers of TLS [19]. This model could give useful information about the role and mechanisms of action of TLS in patients with cystic fibrosis and could bring new insights into the role of chronic inflammation in the induction and maintenance of TLS in infected or tumor tissues. Notably, this model can be used to decipher the role of B cells present in these ectopic structures and to evaluate the clinical risks and biological events associated with anti-B-cell therapy given to CF patients with autoimmune diseases or before lung transplantation [20]. The technique relies on the use of agarose beads where live bacteria (PA or SA) are entrapped. After intratracheal instillation of the beads, animals develop a chronic pulmonary infection marked by the presence of TLS. TLS induced by a bronchial persistent infection in mice are shown in Fig. 1. These infected animals can then be manipulated using various immune intervention protocols to define the role of immune cell subsets in the formation, maintenance, and functions of TLS. A protocol for depleting

immune cells in these infected animals is also given here as an example of immune intervention.

2 Materials

Access to a safety-level microbiology L2 laboratory and to an animal facility with a dedicated room for PA and SA experiments on rodents is needed.

2.1 Reagents

1. Trypticase soy (TS) medium (broth or agar).
2. Mineral oil—heavy (Sigma-Aldrich, now Merck).
3. Agarose High EEO, for molecular biology (Sigma-Aldrich, now Merck).
4. Black Indian ink (Dr. Ph. Martin's 800,815-7BY Bombay India ink).
5. 1× Phosphate-buffered saline (PBS): Dissolve 8 g NaCl (137 mM), 0.2 g KCl (2.7 mM), 1.44 g Na_2HPO_4 (10 mM), 0.24 g KH_2PO_4 (1.8 mM) in 800 mL distilled H_2O. If needed adjust pH to 7.4 (or 7.2 if needed) with 1 N HCl or NaOH solution under agitation. Add then distilled H_2O to a total volume of 1 L. Sterilize by autoclaving (20 min, 121 °C, liquid cycle). Alternatively, RNase-free 10× PBS can be purchased (AM9624, Thermo Fisher Scientific). Store 10× PBS at room temperature (RT).
6. Saline (sterile 0.9% NaCl solution): Dissolve 9 g NaCl in distilled H_2O to a total volume of 1 L. Sterilize by autoclaving (20 min, 121 °C, liquid cycle). Store at RT.
7. Ammonium chloride potassium lysing buffer (ACK buffer) (Thermo Fisher Scientific).
8. Ethanol solutions: 100% (absolute, 99.8%), 95%, 70%, and 50%.
9. Sodium deoxycholate (BioXtra, ≥98.0%) (dry matter) (Sigma-Aldrich, now Merck).
10. Ketamine hydrochloride/xylazine hydrochloride solution (store tightly sealed at 4 °C): Available only at the animal facility under the supervision of a licensed veterinarian as it is classified as a *Schedule III* drug in the USA and as a psychotropic drug in other countries. Purchaser must determine the suitability of the product for their particular use. Additional terms and conditions may apply. Observe all local, state, and federal laws.
11. 4% Paraformaldehyde (PFA) in PBS: Heat 800 mL 1× PBS to around 60 °C. Add 40 g of paraformaldehyde powder while stirring (use a ventilated chemical fume hood). Slowly raise the pH by adding 1 N NaOH dropwise from a pipette until the

solution clears. Cool and filter the solution. Adjust to 1 L with 1× PBS. Aliquot and freeze (−20 °C) or store at 4 °C (it can be stored for up to 1 month).

12. *Streptomyces griseus* protease (0.01 g in 15 mL PBS) (Sigma-Aldrich, now Merck).
13. Bovine serum albumin (BSA) (Fraction V).
14. 100% Xylene.
15. 98% Methanol (histological grade).
16. Hydrogen peroxide (H_2O_2).
17. Citrate buffer, pH 6.0, 10×, Antigen Retriever (Sigma-Aldrich, now Merck).
18. Vectastain Elite ABC HRP kit or Vectastain ABC HRP kit (Vector Laboratories).
19. 3,3′-Diaminobenzidine (DAB) substrate.
20. Limonene mounting medium (Abcam).

2.2 Materials and Supplies Necessary

1. Cryotube vials (Nunc® CryoTubes®, cryogenic vial, 1.8 mL, internal thread, round bottom, free standing, 1800/cs).
2. Gloves and eye protection.
3. Glassware and stir bars (one dedicated for formaldehyde solution preparation).
4. Plastic sterile consumables (pipettes, flasks, centrifuge and culture tubes, pipette tips).
5. Single and multichannel pipettes.
6. 50 mL Capped conical polystyrene tubes.
7. Sterile Petri dishes (90 × 15 mm).
8. Disposable sterile polycarbonate Erlenmeyer flasks.
9. Sterile 400 μm (code: 951019) and 300 μm (code: 951017) stainless steel test sieves Retsch® (Fisher Scientific) for the separation of agarose beads with predefined size (≥300 μm and ≤400 μm).
10. Stirrer (mixer) (IKA® RW 16 Basic Labo Technic) with sterile plastic-covered stirring blades (Sigma-Aldrich, now Merck).
11. 20 Gauge (20G) cannula for intratracheal instillation [1.5 in. long, 20 gauge IV catheter (BD Insylte, Sparks, MD, or Jelco Optiva, Carlsbad, CA) or Dominique Dutscher SAS (code: 075473) (Brumath, France)]. A single sterile cannula is used for each group of mice. The cannula can be reused in other experiments after sterilization by soaking in 70% ethanol overnight (o/n), washing in distilled H_2O_2, and autoclaving.
12. Disposable individually ventilated cages.

13. Syringe and needle for intraperitoneal (i.p.) and intradermal (i.d.) injections.
14. 23 or 25 gauge (23 G or 25 G) needle for peripheral blood collection.
15. Tailveiner restrainer (BrainTree Scientific, Inc.).
16. Gauze sponge.
17. Adhesive tape.
18. Refrigerated centrifuge.
19. Hot plate with magnetic stirrer.
20. Thermometer.
21. ImmEdge hydrophobic barrier PAP pen (code: H-4000) (Vector Laboratories).
22. Slides and cover glass (coverslips) for immunohistochemistry (IHC).
23. Slide boxes and embedding cassettes.
24. Laboratory water bath.
25. −86 °C Ultralow laboratory freezer.
26. Chemical fume hood.
27. Microbiology shaking incubator.
28. Microtome (Leica Microsystems).
29. Heating lamp with 250 W (infrared) bulb.
30. Flow cytometer (for phenotyping).
31. Induction chamber for isoflurane anesthesia.

2.3 Antibodies

1. Anti-mouse CD20 monoclonal antibody (mAb) (endotoxin-free, azide-free): A mouse anti-mouse CD20 mAb can be obtained from companies like Genentech. Signature of a Material Transfer Agreement (MTA) is requested.
2. IgG isotype control (irrelevant mAb exhibiting the same IgG species subclass as the anti-CD20 mAb used) (endotoxin-free, azide-free).
3. Rat anti-mouse CD19-phycoerythrin (PE) and rat anti-mouse CD45R (B220)-allophycocyanin (APC) antibodies for double staining of B cells (eBiosciences).
4. Examples of primary antibodies for immunostaining of paraffin-embedded lung tissue are indicated in Table 1.
5. Biotinylated anti-rabbit or -goat or -rat IgG (secondary antibodies).

2.4 Bacterial Strains

1. P*seudomonas aeruginosa* (PA) laboratory strain PAO1.
2. Alternatively, a *Pseudomonas aeruginosa* (PA) clinical strain can be isolated from the sputum of a CF patient. We use a PA clini-

Table 1
Antibodies for detecting TLS in instillated lungs (by immunohistochemistry)

Specificity	Supplier	Clone	Working dilution	Ag unmasking	Secondary antibody
CD20 (B cell)	Santa Cruz	Sc-7735	1:100	–	Goat
CD3 (T cell)	Novus Biological	SP7	1:50	Citrate	Rabbit
CD21 (follicular dendritic cell)	Abcam	Ab75985	1:200	Citrate	Rabbit
PCNA (germinal center)	Calbiochem	247*261	1:200	Protease	Rabbit
PMN[a]	Santa Cruz	Sc-71674	1:200	Protease	Rat
PNAd[b] (HEV)	BD Pharmingen	BD553863	1:50	Citrate	Rat
F4/80 (macrophages)	Santa Cruz	Sc-71,085	1:100	Protease	Rat

[a] *PMN* Polymorphonuclear cells (neutrophils)
[b] *PNAd* Peripheral node addressin (staining of high endothelial venules, HEV)

cal strain isolated from the sputum of an 8-year-infected CF patient from the adult CF center at the Cochin Hospital (Paris, France).

3. A *Staphylococcus aureus* (SA) clinical strain isolated from the sputum of a 10-year-infected CF patient at the adult CF center at the Cochin Hospital (Paris, France). This SA strain is methicillin sensitive (MSSA) (*see* **Note 1**) and makes it possible to closely mimic the infection observed in a large number of CF patients in Europe (where the prevalence of MSSA strains is higher than MRSA, i.e., methicillin-resistant SA).
4. Bacteria strains are kept frozen at −80 °C in 1.8 mL cryotube vials.

2.5 Animals

All procedures performed on mice should be approved with the local animal ethic committee and carried out in accordance to the rules enacted by the relevant regulatory agencies of the country where the experiment is performed. See the ILAR and European guidelines [21, 22] for the care and use of laboratory animals.

1. House 6-week-old C57Bl/6J female mice in conventional conditions (*see* **Note 2**).
2. Monitor regularly mice for infection by typical pathogens according to the FELASA recommendations [23].

2.6 Lung Removal and Lung Tissue Homogenates

1. Surgical scissors, forceps, and tweezers.
2. Tissue homogenizer (Homogenizer Turrax T18 Digital Deutscher).
3. 1× PBS (*see* Subheading 2.1, **step 5**).

3 Methods

The murine model of chronic infection is based on the use of a single intratracheal nontraumatic instillation of agarose beads containing live PA or SA. This instillation induces a long-term bronchopulmonary infection (*see* **Note 3**) and does not require to be repeated. The infection kinetics in the instilled mice can be followed up by in vitro bacterial cultures of lung homogenates of sacrificed mice at different time points post-instillation. PA or SA infection can be detected up to 2 months after instillation of C57Bl/6 mice.

3.1 Preparation of Bacteria Stock Solutions

1. PA or SA colonies are isolated on Petri dishes [cultured on trypticase soy (TS) agar].
2. Bacteria are then cultured in broth TS medium for 72 h at 37 °C under constant agitation in a 50 mL culture tube. Cultures are then centrifuged and the bacterial pellet is resuspended in PBS to obtain a bacterial suspension of 10^9–10^{10} CFU (colony-forming unit)/mL. The latter is immediately used for preparing PA- or SA-entrapped beads.

3.2 Agarose Bead Preparation

PA or SA is entrapped into agarose beads, as described by van Heeckeren and Schluchter [24] with some minor modifications.

1. Heat 150 mL heavy mineral oil in a water bath up to 50 °C.
2. In parallel, agarose (high EEO) is melted at a 100 °C water bath (0.3 g agarose in 15 mL PBS). Cool the solution down to 50 °C under sterile conditions.
3. Keep equilibrated both solutions at 50 °C under sterile conditions.
4. Mix 8.5 mL agarose with 1 mL bacteria in culture medium (10^9–10^{10} CFU/mL) and 0.5 mL undiluted Indian ink (Indian ink will make it possible to visualize beads when resected lungs will be examined).
5. The agarose-bacteria-Indian ink mix (10 mL) is then added to mineral oil (150 mL) and the resulting solution is stirred first for 6 min at room temperature (RT) and then cooled on ice with continuous stirring for 20 min using a stirrer (IKA RW 16 Basic Labo Technic) equipped with sterile plastic-covered blades (speed: 4) (*see* **Note 4**).

6. Bead washing and resuspension in PBS: The mix is then centrifuged at 3000 × *g* at 4 °C for 20 min (this speed is required due to the viscosity of the heavy mineral oil in the mix). After removing supernatant, 0.5% sodium deoxycholate (1.5 g sodium deoxycholate in 300 mL PBS) is added and the bead pellet is gently resuspended. After centrifugation at 1200 × *g* for 20 min at 4 °C, the bead pellet is resuspended in 0.25% sodium deoxycholate (0.75 g sodium deoxycholate in 300 mL PBS) and centrifuged at 1200 × *g* for 20 min at 4 °C. Beads are then washed similarly twice in PBS.
7. To get a homogeneous size of beads (median size: 300 μm), the bead solutions are first filtered through a 400 μm stainless steel test sieve (gently add PBS with a 10 mL sterile plastic pipette to allow all the bead solution to be filtered). The flow-through is then filtered through a 300 μm stainless steel test sieve to remove beads <300 μm from the bead preparation (make sure that agarose beads are not drying by gently adding PBS with a 10 mL sterile plastic pipette) (*see* **Note 5**). Beads remaining in the upper part of the sieve with a size ranging between 300 and 400 μm are then gently collected with a 5 or 10 mL pipette and diluted in sterile PBS to a 5% final stock solution at 4 °C. They can be stored for up to 3 days before use. All steps require a gentle manipulation to avoid disruption of the agarose beads.
8. To estimate the number of bacteria entrapped within beads, aliquots of bead suspensions are homogenized and plated on TS agar for bacterial culture and CFU are estimated.
9. Control beads are prepared as described above without the addition of PA or SA. They should be found sterile when cultured on TS soy agar.

3.3 Mouse Intratracheal Instillation

Intratracheal instillation bypasses the initial host immune response conducted by the respiratory epithelium of the upper airways.

1. 7–8-Week-old mice (*see* **Note 6**) are anaesthetized by intraperitoneal (i.p.) injection (20 G needle) of a ketamine/xylazine solution (0.1 mL per 10 g of weight) (light anesthesia).
2. Assess the level of anesthesia by pedal reflex (firm toe pinch) and adjust anesthetic delivery as appropriate to maintain surgical plane.
3. Monitor the mouse vital signs during anesthesia (respiratory rate and effort, color of mucous membranes, and reflected eye color (in albino animals) at regular intervals (<15-min intervals).
4. Mice are then intubated with a 20 gauge (20 G) cannula attached to a 1 mL syringe.

5. Introduce cannula as described by Das et al. [25]: place the anesthetized mouse on a vertical support, suspended by its upper incisors. The best visualization is with the ventral side of the mouse facing the investigator. Very gently pull out the tongue and hold with thumb and forefinger. The middle finger is placed between the neck and plastic support. Traction on the tongue with the index finger and thumb allows the opening of the mouth. The angle of the head is adjusted with the middle finger behind the neck to straighten the insertion of the cannula into the trachea.
6. Lay the mouse down. The cannula is secured using a piece of tape. Be careful not to move the cannula.
7. Connect the Luer end of the cannula to the 1 mL syringe.
8. Instillate 40 μL inoculum of sterile or PA- or SA-entrapped beads (containing $6 \times 10^5 \pm 3 \times 10^5$ CFU/mL) through the cannula into the trachea of the anesthetized animal.
9. To prevent respiratory distress and improve oxygenation, place the anaesthetized mouse in an individual ventilation-sealed cage and mechanically supply a mixture of air and medical-grade oxygen for 10–15 min.
10. Then, place each anesthetized animal in a clean, dry, and quiet environment, away from other animals.
11. Cover bedding material (usually made of aspen shavings or shreds) with toweling material as bedding material can stick to eyes or be inhaled while animals are recovering from anesthesia.
12. Provide warmth during recovery [surgical heating pad or incandescent lamp (50–70 Watts) (30–35 cm away, i.e., about 12–14 in.) or use of a temperature-controlled cage].
13. Monitor each animal until it maintains upright posture and walks normally about the cage. Then, return it to the animal housing room.
14. Mice are sacrificed by i.p. injection of 200 μL per 10 g weight of ketamine (15 mg/mL) and xylazine (2 mg/mL) and mix whenever requested by the experimental setting after bead instillation (*see* **Note 7**).

3.4 B-Cell Depletion

This method is given as an example of immune intervention aimed at deciphering the role of immune cells in the generation, maintenance, and functions of TLS. This part of the protocol can be adapted to use any other depleting antibody targeting a specific immune cell subset.

1. In the tail vein of C57Bl/6J mice, perform a single intravenous (i.v.) injection of 250 μg/mouse of an anti-mouse CD20 antibody or of an isotype control (in 200 μL sterile PBS) 1

week before the instillation of PA- or SA-entrapped beads. A heating lamp with a 250 W (infrared) bulb can be used to warm up mice until the tail vein is clearly dilated (at about 1 ft. distance). A tail veiner restrainer can be used to make the i.v. injection into the tail vein easier.

2. Collect blood (at day 2 after anti-CD20 injection) by submandibular puncture into capillary tubes containing heparin (as anticoagulant) with a 23 or 25 gauge needle slightly behind the mandible, but in front of the ear canal. This procedure requires gas anesthesia (with isoflurane in an induction chamber).
3. Apply gentle pressure to the blood collection site with a gauze sponge until bleeding has stopped.
4. Lyse red cells of the collected blood with ACK buffer according to the manufacturer's recommendations. Wash cells once in 1× PBS and adjust at 10^6/mL before phenotyping.
5. Analyze B-cell presence in the cell preparation by flow cytometry using anti-mouse CD19-PE and anti-mouse CD45R (B220)-APC antibodies (double labeling). Compare with untreated mice using the same procedures.

3.5 Bacterial Analysis of Lung Tissue Homogenates

This assay makes it possible to control the success of instillation of PA- or SA-entrapped beads. Only one mouse/experiment is evaluated as the technique of instillation is very robust and reproducible.

1. Remove aseptically the lungs from the thoracic cavity of sacrificed mice (*see* **Note 8**) and prepare lung tissue homogenates in saline (0.9% NaCl) (*see* **Note 9**) under sterile conditions in a laminar flow hood.
2. Plate tenfold serial dilutions of lung tissue homogenates on TS agar. After incubation at 37 °C for 24 h, perform bacterial colony counts (expressed as CFU/lung).

3.6 Histological Analysis of Resected Lungs

1. Puncture the right ventricle of the heart using an intradermic (i.d.) needle to remove blood.
2. To clear lungs of blood, flush 1 mL of 4% PFA in PBS through the right ventricle of the heart before resection (*see* **Notes 10** and **11**).
3. *Rinse* resected lung once in PBS and treat with 4% PFA in PBS ethanol 100% at 4 °C for 48 h (*see* **Note 12**).
4. Dehydrate lung after successive incubations of lungs in PBS, 30% ethanol, and 50% ethanol for 15 min each. Keep lungs in 70% ethanol before inclusion.
5. Inclusion of lung in paraffin: Incubate lung overnight in 100% ethanol at RT and then in 100% xylene for 5 h at RT. Immerse then lung in molten paraffin for 4–5 h.

6. Prepare 5 μm sections of paraffin-embedded lung with a microtome.
7. Deparaffinize lung tissue sections by a 3-min incubation at RT of the slides in a rack containing 100% xylene. Repeat the incubation once.
8. Rehydrate by successive 3-min incubations (1:1 100% xylene:100% ethanol; 100% ethanol twice; 95% ethanol; 70% ethanol; 50% ethanol).
9. Depending on the antibody tested, antigen unmasking (retrieval antigen) may be required (*see* **Note 13**). Incubate slides with protease (from *Streptomyces griseus)* for 20 min at RT or incubate in boiling 10 mM citrate buffer, pH 6.0, for 20–40 min (use microwave) (optimal incubation time should be determined by user).
10. Treat tissue sections with 0.3% H_2O_2 in methanol for 20–30 min at RT to block endogenous peroxidase activity. H_2O_2 treatment can be done before unmasking with protease.
11. Rinse slides with running cold tap water or distilled H_2O_2 for 3 min (*see* **Note 14**).
12. Incubate lung sections with PBS-2% BSA for 30 min at RT to prevent nonspecific binding of antibodies.
13. To keep reagents localized on the tissue section to be stained with antibodies, one can use a pen that delineates a hydrophobic barrier on the slide.
14. Sections that contain agarose beads (detected thanks to their Indian ink content) are stained with antibodies. Sections derived from the same infected lung but where beads are not detected are stained for comparison. Sections derived from animals that received sterile beads are stained and used as negative controls.
15. Remove PBS-2% BSA and stain lung sections with relevant primary antibodies diluted in PBS-0.05% Tween 20–1% BSA for 1 h at RT or overnight (O/N) at 4 °C (depending on the antibodies) in a humid atmosphere.
16. Examples of primary antibodies are given in Table 1 (dilution and antigen retrieval techniques are indicated).
17. Wash three times the stained lung sections with PBS at RT.
18. Incubate lung sections with biotinylated anti-rabbit or -goat or -rat IgG antibodies (final dilution: 1:200) as secondary reagents (depending on the species origin of the primary antibodies) for 1 h at RT (*see* **Note 15**).
19. Wash three times the stained lung sections with PBS at RT.

20. Reveal bound antibodies by the avidin–biotin–peroxidase complex method (Elite ABC HRP kit) according to the manufacturer's instructions using DAB substrate.
21. Counterstain tissue sections with hematoxylin/eosin solution.
22. Wash three times the stained lung sections with distilled H_2O at RT.
23. Dehydrate sections by successive 3-min incubations (50% ethanol; 70% ethanol; 95% ethanol; 100% ethanol; 1:1 100% xylene:100% ethanol) and 2-min incubation with 100% xylene twice.
24. Adhere a coverslip to the tissue section. An organic mounting media such as the limonene mounting medium can be used when DAB is used as substrate (a chromogen resistant to organic solvent). Add 2–3 drops of mounting medium. Apply coverslip carefully, avoiding air bubbles.
25. Negative controls are obtained by omission of primary antibodies and incubation with irrelevant immunoglobulins. The execution of every step is identical.

3.7 Detection and Quantification of TLS

Quantification of TLS and calculation of the area of lung tissue sections can be performed using dedicated image algorithms that generate mathematical descriptions of expression and morphological patterns in tissues. The steps presented below correspond to a manual quantification that can be performed if no imaging software is available.

1. The antibodies used to detect the various immune cell subsets present in TLS (peribronchial and perivascular) are listed in Table 1.
2. Count manually TLS under photonic microscopy [26]. All peribronchial TLS detected in one lung section are counted. For a given mouse, count two sections separated by at least 300–400 μm.
3. Microphotograph lung sections (×10).
4. Overlay a counting grid with regularly disposed points on microphotographs.
5. Count every point intersecting lung parenchyma.
6. For each lung section, calculate the total lung surface according to the formula $[\Sigma\text{counted points} \times (2.36)]^2/[\text{Final magnification}]^2$. The number of lymphoid aggregates is then expressed by square centimeter of lung. Lung surface is evaluated using the point counting method.

4 Notes

1. SA methicillin resistance is due to the acquisition of the mecA gene that encodes a penicillin-binding protein. It leads to an increased resistance to antibiotics treatment, making treatments more difficult, although it is not considered as a virulence factor. Thus, the pathogenicity of the bacteria is not modified [27]. SA persistence in bronchial tree of the patients is due to the capacity of the bacteria to adapt themselves in front of the patient immune system, antibiotics pressure, and interspecies competition when several pathogens are colonizing the tree [28].
2. It has been reported that mice older than 4 months are more susceptible to an infection with *Pseudomonas aeruginosa* than younger mice that are more or less resistant [29]. Whether the sensitivity of mice to intratracheal instillation of PA- or SA-entrapped beads is also dependent on their age has not been documented so far. Use C57Bl/6 mice for intratracheal instillation of PA-entrapped beads. It has been demonstrated that DBA/2 and C57Bl/6 are susceptible to *P. aeruginosa* infection while BALB/c mice are resistant [30].
3. Direct intratracheal instillation of live PA or SA bacteria (without trapping into agarose beads) does not induce chronic infection. It provokes an acute pneumonia that leads to a rapid animal death or to the cure of infection with a whole clearance of bacteria [24].
4. The size of the beads depends on the speed of the stirring and of the rate of cooling.
5. One has to produce beads with a diameter larger than 300 μm. This threshold allows beads to stay within bronchi and bronchioles, and thus prevent them to reach alveoli.
6. Animals should be kept housed without any experimental manipulation for 1–2 weeks after purchase and delivery to the animal facility.
7. A rapid intraluminal bronchia infiltration of inflammatory cells (mostly neutrophils and, to a lesser extent, macrophages) can be detected 24 h after instillation of PA- or SA-entrapped beads and is still detectable at day 14. Immunochemistry analysis also shows the recruitment of subepithelial B lymphocytes around bronchia exhibiting PA- or SA-entrapped agarose beads as early as 24 h after instillation. During the following days, round B-cell aggregates are detected and become surrounded by T cells at days 4–7. Fully structured TLS are observed at day 14.

8. To confirm that persistent airway infection is present after instillation of PA- or SA-encapsulated beads, control animals can be sacrificed at day 7. Tenfold dilutions of left lung homogenates are then prepared and plated on trypticase soy agar. Bacterial counts should confirm that a persistent airway infection is present. No bacteria should be detected in lung homogenates of animals that are instilled with sterile beads (data not shown).
9. Homogenate from one lung is diluted in sterile 500 μL saline (0.9% NaCl solution).
10. The lungs will slightly inflate. It will transition from a red/pink color to a completely white aspect when the procedure is complete.
11. Inflation of the lungs with PFA is critical to some histological analysis. The volume of PFA required to properly inflate the lung tissue is usually ≤1.5 mL. To prevent overinflation of the lungs, the infusion step can be completed with the lungs in situ, with PFA infusion stopping when the lung volume completely fills the thoracic cavity.
12. Instillated agarose beads appear as tiny black spots that can be observed macroscopically at the surface of the resected lungs. It shows that the instillation has been successfully performed. If no spot is observed, the instillation experiment should be performed again (*see* Subheading 3.3, **step 1**).
13. Keep the slides in the tap water until ready to perform antigen unmasking (retrieval antigen). The slides should not be allowed to dry. Drying out will cause nonspecific antibody binding, leading to high background staining.
14. Antigen unmasking is required to improve the quality of staining when polyclonal rabbit antibodies to the endothelial marker von Willebrand factor (vWF) (Dako) are used to identify peribronchial blood vessels.
15. Most of these antibodies are supplied in lyophilized form and can be reconstituted with 1 mL sterile distilled H_2O_2. With some exceptions the recommended dilution for most applications is 1:200.

Funding

This work was supported by a grant from Association Vaincre la Mucoviscidose (RF201605016 22/1/2/51), by INSERM, and by Paris Descartes and Sorbonne Universities.

References

1. Bienenstock J, Johnston N, Perey DY (1973) Bronchial lymphoid tissue. I. Morphologic characteristics. Lab Investig 28:686–692
2. Bienenstock J, Johnston N, Perey DY (1973) Bronchial lymphoid tissue. II. Functional characteristics. Lab Invest 28:693–698
3. Pabst R, Gehrke I (1990) Is the bronchus-associated lymphoid tissue (BALT) an integral structure of the lung in normal mammals, including humans? Am J Respir Cell Mol Biol 3:131–135. https://doi.org/10.1165/ajrcmb/3.2.131
4. Ruddle NH (1999) Lymphoid neo-organogenesis: lympho-toxin's role in inflammation and development. Immunol Res 19:119–125. https://doi.org/10.1007/BF02786481
5. Hogg JC, Chu F, Utokaparch S et al (2004) The nature of small-airway obstruction in chronic obstructive pulmonary disease. N Engl J Med 350:2645–2653. https://doi.org/10.1056/NEJMoa032158
6. Perros F, Dorfmüller P, Montani D et al (2012) Pulmonary lymphoid neogenesis in idiopathic pulmonary arterial hypertension. Am J Respir Crit Care Med 185:311–321. https://doi.org/10.1164/rccm.201105-0927OC
7. Marchal-Sommé J, Uzunhan Y, Marchand-Adam S et al (2006) Cutting edge: non-proliferating mature immune cells form a novel type of organized lymphoid structure in idiopathic pulmonary fibrosis. J Immunol 176:5735–5739. https://doi.org/10.4049/jimmunol.176.10.5735
8. Elliot JG, Jensen CM, Mutavdzic S et al (2004) Aggregation of lymphoid cells in the airways of nonsmokers, smokers and subjects with asthma. Am J Respir Crit Care Med 169:712–718. https://doi.org/10.1164/rccm.200308-1167C
9. Rangel-Moreno J, Harton L, Navarro C et al (2006) Inducible bronchus-associated lymphoid tissue (iBALT) in patients with pulmonary complications of rheumatoid arthritis. J Clin Invest 116:3183–3194. https://doi.org/10.1172/JCI28756
10. Dieu-Nosjean MC, Antoine M, Danel C et al (2008) Long-term survival for patients with non-small-cell lung cancer with intratumoral lymphoid structures. J Clin Oncol 26:4410–4417. https://doi.org/10.1200/JCO.2007.15.0284
11. Sautès-Fridman C, Lawand M, Giraldo NA et al (2016) Tertiary lymphoid structures in cancers: prognostic value, regulation, and manipulation for therapeutic intervention. Front Immunol 7:407. https://doi.org/10.3389/fimmu.2016.00407
12. Frija-Masson J, Martin C, Regard L et al (2017) Bacteria-driven peribronchial lymphoid neogenesis in bronchiectasis and cystic fibrosis. Eur Respir J 49(4). pii: 1601873. https://doi.org/10.1183/13993003.01873-2016
13. Vaincre la Mucoviscidose, INED. French cystic fibrosis registry. Annual data report 2015. http://www.vaincrelamuco.org/sites/default/files/french_cf_patient_registry_2015.pdf
14. Cystic Fibrosis Foundation 2016-Patient Registry-Annual data report. https://www.cff.org/Research/Researcher-Resources/Patient-Registry/2016-Patient-Registry-Reports/
15. Foo SY, Phipps S (2010) Regulation of inducible BALT formation and contribution to immunity and pathology. Mucosal Immunol 3:537–544. https://doi.org/10.1038/mi.2010.52
16. Crother TR, Ma J, Jupelli M et al (2012) Plasmacytoid dendritic cells play a role for effective innate immune responses during chlamydia pneumoniae infection in mice. PLoS One 7(10):e48655. https://doi.org/10.1371/journal.pone.0048655
17. Finkin S, Yuan D, Stein I et al (2015) Ectopic lymphoid structures function as microniches for tumor progenitor cells in hepatocellular carcinoma. Nat Immunol 16:1235–1244. https://doi.org/10.1038/ni.3290
18. Joshi NS, Akama-Garren EH, Lu Y et al (2015) Regulatory T cells in tumor-associated tertiary lymphoid structures suppress anti-tumor T cell responses. Immunity 43:579–590. https://doi.org/10.1016/j.immuni.2015.08.006
19. Martin C, Thevenot G, Danel S et al (2011) Pseudomonas aeruginosa induces vascular-endothelial growth factor synthesis in airway epithelium in vitro and in vivo. Eur Resp J 38:939–946. https://doi.org/10.1183/09031936.00134910
20. Ius F, Sommer W, Tudorache I et al (2015) Preemptive treatment with therapeutic plasma exchange and rituximab for early donor-specific antibodies after lung transplantation. J Heart Lung Transplant 34:50–58. https://doi.org/10.1016/j.healun.2014.09.019
21. National Research Council (US) Committee for the Update of the Guide for the Care and Use of Laboratory Animals (2011) Guide for the care and use of laboratory animals, 8th ed. National Academies Press (US), Washington (DC). https://doi.org/10.17226/12910

22. The European Parliament and the Council of the European Union. 2010. Directive 2010/63/EU of the European Parliament and of the Council of 22 September 2010 on the Protection of Animals Used for Scientific Purposes. Off J Eur Communities L276:33–79
23. Nicklas W, Baneux P, Boot R et al (2002) Recommendations for the health monitoring of rodent and rabbit colonies in breeding and experimental units. Lab Anim 36:20–42. https://doi.org/10.1258/0023677021911740
24. Van Heeckeren AM, Schluchter MD (2002) Murine models of chronic Pseudomonas aeruginosa lung infection. Lab Anim 36:291–312. https://doi.org/10.1258/002367702320162405
25. Das S, MacDonald K, Chang HY, Mitzner W (2013) A simple method of mouse lung intubation. J Vis Exp 73:e50318. https://doi.org/10.3791/50318
26. Hsia CC, Hyde DM, Ochs M, Weibel ER, ATS/ERS Joint Task Force on Quantitative Assessment of Lung Structure (2010) An Official Research Policy Statement of the American Thoracic Society/European Respiratory Society: standards for quantitative assessment of lung structure. Am J Respir Crit Care Med 181:394–418. https://doi.org/10.1164/rccm.200809-1522ST
27. Palavecino EL (2014) Clinical, epidemiologic, and laboratory aspects of methicillin-resistant Staphylococcus aureus infections. Methods Mol Biol 1085:1–24. https://doi.org/10.1007/978-1-62703-664-1_1
28. Goerke C, Wolz C (2010) Adaptation of Staphylococcus aureus to the cystic fibrosis lung. Int J Med Microbiol 300:520–525. https://doi.org/10.1016/j.ijmm.2010.08.003
29. Teichgräber V, Ulrich M, Endlich N et al (2008) Ceramide accumulation mediates inflammation, cell death and infection susceptibility in cystic fibrosis. Nat Med 14:382–391
30. Morissette C, Skamene E, Gervais F (1995) Endobronchial inflammation following Pseudomonas aeruginosa infection in resistant and susceptible strains of mice. Infect Immun 63:1718–1724

Chapter 14

Identification and Characterization of Tertiary Lymphoid Structures in Murine Melanoma

Anthony B. Rodriguez, J. David Peske, and Victor H. Engelhard

Abstract

Tertiary lymphoid structures (TLS) are transient ectopic lymphoid aggregates that often share structural similarities to conventional secondary lymphoid organs. In a variety of solid cancers, the presence of these structures commonly correlates with high densities of tumor-infiltrating T lymphocytes and prolonged patient survival. These observations suggest that TLS act as sites for the development of beneficial antitumor immune responses. However, few murine tumor models have been described that could enable a more comprehensive understanding of the functionality of TLS in solid cancers. We previously reported that murine B16-F1 melanoma or Lewis lung carcinoma cells transfected to express the model antigen ovalbumin form intratumoral TLS after implantation into the peritoneal cavity of C57BL/6 mice. In this chapter, we describe immunofluorescent microscopy and flow cytometry approaches for identifying and characterizing intratumoral TLS. Additionally, we describe an adoptive transfer method for demonstrating the infiltration of naïve T cells into B16-OVA melanoma tumors *via* the lymph node-like vasculature, which is an essential functional feature of tumor-associated TLS.

Key words Tertiary lymphoid structure, Melanoma, CD8$^+$ T lymphocyte, Peripheral node addressin, Cancer-associated fibroblast, Immunofluorescence, Flow cytometry, Adoptive cell transfer

1 Introduction

It is well established that the immune system plays an important role in cancer immunosurveillance and tumor eradication. A high density of CD8$^+$ T lymphocytes infiltrating solid tumors is commonly associated with favorable clinical outcomes and patient survival (reviewed in [1–3]). Cytokine infusion, checkpoint blockade inhibition, vaccination, and adoptive transfer strategies have all been used to increase the representation of intratumoral CD8$^+$ T lymphocytes and bolster antitumor immunity [4–7]. However, only a small fraction of patients respond favorably to these immunotherapies. Gene expression profiling of patients who respond favorably to these immunotherapies has been shown to have a preexisting immune infiltrate prior to treatment [8–10]. This suggests

Marie-Caroline Dieu-Nosjean (ed.), *Tertiary Lymphoid Structures: Methods and Protocols*, Methods in Molecular Biology, vol. 1845, https://doi.org/10.1007/978-1-4939-8709-2_14,

that the limited representation of intratumoral CD8+ T lymphocytes is a fundamental barrier to the success of current cancer immunotherapies. One potential strategy to increase the representation of CD8+ T lymphocytes in solid tumors is by increasing their exogenous infiltration through vaccination or alterations in tumor-associated vasculature. An alternative potential strategy is to enhance the intratumoral immune response by promoting the development of tertiary lymphoid structures (TLS).

TLS were initially identified as ectopic accumulations of immune cells that develop in and/or near chronically inflamed non-lymphoid tissues in association with microbial infections, graft rejection, and autoimmune disorders [reviewed in [11]]. Some of these TLS have considerable morphological similarities to conventional secondary lymphoid organs. For example, TLS often exhibit organized T- and B-cell compartments, a stromal infrastructure that produces homing chemokines and survival factors, lymphatic vessels, and high endothelial-like vessels that express peripheral node addressin (PNAd) [12–14]. Alternatively, TLS-like structures found in adipose tissue display all of the above characteristics expect for discernable T- and B-cell compartmentalization [15, 16]. TLS have been documented in association with a wide variety of primary and metastatic solid tumors in humans. Their presence is almost always a favorable prognostic indicator for patient survival [17, 18]. Higher densities of TLS correlate with higher representation of tumor-infiltrating CD8+ T lymphocytes [19, 20]. Additionally, the presence of TLS associates with infiltrates that display an activated and cytotoxic immune signature [21]. These observations suggest that tumor-associated TLS serve as productive sites for in situ activation of CD8+ T lymphocytes, which in turn control tumor growth.

The availability of animal models that could enable a more comprehensive understanding of the functionality of TLS in solid cancers has been limited. Recently, we demonstrated that naïve CD8+ T cells can directly infiltrate tumors formed from two transplantable murine cell lines: B16-F1 melanoma and Lewis lung carcinoma. Once in the tumor, these naïve cells become activated, proliferate, and differentiate into immune effectors [22]. This infiltration is dependent on the development of tumor-associated blood vessels that express PNAd and CCL21, the ligands that engage CD62L and CCR7 on naïve and central memory T cells, respectively, and enable them to enter lymph nodes (LN) [23]. Interestingly, tumors growing in the peritoneal cavity, but not subcutaneously, develop intratumoral TLS in association with this PNAd+/CCL21+ LN-like tumor vasculature. In this chapter, we describe methods for the development, identification, and characterization of intratumoral TLS in intraperitoneal B16 melanoma tumors. Additionally, we describe an adoptive transfer method to demonstrate the function of the PNAd+/CCL21+ LN-like tumor vasculature in promoting naïve T-cell infiltration.

2 Materials

2.1 Implantation of Murine Melanoma Tumors

1. B16-OVA melanoma cell line (*see* **Note 1**).
2. Complete medium: RPMI-1640 supplemented to a final concentration of 5% (v/v) fetal bovine serum (FBS), 2 mM L-glutamine, and 15 mM HEPES.
3. Trypsin-EDTA solution: 0.5% Trypsin-EDTA diluted 1:10 in Ca^{2+}/Mg^{2+}-free Hanks' balanced salt solution with sodium bicarbonate.
4. PBS: Ca^{2+}/Mg^{2+}-free phosphate-buffered saline, pH 7.4.
5. 15 mL Capped conical polystyrene tubes.
6. T75 cm^2 culture flask.
7. MACS 70 μm Smart Strainers (Miltenyi).
8. 6–8-Week-old C57BL/6 mice.
9. Tribromoethanol working solution: Dissolve 1.25 g of tribromoethanol in 25 mL of tert-amyl alcohol. Dilute 1.25 mL of this solution into 50 mL of water.
10. 1 mL Tuberculin syringes pre-attached with a 25 G × 5/8 in. needle.

2.2 Preparation of Murine Melanoma Tumors

1. Tribromoethanol working solution (as described in Subheading 2.1, **step 9**).
2. Surgical scissors, forceps, and tweezers.
3. 50 mL Capped conical polystyrene tubes.
4. Platform rocker.
5. PBS (*see* Subheading 2.1).
6. Fixative solution: 4% (w/v) Paraformaldehyde (PFA) in PBS.
7. Cryopreservation solution: 30% (w/v) Sucrose in PBS.
8. 25 mm × 20 mm × 5 mm Cryomolds (Tissue-Tek).
9. O.C.T. compound (Tissue-Tek).
10. Superfrost Plus Microscope Slides (Fisher Scientific).
11. Cryostat preset to −20 °C.
12. Dry ice.

2.3 Immunofluorescent Staining

1. Glass Coplin jar.
2. Slide humidity chamber.
3. −20 °C Freezer.
4. KimWipes.

5. Rat anti-mouse CD16/CD32 monoclonal blocking antibody (BioXcell).
6. Methanol, histological grade, 98%.
7. Staining buffer: 5% (w/v) Bovine serum albumin (BSA) in PBS.
8. Avidin/biotin blocking kit (Vector Laboratories).
9. Quenching solution: 3% Hydrogen peroxide, 0.1% (w/v) sodium azide in PBS.
10. Tris–NaCl blocking buffer (TNB): 0.1 M Tris–HCl, pH 7.5, 150 mM NaCl, 0.5% (w/v) tyramide signal amplification blocking reagent (PerkinElmer).
11. Tyramide signal amplification (TSA) plus biotin kit (Perkin Elmer).
12. Monoclonal antibodies for immunofluorescent staining (Table 1).
13. DyLight-550-conjugated streptavidin (Thermo Fisher Scientific).
14. ProLong Gold Antifade Mountant with DAPI (Thermo Fisher Scientific).
15. 25 × 50 Premium cover glasses.
16. Horseradish peroxidase-conjugated streptavidin.

2.4 Preparation of Tumor Tissue

1. 10× MACS buffer: 0.5% (w/v) BSA, 2 mM EDTA.
2. 10× PBS.
3. Awesome MACS buffer: 100 mL of 10× MACS buffer, 100 mL of 10× PBS; 10 mL of 200 mM L-glutamine solution, 10 mL of 100× sodium pyruvate solution, 10 mL of 100× non-essential amino acid solution, 20 mL of 50× essential amino acid solution, and 4.5 g of glucose in 1 L final volume.

Table 1
Antibodies for detecting TLS in tumors by immunofluorescence

Specificity	Clone	Conjugate	Supplier	Working dilution
PNAd	MECA-79	Biotin	BioLegend	1:50
CD31	390	Alexa Fluor 647	BioLegend	1:100
Podoplanin	8.1.1	eFluor 660	ThermoScientific/eBioscience	1:100
B220	RA3-6B2	Alexa Fluor 488	BioLegend	1:100
CD11c	N418	Biotin	BioLegend	1:50
CD3	17A2	Alexa Fluor 647	BioLegend	1:50

Adjust pH to 7.4 and filter solution with a 0.22 μm steritop filter.

4. Digestion buffer: 10 mL of FBS, 5 mL of 200 mM L-glutamine, 5 mL of 100× sodium pyruvate, 5 mL of 100× non-essential amino acids, 10 mL of 50× essential amino acids, 500 μL of 10 mg/mL gentamicin, and 7.5 mL of 1 M HEPES in 500 mL final volume of L-glutamine-free and sodium pyruvate-free Dulbecco's modified Eagle's medium (DMEM).
5. Working buffer: 0.42 U/mL of Liberase™ (Sigma) and 60 U/mL of DNase I (Sigma) in digestion buffer.
6. Harvest buffer: 50 mL of FBS, 5 mL of 200 mM L-glutamine, 5 mL of 100× sodium pyruvate, 5 mL of 100 × non-essential amino acids, 10 mL of 50× essential amino acids, 500 μL of 10 mg/mL gentamicin, and 7.5 mL of 1 M HEPES in 500 mL final volume of DMEM.
7. MACS 70 μm Smart Strainers (Miltenyi).
8. Red Blood Cell Lysing Buffer Hybri-Max (Sigma).
9. Water or bead bath set at 37 °C.
10. Mouse CD45 MicroBeads (Miltenyi Biotec).
11. Anti-biotin MicroBeads (Miltenyi Biotec).
12. LS columns (Miltenyi Biotec).
13. MACS manual magnetic separator (Miltenyi Biotec).
14. Monoclonal antibodies for enrichment (Table 2).
15. Monoclonal antibodies for cell surface staining (Table 3).
16. Rat anti-mouse CD16/CD32 monoclonal blocking antibody (BioXcell).
17. Polystyrene 96-well, No Lid, V-bottom plate.
18. 5 mg/mL DAPI viability dye.

2.5 Adoptive Transfer of $CD8^+$ T Lymphocytes

1. 6–8-Week-old C57BL/6 mice bearing 10–14-day-old B16-OVA tumors (Subheading 3.1).
2. 6–8-Week-old congenic Thy1.1 mice (*see* **Note 2**).
3. Tribromoethanol working solution (*see* Subheading 2.1, **step 9**).
4. CTL medium: 50 mL of FBS, 5 mL of 200 mM L-glutamine, 5 mL of 100× sodium pyruvate, 5 mL of 100× non-essential amino acids, 10 mL of 50× essential amino acids, 500 μL of 10 mg/mL gentamicin, 7.5 mL of 1 M HEPES, and 454 μL of 55 mM β-mercaptoethanol in a final volume of 500 mL of RPMI-1640.
5. Autoclaved 7 mL Dounce homogenizer.
6. MACS 70 μm Smart Strainers (Miltenyi).

Table 2
Antibodies for magbead enrichment of stromal populations for flow cytometry

Specificity	Clone	Conjugate	Supplier	Working dilution
Podoplanin	8.1.1	Biotin	BioLegend	1:1000
CD31	390	Biotin	BioLegend	1:1000

Table 3
Antibodies for flow cytometry staining of cell surface markers on stromal and lymphocyte populations

Specificity	Clone	Conjugate	Supplier	Working dilution
CD45	30-F11	Alexa Fluor 488	BioLegend	1:2000
CD3	17A2	Alexa Fluor 647	BioLegend	1:500
CD19	6D5	PE-Cy7	BioLegend	1:1000
CD8α	53–6.7	APC-eFluor780	ThermoScientific/eBioscience	1:1000
Podoplanin	8.1.1	APC	BioLegend	1:1000
CD31	390	PerCP-Cy5.5	BioLegend	1:1000
Ter119	Ter119	PE-Cy7	BioLegend	1:500
Thy1.1	HIS51	PE	ThermoScientific/eBioscience	1:1000

7. Red Blood Cell Lysing Buffer Hybri-Max (Sigma).
8. Awesome MACS buffer (Subheading 2.4, **step 3**).
9. Naïve $CD8^+$ T cell isolation kit (Miltenyi Biotec).
10. LS columns (Miltenyi Biotec).
11. MACS manual magnetic separator (Miltenyi Biotec).
12. Heating lamp with a 250 W (infrared) bulb.
13. Tailveiner restrainer (BrainTree Scientific, Inc.).
14. 1 mL Tuberculin syringes pre-attached with a 25 G × 5/8 in. needle.

3 Methods

3.1 Implantation of Subcutaneous and Intraperitoneal Murine Melanoma Tumors

1. Culture B16-OVA melanoma cells in complete medium in a T75 flask to 60–70% confluency.
2. Aspirate supernatant, rinse flask with 5 mL room-temperature trypsin-EDTA solution, and aspirate again. Add 5 mL trypsin-EDTA solution and tilt to cover the bottom of the flask. Incubate for 2–3 min at 37 °C, or until cells have fully detached.

3. Add 5 mL cold complete medium and transfer cell suspension to a 15 mL conical tube. Rinse flask with 5 mL cold complete medium and add to the 15 mL conical tube. Centrifuge for 5 min at 600 × *g* at 4 °C.
4. Aspirate supernatant, resuspend in 5 mL cold complete medium, and centrifuge for 5 min at 600 × *g* at 4 °C.
5. Aspirate supernatant, resuspend in 5 mL cold PBS, and centrifuge for 5 min at 600 × *g* at 4 °C. Repeat once more.
6. Resuspend in 5 mL cold PBS, pass through MACS Smart Strainer into a new 15 mL conical tube, count live cells, and adjust to 2×10^6 cells/mL with cold PBS.
7. For subcutaneous tumors only, anesthetize mice by intraperitoneal injection of 15 μL tribromoethanol working solution per gram of mouse weight (*see* **Note 3**).
8. Subcutaneously or intraperitoneally inject 200 μL (4×10^5 cells) of cell suspension into C57BL/6 mice with a 1 mL syringe with a 25 G × 5/8 in. needle. Allow subcutaneous tumors to grow for 14 days and intraperitoneal tumors to grow for 12 days (*see* **Note 4**).

3.2 Preparation of Murine Melanoma Tumors for Immunofluorescence Microscopy

1. Anesthetize mice by intraperitoneal injection of 25 μL tribromoethanol working solution per gram of mouse weight. Euthanize by cervical dislocation and dissect out tumor with surgical scissors and forceps.
2. Transfer each tumor to a separate 50 mL conical tube containing 10 mL room-temperature PBS. Rock on platform rocker for 5 min at room temperature.
3. Using forceps, transfer tumor to a new 50 mL conical tube containing 30 mL room-temperature fixative solution. Cap and gently rock for 1 h at room temperature (*see* **Note 5**).
4. Using forceps, transfer tumor to a new 50 mL conical tube containing 30 mL cold cryopreservation solution and gently rock overnight at 4 °C.
5. Aspirate cryopreservation solution, transfer tumor to Cryomold with forceps, embed it in OCT, and place on dry ice for 30 min.
6. Cut 7 μm sections with a −20 °C cryostat and mount on Superfrost Plus microscope slides.

3.3 Immunofluorescent Staining of Cell Surface Markers on Formalin-Fixed Tumor Sections

1. Immerse slides in a Coplin jar containing cold methanol for 10 min at −20°C.
2. Remove slides, wipe off excess methanol with KimWipes, and air-dry for 10 min at room temperature.
3. Immerse slides in a Coplin jar containing PBS for 10 min at room temperature.

4. Remove slides, place in a humidity chamber, and pipette 200 μL 0.5 μg/mL anti-CD16/32 antibody in staining buffer uniformly across sections. Incubate for 15 min at room temperature to block Fc receptors.
5. Immerse slides in a Coplin jar containing PBS for 5 min at room temperature. Remove slides, blot off liquid with KimWipes, and place in humidity chamber.
6. Pipette 200 μL Avidin D solution from avidin/biotin blocking kit uniformly across sections. Incubate for 15 min at room temperature to block endogenous biotin. Wash as in **step 5**.
7. Pipette 200 μL biotin solution from avidin/biotin blocking kit uniformly across sections. Incubate for 15 min at room temperature to block Avidin D. Wash as in **step 5**.
8. Pipette 200 μL quenching solution from avidin/biotin blocking kit uniformly across sections. Incubate for 30 min at room temperature to block endogenous peroxidases. Wash as in **step 5**.
9. Pipette 200 μL biotin-conjugated anti-PNAd antibody in TNB buffer uniformly across sections. Incubate overnight at 4°C. Wash as in **step 5**.
10. Pipette 200 μL horseradish peroxidase-conjugated streptavidin in TNB buffer uniformly across sections. Incubate for 45 min at room temperature. Wash as in **step 5** (*see* **Note 6**).
11. Pipette 200 μL 0.5 μg/mL biotin-conjugated tyramide from TSA kit uniformly across sections. Incubate for 10 min at room temperature. Wash as in **step 5**.
12. Pipette 200 μL 0.5 μg/mL of DyLight550-conjugated streptavidin in staining buffer uniformly across sections. Incubate for 1 h at room temperature. Wash as in **step 5**.
13. Pipette cell surface marker antibody cocktail in staining buffer (Table 1) (*see* **Note 7**) uniformly across sections. Incubate for 1 h at room temperature. Wash as in **step 5**.
14. Apply ProLong Gold DAPI Antifade Mountant and apply coverslip.

3.4 Identification and Characterization of TLS in B16 Melanoma by Immunofluorescence

Acquisition and analysis of immunofluorescent images can be performed with any fluorescent microscope and image software package, respectively. We use a Zeiss AxioImager with Apotome and an AxioCam MRm camera, and Zeiss Zen image analysis software. We define intratumoral TLS to have the following features:

1. Aggregates of 50 or more $B220^+$ B lymphocytes in juxtaposition to $PNAd^+$ $CD31^+$ vasculature: Note that such aggregates are present in intraperitoneal tumors (Fig. 1e–h), but lacking in subcutaneous tumors (Fig. 1a–d), despite the presence of

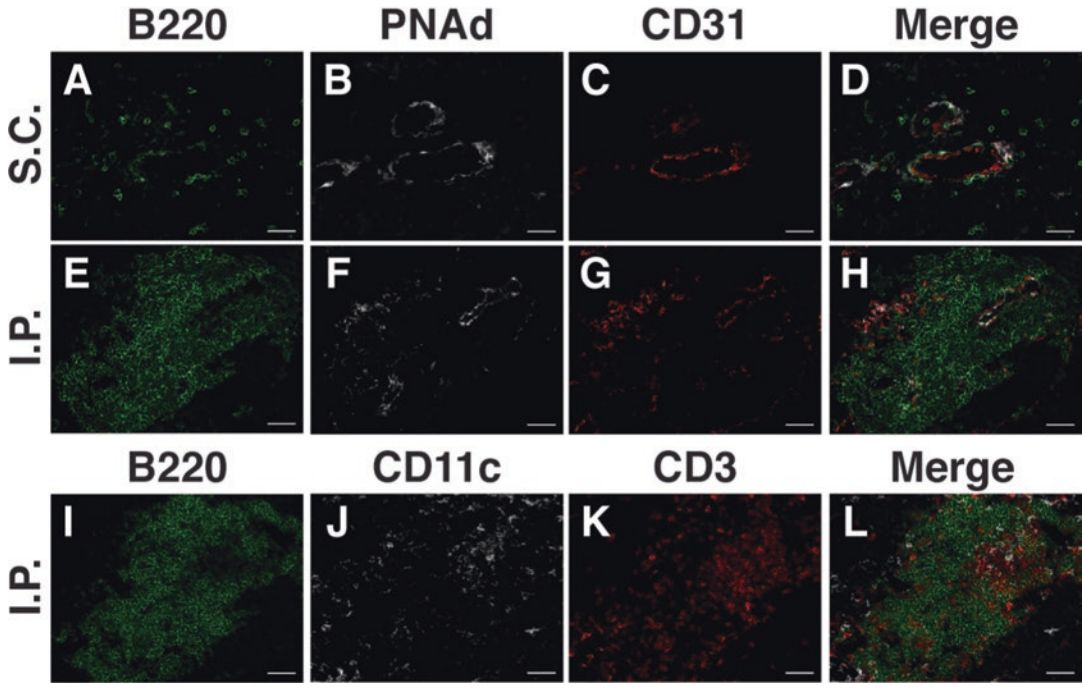

Fig. 1 B16-OVA tumors grown in the subcutaneous (**a**–**d**) or intraperitoneal (**e**–**l**) cavities of C57BL/6 mice were harvested, histologically prepared, and stained for immunofluorescent microscopy, as outlined in Subheadings 3.1–3.3. Tumor sections were stained with antibodies of the indicated specificities (Table 1). (**e**–**h**) and (**i**–**l**) are serial sections of a single B16-OVA intraperitoneal tumor. *Abbreviations*: *S.C.* subcutaneous and *I.P.* intraperitoneal. Scale bar = 50 μm

PNAd$^+$ vasculature and small numbers of B220$^+$ B lymphocytes.

2. T lymphocytes and CD11c$^+$ antigen-presenting cells intermingled with B lymphocyte aggregates (Fig. 1i–l).
3. A co-extensive reticular network of podoplanin$^+$ fibroblasts (Fig. 2a–d).
4. Additional characteristics of TLS in B16-OVA tumors are shown in Fig. 2e–h.

3.5 Preparation, Enrichment, and Cell Surface Marker Staining of Tumor-Associated Hematopoietic and Stromal Cells for Flow Cytometry

1. Anesthetize mice by intraperitoneal injection of 25 μL tribromoethanol working solution per gram of mouse weight. Euthanize by cervical dislocation and dissect out tumor with surgical scissors and forceps. Transfer to a weigh boat filled with cold digestion buffer (*see* **Note 8**).
2. Aspirate digestion buffer from weigh boat and mince tumor with scissors into ~1 mm^3 pieces. Flush minced tumor into a 15 mL conical tube with 5 mL of working buffer (*see* **Note 9**). Incubate for 30 min in a 37°C water bath. Pipette suspension gently at 5-min intervals to break up aggregates (*see* **Note 10**).

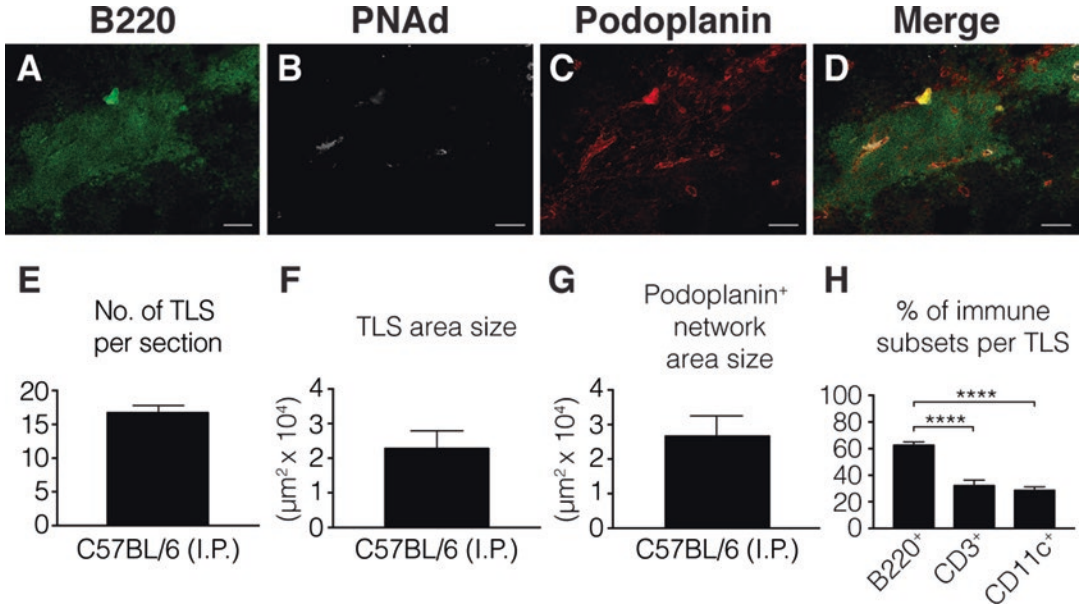

Fig. 2 A B16-OVA tumor growing in the intraperitoneal cavity of a C57BL/6 mouse was harvested, histologically prepared, and stained for immunofluorescent microscopy (**a**–**d**), as outlined in Subheadings 3.1–3.3. Tumor sections were stained with antibodies of the indicated specificities (Table 1). Scale bar = 100 μm. (**f**–**g**) Area measurements were done by drawing a perimeter around TLS and podoplanin⁺ structures with the polygon tool in Zen software. Frequency of TLS (**e**) and individual immune subsets (**h**) was assessed by using the manual count tool in Zen software. *Abbreviation*: *IP* intraperitoneal. Error bars represent mean ± SEM. ns: $P > 0.05$, *$P < 0.05$, **$P < 0.01$, ***$P < 0.001$, ****$P < 0.0001$. *P* values in (**h**) were calculated using the Mann-Whitney test

3. Pass suspension through MACS Smart Strainer into a new 15 mL conical tube. Wash digestion tube with 5 mL cold harvest buffer and pass through filter. Centrifuge for 5 min at 600 × *g* at 4°C.
4. Aspirate supernatant, resuspend in 5 mL cold harvest buffer, centrifuge for 5 min at 600 × *g* at 4°C, and aspirate supernatant.
5. Resuspend in 2 mL Red Blood Cell Lysing Buffer Hybri-Max. Incubate for 1 min at 37°C.
6. Add 8 mL cold harvest buffer, centrifuge for 5 min at 600 × *g* at 4°C, and aspirate supernatant. Repeat this step twice.
7. Resuspend in 5 mL cold Awesome MACS buffer (*see* **Note 8**) and count viable cells. A typical cell yield for a B16-OVA tumor is 5×10^7. Centrifuge for 5 min at 600 × *g* at 4°C and aspirate supernatant.
8. Resuspend in 80 μL cold Awesome MACS buffer and 20 μL CD45 MicroBeads per 10^7 cells. Mix by inverting the 15 mL conical tube and incubate on ice for 15 min. Centrifuge for

5 min at 600 × *g* at 4°C and aspirate supernatant. Resuspend in cold Awesome MACS buffer to 2×10^8 cells/mL. Proceed immediately to magnetic separation.

9. Rinse LS column in a MACS manual magnetic separator with 3 mL of cold Awesome MACS buffer.
10. Pipette cell suspension onto column and allow to flow by gravity. Collect $CD45^{Neg}$ cells that flow through into a new 15 mL conical tube. Rinse column with 3 mL of cold Awesome MACS buffer three times, collecting $CD45^{Neg}$ cells that flow though into same collection tube. Count viable cells, cap tube, and keep on ice. A typical cell yield of $CD45^{Neg}$ cells from a B16-OVA tumor is 4×10^7.
11. Remove column from magnetic separator and insert into a new 15 mL conical tube. Apply 3 mL of cold Awesome MACS buffer and firmly flush out $CD45^{Pos}$ cells with supplied plunger. Count viable cells, cap tube, and keep on ice. A typical cell yield of $CD45^{Pos}$ cells from a B16-OVA tumor is 1×10^7.
12. Centrifuge $CD45^{Neg}$ cells for 5 min at 600 × *g* at 4°C. Aspirate supernatant, and resuspend in cold Awesome MACS buffer at 10^7 cells/mL. Add biotinylated anti-podoplanin and/or anti-CD31 (Table 2) to a final concentration of 0.5 μg/mL. Incubate on ice for 30 min. Centrifuge for 5 min at 600 × *g* at 4°C and aspirate supernatant.
13. Resuspend $CD45^{Neg}$ cells in 80 μL cold Awesome MACS buffer and 20 μL of anti-biotin MicroBeads per 10^7 cells. Mix by inverting the tube and incubate for 15 min on ice. Centrifuge for 5 min at 600 × *g* at 4°C and aspirate supernatant. Resuspend in cold Awesome MACS buffer to 2×10^8 cells/mL.
14. Repeat **steps 9–11** with a new LS column using these $CD45^{Neg}$ cells as input. Discard cells that flow through while the column is in the magnetic separator, and collect the $podoplanin^+$ and/or $CD31^+$ cells that are eluted with the plunger after the column is removed from the separator.
15. Centrifuge the $CD45^{Pos}$ cells collected in **step 11** and enriched stromal fraction collected in **step 14** for 5 min at 600 × *g* at 4°C. Aspirate supernatant and resuspend in 5 mL of cold Awesome MACS buffer. Centrifuge for 5 min at 600 × *g* at 4°C and aspirate supernatant.
16. Resuspend $CD45^{Neg}$ cells in 100 μL cold Awesome MACS buffer and pipet entire suspension to a 96-well plate. Resuspend $CD45^{Pos}$ cells in 1 mL cold Awesome MACS buffer and pipet 100 μL (1×10^6 cells) to same 96-well plate. Centrifuge for 5 min at 600 × *g* at 4 °C and aspirate supernatant.
17. Resuspend both fractions in 100 μL cold Awesome MACS buffer containing 0.5 μg/mL of anti-CD16/32. Incubate for

15 min at 4°C, centrifuge for 5 min at 600 × g at 4 °C, and aspirate supernatant.

18. Resuspend $CD45^{Pos}$ cells in 100 μL cold Awesome MACS buffer with CD45, CD3, CD8α, and CD19 antibodies, and the $CD45^{Neg}$ cells in 100 μL of cold awesome MACS buffer with CD45, Ter119, CD31, and gp38 antibodies (Table 3). Incubate for 30 min at 4°C, centrifuge for 5 min at 600 × *g* at 4 °C, and aspirate supernatant.
19. Resuspend both fractions in 5 mL cold Awesome MACS buffer. Centrifuge for 5 min at 600 × *g* at 4°C and aspirate supernatant. Repeat this step twice.
20. Resuspend both fractions in 1 mL cold Awesome MACS buffer containing 0.2 μg/mL DAPI. Incubate for 30 min at 4°C, and analyze by flow cytometry.

3.6 Cellular Characteristics of TLS Containing B16 Melanoma Tumors by Flow Cytometry

We utilize Beckman Coulter CytoFlex S units for acquisition, and imported FCS files into FlowJo software (TreeStar) for analysis. While flow cytometry does not enable TLS-associated cells to be directly distinguished from non-TLS-associated cells in tumors, we have found significant quantitative differences between IP and SC tumors in certain populations that are TLS-associated. For comparably sized tumors, the number of $CD31^+$ endothelial cells is actually lower in IP tumors (Fig. 3a). However, the number of $podoplanin^+$ fibroblasts is substantially higher (Fig. 3b). While the podoplanin/CD31 ratio in SC tumors is slightly less than 1, the ratio in IP tumors is about 3.5, consistent with the presence of the reticular network that is evident by immunofluorescence (Fig. 3c). This provides a method to further delineate the characteristics of both populations in these different tumor microenvironments. Similarly, the average number of B lymphocytes in IP tumors is about tenfold greater than in SC tumors (Fig. 3d), and these are largely concentrated in TLS. The number of T cells in both tumors is comparable, about 10^6 cells.

3.7 Adoptive Transfer of Naïve $CD8^+$ T Lymphocytes into Mice with Established Tumors

1. Follow steps in Subheading 3.1 to grow intraperitoneal or subcutaneous B16-OVA melanoma cells in C57BL/6 mice.
2. Eighteen hours prior to tumor harvest, anesthetize one or more (*see* **Note 11**) congenic Thy1.1 mice by intraperitoneal injection of 25 μL tribromoethanol working solution per gram of mouse weight. Euthanize by cervical dislocation and dissect lymph nodes (axillary, brachial, inguinal, cervical, and mesenteric) and spleen with surgical scissors and forceps. Pool tissues into an autoclaved Dounce homogenizer containing 5 mL of cold CTL medium and homogenize to create a single-cell suspension.

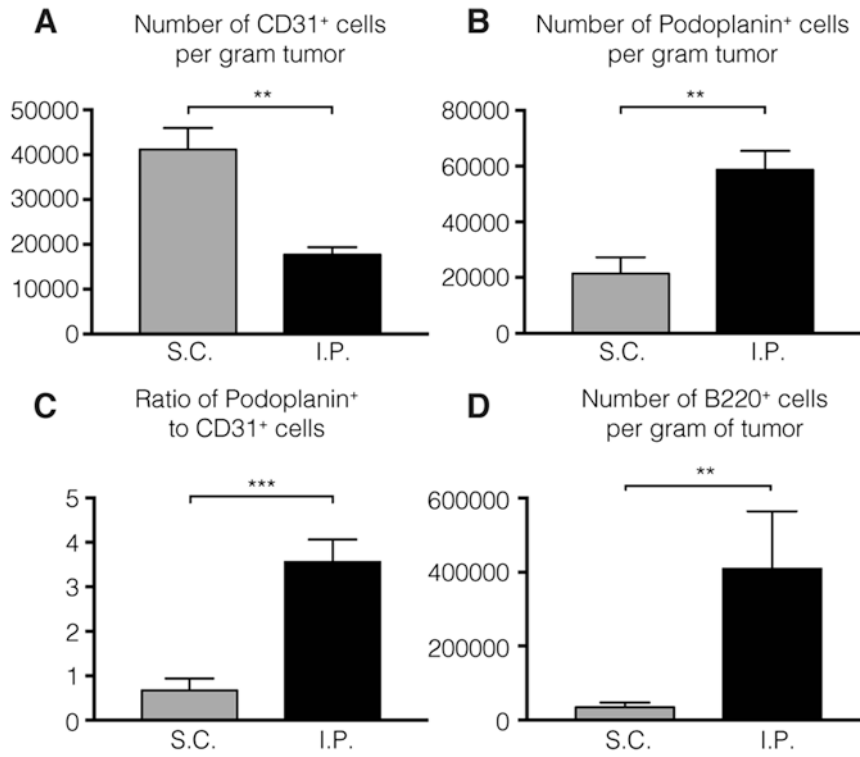

Fig. 3 Intraperitoneal and subcutaneous B16-OVA tumors grown in C57BL/6 mice were prepared for flow cytometry, as outlined in Subheadings 3.1 and 3.4. Endothelial cells were gated as live singlet $CD45^{neg}$ $Ter119^{neg}$ $CD31^{pos}$. Fibroblasts are gated as live singlet $CD45^{neg}$ $Ter119^{neg}$ $podoplanin^{pos}$. B cells are gated as live singlet $CD45^{pos}$ $CD3^{neg}$ $CD19^{pos}$. *Abbreviations*: *SC* subcutaneous and *IP* intraperitoneal. Error bars represent mean ± SEM. ns: $P > 0.05$, $^{*}P < 0.05$, $^{**}P < 0.01$, $^{***}P < 0.001$, $^{****}P < 0.0001$. *P* values were calculated using the Mann-Whitney test

3. Pipet suspension through MACS Smart Strainer into a 15 mL conical tube. Wash homogenizer with 5 mL cold CTL medium and pipet through filter. Centrifuge for 5 min at 600 × *g* at 4°C and aspirate supernatant.
4. Resuspend in 2 mL Red Blood Cell Lysing Buffer Hybri-Max and incubate for 1 min in a 37°C water bath. Add 8 mL cold CTL medium, centrifuge for 5 min at 600 × *g* at 4°C, and aspirate supernatant.
5. Resuspend in 5 mL cold Awesome MACS buffer, count viable cells, and adjust to 10^8/400 μL. Add 100 μL of naïve CD8α T-cell biotin-antibody cocktail (supplied with kit) per 10^8 cells. Mix by inverting tube and incubate for 5 min on ice.
6. Add 200 μL cold Awesome MACS buffer, 200 μL anti-biotin Microbeads, and 100 μL of CD44 MicroBeads per 10^8 cells (both supplied with kit). Mix by inverting tube and incubate for 10 min on ice.

7. Add 10 mL cold Awesome MACS buffer, centrifuge for 5 min at 600 × *g* at 4 °C, and aspirate supernatant. Resuspend in 500 μL cold Awesome MACS buffer per 10^8 cells.
8. Apply suspension to a pre-rinsed LS column (Subheading 3.5) attached to a magnetic separator. Collect flow-through into a new 15 mL conical tube. Rinse column with 3 mL cold Awesome MACS buffer and collect flow-through into the same tube. Centrifuge collection tube for 5 min at 600 × *g* at 4°C and aspirate supernatant.
9. Resuspend in 5 mL cold PBS, centrifuge for 5 min at 600 × *g* at 4 °C, and aspirate supernatant. Resuspend in 5 mL of cold PBS, determine the cell count, and adjust to a final concentration of 2×10^7 cells/mL.
10. Place a single tumor-bearing C57BL/6 mice under an infrared heat lamp until lateral tail veins are apparent (typically 3–5 min).
11. Restrain mouse in a Tailveiner and inject 200 μL (4×10^6 cells) into the lateral tail vein using a 1 mL syringe with a 25 G × 5/8 in. needle. Repeat **steps 10** and **11** for additional tumor-bearing animals.
12. Eighteen hours after adoptive transfer (*see* **Note 12**), tumor-infiltrating $CD8^+$ T lymphocytes can be isolated and quantitated as described in Subheading 3.5 using the antibody cocktail described in Table 3, with the addition of anti-Thy1.1. Typical results are shown in Fig. 4.

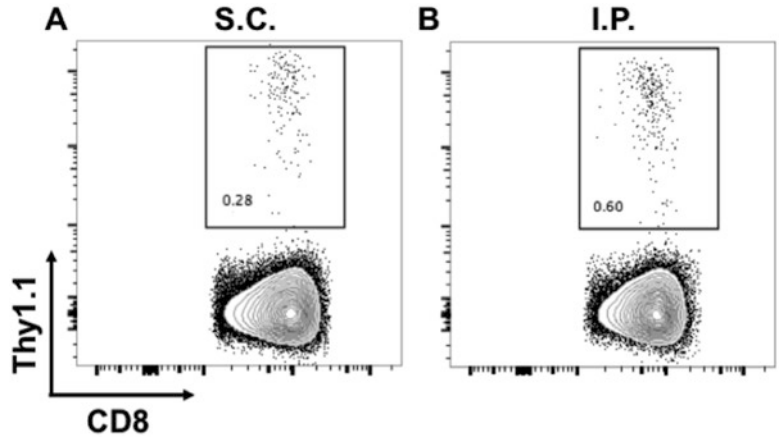

Fig. 4 Naïve $CD8^+$ T cells from congenic Thy1.1 mice were intravenously injected into C57BL/6 mice with established subcutaneous (**a**) and intraperitoneal (**b**) B16-OVA tumors. Tumors were harvested 18 h later and infiltrating $Thy1.1^{pos}$ T cells were enumerated by flow cytometry. Numbers on plots indicate the percentage of $Thy1.1^{pos}$ cells out of the live singlet $CD45^{pos}$ $CD3^{pos}$ $CD8\alpha^{pos}$ parent gate. *Abbreviations*: *S.C.* subcutaneous and *I.P.* intraperitoneal

4 Notes

1. We use a B16-F1 melanoma cell line (ATCC) transfected to stably express chicken ovalbumin (B16-OVA). These cells present the OVA_{257} epitope on H2-K^b [24]. This was determined by flow cytometry after incubating cultured B16-OVA cells overnight at 37 °C with 100 U/mL of murine recombinant IFNγ, staining with anti-mouse SIINFEKL-H-2K^b (BioLegend), and evaluating by flow cytometry.
2. We utilize congenic Thy1.1 mice to distinguish exogenous *versus* endogenous $CD8^+$ T lymphocytes. An alternative congenic marker, such as CD45.1, can be substituted.
3. We use tribromoethanol to minimize movement during subcutaneous tumor implantation. This maneuver diminishes spreading of cells after injection, and results in more regularly formed tumors.
4. These conditions lead to subcutaneous tumors that are 2 mm in each of the two measurable dimensions. Intraperitoneal tumors grow somewhat faster and may be harvested earlier for that reason. Since intraperitoneal tumors cannot be measured directly, ensure that mice do not gain more than 5–10% in bodyweight and do not show any signs of discomfort.
5. Overnight fixation provides excellent preservation of tumor morphology. However, some cell surface markers become undetectable (i.e., CD31). We've determined that 1-h fixation still provides excellent tumor morphology and detection of all markers described.
6. PNAd is expressed at relatively low levels on tumor vasculature when compared to LN-HEV. Tyramide signal amplification enables successful visualization.
7. We use B220, CD31, and PNAd to identify TLS, CD3 and CD11c to identify T cells and antigen-presenting cells, respectively, and podoplanin to identify fibroblasts. Specific fluorochromes for each are shown in Table 1, and representative staining combinations are shown in Figs. 1 and 2.
8. The steps in Subheadings 3.5 and 3.6 should be carried out as quickly as possible. Isolated endothelial cells and fibroblasts from lymphoid organs and tumors are fragile and significantly lose viability over a few hours. Awesome MACS buffer provides with nutrients to maintain their survival for the duration of the experiment. Enrichment steps and staining of isolated stromal cells should always be carried out in this buffer.
9. Liberase TM and DNase I at the concentrations specified in working buffer enable high-yield isolation of tumor-associated stromal cells from B16 without substantial loss of CD3, CD8,

CD4, and B220 on tumor-infiltrating lymphocytes. If you are assessing alternative markers or tumors, optimizing enzyme concentrations and incubation times is recommended.

10. Cell suspension should initially be pipetted several times with a cut 1000 μL pipette tip. After 10 min, aggregates should easily be pipetted with an uncut 1000 μL tip. If not, prepare a single-cell suspension using a Dounce homogenizer.
11. Pooled lymph nodes and spleen from a single congenic Thy1.1 mouse provide 4.0×10^6 naïve $CD8^+$ T cells, sufficient for two tumor-bearing animals. It is recommended to use three congenic Thy1.1 mice for a maximum of seven tumor-bearing animals.
12. Our lab and others have reported that 18 h after adoptive transfer of T lymphocytes is a sufficient amount of time to visualize their infiltration into tumors [23, 25–28]. We have also observed substantially similar levels of infiltration in 1 h [23].

Funding

This work was supported by the United States Public Health Service (USPHS) grants R01 CA78400 and R01 CA181794 (V.H.E.). Additional support was provided by USPHS grant P30 CA0044579 to the University of Virginia Cancer Center. A.B.R. was supported by USPHS training grant AI007496 and the Wagner Fellowship. J.D.P. was supported by USPHS training grant GM007276 and the Farrow Fellowship.

References

1. Vesely M, Kershaw M, Schreiber R, Smyth M (2011) Natural innate and adaptive immunity to cancer. Annu Rev Immunol 29:235–271
2. Fridman WH, Pagès F, Sautès-Fridman C, Galon J (2012) The immune contexture in human tumours: impact on clinical outcome. Nat Rev Cancer 12:298–306. https://doi.org/10.1038/nrc3245
3. Galon J, Angell HK, Bedognetti D, Marincola FM (2013) The continuum of cancer immunosurveillance: prognostic, predictive, and mechanistic signatures. Immunity 39:11–26. https://doi.org/10.1016/j.immuni.2013.07.008
4. Rosenberg SA, Restifo NP, Yang JC et al (2008) Adoptive cell transfer: a clinical path to effective cancer immunotherapy. Nat Rev Cancer 8:299–308. https://doi.org/10.1038/nrc2355
5. Klebanoff CA, Acquavella N, Yu Z, Restifo NP (2011) Therapeutic cancer vaccines: are we there yet? Immunol Rev 239:27–44. https://doi.org/10.1111/j.1600-065X.2010.00979.x
6. Lee S, Margolin K (2011) Cytokines in cancer immunotherapy. Cancers 3:3856–3893. https://doi.org/10.3390/cancers3043856
7. Pardoll DM (2012) The blockade of immune checkpoints in cancer immunotherapy. Nat Rev Cancer 12:252–264. https://doi.org/10.1038/nrc3239
8. Gajewski TF, Louahed J, Brichard VG (2010) Gene signature in melanoma associated with

clinical activity. Cancer J 16:399–403. https://doi.org/10.1097/PPO.0b013e3181eacbd8

9. Ji R-R, Chasalow SD, Wang L et al (2012) An immune-active tumor microenvironment favors clinical response to ipilimumab. Cancer Immunol Immunother 61:1019–1031. https://doi.org/10.1007/s00262-011-1172-6
10. Gajewski TF, Schreiber H, Fu Y-X (2013) Innate and adaptive immune cells in the tumor microenvironment. Nat Immunol 14:1014–1022. https://doi.org/10.1038/ni.2703
11. Pitzalis C, Jones GW, Bombardieri M, Jones SA (2014) Ectopic lymphoid-like structures in infection, cancer and autoimmunity. Nat Rev Immunol 14:447–462. https://doi.org/10.1038/nri3700
12. Kratz A, Campos-Neto A, Hanson MS, Ruddle NH (1996) Chronic inflammation caused by lymphotoxin is lymphoid neogenesis. J Exp Med 183:1461–1472. https://doi.org/10.1084/jem.183.4.1461
13. Buckley CD, Barone F, Nayar S et al (2015) Stromal cells in chronic inflammation and tertiary lymphoid organ formation. Annu Rev Immunol 33:715–745. https://doi.org/10.1146/annurev-immunol-032713-120252
14. Ruddle NH (2016) High endothelial venules and lymphatic vessels in tertiary lymphoid organs: characteristics, functions, and regulation. Front Immunol 7:491. https://doi.org/10.3389/fimmu.2016.00491
15. Randall TD, Mebius RE (2014) The development and function of mucosal lymphoid tissues: a balancing act with micro-organisms. Mucosal Immunol 7:455–466. https://doi.org/10.1038/mi.2014.11
16. Cruz-Migoni S, Caamaño J (2016) Fat-associated lymphoid clusters in inflammation and immunity. Front Immunol 7:612. https://doi.org/10.3389/fimmu.2016.00612
17. Dieu-Nosjean M-C, Goc J, Giraldo NA et al (2014) Tertiary lymphoid structures in cancer and beyond. Trends Immunol 35:571–580. https://doi.org/10.1016/j.it.2014.09.006
18. Goc J, Fridman W-H, Sautès-Fridman C, Dieu-Nosjean M-C (2013) Characteristics of tertiary lymphoid structures in primary cancers. OncoImmunology 2:e26836. https://doi.org/10.4161/onci.26836
19. Behr DS, Peitsch WK, Hametner C et al (2014) Prognostic value of immune cell infiltration, tertiary lymphoid structures and PD-L1 expression in Merkel cell carcinomas. Int J Clin Exp Pathol 7:7610–7621
20. Caro GD, Bergomas F, Grizzi F et al (2014) Occurrence of tertiary lymphoid tissue is associated with T-cell infiltration and predicts better prognosis in early-stage colorectal cancers. Clin Cancer Res 20:2147–2158. https://doi.org/10.1158/1078-0432.CCR-13-2590
21. Goc J, Germain C, Vo-Bourgais TKD et al (2014) Dendritic cells in tumor-associated tertiary lymphoid structures signal a Th1 cytotoxic immune contexture and license the positive prognostic value of infiltrating CD8+ T cells. Cancer Res 74:705–715. https://doi.org/10.1158/0008-5472.CAN-13-1342
22. Thompson ED, Enriquez HL, Fu Y-X, Engelhard VH (2010) Tumor masses support naive T cell infiltration, activation, and differentiation into effectors. J Exp Med 207:1791–1804. https://doi.org/10.1084/jem.20092454
23. Peske JD, Thompson ED, Gemta L et al (2015) Effector lymphocyte-induced lymph node-like vasculature enables naive T-cell entry into tumours and enhanced anti-tumour immunity. Nat Commun 6:7114. https://doi.org/10.1038/ncomms8114
24. Hargadon KM, Brinkman CC, Sheasley-O'Neill SL et al (2006) Incomplete differentiation of tumor-specific CD8+ T cells in tumor-draining lymph nodes. J Immunol 177:6081–6090
25. Palazón A, Teijeira A, Martínez-Forero I et al (2011) Agonist anti-CD137 mAb act on tumor endothelial cells to enhance recruitment of activated T lymphocytes. Cancer Res 71:801–811. https://doi.org/10.1158/0008-5472.CAN-10-1733
26. Sasaki K, Zhu X, Vasquez C et al (2007) Preferential expression of very late antigen-4 on type 1 CTL cells plays a critical role in trafficking into central nervous system tumors. Cancer Res 67:6451–6458. https://doi.org/10.1158/0008-5472.CAN-06-3280
27. Scimone ML, Aifantis I, Apostolou I et al (2006) A multistep adhesion cascade for lymphoid progenitor cell homing to the thymus. Proc Natl Acad Sci 103:7006–7011. https://doi.org/10.1073/pnas.0602024103
28. Walch JM, Zeng Q, Li Q et al (2013) Cognate antigen directs CD8+ T cell migration to vascularized transplants. J Clin Invest 123:2663–2671. https://doi.org/10.1172/JCI66722

Chapter 15

Investigating Tumor-Associated Tertiary Lymphoid Structures in Murine Lung Adenocarcinoma

Kelli A. Connolly, Mursal Nader, and Nikhil Joshi

Abstract

Genetically engineered mouse models (GEMMs), in which autochthonous tumors develop into advanced-stage disease in the presence of a functional immune system, have contributed significantly to the understanding of most types of cancer. Using a GEMM of lung adenocarcinoma, we have found that immune cells are present in complex, highly organized, lymph node (LN)-like structures known as the tumor-associated tertiary lymphoid structures (TA-TLS). TA-TLS have been characterized in human lung cancer patients, but not in animal tumor models, and hence remain untapped targets for therapeutic interventions. We have shown that TA-TLS emerge as a result of tumor growth and that therapeutically depleting regulatory T cells (T_{regs}) from TA-TLS results in tumor elimination. Hence, a strong antitumor immune response exists but is suppressed in TA-TLS. Here, we describe a high-throughput immunofluorescence (IF) analysis pipeline for visualization and quantification of TA-TLS. Imaging the relatively small size of TA-TLS within tumor-bearing lung lobes using confocal microscopy is a labor-intensive process that can take up to 1 month. We have optimized this process and reduced the time required per lung lobe to 1–2 weeks using automated microscopy methods. Combining IF with multicolor fluorescence-activated cell sorting (FACS), we are able to interrogate not only the size and location of TA-TLS but also the activation status of immune cells within these structures. Using these techniques, investigation of TLS in lung adenocarcinoma combines cutting-edge technological tools in cancer biology and immunology to interrogate a fundamental, but poorly understood, tumor-associated immune structure.

Key words Tertiary lymphoid structure, Tumor-associated tertiary lymphoid structure, Genetically engineered mouse model, Lung adenocarcinoma, Immunofluorescence, Fluorescence-activated cell sorting

1 Introduction

Tumor-associated tertiary lymphoid structures (TA-TLS) are lymph node-like aggregates that develop at sites of chronic inflammation, and have been identified in many types of human cancers. The increased presence of TLS has been correlated with improved patient outcomes in various cancer types including non-small cell lung cancer (NSCLC) [1], colorectal [2], pancreatic [3], and ovarian cancer [4]. TA-TLS share many features with secondary

Marie-Caroline Dieu-Nosjean (ed.), *Tertiary Lymphoid Structures: Methods and Protocols*, Methods in Molecular Biology, vol. 1845, https://doi.org/10.1007/978-1-4939-8709-2_15,

lymphoid tissues and are thought to play an important role in regulating the antitumor immune response [5]. Therefore, TA-TLS represent an exciting potential therapeutic target in cancer therapy. Regardless, the mechanisms by which TA-TLS impact the local and systemic immune response have not been fully elucidated. Even less is known regarding when and how TA-TLS are generated and maintained within tumor microenvironments. In large part, this is due to the dearth of appropriate preclinical models in which to study the development of TA-TLS in the context of a fully intact immune system.

Immunocompetent mouse models of cancer can be divided into two main types: injected syngeneic mouse models and genetically engineered mouse models (GEMMs). Both syngeneic mouse models and GEMMs of cancer possess caveats which provide insight regarding the absence of TA-TLS. In syngeneic models, tumor tissue or tumor cell lines are implanted into mice with the same genetic background. In these cases, tumors develop within weeks and progress rapidly, often so rapidly that the mice succumb to disease before the development of a chronic inflammatory environment present in human disease [6]. It is likely that this rapid progression from initiation of tumors to humane endpoint does not allow for the full development of TA-TLS. GEMMs, on the other hand, develop tumors over several months, and more closely mirror the histopathological features of cancer progression in humans [7]. Nevertheless, GEMMs have been shown to have a very low mutational burden compared to human cancers. In particular, oncogene-driven GEMMs of lung adenocarcinoma have been shown to harbor ~50-fold fewer somatic mutations compared to their human counterparts [8], and therefore are thought to be less "immunogenic," easily evading immune recognition [9]. To overcome these restrictions, we have designed a novel GEMM of lung adenocarcinoma in which the expression of neoantigens by tumor cells can be programmed using lentiviruses [10]. Intriguingly, the induction of neoantigen expression in tumors results in the formation of TA-TLS, highlighting the role of tumor antigens in this process.

To date, several different strategies have been used to identify and quantify the presence of TLS in human tumors. These studies assess the density of TA-TLS by identifying the presence of various immune cell populations, with the use of immunohistochemistry and/or fluorescence-activated cell sorting (FACS), or by gene expression assays to identify TLS-related gene signatures. In order to enumerate and characterize the TA-TLS in our murine model, we use a combination of immunofluorescence staining of frozen sections (IF-F) and FACS. IF-F of sequential tumor sections allows us to assess the presence and relative location of TLS in relation to the tumors themselves while concurrently determining the size of immune cell compartments within these structures. Additionally, we are able to determine the activation status of certain cell populations

within TLS, such as tumor-specific $CD8^+$ T cells, by FACS of the single-cell suspensions from these lung tumors. Using these complementary techniques, we previously demonstrated that regulatory T cells (T_{regs}) within TA-TLS actively suppress antitumor immune responses. Furthermore, immune-mediated tumor destruction is enhanced following the depletion of T_{regs} [10]. Combining these techniques to investigate TA-TLS in our clinically relevant mouse model of lung adenocarcinoma permits an in-depth interrogation of the formation, maintenance, and functions of TA-TLS.

2 Materials

2.1 Tissue Collection and Preparation

1. 1× Phosphate-buffered saline (PBS).
2. Surgical tools (i.e., scissors, forceps).
3. Fluorescently labeled anti-CD45 antibody.
4. 3 mL Syringes.
5. 18 Gauge × 1.16 mm catheter.
6. 23 Gauge needles.
7. 20 mL Syringes.
8. Periodate-lysine-paraformaldehyde fixative (PLP): 50 mM Phosphate buffer, 1% paraformaldehyde (PFA), 0.1 M L-lysine buffer (pH 7.4), 0.2% $NaIO_4$ (*see* **Note 1**).
9. 30% Sucrose in H_2O (*see* **Note 2**).
10. 30% Optimal cutting temperature (OCT) compound in 1× PBS (*see* **Note 2**).
11. Standard plastic cryomolds (25 × 20 × 5 mm) (*see* **Note 2**).
12. 100% OCT compound (*see* **Note 2**).
13. Dry ice (*see* **Note 2**).

2.2 Immunofluorescence Staining of Frozen Sections (IF-F)

1. 1× PBS.
2. Permeabilization Immunomix solution: 0.2% Bovine serum albumin (BSA), 0.05% sodium azide, 0.3% Triton X-100, and 10% mouse-specific serum antibodies in PBS. Store at 4 °C.
3. PAP pen.
4. Kimwipes.
5. Slide-staining tray.
6. Polyethylene transfer pipettes.
7. Primary antibodies against CD3, B220, and/or NKX2.1: Detailed information on the primary antibodies used in our studies is listed in Table 1 (*see* **Note 3**).
8. 0.1% Triton X-100/1× PBS.

Table 1
Antibodies for detection of TLS in IF and FACS

Marker	Species	Clone	Conjugate	Working dilution	Supplier	Method
CD3	Rabbit	Polyclonal	Unconjugated	1:100	Abcam	IF
B220	Rat	Polyclonal	FITC	1:100	BioLegend	IF
NKX2.1	Rabbit	Polyclonal	Unconjugated	1:1000	Abcam	IF
CD4	Rat	GK1.5	AF647	1:500	BioLegend	FACS
CD8	Rat	53.6.7	AF421	1:200	BioLegend	FACS
CD103	Hamster	2.00E+07	APC	1:100	eBioscience	FACS
CD44	Rat	IM7	BV421	1:200	BD Biosciences	FACS
PD-1	Rat	29F.1A12	AF421	1:200	BioLegend	FACS
CD45 (in vivo)	Rat	30-F11	PECF594	1:200	Invitrogen	FACS

9. Secondary antibodies (*see* **Note 4**).
10. 1% PFA in 1× PBS (*see* **Note 1**).
11. 1 μg/mL 4′,6-Diamidino-2-phenylindole (DAPI).
12. Antifade mounting medium.
13. Top-coat nail polish.
14. Microscope slide box(s).

2.3 Fluorescence-Activated Cell Sorting (FACS)

1. 12 × 75 mm Round-bottom polystyrene tubes.
2. 1× PBS.
3. 1× HBSS containing $MgCl_2$ and $CaCl_2$.
4. Heat-inactivated fetal bovine serum (FBS).
5. FACS buffer: 1× PBS without Mg^{2+}/Ca^{2+}, 0.5% heat-inactivated FBS, 0.1% sodium azide (*see* **Note 5**).
6. 2% PFA in FACS buffer (*see* **Note 6**).
7. Conjugated primary antibodies against CD4, CD8, CD103, CD44, and PD-1. Detailed information on the primary antibodies used in our studies is listed in Table 1 (*see* **Note 7**).
8. GentleMACS C-Tubes and dissociator (Miltenyi Biotec).
9. RPMI-1%: RPMI-1640 media containing 1% heat-inactivated FBS, 55 μM β-mercaptoethanol, 100 units/mL penicillin, 100 μg/mL streptomycin, 2 mM L-glutamine. Store at 4 °C.
10. HEPES buffer: 10 mM HEPES-NaOH (pH 7.4), 150 mM NaCl, 5 mM KCl, 1 mM $MgCl_2$, 1.8 mM $CaCl_2$. Store at 4 °C.

11. Collagenase IV stock (400×): 5 g Collagenase Type 4 (Worthington-Biochemical Corporation) diluted to 1.5 U/mL (Collagenase IV ≥160 U/mg) in HEPES buffer. Store 100 μL aliquots at −20 °C.
12. DNase I stock (400×): 100 mg DNase I grade II (Roche) diluted to 8 mg/mL in 1× HBSS containing $MgCl_2$ and $CaCl_2$. Store 50 μL aliquots at −20 °C.
13. Collagenase/DNase buffer: 1× HEPES buffer + 1× Collagenase IV and 1× DNase I (in 1× HBSS containing $MgCl_2$ and $CaCl_2$). Store at −20 °C.
14. Ammonium-chloride-potassium (ACK) lysis buffer.
15. LIVE/DEAD Fixable Dead Cell Stain kit (Thermo Fisher Scientific).
16. 20 mL Syringe and 23 gauge needle.
17. Secondary container with ice.
18. 15 mL Conical tubes.
19. 50 mL Conical tubes.
20. Hemocytometer.
21. 70 mm Strainers.
22. Trypan blue.

3 Methods

For these studies, Kras $^{\text{Lox-STOP-Lox (LSL)-G12D}}$ p53 flox/flox (KP mice) mice were used (*see* **Note 8**). As an additional tool to track tumor cell fate, KP mice were crossed with Rosa26$^{\text{LSL-tdTomato(tdT)}}$ mice to generate "KPT" mice [11] (*see* **Note 8**). In KPT mice, Cre-inducible tdT expression [12] is useful for identifying tumor cells by immunofluorescence as transformed cells fluoresce red (*see* Fig. 1). Tumors were initiated by intratracheal administration of 2.5×10^4 to 5×10^4 PFU of non-replicating lentiviruses (LVs) which co-express LucOS (firefly luciferase fused to a portion of ovalbumin and the antigenic 2C peptide) and Cre-recombinase [10]. Lungs were harvested 8–20 weeks after infection. All mice were handled according to IACUC-approved protocols and were humanely sacrificed prior to natural expiration.

If working with infected tissues, all work should be performed in a tissue culture hood. Appropriate personal protective equipment (PPE) should be worn for handing BL2 materials. Use safety caps for any centrifugation steps. Allow pipette tips and waste to soak for 30 min in 10% bleach solution inside hood, and then discard. Wipe hood surfaces with 10% bleach to disinfect, followed by 70% ethanol.

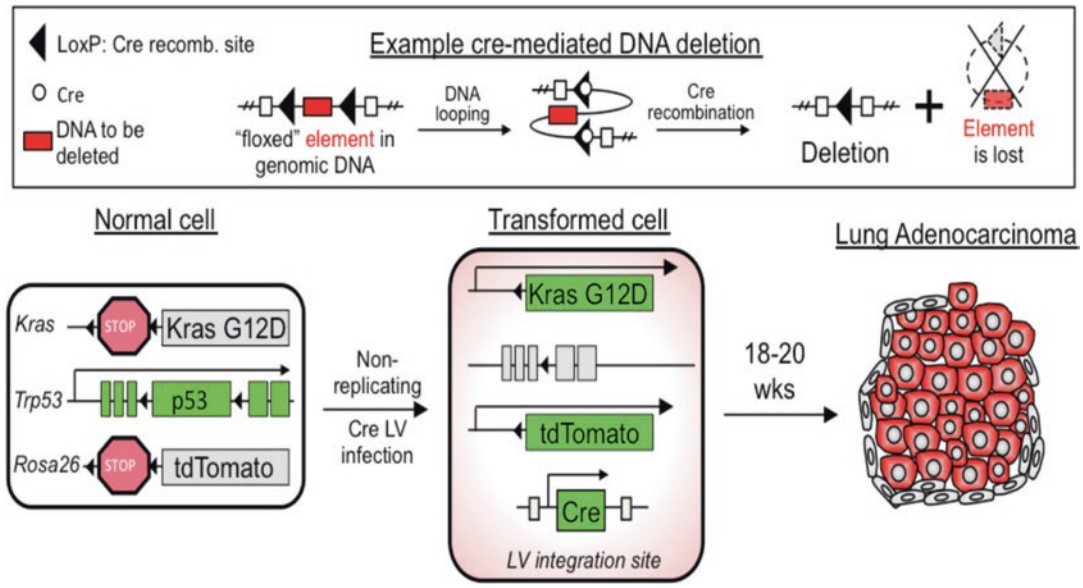

Fig. 1 Expression of the fluorescent protein Tomato in transformed lung epithelial cells. Schematic illustrating Cre recombinase-mediated DNA deletion which results in the induction of tdTomato expression by tumor cells. tdTomato provides a strong signal and facilitates the detection of small tumor cell clusters with the use of a dissecting microscope and immunofluorescence (IF) sections

3.1 Isolation and Preparation of Tumor-Bearing Lungs for IF-F

1. Following euthanasia, perform cardiac lung perfusion to flush out all blood cells from circulation: Pin ribs down to expose the lungs and heart. Gently immobilize heart with forceps. Using a 20 mL syringe and 23 gauge needle, inject 10–20 mL PBS into the right ventricle of the heart (the right ventricle is the bottom left portion of the heart from your perspective). Lungs should inflate and turn white while perfusion occurs. Allocate lung lobes for staining.
2. Preserve tissue by overnight fixation at 4 °C with PLP.
3. Perfuse and cryoprotect PLP-fixed tissues by injecting 30% sucrose solution into lung lobes and incubating lobes in 30% sucrose solution for 4–6 h at 4 °C (*see* **Note 9**).
4. Inject tissue with 30% OCT compound solution.
5. Place tissue in cryomolds and cover with 100% OCT compound and freeze by placing on dry ice.
6. Once frozen (OCT will be white and hardened), store at −80 °C.

3.2 Immunofluorescence Staining

All steps, unless otherwise noted, are done at room temperature (RT).

1. Cut sections (ranging 20–70 μm thick) at −20 °C using cryostat (*see* **Note 10**).

2. Dry tissue sections for 90 min at RT on slide-staining tray.
3. While sides are on slide-staining tray, use transfer pipette to wash tissue sections with 1× PBS for 7 min. Repeat this step two times.
4. Tip staining tray to dump liquid off of slides and into the bottom of the staining tray.
5. With a Kimwipe, gently dry the area around each tissue section.
6. Draw hydrophobic circles around tissue sections on the slides with PAP pen (*see* **Note 11**).
7. Using a transfer pipette, add drops of PBS onto the slides.
8. Block tissue sections in Immunomix for 1 h at RT.
9. Incubate sections with primary antibodies against CD3, B220, and/or NKX2.1 (*see* **Note 3**) diluted in the blocking Immunomix solution overnight at RT. Working concentrations of these antibodies are listed in Table 1.
10. Wash slides with 0.1% Triton X-100/1× PBS for 7 min. Repeat this step five times.
11. Dilute 1:500 species-specific secondary antibodies in Immunomix (*see* **Note 4**).
12. Incubate sections in secondary antibody cocktail overnight at RT.
13. Repeat **step 11**.
14. Fix tissue sections with cold 1% PFA for 15 min at RT. Once fixed, sections can be stored indefinitely.
15. If desired, incubate slides with DAPI (working concentration: 1 μg/mL) in PBS for 10 min.
16. Wash slides with 1× PBS for 7 min. Repeat this step five times.
17. Pipette antifade mounting medium onto slides, and place coverslips on top.
18. Seal slides with top coat on all sides of coverslip.
19. Store slides at 4 °C in a microscope slide box. Fixed sections can be stored indefinitely for later imaging of fluorescence. However, if DAPI is used, it is ideal to image within a few days.

3.3 Microscopy Imaging

Images were acquired on an EVOS FL Auto 2 imaging system (Thermo Fisher; *see* **Note 12**) and high-resolution Leica SP8 TCS STED confocal microscopy with ×10, ×20, and ×30 objectives. Images were analyzed using ImageJ (NIH) and Photoshop CC (Adobe Creative) (*see* **Note 13**).

3.4 Tissue Isolation and Preparation for FACS

When there is excessive tumor burden, avoid using KPT mice, or any model in which tumor cells express fluorescent protein, for FACS analysis. Differentiation of immune cells from tumor cells is made difficult as various phagocytic immune cells are capable of engulfing tumor cells along with fluorescent proteins. Note: This engulfment likely occurs during processing of tissues.

1. For in vivo labeling and exclusion of circulatory immune cells, inject fluorescently labeled anti-CD45 antibody intravenous (i.v.) for 2–5 min prior to sacrifice (*see* **Note 14**). Full information on this antibody is included in Table 1.
2. Euthanize mouse without performing cervical dislocation (*see* **Note 15**).
3. To reduce autofluorescence in FACS analysis, perform bronchoalveolar lavage (BAL): Open the peritoneal and thoracic cavity, and expose the trachea. Identify the wider opening between tracheal rings and snip using fine scissors (*see* **Note 16**). Insert needleless catheter attached to 3 mL syringe filled with 1 mL PBS, and inject PBS into trachea. Lungs should inflate. Use plunger to pull the liquid back into the syringe. While catheter remains inserted, detach syringe and discard liquid. Flush lungs with an additional 0.5–1 mL PBS and repeat this **steps 2–3** times.
4. Perform cardiac lung perfusion, as previously described (*see* Subheading 3.1, **step 1**) (*see* **Note 17**).
5. Remove mediastinal lymph node: Flip out the lungs and locate mediastinal lymph node, within the thoracic cavity, attached to the back of the trachea. Isolate with curved forceps and add it to a 15 mL conical tube with 5 mL RPMI-1% (*see* **Note 18**).
6. Isolate lungs and place lobes for FACS into gentleMACS C-Tubes containing 2.5 mL Collagenase/DNase buffer (*see* **Note 19**).
7. Isolate distant non-mediastinal lymph node for staining controls and add to 15 mL conical tube containing 5 mL RPMI-1%.
8. Place samples on ice and stain as soon as possible following isolation.

3.5 Tissue Dissociation and Staining for FACS

1. Place gentleMACS C-Tubes containing lungs and Collagenase/DNase buffer in the MACS dissociator and run on gentleMACS program m_Lung_01. Repeat the program if samples get stuck during the first run.
2. Incubate lung tissue inside gentleMACS C-Tubes at 37 °C on a shaker for 30 min.
3. While lung tissues are incubating, lymph nodes and 5 mL RPMI-1% should be transferred from 15 mL tubes into petri

dishes. Dissociate lymph nodes between two frosted glass slides and rinse slides with RPMI-1% from the petri dish so that all cells are washed off of the slides and into the dish.

4. Transfer lymph node cell suspension from petri dishes back into 15 mL tubes and wash slides with 2–3 mL additional RPMI-1%. Pool cell suspension in 15 mL tube and discard slides in sharps container.
5. Centrifuge 15 mL tubes containing lymph node cell suspensions for 5 min at 563 × *g*. Aspirate and discard the supernatant.
6. Resuspend cell pellets and count cells using a hemocytometer (*see* **Note 20**).
7. Adjust the concentration of cells to 1×10^7 cells/mL and leave on ice until they are ready to be stained alongside lung samples.
8. Following incubation, place the gentleMACS C-Tubes containing the lung tissues onto the MACS dissociator and run on gentleMACS program m_Lung_02. Again, repeat this program if samples get stuck during the first run.
9. To quench the enzymatic dissociation of lung tissues, add 0.5 mL heat-inactivated FBS, and centrifuge for 5 min at 563 × *g*.
10. Aspirate and discard supernatants from gentleMACS C-Tubes.
11. Resuspend cell pellets in 10 mL RPMI-1% and filter through 70 μm strainers into 50 mL conical tubes. Wash strainer with an additional 5 mL RPMI-1%.
12. Centrifuge samples at RT for 10 min at 563 × *g*, and discard supernatants.
13. Resuspend cell pellets in 1–2 mL ACK lysis buffer for 2 min at RT to remove any red blood cells from the samples.
14. Following red blood cell lysis, centrifuge samples at 4 °C for 10 min at 563 × *g*, discard supernatant, and resuspend pellets in 1–10 mL RPMI-1% in order to count cells with hemocytometer, as with lymph node samples in **step 6** (*see* **Note 20**).
15. Resuspend all sample cell suspensions to 10×10^7 cells/mL, and pipette 100 μL from these into appropriate flow tubes for approximately 1×10^6 cells/tube (*see* **Note 21**).
16. Wash each tube with 200 μL PBS (*see* **Note 22**), centrifuge at 4 °C for 5 min at 563 × *g*, and discard supernatant. Resuspend in 1 mL PBS.
17. To distinguish dead cells from viable cells: Use LIVE/DEAD Fixable Dead Cell Stain according to the manufacturer's instructions: Thaw supplied tube of DMSO and add 50 μL to one vial of LIVE/DEAD Fixable Aqua Dead Cell Stain (or

preferred live/dead stain). Add 1 μL of diluted Dead Cell Stain to each tube.

18. Incubate for 15 min at 4 °C in the dark.
19. Wash samples with 200 μL PBS, centrifuge at 4 °C for 5 min at 563 × *g*, and discard supernatant.
20. Prepare a cocktail of directly conjugated antibodies you wish to use, with or without tetramers (*see* **Note 23**), diluted in FACS buffer at their optimal concentrations (*see* **Note 24**). Minimally, antibodies against CD4, CD8, CD103, CD44, and PD-1 should be used to assess TLS. *See* Table 1 for information on these antibodies including species, clone, and working dilution.
21. Resuspend cells in 50 μL of antibody cocktails.
22. Incubate for 15 min at 4 °C in the dark.
23. Wash with 200 μL FACS buffer, centrifuge at 4 °C for 5 min at 563 × *g*, and discard supernatant.
24. For same-day FACS analysis, resuspend samples in 400 μL cold FACS buffer and run tubes on cytometer.
25. If not analyzing on the same day, fix samples in 2% PFA: Resuspend samples in 100 μL of 2% PFA in FACS buffer and incubate at 4 °C for 10 min (*see* **Note 25**).
26. Wash with 200 μL cold FACS buffer, centrifuge for 5 min at 563 × *g* at 4 °C, and discard supernatant.
27. Resuspend samples in 200 μL cold FACS buffer, cap tubes, and store at 4 °C in the dark for up to 3 weeks until analysis (*see* **Note 26**).
28. Analyze samples on LSRII FACS machine (or other suitable alternative).
29. Process data from FACS analysis using FlowJo software (or other suitable alternative).

4 Notes

1. PLP is not stable and has to be prepared fresh each time. We suggest diluting the remaining 16% PFA in 1× PBS and storing aliquots at −18 to −20 °C to be used in subsequent steps as needed.
2. Necessary only for IF-F.
3. Choice of antibodies will vary based on your specific experimental aims. As shown in Table 1, we most commonly stain with an unconjugated primary antibody against cluster of differentiation 3 (CD3) and a primary antibody against CD45R (B220) conjugated to fluorescein isothiocyanate (FITC) for

the identification of T cells and B cells, respectively. In place of one of the previously mentioned primary antibodies, we occasionally stain with a primary antibody against NK2 homeobox 1 (NKX2.1), also known as thyroid transcription factor 1 (TTF-1), in order to stain for tumor cells. TTF-1 is expressed strongly by lung adenocarcinoma cells [13] and is therefore a good marker to distinguish tumor cells from normal in IF-F sections. For a more thorough analysis of TLS, you may consider adding antibodies against the following proteins to your sections: CXCL13 (B cell chemokine), CR1 (follicular dendritic cell marker), CCL21 (T-cell chemokine), ER-TR7 (follicular reticular cell marker), CD31 (endothelial cell marker), and/or PNAd (HEV marker).

4. Secondary antibodies should be carefully chosen based on both the fluorescence spectra of chosen fluorophores and the configuration of your microscope. We commonly use goat anti-rabbit Alexa Fluor-568 (1:500) and anti-FITC Alexa Fluor-488 (1:500) in combination with the primary antibodies mentioned above (*see* **Note 3**).
5. To 500 mL of PBS, add 2.5 mL of thawed, heat-inactivated FBS and 2.5 mL of 20% sodium azide solution. Store at 4 °C.
6. From 16% PFA ampule, add 125 μL 16% PFA per 1 mL FACS buffer. Make fresh each use.
7. *See* Table 1 for detailed information regarding the antibodies used. Conjugated fluorophores should be carefully chosen based on both the fluorescence spectra of chosen fluorophores and the configuration of your flow cytometer. For our work, stained cells were run using 9–11-color FACS on an LSR II (BD) with 405, 488, 561, and 635 lasers.
8. "KP" mice were produced by crossing two commercially available mouse strains: $Kras^{LSL\text{-}G12D}$ (Jackson Laboratory; Stock No: 008179) and $p53^{LoxP}$ (Jackson Laboratory; Stock No: 008462). To obtain "KPT" mice, "KP" mice were crossed with commercially available Ai14 Cre reporter mice (Jackson Laboratory; Stock No: 007914).
9. Staining for the presence of B and T cells in mouse spleens serves as a good positive staining control. Having a positive control is essential for correct interpretation of microscopy images.
10. Tumors span several hundred microns. Therefore, TLS within tumors can easily be underrepresented or missed altogether if thin tumor sections (5 μm) are analyzed. For our studies, we have found that cutting 30-μm-thick sections is ideal for identification of TLS [10].

11. From this step forward, make sure that the sample never fully runs dry. Add 10–20 μL PBS to keep parts of samples hydrated, as needed. Add water to the bottom of black slide-staining trays and cover with lid to keep slides humidified and prevent drying.
12. Imaging sections with confocal microscopy is a labor-intensive protocol that takes about 1 month. We have optimized this process using EVOS FL Auto 2 and reduced the time required per lung lobe to 12 days maximum (*see* Fig. 2).
13. We have defined TLS as ≥20 aggregated B cells.
14. To ensure that analysis of intratumoral immune cells is not complicated by the presence of immune cells from circulation, we suggest that you first stain all circulatory $CD45^+$ immune cells via i.v. injection of a fluorescently conjugated anti-CD45 antibody prior to euthanasia. In this way, immune cells present in tumor homogenates that were trapped in the vasculature at the time of tissue harvest can be excluded during data analysis (*see* Fig. 3).
15. Cervical dislocation results in rapid death but can easily damage the trachea, making bronchoalveolar lavage more challenging to perform.
16. The smaller the incision the better. Optional: To improve digestion, fill the lungs with 0.5 mL Collagenase/DNase mixture. Use caution with syringes and discard in sharps container after use. Do not attempt to re-cap.
17. At this step, lobes can be used for either IF-F or FACS. Lobes for IF-F should be infused with and placed in PLP (*see* Subheading 3.1, **step 2**).
18. The tumor-draining lymph node, in the case of murine lung tumors, is the mediastinal lymph node. Therefore, FACS analysis of the mediastinal lymph node provides a useful comparison for the activation status of different immune cell subsets within the tumor. Likewise, performing FACS on cells from control lymph nodes that are not tumor draining (inguinal lymph nodes, for example), in addition to cells from the tumor and from the tumor-draining lymph node, is suggested.
19. Without gentleMACS dissociator, you may alternatively dissociate lung tumor tissue mechanically with small surgical scissors and incubate samples in Collagenase/DNase buffer on a rotator at 37 °C for 30 min. Following incubation, samples should be filtered through 40–100 μM cell strainers, washed with FACS buffer, and kept on ice prior to obtaining cell counts.
20. To perform a simple hemocytometer count, pipette 10 μL of cell suspension into a tube containing 390 μL of trypan blue

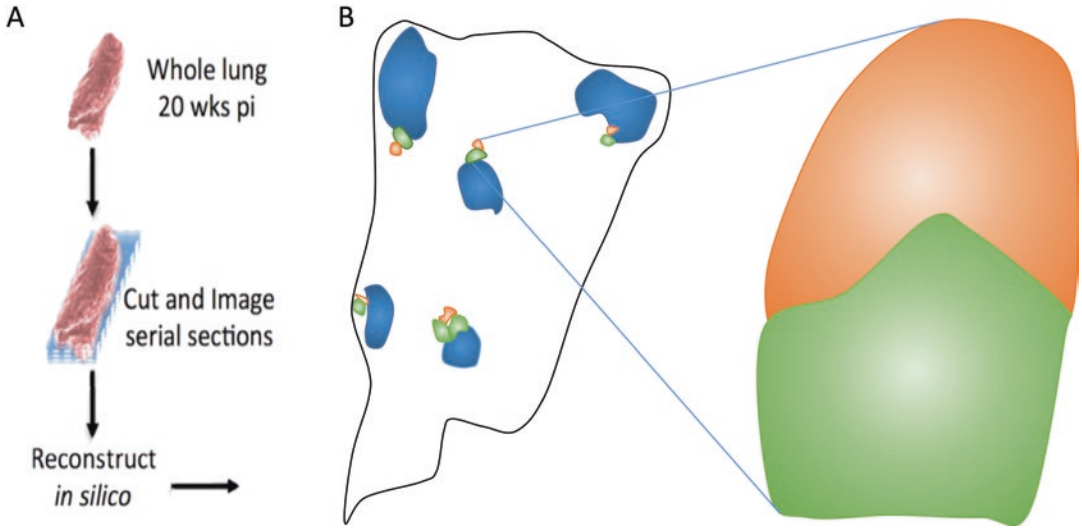

Fig. 2 Visualizing TA-TLS associated with LucOS-expressing tumors in whole tumor-bearing lung lobe 20 weeks postinfection. (**a**) Schematic illustrating the serial sectioning of whole lung lobe and reconstruction of IF sections in silico. (**b**) Artistic rendering of a reconstructed lung lobe stained for T cells (anti-CD3; orange), B cells (anti-B220; green), and tumor cells (anti-NKX2.1; blue) (left). Rendering of an individual tumor-associated tertiary lymphoid structure showing distinct clusters of T and B cells (right)

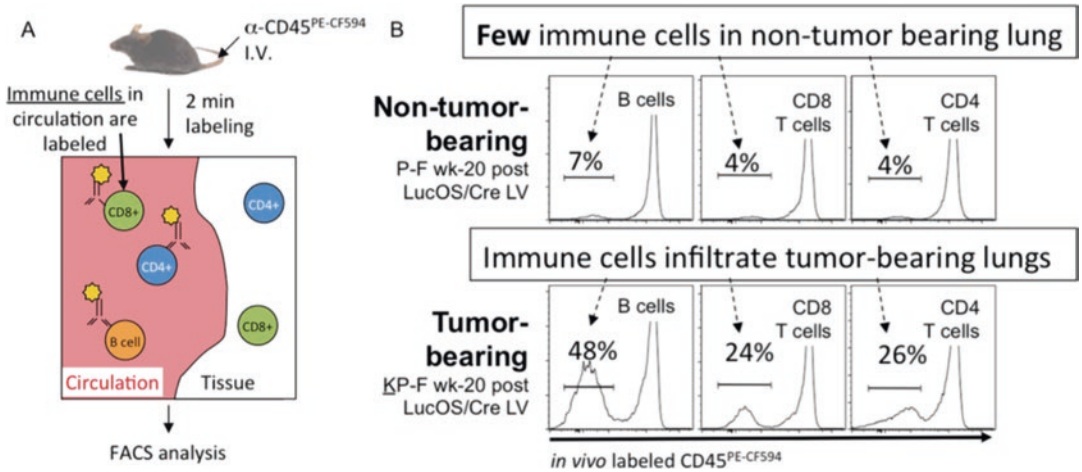

Fig. 3 Immune cells associated with advanced LucOS/Cre LV-infected KP mice 20 weeks postinfection. (**a**) Schematic for in vivo labeling of circulating immune cells. (**b**) Histograms show proportions of B cells, $CD8^+$ T cells, and $CD4^+$ T cells in week-20 non-tumor-bearing or tumor-bearing lungs from "P-F" and "KP-F" mice, respectively. "P-F" and "KP-F" mice were generated by crossing "KP" mice or commercially available $p53^{LoxP}$ mice (Jackson Laboratory; Stock No: 008462), respectively, with $Foxp3^{IRES\text{-}DTR\text{-}GFP}$ mice, generously provided by Professor Alexander Rudensky (Memorial Sloan-Kettering Cancer Center). Gates show tissue infiltrating ($CD45^{PE\text{-}CF594}$-negative cells). Control mouse lacks $Kras^{G12D}$ allele. *Abbreviations*: *i.v.* intravenous and *LV* lentivirus

for a 1:40 dilution. From this, pipette 10 μL onto hemocytometer with coverslip and, using a compound microscope, bring the etched grid located in the center of the hemocytometer into focus. Count the number of trypan blue-negative, viable cells within the four outer squares of the grid, and divide by four to obtain the average number of cells per square. Multiply by 40 (trypan blue dilution factor) and divide this by 0.0001 mL (volume of square on hemocytometer) to calculate the number of live cells per mL. In order to calculate the total number of cells, multiply the number of cells/mL by the volume (mL) of the cell suspension you counted.

21. As an alternative to polystyrene tubes, cells can be stained in 96-well U-bottom plates.
22. FBS must be washed out of cells as it will interfere with Live/Dead stain. Ensure that wash is performed with PBS only.
23. If staining with tetramers to identify antigen-specific T cells, tetramer staining can occur at the same time as staining with directly conjugated antibodies (*see* Subheading 3.5, **step 20**), depending on available fluorophores. If you wish to stain cells with tetramers, the tetramers should be thawed on ice and diluted in FACS buffer. Resuspend cells in 50 μL for lymph nodes, or 150 μL for lung tissue/tumors, and incubate for 15 min at 4 °C in the dark. Always fix tetramer-stained cells, even when planning to run samples on cytometer immediately. For a more thorough analysis of TLS, you may consider adding antibodies against the following proteins to your panel in order to assess the presence and activation status of other cell types within TLS: CD11c, CD11b, MHC class II, Thy1.2, CD103, KLRG1, GITR, CD62L, CD39, CTLA-4, and CD80.
24. Optimal dilutions of antibodies and tetramers should be determined prior to experimental FACS. This is most commonly achieved by making a series of dilutions of each individual antibody/tetramer and performing titration experiments.
25. Some fluorophores, like PE-Cy5, are sensitive to fixation in PFA. Therefore, when PE-Cy5 is included in your panel we suggest running samples fresh on the same day as staining. For the fluorophores included in this chapter, we did not see a measurable effect of fixation on fluorophore brightness. This is due to a relatively short fixation period (10 min).
26. Ideally, run samples on cytometer within 1 week of fixing for optimal detection of tetramers and conjugated stains. Samples that are not fixed should be run as soon as possible on the same day as staining.

Acknowledgements

We thank Professor Tyler Jacks (Massachusetts Institute of Technology) and Jacks lab members for their generous gift of reagents, advice, and time.

Funding: This work was supported by the National Cancer Institute K22 Transition Career Award.

References

1. Dieu-Nosjean MC, Antoine M, Danel C et al (2008) Long-term survival for patients with non-small-cell lung cancer with intratumoral lymphoid structures. J Clin Oncol 26(27):4410–4417. https://doi.org/10.1200/JCO.2007.15.0284
2. Ogino S, Nosho K, Irahara N et al (2009) Lymphocytic reaction to colorectal cancer is associated with longer survival, independent of lymph node count, microsatellite instability, and CpG island methylator phenotype. Clin Cancer Res 15(20):6412–6420. https://doi.org/10.1158/1078-0432.CCR-09-1438
3. Hiraoka N, Ino Y, Yamazaki-Itoh R et al (2015) Intratumoral tertiary lymphoid organ is a favourable prognosticator in patients with pancreatic cancer. Br J Cancer 112(11):1782–1790. https://doi.org/10.1038/bjc.2015.145
4. Kroeger DR, Milne K, Nelson BH (2016) Tumor-infiltrating plasma cells are associated with tertiary lymphoid structures, cytolytic T-cell responses, and superior prognosis in ovarian cancer. Clin Cancer Res 22(12):3005–3015. https://doi.org/10.1158/1078-0432.CCR-15-2762
5. Germain C, Gnjatic S, Tamzalit F et al (2014) Presence of B cells in tertiary lymphoid structures is associated with a protective immunity in patients with lung cancer. Am J Respir Crit Care Med 189(7):832–844. https://doi.org/10.1164/rccm.201309-1611OC
6. Sanmamed MF, Chester C, Melero I, Kohrt H (2016) Defining the optimal murine models to investigate immune checkpoint blockers and their combination with other immunotherapies. Ann Oncol 27(7):1190–1198. https://doi.org/10.1093/annonc/mdw041
7. Politi K, Pao W (2011) How genetically engineered mouse tumor models provide insights into human cancers. J Clin Oncol 29(16):2273–2281. https://doi.org/10.1200/JCO.2010.30.8304
8. McFadden DG, Politi K, Bhutkar A et al (2016) Mutational landscape of EGFR-, MYC-, and Kras-driven genetically engineered mouse models of lung adenocarcinoma. Proc Natl Acad Sci U S A 113(42):E6409–E6417. https://doi.org/10.1073/pnas.1613601113
9. DuPage M, Mazumdar C, Schmidt LM et al (2012) Expression of tumour-specific antigens underlies cancer immunoediting. Nature 482(7385):405–409. https://doi.org/10.1038/nature10803
10. Joshi NS, Akama-Garren EH, Lu Y et al (2015) Regulatory T cells in tumor-associated tertiary lymphoid structures suppress anti-tumor T cell responses. Immunity 43(3):579–590. https://doi.org/10.1016/j.immuni.2015.08.006
11. Caswell DR, Chuang CH, Yang D et al (2014) Obligate progression precedes lung adenocarcinoma dissemination. Cancer Discov 4(7):781–789. https://doi.org/10.1158/2159-8290.CD-13-0862
12. Madisen L, Zwingman TA, Sunkin SM et al (2010) A robust and high-throughput Cre reporting and characterization system for the whole mouse brain. Nat Neurosci 13(1):133–140. https://doi.org/10.1038/nn.2467
13. Nakamura N, Miyagi E, Murata S et al (2002) Expression of thyroid transcription factor-1 in normal and neoplastic lung tissues. Mod Pathol 15(10):1058–1067. https://doi.org/10.1097/01.MP.0000028572.44247.CF

Chapter 16

Targeting Tertiary Lymphoid Structures for Tumor Immunotherapy

Haidong Tang, Xiangyan Qiu, Casey Timmerman, and Yang-Xin Fu

Abstract

Tumor microenvironments (TME) are usually immunosuppressive and prevent lymphocyte priming. Recent clinical trials have shown that cancer immunotherapy such as immune checkpoint inhibitors can induce unprecedented durable responses in patients with a variety of cancers. Tertiary lymphoid structures (TLS) can form inside or adjacent to tumor tissues due to persistent inflammation. The formation of TLS facilitates lymphocyte trafficking and infiltration into tumor tissues. It can also support effective antigen presentation and lymphocyte activation. Thus, TLS have become an intriguing target to manipulate antitumor immunity. Several therapeutics targeting TLS have been developed and shown promising antitumor effects in various mouse models. In this chapter, we describe the general approach to establish transplantable mouse tumor models for the study of immunotherapy. We introduce the strategies for therapy through systemic or local treatment targeting TLS. We also present approaches to evaluate the antitumor immune responses provoked by the therapies.

Key words Tertiary lymphoid structure, Immunotherapy, Cancer, Mouse tumor model

1 Introduction

Conventional cancer therapies target the tumor tissues and can increase survival in some cancer patients. However, despite initial responses, many tumors relapse and develop resistance after prolonged treatment [1]. In contrast, immunotherapy targets the immune system to provoke a systemic response against tumors. Recent clinical trials with cancer immunotherapy have shown unprecedented durable responses in patients with a variety of advanced cancers, representing one of the major breakthroughs in oncology [2, 3].

In an antitumor immune response, antigen-presenting cells (APCs) uptake tumor antigens from tumor tissues, migrate to draining lymph nodes (LNs), and present processed antigens to T cells, leading to T-cell activation [4]. In many cancers, the presence of tumor-infiltrating lymphocytes (TILs) correlates with better

Marie-Caroline Dieu-Nosjean (ed.), *Tertiary Lymphoid Structures: Methods and Protocols*, Methods in Molecular Biology, vol. 1845, https://doi.org/10.1007/978-1-4939-8709-2_16,

prognosis, indicating the important roles of lymphocyte infiltration and immune responses [5]. During the persistent inflammation seen in tumors, the migration and positioning of immune cells form patterns similar to secondary lymphoid organs (SLOs). Such structures are known as tertiary lymphoid structures (TLS). TLS can be induced both inside and adjacent to tumors. Compared to draining lymph nodes, TLS may be a better place for T-cell priming (Fig. 1) [6]. As TLS are close to tumor tissues, it takes less effort for APCs to migrate to TLS and to present antigenic peptides to T cells than to emigrate to the draining LNs, knowing that each step is not exclusive of the other. After activation, effector T cells can go to the tumor tissues with fewer barriers. In addition, tumor antigen load may be higher in TLS than in draining LNs [7]. The microenvironment in TLS can induce better T-cell priming and prevent exhaustion or anergy. Since TLS can support effective antigen presentation and lymphocyte activation, it has become an intriguing target for cancer immunotherapy [8].

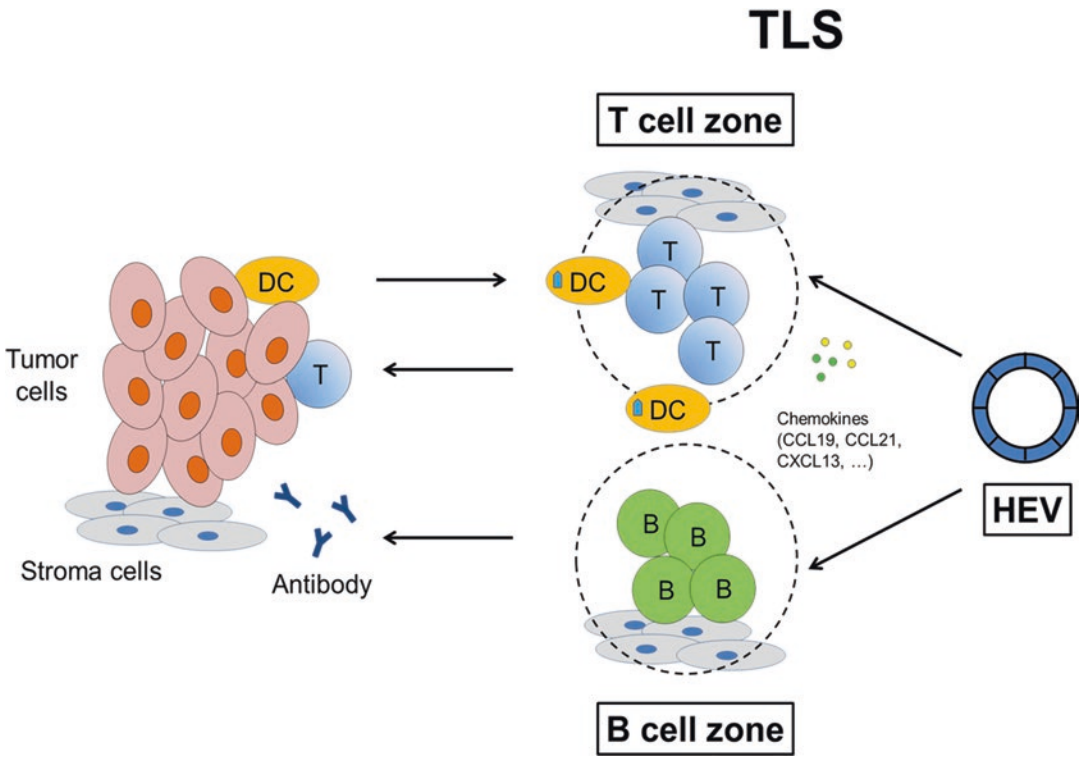

Fig. 1 Immune responses mediated by tumor-associated tertiary lymphoid structures. Circulating lymphocytes are recruited from HEV to tumor-associated TLS through a gradient of lymphoid chemokines. Intra-tumoral DCs uptake antigens and present processed antigens to specific T cells in the T-cell-rich areas of TLS, leading to T-cell (re)activation and differentiation. Effector T cells migrate to tumor nests for destruction of malignant cells. Tumor-infiltrating B cells are activated within the B-cell follicle of TLS and mediate antibody production. *Abbreviations*: *B* B cell, *DC* dendritic cell, *HEV* high endothelial venule, *T* T cell, and *TLS* tertiary lymphoid structure

Strategies aiming at inducing TLS have shown antitumor effects in several different mouse tumor models. In one study, systemic treatment with an agonist antibody against lymphotoxin beta receptor (LTβR) increases lymphocyte infiltration and antitumor immune responses in both mouse and human xenograft models [9]. In another study, a lymphotoxin alpha (LTα) fusion protein induces the formation of high endothelial venule (HEV)-like structures in a mouse model of melanoma [10]. Further, LTα therapy inhibits the growth of primary tumors as well as lung metastasis [10]. Our group and others have shown that recombinant proteins targeting the TNF superfamily member LIGHT can induce the formation of TLS, normalize blood vessels, support lymphocyte trafficking to tumor tissues, and lead to better antitumor responses [7, 11–13]. Clinically, the presence of TLS usually correlates with active antitumor immunity and better prognosis [14–16]. In colorectal carcinoma patients, TLS are associated with a higher number of $CD3^+$ T-cell infiltration and improved survival [17–19]. A 12-chemokine gene expression signature, most of which are critical for the formation of SLOs and TLS, correlates with better survival in melanoma and colorectal carcinoma patients [17, 20].

One major characteristic of TLS is the unique organization of immune cells, primarily dendritic cells (DCs), B cells, and T cells [21]. The organization of TLS is highly dependent on the expression of chemokines such as CCL19, CCL21, and CXCL13 [8, 16]. In this chapter, we describe the general approaches to established mouse tumor models and their applications in evaluating immunotherapies targeting TLS.

2 Materials

2.1 Cell Culture

1. Tumor cell lines B16F10 (ATCC CRL-6475) and Ag104Ld (*see* **Note 1**) [22].
2. Cell culture medium: Dulbecco's modified Eagle's medium (DMEM, Corning) supplemented with 10% fetal bovine serum (FBS, heat-inactivated or not), 100 U/mL penicillin, and 100 U/mL streptomycin.
3. 37 °C Water bath.
4. Humidified CO_2 incubator.
5. 0.25% Trypsin (Corning).
6. 1× Phosphate-buffered saline (PBS) without calcium or magnesium.
7. Sterile cell culture plastics: 100 or 150 mm petri dishes, 6-well plates, 15 or 50 mL polypropylene tubes, pipets.
8. Sterile 1.5 mL microcentrifuge tubes.

9. 2× Trypan blue solution.
10. Hemocytometer.
11. Benchtop centrifuge.

2.2 Tumor Inoculation, Treatment, and Monitoring

1. C57BL/6 and C3B6F1 mice (5–10 mice per treatment group).
2. Ear tags and applier.
3. 0.3 mL Insulin syringes with 31 gauge needle.
4. 0.5 mL Tuberculin syringes with 27 gauge needle.
5. Shaver.
6. Vernier caliper (Scienceware).
7. Drug of interest, i.e., TLS inducer (*see* **Note 2**).

2.3 Analysis of Tumor Immune Infiltrate

1. CO_2 euthanasia chamber.
2. Dissection supplies: Dissection board, scissors, and forceps.
3. 75% Alcohol spray.
4. RPMI-1640 medium.
5. 0.5 M EDTA solution, pH 8.0.
6. 100 mg/mL Collagenase IV (Sigma-Aldrich).
7. 10 mg/mL DNase I (Sigma-Aldrich).
8. 37 °C Shaker.
9. 40 μm Cell strainer.
10. FACS buffer: 1% FBS, 1 mM EDTA, 0.05% sodium azide in PBS.
11. Antibodies for flow cytometry (*see* Table 1).
12. 12 × 75 mm Round-bottom polystyrene tubes.

2.4 Analysis of Chemokines/ Cytokines

1. Scale.
2. TRIzol (Invitrogen).
3. FastPrep-24 5 G benchtop homogenizer (MP Biomedicals), or Polytron homogenizer (Kinematica).
4. 100% Chloroform.
5. 100% Isopropyl alcohol.
6. Vortex mixer.
7. 75% Ethanol.
8. Nuclease-free water.
9. NanoDrop 2000 spectrophotometer (Thermo Scientific).
10. RNase-free DNase set (QIAGEN).
11. Maxima first-strand cDNA synthesis kit (Thermo Scientific).
12. SsoAdvanced universal SYBR green supermix (Bio-Rad).
13. Primers for real-time PCR (Table 2).
14. PTC-200 Thermal Cycler (MJ Research).

Table 1
List of antibody for flow cytometry

Antibody	Supplier	Catalog number	Dilution
FITC-rat anti-mouse B220	BioLegend	103206	1:200
PE-hamster anti-mouse CD3ε	BioLegend	100308	1:500
PE/Cy7-rat anti-mouse CD4	BioLegend	100422	1:1000
APC/Cy7-rat anti-mouse CD8α	BioLegend	100714	1:500
7-AAD	BioLegend	420404	1:100
BV421-rat anti-mouse CD45	BioLegend	103133	1:500

Table 2
Primers for real-time PCR [28, 29]

Gene		Sequence
Ccl19	Forward	5'-CTGCCTCAGATTATCTGCCAT-3′
	Reverse	5'-AGGTAGCGGAAGGCTTTCAC-3′
Ccl21	Forward	5'-AAGGCAGTGATGGAGGGG-3′
	Reverse	5'-CGGGTAAGAACAGGATTG-3′
Cxcl13	Forward	5'-CATAGATCGGATTCAAGTTACG-3′
	Reverse	5'-TCTTGGTCCAGATCACAACTTCA-3′
Gapdh	Forward	5'-CCACCCCAGCAAGGACACT-3′
	Reverse	5'-GAAATTGTGAGGGAGATGCTCA-3'

3 Methods

3.1 Preparation of Tumor Cells Before Inoculation

1. In a 15 mL tube, add 10 mL pre-warmed complete DMEM medium.
2. Thaw the frozen cell line rapidly in a 37 °C water bath.
3. Transfer 1 mL of cells into pre-warmed complete DMEM medium.
4. Centrifuge at 180 × *g* for 3 min. Then, discard the supernatant.

5. Resuspend cells with 8 mL of complete DMEM medium. Seed the cells into a 100 mm dish.
6. Culture the cell line in 37 °C incubator with 5% CO_2.
7. When cells reach 80–90% confluency, remove the growth medium. Wash the cells with 5 mL of PBS.
8. Aspirate PBS. Add 0.5 mL of 0.25% trypsin and incubate the cells in 37 °C until they have detached.
9. Quench trypsin by adding 5 mL of complete DMEM medium. Pellet cells by centrifugation at 180 × *g* for 3 min.
10. Resuspend the cells with 1 mL of complete DMEM medium. Seed the cells into a new dish by 1:5–1:10 dilution. Add 8 mL of fresh complete DMEM medium.
11. Before the tumor inoculation, harvest the cells from dishes by trypsin digestion, as described in **step 8** (*see* **Note 3**).
12. Centrifuge at 180 × *g* for 3 min. Wash the cells twice by PBS.
13. Resuspend the cells in 10 mL of PBS. Take 10 μL of cells, and mix 1:1 with trypsin blue solution. Count the cell number with a hemocytometer (*see* **Note 3**).
14. Pellet the cells by centrifugation at 180 × *g* for 3 min.
15. Resuspend the cells with PBS to obtain a desired concentration of cells for injection. For B16F10 or Ag104Ld cells, a 5×10^6/mL of suspension is made to achieve an inoculation number of 5×10^5/100 μL/mouse (*see* **Note 4**). Keep the cells on ice before the inoculation for a better viability.

3.2 Tumor Inoculation and Treatment

1. Shave the mice on their flank.
2. (Optional) Anesthetize the mice with isoflurane (*see* **Note 5**).
3. Mix the cells, and slowly draw 100 μL of cells into an insulin syringe (*see* **Note 6**).
4. Restrain mouse with the nondominant hand while holding the syringe with dominant hand (*see* **Note 7**). Inject 5×10^5 cells/100 μL subcutaneously (s.c.) into the shaved flank of the mice.
5. Slowly withdraw the needle. Place the mice back to its cage.
6. Tumors usually become palpable 3–4 days after the inoculation of the malignant cells. Identify tumor-bearing mice by ear tags. Tumor sizes are measured with vernier caliper. The volume is calculated as

$$\text{Volume } (\text{mm}^3) = \text{Length} \times \text{Width} \times \text{Height}/2$$

7. Measure tumor sizes two to three times per week.
8. When the tumors reach a certain size, treat mice with the drug of interest (*see* **Note 8**).

9. Preload the syringe with drugs pre-diluted in PBS. Ensure that no air bubbles are apparent.
10. Restrain mouse with the nondominant hand while holding the syringe with dominant hand.
11. (Option 1: intraperitoneal injection) Lay animal on its back and tilt the head downwards at approximately 15–20° angle. Inject needle, bevel up, into the lower left abdominal quadrant. Push the solution (100–200 μL) in, and then pull out the needle before placing the mouse back in the cage.
12. (Option 2: intratumoral injection) Inject needle, bevel up, directly into the tumor. Slowly push the solution (25–50 μL) in. Wait for few seconds before pulling the needle out. Place the mice back in the cage (*see* **Note 9**).

3.3 Analysis of Tumor Immune Infiltrate

1. Euthanize the mice by CO_2 asphyxiation.
2. Dissect subcutaneous tumors. Place into a 6-well plate with 0.5 mL serum-free RPMI-1640 medium. Keep all samples on ice while collecting tissues.
3. Cut tumors into small pieces (~1–2 mm) with scissors.
4. Add serum-free RPMI-1640 medium into a final volume of 5 mL. Add collagenase IV and DNase I to a final concentration of 1 mg/mL and 100 μg/mL, respectively.
5. Digest samples for 15 min for B16F10 tumor, or 60 min for Ag104Ld tumor, while shaking at 100 rpm in 37 °C (*see* **Note 10**).
6. After the digestion, add 40 μL of 0.5 M EDTA to terminate digestion. Disrupt remaining pieces by pipetting several times with a 5 mL pipet.
7. Strain the cells through a 40 μm cell strainer. Further mash clumps using a stopper from a 1 mL syringe. Wash the cell strainer with a few mL of RPMI-1640 medium.
8. Spin down the cells at 400 × *g* for 10 min.
9. Wash the cells twice with the FACS buffer.
10. Count cells with a hemocytometer. Resuspend the cells into 1×10^7/mL with FACS buffer.
11. Aliquot cells into 100 μL/tube. Add 10 μg/mL Fc-blocking antibodies (anti-CD16/CD32, clone 2.4G2). Incubate on ice for 20 min.
12. Wash the cells once with the FACS buffer.
13. (Optional) As a positive control for the Live/Dead dye, incubate one aliquot of cells at 60 °C for 1 min. Then, chill on ice for at least 1 min before proceeding.
14. Centrifuge the cells at 400 × *g* for 10 min. Discard the supernatant.

15. Resuspend the cells with 100 μL of staining cocktail (FITC-anti-mouse B220, PE-anti-mouse CD3e, PE/Cy7-anti-mouse CD4, APC/Cy7-anti-mouse CD8a, BV421-anti-mouse CD45 antibodies, 7-AAD) diluted in FACS buffer (*see* Table 1). Incubate on ice for 20 min in the dark.
16. Wash the samples twice with FACS buffer.
17. Resuspend samples with 300 μL of FACS buffer. Transfer the stained cells to polystyrene tubes. Proceed to acquisition using a flow cytometer.

3.4 Analysis of Cytokine/Chemokine Expression

1. Euthanize the mice by CO_2 asphyxiation.
2. Dissect the subcutaneous tumors. Weigh the tumor tissues on a scale. Add 1 mL of TRIzol per 50–100 mg of tissues. Store at −80 °C until use.
3. Homogenize the tumors with FastPrep-24 5 G benchtop homogenizer or Polytron homogenizer. Place the tubes on ice.
4. Centrifuge at 12,000 × *g* for 5 min at 4 °C to remove the pellet debris. Transfer the supernatant to a new tube at 4 °C.
5. Add 0.2 mL of 100% chloroform. Vortex the cells for 15 s. Then, incubate at RT for 2 min.
6. Centrifuge the cells at 12,000 × *g* for 15 min at 4 °C.
7. Transfer the supernatant to a new tube at 4 °C.
8. Add 0.5 mL of 100% isopropyl alcohol. Incubate at RT for 10 min.
9. Centrifuge at 12,000 × *g* for 10 min in 4 °C.
10. Discard the supernatant. Wash pellet by 1 mL of 75% ethanol.
11. Centrifuge at 6000 × *g* for 5 min at 4 °C.
12. Air-dry the RNA pellet for 5–10 min. Dissolve it by 50 μL of nuclease-free water.
13. RNA concentration is determined in a Nanodrop spectrophotometer. RNA can be stored at −80 °C for at least 1 year.
14. Prepare the genomic DNA elimination mix for each sample according to Table 3.
15. Incubate for 15 min at RT.
16. Add 1.0 μL of stop solution. Incubate for 10 min at 70 °C to inactivate enzyme. Chill on ice for at least 1 min.
17. Prepare the reverse-transcription mix according to Table 4.
18. Incubate for 10 min at 25 °C, followed by 60 min at 50 °C.
19. Terminate the reaction by heating at 85 °C for 5 min. The product cDNA can be stored at −20 or −80 °C for long-term storage.

Table 3
Genomic DNA elimination mix

Component	Amount
10× Buffer	1.0 μL
RNA	25 ng–5 μg
RNase-free DNase I	1.0 μL
Nuclease-free water	Add to 10 μL

Table 4
Reverse transcription mix

Component	Amount
5× Reaction buffer	2.0 μL
RiboLock RNase inhibitor	1.0 μL
Random primer	0.2 μg
dNTP mix, 10 mM each	2.0 μL
Maxima reverse transcriptase	1.0 μL
Nuclease-free water	Add to 20 μL

Table 5
qPCR mix

Component	Amount
SsoAdvanced universal SYBR green supermix (2×)	10 μL
Forward and reverse primers	1.0 μL
cDNA	1.0 μL
Nuclease-free water	Add to 20 μL

20. Prepare the qPCR mix according to Table 5.
21. Load the qPCR tubes into the real-time PCR instrument and start the PCR run (95 °C 5 min; 95 °C 15 s → 55 °C 30 s → 72 °C 30 s, 40 cycles; 72 °C 5 min).
22. Perform data analysis according to the instrument-specific instructions.

4 Notes

1. Different models vary in their tumor microenvironments, and thus may have different responses to therapy. Both B16F10 and Ag104Ld cell lines characteristically have a low level of spontaneous T-cell infiltration. They are more sensitive to therapies that are able to manipulate lymphocyte infiltration.
2. Different therapeutics have been developed to induce the formation of TLS and have shown an antitumor activity. These include, but are not limited to, antibodies [23, 24], recombinant cytokines/chemokines [11, 13, 25, 26], and antibody-cytokine fusion proteins [10, 27, 12].
3. It is important to use cells in good condition for inoculation (viability >90%). Using cells in the log phase of proliferation curve will increase tumor take rate in mice.
4. For our experiments, we usually use 5×10^5 for both B16F10 and Ag104Ld cell lines. However, the tumor growth curve may vary depending on various factors, such as condition of the cells, different tumor models, animal facility, and genetic background of the mice. Thus, it is recommend to titrate tumor cell numbers before starting any experiment.
5. While it is not necessary to anesthetize mice during tumor inoculation, mice may struggle and thus doing so can improve the reproducibility of the tumor growth curve in vivo.
6. If using syringes with permanently attached needles, cells should be drawn and injected slowly. Do not aspirate cells with the needle as this may damage the cells, leading to low tumor take rate.
7. While restraining mouse with the nondominant hand, hold one rear foot with ring and baby fingers. Mouse often tries to kick back during injection. This will help to keep the injection site steady especially during *i.p.* injection.
8. The time to start therapy may vary depending on the purposes. It usually takes about 7 days for the adaptive immune responses to take place. So, it is recommended to start treatment at least 7 days after the tumor inoculation when studying T-cell response.
9. Drugs may leak out quickly from the tumor after intra-tumoral injection. To increase retention, drugs can be mixed with Matrigel (Corning) before its injection.
10. Digestion time varies depending on tumor types. Soft tumors such as B16F10 take a short time to digest. In contrast, rigid tumors such as Ag104Ld take longer. However, do not over-digest as it may result in loss of cell surface markers or even cell death.

Funding

Y.X.F. holds the Mary Nell and Ralph B. Rogers Professorship in Immunology. This work was in part supported by the US National Institutes of Health through National Cancer Institute grants CA141975 and CA97296, CPRIT grant RR150072, grants from the Chinese Academy of Sciences (XDA09030303), and the Chinese Ministry of Science and Technology (2012ZX10002006, 2011DFA31250, and 2012AA020701) to Y.X.F.

References

1. Holohan C, Van Schaeybroeck S, Longley DB, Johnston PG (2013) Cancer drug resistance: an evolving paradigm. Nat Rev Cancer 13(10):714–726
2. Couzin-Frankel J (2013) Cancer immunotherapy. Science 342(6165):1432–1433
3. Sunshine J, Taube JM (2015) Pd-1/Pd-L1 Inhibitors. Curr Opin Pharmacol 23:32–38
4. Chen DS, Mellman I (2013) Oncology meets immunology: the cancer-immunity cycle. Immunity 39(1):1–10
5. Woo S-R, Corrales L, Gajewski TF (2015) Innate immune recognition of cancer. Annu Rev Immunol 33:445–474
6. Tang H, Zhu M, Qiao J, Fu Y-X (2017) Lymphotoxin signalling in tertiary lymphoid structures and immunotherapy. Cell Mol Immunol 14:809–818
7. Yu P, Lee Y, Liu W et al (2004) Priming of naive T cells inside tumors leads to eradication of established tumors. Nat Immunol 5(2):141–149
8. Sautès-Fridman C, Fridman WH (2016) TLS in tumors: what lies within. Trends Immunol 37(1):1–2
9. Lukashev M, LePage D, Wilson C et al (2006) Targeting the lymphotoxin-β receptor with agonist antibodies as a potential cancer therapy. Cancer Res 66(19):9617–9624
10. Schrama D, thor Straten P, Fischer WH et al (2001) Targeting of lymphotoxin-α to the tumor elicits an efficient immune response associated with induction of peripheral lymphoid-like tissue. Immunity 14(2):111–121
11. Johansson-Percival A, Li Z-J, Lakhiani DD et al (2015) Intratumoral LIGHT restores pericyte contractile properties and vessel integrity. Cell Rep 13(12):2687–2698
12. Tang H, Wang Y, Chlewicki LK et al (2016) Facilitating T cell infiltration in tumor microenvironment overcomes resistance to PD-L1 blockade. Cancer Cell 29(3):285–296
13. Johansson-Percival A, He B, Li Z-J et al (2017) De novo induction of intratumoral lymphoid structures and vessel normalization enhances immunotherapy in resistant tumors. Nat Immunol 18:1207
14. Dieu-Nosjean MC, Giraldo NA, Kaplon H et al (2016) Tertiary lymphoid structures, drivers of the anti-tumor responses in human cancers. Immunol Rev 271(1):260–275
15. Dieu-Nosjean M-C, Goc J, Giraldo NA et al (2014) Tertiary lymphoid structures in cancer and beyond. Trends Immunol 35(11):571–580. https://doi.org/10.1016/j.it.2014.09.006
16. Weinstein AM, Storkus WJ (2015) Therapeutic lymphoid organogenesis in the tumor microenvironment. In: Xiang-Yang W, Paul BF (eds) Advances in cancer research, vol 128. Academic Press, pp 197–233. https://doi.org/10.1016/bs.acr.2015.04.003
17. Coppola D, Nebozhyn M, Khalil F et al (2011) Unique ectopic lymph node-like structures present in human primary colorectal carcinoma are identified by immune gene Array profiling. Am J Pathol 179(1):37–45. https://doi.org/10.1016/j.ajpath.2011.03.007
18. Di Caro G, Bergomas F, Grizzi F et al (2014) Occurrence of tertiary lymphoid tissue is associated with T-cell infiltration and predicts better prognosis in early-stage colorectal cancers. Clin Cancer Res 20(8):2147–2158
19. McMullen T, Lai R, Dabbagh L et al (2010) Survival in rectal cancer is predicted by T cell infiltration of tumour-associated lymphoid nodules. Clin Exp Immunol 161(1):81–88
20. Messina JL, Fenstermacher DA, Eschrich S et al (2012) 12-Chemokine gene signature identifies lymph node-like structures in melanoma: potential for patient selection for immunotherapy? Sci Rep 2:765

21. Pitzalis C, Jones GW, Bombardieri M, Jones SA (2014) Ectopic lymphoid-like structures in infection, cancer and autoimmunity. Nat Rev Immunol 14(7):447
22. Wick M, Dubey P, Koeppen H et al (1997) Antigenic cancer cells grow progressively in immune hosts without evidence for T cell exhaustion or systemic anergy. J Exp Med 186(2):229–238
23. Lee Y, Chin RK, Christiansen P et al (2006) Recruitment and activation of naive T cells in the islets by lymphotoxin β receptor-dependent tertiary lymphoid structure. Immunity 25(3):499–509
24. Yang D, Ud Din N, Browning DD et al (2007) Targeting lymphotoxin β receptor with tumor-specific T lymphocytes for tumor regression. Clin Cancer Res 13(17):5202–5210
25. Sharma S, Stolina M, Luo J et al (2000) Secondary lymphoid tissue chemokine mediates T cell-dependent antitumor responses in vivo. J Immunol 164(9):4558–4563
26. Hillinger S, Yang S, Batra R et al (2006) CCL19 reduces tumour burden in a model of advanced lung cancer. Br J Cancer 94(7):1029–1034
27. Reisfeld RA, Gillies SD, Mendelsohn J et al (1996) Involvement of B lymphocytes in the growth inhibition of human pulmonary melanoma metastases in athymic nu/nu mice by an antibody-lymphotoxin fusion protein. Cancer Res 56(8):1707–1712
28. Moussion C, Girard J-P (2011) Dendritic cells control lymphocyte entry to lymph nodes through high endothelial venules. Nature 479(7374):542–546
29. Chai Q, Onder L, Scandella E et al (2013) Maturation of lymph node fibroblastic reticular cells from myofibroblastic precursors is critical for antiviral immunity. Immunity 38(5):1013–1024

INDEX

Marie-Caroline Dieu-Nosjean (ed.), *Tertiary Lymphoid Structures: Methods and Protocols*, Methods in Molecular Biology, vol. 1845, https://doi.org/10.1007/978-1-4939-8709-2, © Springer Science+Business Media, LLC, part of Springer Nature 2018

L

M

O

P

Q

R

S

T

V